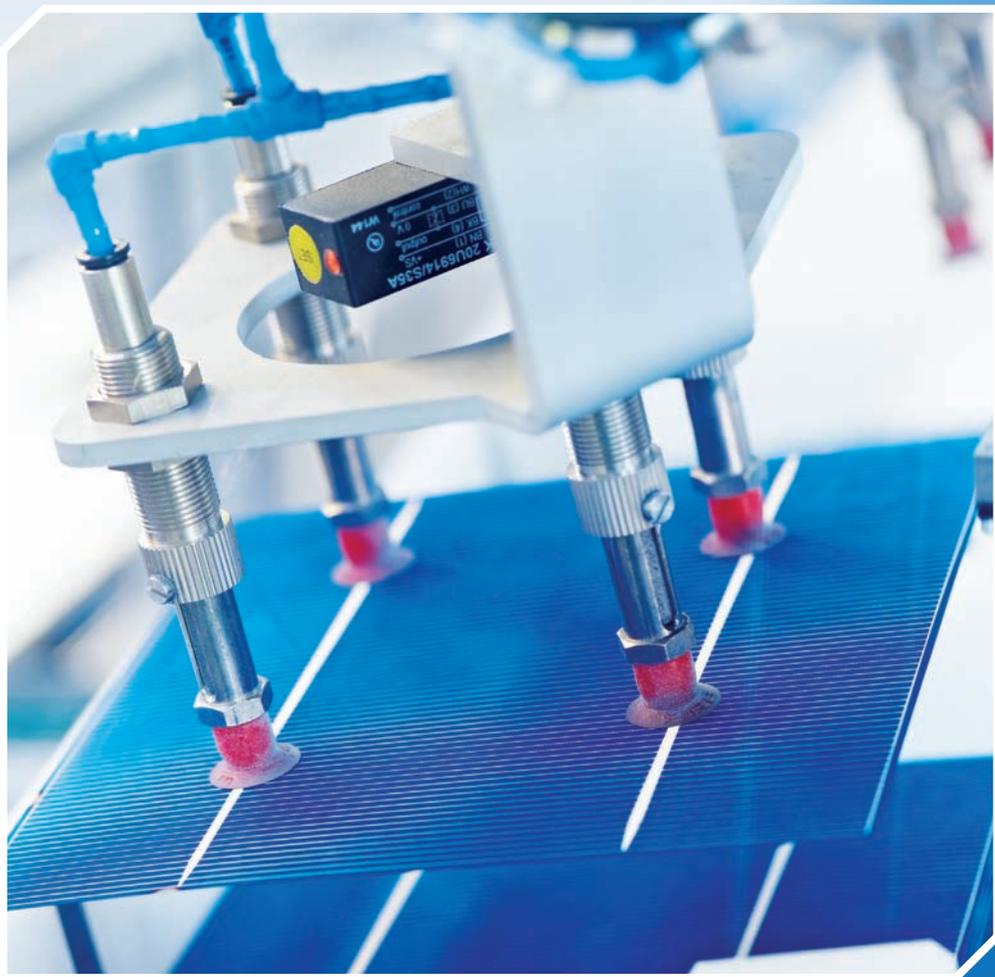Konrad Mertens

Photovoltaics

Fundamentals, Technology and Practice

WILEY

PHOTOVOLTAICS

PHOTOVOLTAICS
FUNDAMENTALS, TECHNOLOGY AND PRACTICE

Konrad Mertens

Münster University of Applied Sciences, Germany

Translated by
Gunther Roth, *Switzerland*

WILEY

Contents

Preface

This book arose from my lectures on the subject of photovoltaics at the Münster University of Applied Sciences. The students repeatedly asked for a suitable textbook that I could recommend to them to accompany the lectures. Unfortunately searching the book market was difficult, although there are a whole series of books on the subject of photovoltaics. Many textbooks concentrate exclusively on cell technologies and look at this from a very theoretical, formalistic point of view. Added to this is that the contents are often out of date. On the other hand, there are books on the planning and design of photovoltaic installations. These can provide the solar plant installer with help but they simplify the issues so much that they do not provide a basis for a real understanding of photovoltaics.

For this reason this book places emphasis on a clear and also correct depiction of the physical and electro-technical fundamentals. Besides cell technologies, the system technology (inverter, plant types, etc.) as well as the planning and operation (selection of sites, monitoring of plants, etc.) are also discussed. A special feature is also the presentation of current methods of surveying and studying the quality of solar modules as is carried out in the photovoltaic test laboratory of the Münster University of Applied Sciences.

Special thanks are due to my students who have enriched the lectures on photovoltaics with great interest and commitment over the years. Their clever questions have entered this book so that the answers can also help the readers. I would also like to thank graduate engineer Josef Lindenbaum for fruitful technical discussions and his assistance in numerous surveys.

"Daddy, since you have been writing this book you haven't any time for us." I have heard this reproach now and again during the writing of this book. For this reason a special thank you to my wife Annette and my children Martin, Barbara and Viktoria who have always supported me during this time.

Steinfurt, August 2011
Konrad Mertens

Preface to the International Edition

A steadily growing number of requests for an English version led to the decision to publish this international version of the Photovoltaics textbook. For this – besides the translation of the German text – several figures, tables and solar radiation maps were extended with worldwide data and information. Moreover, as the photovoltaic market and technology has developed very quickly, numerous updates have found room in this first international version.

I would like to express my thanks to John Wiley & Sons, Ltd for making this book possible. My special thanks to Gunther Roth for the translation, Richard Davies for managing the whole book project and Laura Bell for taking care for all the small problems that arose.

A new English website has been created at www.textbook-pv.org.

Here the reader can find the most figures of the book (in colours!) as a free download, supporting software and solutions to the exercises (and possibly corrections to the book).

I am very glad that the book is now accessible for a worldwide readership. We all know that the transformation of the current worldwide energy system into an environmentally friendly and sustainable one is a giant challenge. Photovoltaics can become an important part in the future energy supply. Hopefully this book will help to deepen the understanding of the technology and the possibilities for photovoltaics, and can therefore support this development.

Steinfurt, January 2014
Konrad Mertens

Abbreviations

ALB	Albedo
AM	Air Mass
a-Si	Amorphous silicon
CAES	Compressed air energy storage
CdTe	Cadmium-telluride
CET	Central European Time
CIGS	Copper-indium-gallium-sulfide
CIGSe	Copper-indium-gallium-selenide
CIS	Copper-indium sulfide
CISe	Copper-indium-selenide
c-Si	Crystalline silicon
EEG	Renewable Energy Law
EMC	Electromagnetic compatibility
EVA	Ethyl-Vinyl-Acetate
FF	Fill factor
GCB	Generator connection box
HIT	Heterojunction with intrinsic thin layer
ITO	Indium tin oxide
LST	Local Solar Time
MET	Middle European Time
MPP	Maximum power point
NOCT	Nominal operating cell temperature
PECVD	Plasma enhanced chemical vapor deposition
PR	Performance ratio
PWM	Pulse width modulation
SR	Sizing ratio
STC	Standard test conditions
TC	Temperature coefficient
tce	Tons of coal equivalent
TCO	Transparent conducting oxide
toe	Tons of oil equivalent
UTC	Coordinated Universal Time
PID	Potential induced degradation

1

Introduction

The supply of our industrial community with electrical energy is indispensable on one hand but, on the other, is accompanied by various environmental and safety problems. In this first chapter, therefore, we will look at the present energy supply and will familiarize ourselves with renewable energies as feasible future alternatives. At the same time, photovoltaics will be presented in brief and its short but successful history will be considered.

1.1 Introduction

In the introduction we will explain why we are occupying ourselves with photovoltaics and who should read this book.

1.1.1 Why Photovoltaics?

In past years it has become increasingly clear that the present method of generating energy has no future. Thus, **finiteness of resources** is noticeably reflected in the rising prices of oil and gas. At the same time we are noticing the first effects of **burning fossil fuels**. The melting of the glaciers, the rise of the ocean levels and the increase in weather extremes, as well as the **nuclear catastrophe in Fukushima**, all show that nuclear energy is not the path to follow in the future. Besides the **unsolved final storage question**, fewer and fewer people are willing to take the risk of large parts of their country being radioactive.

Fortunately there is a **solution** with which a sustainable energy supply can be assured: **renewable energy sources**. These use infinite sources as a basis for energy supplies and can ensure a full supply with a suitable combination of different technologies such as biomasses, photovoltaics, wind power, and so on. A particular role in the number of renewable energies is played by **photovoltaics**. They permit an emission-free conversion of sunlight into electrical energy and, because of their great potential, **will be an important pillar in future energy systems**.

However, the changeover of our energy supply will be a **huge task** that will only be mastered with the **imagination** and **knowledge of engineers and technicians**. The object of this book is to increase this technical knowledge in the field of photovoltaics. For this purpose it will deal with the fundamentals, technologies, practical uses and commercial framework conditions of photovoltaics.

1.1.2 Who Should Read this Book?

This book is meant mostly for **students of the engineering sciences** who wish to deepen their knowledge of photovoltaics. But it is written in such a way that it is also suitable for **technicians, electricians and the technically-interested layman**. Furthermore, it can be of use to **engineers in the profession** to help them to gain knowledge of the current technical and commercial position of photovoltaics.

1.1.3 Structure of the Book

In this **introduction** we will first deal with the **subject of energy**: What is energy and into what categories can it be divided? From this base we will then consider the present energy supply and the problems associated with it. A solution to these problems is renewable energies and will be presented next in a brief overview. As we are primarily interested in photovoltaics in this book we will finish with the relatively young but stormy history of photovoltaics.

The **second chapter** deals with the **availability of solar radiation**. We become familiar with the features of sunlight and investigate how solar radiation can be used as efficiently as possible. Then in the Sahara Miracle, we will consider, what areas would be necessary to cover the whole of the world's energy requirements with photovoltaics.

In the **third chapter** we deal with the **basics of semiconductor physics**. Here we will concentrate on the structure of semiconductors and an understanding of the p-n junction. Besides this, the phenomenon of light absorption will be explained, without which no solar cell can function. Those familiar with semiconductors can safely skip this chapter.

In **Chapter 4** we get to the details: We learn of the **structure, method of operation and characteristics of silicon solar cells**. Besides this, we will view in detail the parameters and degree of efficiency on which a solar cell depends. On the basis of world records of cells we will then see how this knowledge can be successfully put to use.

Chapter 5 deals with **cell technologies**: What is the path from sand, via silicon solar cell, to the solar module? What other materials are there and what does the cell structure look like in this case? Besides these questions we will also look at the ecological effects of the production of solar cells.

The **structures and properties of solar generators** are the subjects of **Chapter 6**. Here we will deal with the optimum interconnection of solar modules in order to minimize the effects of shading. Besides this we will present various types of plants such as pitched roof and ground-mounted plants.

Chapter 7 deals with **system technology**. At the start there is the question of how to convert direct current efficiently into alternating current. Then we will become familiar with the various types of inverters and their advantages and disadvantages. Off-grid systems are handled in their own section.

In **Chapter 8** we concentrate on **photovoltaic metrology**. Besides the acquisition of solar radiation we deal especially with the determination of the real power of solar modules. Furthermore we become familiar with modern methods of quality analysis such as thermography and electroluminescence metrology.

Design and operation of grid-coupled plants are both presented in **Chapter 9**. Besides the optimum planning and dimensioning of plants, methods of feasibility calculation are also discussed. In addition, methods for monitoring plants are shown and the operating results of particular plants are presented.

Chapter 10 provides a view of the **future of photovoltaics**. First we will estimate power generation potential in Germany. This is followed by a consideration of price development. Finally we will discuss the role that photovoltaics can play in the energy systems of the future.

Each chapter has **exercises** associated with it, which will assist in repeating the material and deepening the knowledge of it. Besides, they provide a control of the students' own knowledge. The **solutions** to the exercises can be found in the Internet under ***www.textbook-pv.org***.

1.2   What is Energy?

We take the **use of energy** in our daily lives as a **matter of course**, whether we are operating the coffee machine in the morning, using the car during the day or returning to a warm home in the evening. Also the **functionality** of our whole modern **industrial community** is based on the availability of energy: production and transport of goods, computer-aided management and worldwide communication are inconceivable without a sufficient supply of energy.

At the same time the recognition is growing that the present type of **energy supply** is partly **uncertain, environmentally damaging** and available only to a **limited extent**.

1.2.1 Definition of Energy

What exactly do we understand about the term energy? Maybe a definition of energy from a famous mouth will help us. **Max Planck** (founder of quantum physics: 1858–1947) answered the question as follows:

> Energy is the ability of a system to bring outside effects (e.g., heat, light) to bear.

For instance, in the field of mechanics we know the **potential energy** (or stored energy) of a mass m that is situated at a height h (Figure 1.1(a)):

$$W_{Pot} = m \cdot g \cdot h \tag{1.1}$$

with

g: Earth's gravity, $g = 9.81 \, \text{m/s}^2$

(a) Potential energy

$$W_{Pot} = m \cdot g \cdot h$$
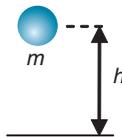
(c) Capacitor energy

$$W_{Cap} = \frac{1}{2} \cdot C \cdot V^2$$
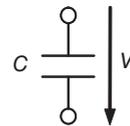
(b) Kinetic energy

$$W_{Kin} = \frac{1}{2} \cdot m \cdot v^2$$
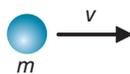
(d) Energy at the resistor

$$W_{El} = \frac{V^2}{R} \cdot t$$
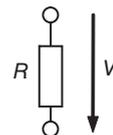
Figure 1.1   Depiction of different forms of energy

If a bowling partner drops his 3 kg bowling ball then the "one meter-high ball" system can have a distinct effect on his foot.

If, on the other hand he propels the ball as planned forward, then he performs **work** on the ball. With this work, energy is imparted to the ball system. Thus, we can say in general:

> The energy of a system can be changed with the addition or transfer of work. To put it another way, energy is stored work.

In the case of the bowling partner, the ball obtains **kinetic energy W_{Kin}** (or movement energy, see Figure 1.1(b)) in being propelled forward:

$$W_{\text{Kin}} = \frac{1}{2} \cdot m \cdot v^2 \tag{1.2}$$

with

v: velocity of the ball

A similar equation describes the electro-technics of the energy stored in a **capacitor W_{Cap}**

$$W_{\text{Cap}} = \frac{1}{2} \cdot C \cdot V^2 \tag{1.3}$$

with

C: capacity of the capacitor
V: voltage of the capacitor

If, again, there is a voltage V at an ohmic resistor R then, in the time t it will be converted into **electrical work W_{El}** (Figure 1.1(d)):

$$W_{\text{El}} = P \cdot t = \frac{V^2}{R} \cdot t \tag{1.4}$$

The power P shows what work is performed in the time t:

$$P = \frac{Work}{Time} = \frac{W}{t} \tag{1.5}$$

1.2.2 Units of Energy

Unfortunately many different units are in use to describe energy. The most important relationship is:

$$1\text{J}(\text{Joule}) = 1\,\text{Ws} = 1\,\text{Nm} = 1\,\text{kg} \cdot \text{m/s}^2 \tag{1.6}$$

Example 1.1   Lifting a sack of potatoes

If a sack of 50 kg of potatoes is lifted by 1 m then this provides it with stored energy of

$$W_{\text{Pot}} = m \cdot g \cdot h = 50\,\text{kg} \cdot 9.81\,\text{m/s}^2 \cdot 1\,\text{m} = 490.5\,\text{Nm} = 490.5\,\text{Ws} \tag{1.7}$$

∎

Table 1.1 Prefixes and prefix symbols

Prefix	Prefix symbol	Factor	Number
Kilo	k	10^3	Thousand
Mega	M	10^6	Million
Giga	G	10^9	Billion
Tera	T	10^{12}	Trillion
Peta	P	10^{15}	Quadrillion
Exa	E	10^{18}	Quintillion

In electrical engineering the unit of the kilowatt hour (kWh) is very useful and results in

$$1\,\text{kWh} = 1000\,\text{Wh} = 1000\,\text{W} \cdot 3600\,\text{s} = 3.6 \cdot 10^6\,\text{Ws} = 3.6\,\text{MWs} = 3.6\,\text{MJ} \qquad (1.8)$$

Due to the fact that in the energy industry very large quantities are often dealt with, a listing of unit prefixes into factors of 10 is useful, see Table 1.1.

1.2.3 Primary, Secondary and End Energy

Energy is typically stored in the form of energy carriers (coal, gas, wood, etc.). This form of energy is typically called **primary energy**. In order to use it for practical purposes it needs to be converted. If one wishes to generate electricity, then for instance, coal is burned in a coal-fired power station in order to generate hot steam. The pressure of the steam is again used to drive a generator that makes electrical energy available at the exit of the power station (Figure 1.2). This energy is called **secondary energy**. This process chain is associated with relatively high **conversion losses**. If the energy is transported on to a household, then further losses are incurred from the cables and transformer stations. These are added together under **distribution losses**. The **end energy** finally arrives at the end customer.

With a **petrol driven car** the oil is the primary energy carrier. It is converted to **petrol** by means of refining (secondary energy) and then brought to the petrol station. As soon as the
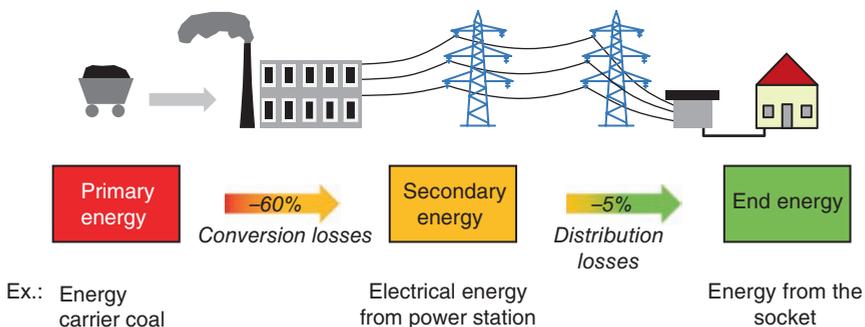
Figure 1.2 Depiction of the types of energy as an example of coal-fired power: Only about one third of the applied primary energy arrives at the socket by the end customer

petrol is in the tank it becomes end energy. This must again be differentiated from **useful energy** and in the case of the car it is the mechanical movement of the vehicle. As a car engine has an efficiency of less than 30%, only a small fraction of the applied primary energy arrives on the road. In the case of electrical energy, the useful energy would be light (lamp) or heat (stove plates).

In order that end energy is available at the socket, the conversion and distribution chain shown in Figure 1.2 must be passed through. As the efficiency of a conventional power station with approximately 40% is relatively small, the **overall degree of efficiency η_{Over}** up to the socket of the end user is:

$$\eta_{\text{Over}} = \eta_{\text{Powerstation}} \cdot \eta_{\text{Distr}} \approx 0.4 \cdot 0.95 \approx 0.38 \tag{1.9}$$

Thus we can state that:

> In the case of conventional electrical energy only about **one third** of the applied **primary energy arrives at the socket**.

And yet electrical energy is used in many fields as it is easy to transport and permits the use of applications that could hardly be realized with other forms of energy (e.g., computers, motors, etc.). At the same time, however, there are uses for which the valuable electricity should not be used. Thus, for the case of electric space heating, only a third of the applied primary energy is used whereas with modern gas energy it is more than 90%.

1.2.4 Energy Content of Various Substances

The conversion factors in Table 1.2 are presented in order to estimate the energy content of various energy carriers.

In the energy industry the unit **toe** is often used. This means **tonnes oil equivalent** and refers to the conversion factor of 1 kg crude oil in Table 1.2. Thus, 1 toe is 1000 kg · 11.63 kWh/kg = 11.630 kWh. Correspondingly there is the conversion of tons of **coal equivalent (tce)** with the factor for coal in Table 1.2.

We can remember the very approximate rule:

> 1 m^3 natural gas ≈ 1 l oil ≈ 1 l petrol ≈ 1 kg coal ≈ 2 kg wood ≈ 10 kWh

Table 1.2 Conversion factors of various energy carriers [121, Wikipedia]

Energy carrier	Energy content (kWh)	Remarks
1 kg coal	8.14	–
1 kg crude oil	11.63	Petrol 8.7 kWh/liter, Diesel: 9.8 kWh/liter
1 m^3 natural gas	8.82	
1 kg wood	4.3	(at 15% moisture)
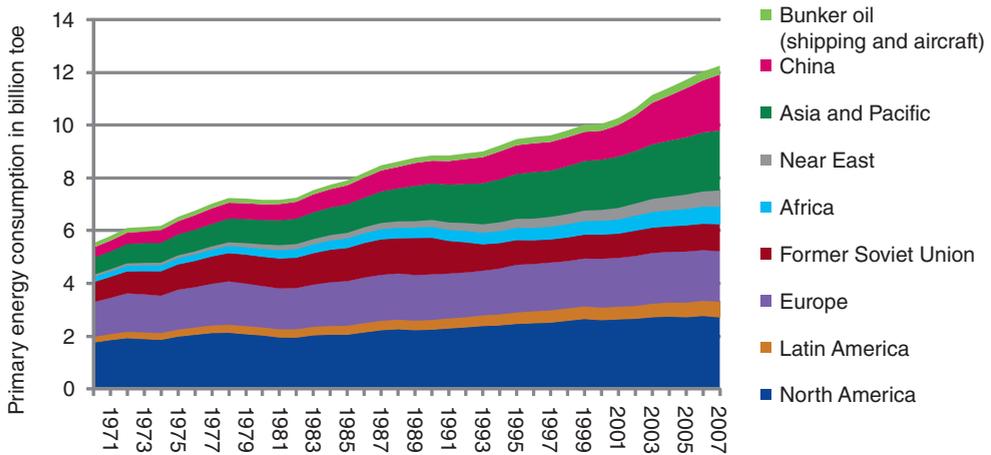
Figure 1.3 Development of worldwide primary energy requirements since 1971 [3]

1.3 Problems with Today's Energy Supply

The present worldwide energy supply is associated with a series of problems; the most important aspects will be presented in the following.

1.3.1 Growing Energy Requirements

Figure 1.3 shows the development of worldwide primary energy usage in the last 40 years. From 1971–2008 this more than doubled, the average annual growth being 2.2%. While at first, mainly Western industrial countries made up the greatest part, emerging countries, especially China, caught up rapidly.

One reason for the growth in energy requirements is the **growth of the world population**. This has almost doubled in the past 40 years from 3.7 billion to the present 7 billion people. By the year 2030 a further rise to more than 8 billion people is expected [2].

The second cause for this development is the **rising standards of living**. Thus, the requirement of **primary energy in Germany** is approximately **45 000 kWh/head**; in a weak industrialized country such as Bangladesh, on the other hand, it is only 1500 kWh/head. With growing standards of living in developing countries, the per-head consumption will increase substantially. In China, as a very dynamic emerging nation it is above 16 000 kWh/head [3]. The International Energy Agency (IEA) assumes that China will increase its energy requirement in the next 25 years by 75% and India by even 100% [4].

The growing energy requirement would not be so grave if this did not cause a series of problems:

1. Tightening of resources
2. Climate change
3. Hazards/disposals

These will now be looked at in more detail.
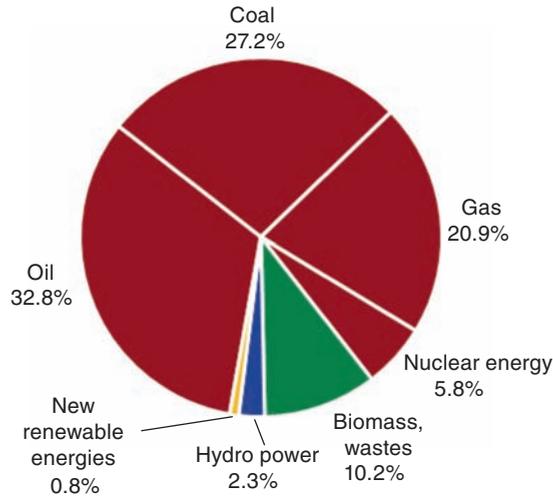
Figure 1.4 Distribution of worldwide primary energy consumption in 2008 according to energy carriers [4]

1.3.2 Tightening of Resources

The worldwide requirement for energy is covered today mainly by the **fossil fuels**: oil, natural gas and coal. From Figure 1.4, it can be seen that they make up a portion of more than 80%, whilst biomass, hydro and renewable energies (wind, photovoltaics, solar heat, etc.) up to now have only reached 10%.

Meanwhile, the strong usage of fossil sources has led to scarcity. Table 1.3 shows the individual extraction quantities in the years 2001 and 2008. Already, in 2001 the **estimated reserves of oil** were estimated to last 43 years and **natural gas** 64 years. Only coal reserves were estimated to last for a relatively long period of 215 years. By 2008 more oil reserves were found but by then the annual consumption had increased substantially. Thus the reserves have reduced from 140 to 41 years.

If one assumes that the world energy consumption continues to grow as previously, then reserves will be reduced drastically in **30–65 years** (see also Exercise 1.3). The scarcity of fuels will lead to **strongly rising prices and distribution wars**.

In the past a start has also been made with the extraction of oil from oil sands and oil shales. This has been carried out particularly in Canada and the USA. However, much engineering

Table 1.3 Extraction and reserves of fossil fuels [5]

	Oil		Nat. gas		Coal	
	2001	2008	2001	2008	2001	2008
Extraction EJ/a	147	163	80	121	91	151
Reserves EJ	6,351	6,682	5,105	7,136	19,620	21,127
Lasting for	43 a	41 a	64 a	59 a	215 a	140 a
Lasting with annual growth of 2.2%		**30 a**		**38 a**		**65 a**

effort is required for the generation of synthetic oil. Extraction in open cast mining leads to the destruction of previously intact ecosystems. Therefore the use of these additional fossil sources is no real future option.

1.3.3 Climate Change

The decomposition of biomasses (wood, plants, etc.) causes **carbon dioxide (CO$_2$)** to be released into the atmosphere. At the same time plants grow due to photosynthesis and take up CO$_2$ from the air. In the course of the history of the Earth this has equalized itself and has led to a relatively constant CO$_2$ concentration in the atmosphere.

CO$_2$ is also created when wood, coal, natural gas or oil are burned and is released into the atmosphere. In the case of wood this is not tragic as long as felled trees are replanted. The newly growing wood binds CO$_2$ from the air and uses it for building up the existing biomasses.

In the case of energy carriers, however, this looks different. These were formed millions of years ago from biomass and have been burned up in one to two centuries. Figure 1.5 shows the course of CO$_2$ concentrations in the atmosphere in the last 20 000 years.

Apparently, in earlier times there were already fluctuations in these concentrations but really **disturbing** is the **steep rise since the start of industrialization**. In the year **2012** the concentration was approximately **400 ppm** (parts per million); a value that has not been reached for millions of years.

Why is the CO$_2$ concentration in the atmosphere so important for us? The reason is that CO$_2$, besides the other trace gases (e.g., methane, CH$_4$) affects the temperature of the Earth through the **greenhouse effect**. For clarity, consider Figure 1.6. The light from the **Sun** (visible and infrared radiation ①) arrives almost unhindered through the atmosphere and is absorbed by the ground ②. This causes the surface ③ to be warmed and emits heat radiation as a so-called **black body source** (see Chapter 2) ④. This radiation is again absorbed by the trace gases ⑤ and released to the environment as heat ⑥. The **heat energy** thus **remains** in the **atmosphere** to a large extent and only a small amount is returned back in to Space.
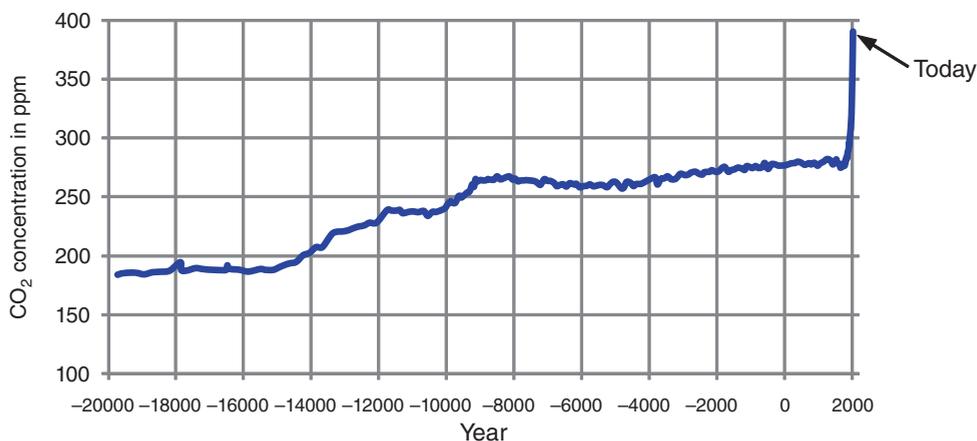
Figure 1.5 Development of the CO$_2$ content in the atmosphere in the last 22 000 years: noticeable is the steep rise since the start of industrialization [6,7,137]
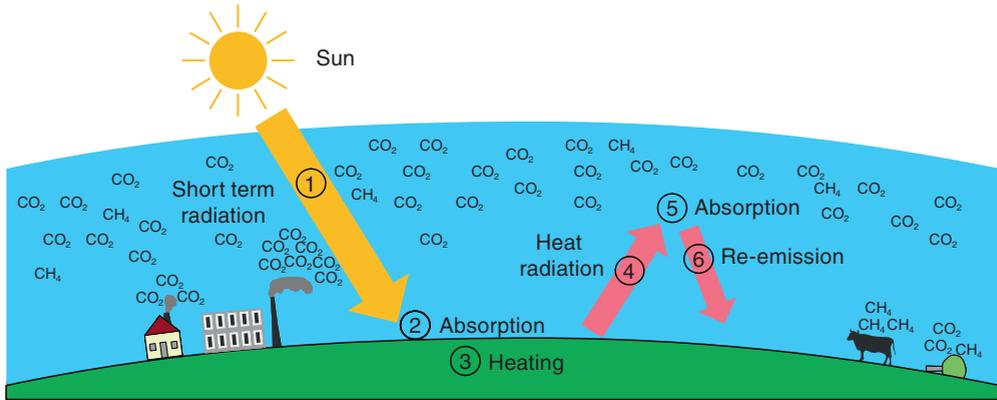
Figure 1.6   Depiction in principle of the greenhouse effect: the heat radiation reflected from the ground is held back by the greenhouse gases

The comparison to a greenhouse is thus fitting: the atmosphere with trace gases acts as the glass of a greenhouse that allows the Sun's rays to pass into the greenhouse but holds back the internally resulting heat radiation. The result is a heating up of the greenhouse.

Now we should be happy that this greenhouse effect even exists. **Without** it, the temperature on the earth would be $-18\,°C$ but because of the **natural greenhouse effect** the actual average temperature is approximately $15\,°C$. However, the additional emissions of CO_2, methane, and so on, caused by people as an **anthropogenic greenhouse effect**, leads to additional heating. Since the start of industrialization this **temperature rise** has been approximately $0.74\,°C$; it is expected in future this rise will accelerate by $0.2\,°C$ per decade [8].

The results of the temperature increase can already be seen in the **reduction of glaciers** and melting of the ice in the North Polar Sea. Besides this, **extreme weather phenomena** (hurricanes, drought periods in some regions) are connected to the rise in temperatures. In the long term further rises in temperatures are expected with a significant **rise** in **water levels** and **displacement of weather zones**.

In order to slow down the climate change, the **Kyoto agreement** was promulgated in 1997 at the World Climate Conference in the Japanese city of Kyoto. There the industrial countries obligated themselves to lower their greenhouse emissions by 5.5% below the 1990 level by 2012. The declared aim was the limitation of the rise of temperature caused by people by $2\,°C$. Of its own will, Germany obligated itself to reduce emissions by 21%. After Germany had achieved its aim, in the year 2010 the Federal Government decided on a **reduction of 40% by 2020** (compared to 1990). Important elements to achieving this goal, besides the increase in **energy efficiency**, are the extensions of renewable energies. After the catastrophe in Fukushima it was also decided to **completely** change over to **renewable energies by 2050**.

1.3.4 Hazards and Disposal

An almost CO_2-free generation of electricity is presented by nuclear energy. However, it is associated with a number of other problems. The reactor catastrophe in Fukushima in 2011 showed that the risk of a **super catastrophe** (largest expected accident) can never be fully

excluded. Even when no tsunami is expected in Germany there is still a great danger as the nuclear power stations here are only **insufficiently protected against terrorist attack**.

Added to this is the **unsolved problem** of final storage of radioactive waste. At present there is no final **storage for highly radioactive waste in the world**. This must be safely stored for thousands of years. There is also the question as to whether it is **ethically correct** to saddle future generations with such a burdensome legacy.

Here, too the **availability** should be taken into account. The known reserves of uranium including estimated stores are approximately 4.6 million tons. Included in these are the ones with relatively poor concentrations of uranium that are difficult to extract. If we accept the current annual requirements of 68 000 t/a as a basis, then the stocks will last for 67 years [9]. Assuming the increase of energy from Table 1.3, then the **reserves** will last for approximately **40 years**. If the whole of today's energy requirement were changed over to nuclear energy, then the stocks of uranium would last for just **4 years**.

1.4 Renewable Energies

1.4.1 The Family of Renewable Energies

Before we turn to photovoltaics in more detail we should allocate them into the family of renewable energies. The term **renewable** (or **regenerative**) means that the supply of energy is not used up. The wind blows every year again and again, the Sun rises every day and plants grow again after the harvest. In the case of geothermic energy, the Earth is cooling off but this will only be noticeable thousands of years in the future.

As Figure 1.7 shows, the actual **primary energies** of the renewable energies are the **movements of the planets**, the **heat of the Earth** and **solar radiation**. Whereas movements of
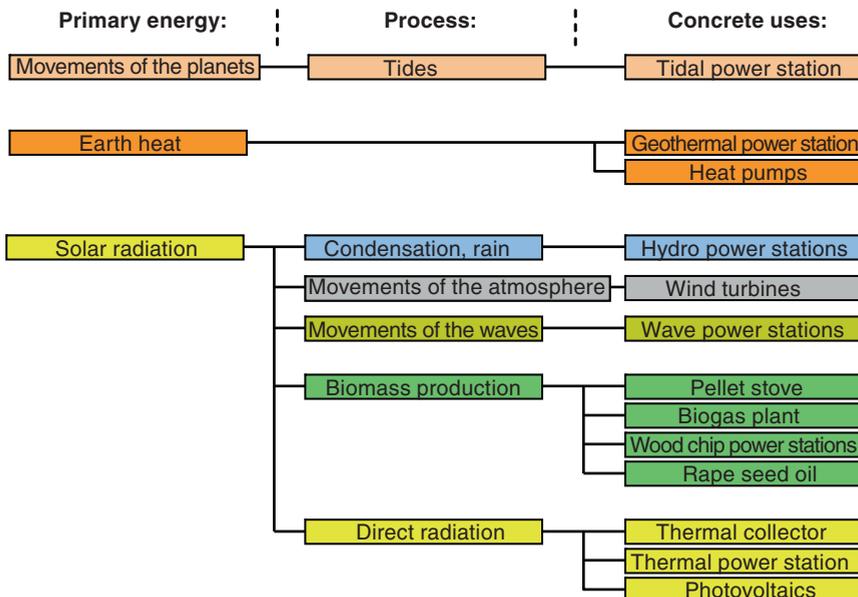
Figure 1.7   Various possibilities for the use of renewable energies

the planets are used only in the somewhat exotic tidal power plants, the heating of the Earth as well as the heating of buildings can be achieved with the aid of a heat pump as well as for generating electrical energy in a geothermal power station.

Solar radiation is the basis for a surprising range of energies. Thus, the use of **hydro power** is only possible by the **condensation of water** and subsequent precipitation onto land. **Atmospheric movement** originates mostly due to solar radiation, which is also the basis for the **use of wind power**. In the case of biomass products it is again sunlight that causes **photosynthesis**, and thus the growth of biomass is conditioned by it.

Solar radiation can also be used directly for the generation of heat, for instance in a **thermal collector** for domestic water or domestic space heating. **Thermal solar power stations** generate process heat from concentrated sunlight in order to drive generators for production of electricity. Last but not least, with **photovoltaics**, solar radiation is directly converted into electrical energy.

Thus we can consider **photovoltaics** as the **young daughter of the large family** of renewable energies. However, they have a very special attraction: they are the only one able to convert sunlight directly into electrical energy without complicated intermediate processes and without using mechanical converters that can wear out.

1.4.2 Advantages and Disadvantages of Renewable Energies

Renewable energies have certain common characteristics. Their greatest advantage is that in contrast to all other energy carriers they are **practically inexhaustible**. Added to this they are almost **free of any emissions** and with only **few environment effects** and **hazards**.

A further important advantage is in the fact that there are practically **no fuel costs**. The Sun shines for free, the wind blows irrespectively and the heat of the Earth is an almost inexhaustible reservoir. On the other hand, the **energy densities** in which the renewable energies are available **are small**. Large areas are needed (solar module area for photovoltaics, rotor area for wind turbines, etc.) in order to "collect" sufficient energy. This means that typically **large investment costs** are incurred as the large surfaces require the **use of a lot of material**.

A further large disadvantage is the **varying energy supply**. **Photovoltaics** and **wind power** are especially affected by this. As a result, further power stations **(backup power stations)** must be kept on reserve in order to ensure a constant supply. **Geothermal power** is not affected by this; it can provide energy practically **independently of time of day or year**. A special case is **biomass** which is the only renewable energy that is **easy to store** (branches in the woods, biogas in the tank, etc.).

In many **developing countries** there is no power grid. There, a further advantage of renewable energies can be used: their **decentralized availability and utility**. Thus autarchic village power supplies can be installed far from large towns without an overland grid being necessary.

1.5 Photovoltaic – The Most Important in Brief

In the following chapters we will work through some fundamentals in which some may perhaps question their necessity. For this reason, in order to increase motivation and for the sake of clarity, we will briefly consider the most important aspects of photovoltaics.

1.5.1 What Does "Photovoltaic" Mean?

The **term photovoltaic** is a combination of the Greek word *phós*, *phōtós* (light, of the light) and the name of the Italian physicist Alessandro Volta (1745–1825). He discovered the first functional electro-chemical battery and the unit of electricity, **Volt**, is named after him. Thus, a translation of the word photovoltaic could be **light battery** or also **light source**. More generally we understand the word **photovoltaics** as the direct conversion of sunlight into electric energy.

1.5.2 What are Solar Cells and Solar Modules?

The basic component of every photovoltaic plant is the solar cell (see Figure 1.8). This consists in most cases of **silicon**, a semiconductor that is also used for diodes, transistors and computer chips. With the introduction of foreign atoms **(doping)** a **p-n junction** is generated in the cell that "installs" an **electrical field** in the crystal. If light falls on the solar cell then charge carriers are dissolved out of the crystal bindings and moved by the electrical field to the outer contacts. The result at the contacts of the solar cells is the creation of a **voltage of** approximately **0.5 V**. The released **current** varies depending on radiation and cell area, and lies between **0 and 10 A**.

In order to achieve a usable voltage in the region of 20–50 V, many cells are switched together in series in a **solar module** (Figure 1.8). Besides this, the solar cells in the modules are mechanically protected and sealed against environmental influences (e.g., entrance of moisture).
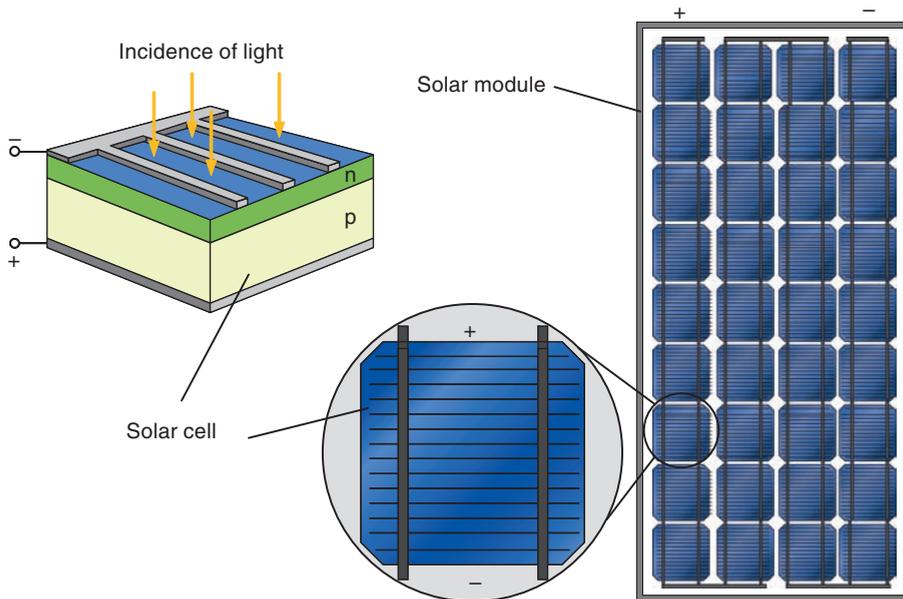
Figure 1.8 The solar cell and solar module as basic components of photovoltaics
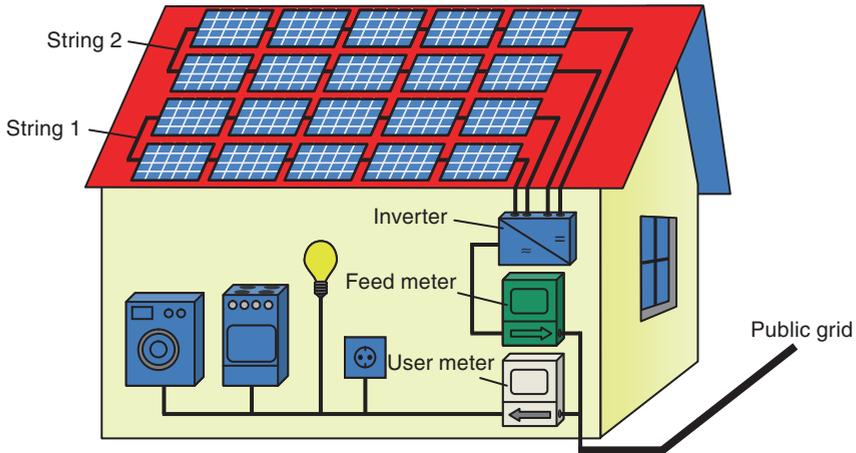
Figure 1.9 Structure of a grid-coupled photovoltaic plant. An inverter converts the direct current supplied by the solar modules into alternating current and feeds it into the public grid

1.5.3 How is a Typical Photovoltaic Plant Structured?

Figure 1.9 shows the structure of a grid-coupled plant typical for Germany. Several solar modules are switched in series into a **string** and connected to an **inverter**. The inverter converts the direct current delivered by the modules into alternating current and feeds it into the public grid. A **feed meter** measures the generated electricity in order to collect payment for the energy generated. The **user meter** counts the current consumption of the household separately.

The plant is financed on the basis of the **Renewable Energy Law (EEG)**. This guarantees that the fed-in **electric energy** is **paid** for by the energy supply company for **20 years** at a guaranteed price. To a certain extent, the owner of the plant becomes a power station operator.

1.5.4 What Does a Photovoltaic Plant "Bring?"

For the owner of a solar power plant the power of his plant is of interest and so is the quantity of energy fed into the grid during the course of a year.

The power of a solar module is measured according to the **Standard-Test-Conditions (STC)** and defined by three limiting conditions:

1. Full Sun radiation (radiation strength $E = E_{STC} = 1000\,\text{W/m}^2$)
2. Temperature of the solar module: $\vartheta_{\text{Module}} = 25\,°\text{C}$
3. Standard light spectrum AM 1.5 (for more details see Chapter 2)

The capacity of the solar module under these conditions is the **rated power** (or **nominal power**) **of the module**. It is given in **Watt-Peak (Wp)** as it actually describes the peak power of the module under optimal conditions.

The **degree of efficiency** η_{Module} of a solar module is the relationship of delivered electric rated power P_{STC} referenced to incidental **optical power** P_{Opt}:

$$\eta_{\text{Module}} = \frac{P_{\text{STC}}}{P_{\text{Opt}}} = \frac{P_{\text{STC}}}{E_{\text{STC}} \cdot A} \tag{1.10}$$

with

A: module surface

The **efficiency** of **silicon solar modules** is in the range of **13–20%**. Besides silicon there are also **other materials** such as cadmium telluride or copper-indium-selenide, which go under the name of **thin film technologies**. These reach module efficiencies of 7–13%.

Example 1.2   Power and yield of a roof plant

Assume that the house owner has a roof area of $40\,\text{m}^2$ available. He buys modules with an efficiency of 15%. The rated power of the plant is:

$$P_{\text{STC}} = P_{\text{Opt}} \cdot \eta_{\text{Module}} = E_{\text{STC}} \cdot A \cdot \eta_{\text{Module}} = 1000\,\frac{\text{W}}{\text{m}^2} \cdot 40\,\text{m}^2 \cdot 0.15 = 6\,\text{kWp}$$

In Germany with a South facing rooftop plant the result is typically a **specific yield w_{Year} of approximately 900 kWh/kWp** (kilowatt hours per kilowatt peak) per year. This brings our house owner the following annual yield W_{year}:

$$W_{\text{Year}} = P_{\text{STC}} \cdot w_{\text{Year}} = 6\,\text{kWp} \cdot 900\,\frac{\text{kWh}}{\text{kWp} \cdot \text{a}} = 5400\,\text{kWh/a}$$

In comparison to the **typical electric power consumption of a household** of **3000–4000 kWh per year** the energy quantity is not bad.

■

After this quick course on the subject of photovoltaics we will now consider the quite recent history of solar power generation.

1.6   History of Photovoltaics

1.6.1   How it all Began

In the year **1839** the French scientist **Alexandre Edmond Becquerel** (the father of Antoine Henri Becquerel, after whom the unit of the activity of radioactive material is named) discovered the **photo-electric effect** while carrying out electro-chemical experiments. He placed two coated platinum electrodes in a container with an electrolyte and determined the current flowing between them (see Figure 1.10(a)) . Becquerel found that the strength of the current changed when exposed to light [10]. In this case it was a matter of the outside photo-effect in which electrons move out of a fixed body when exposed to light.

In **1873** the British engineer **Willoughby Smith** and his assistant **Joseph May** discovered that the semiconductor selenium changed its resistance when exposed to light. They thus saw
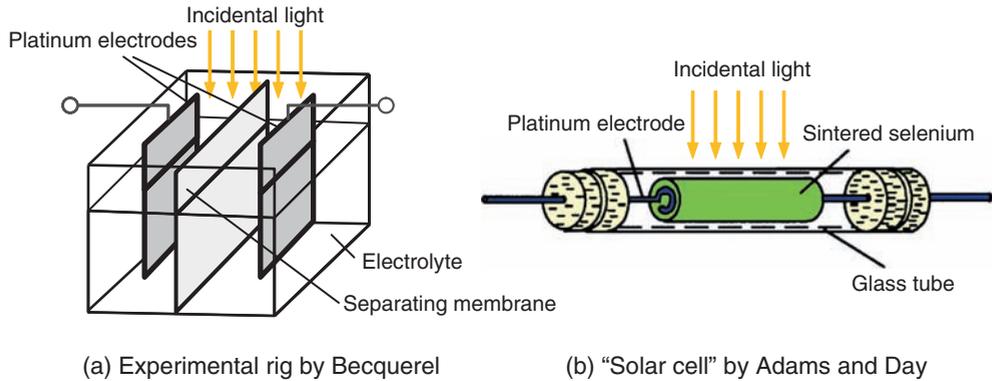
Figure 1.10   The beginnings of photovoltaics: Electrochemical experiment of A.E. Becquerel and the first solar cell by Adams and Day [16,17]

for the first time the internal photo-effect relevant for photovoltaics in which electrons in the semiconductor are torn from their bindings by light and are thus available as free charge carriers in the solid-state body.

Three years later the Englishmen **William Adams** and **Richard Day** found out that a **selenium rod** provided with platinum electrodes can **produce electrical energy** when it is exposed to light (see Figure 1.10(b)) With this it was proven for the first time that a solid body can directly convert light energy into electrical energy.

In 1883 the New York inventor Charles Fritts built a small "**Module**" of selenium cells with a surface area of approximately $30\,cm^2$ that had an **efficiency of almost 1%**. For this purpose he coated the selenium cells with a very thin electrode of gold. He sent a module to **Werner von Siemens** (German inventor and entrepreneur, 1816–1892) for assessment. Siemens recognized the importance of the discovery and declared to the Royal Academy of Prussia that with this "The direct conversion of light into electricity has been shown for the first time." [11]. As a result Siemens developed a lighting measuring instrument based on selenium.

In the following years the physical background of the photo-effect became better explained. In part this was particularly due to **Albert Einstein** (1879–1955) who presented his **light quantum theory** in 1905, for which he was awarded the Nobel Prize 16 years later. At the same time there were technological advances: in 1916 the Polish chemist **Jan Czochralski** at the AEG Company discovered the **crystal growth process** named after him. With the Czochralski process it became possible to produce semiconductor crystals as single crystals of high quality.

1.6.2   The First Real Solar Cells

In 1950, the co-inventor of the transistor, the American Nobel laureate **William B. Shockley** (1910–1989) presented an explanation of the method of **functioning of the p-n junction** and thus laid the theoretical foundations of the solar cells used today. On this basis, **Daryl Chapin**, **Calvin Fuller and Gerald Pearson** in the Bell Labs developed the **first silicon solar cell** with an area of $2\,cm^2$ and an **efficiency of up to 6%** and presented it to the public on **25 April 1954** (Figure 1.11) [12]. The *New York Times* published this on its front page the next day and promised its readers "The fulfilment of one of the greatest desires of mankind – the use of the almost limitless energy of the sun."
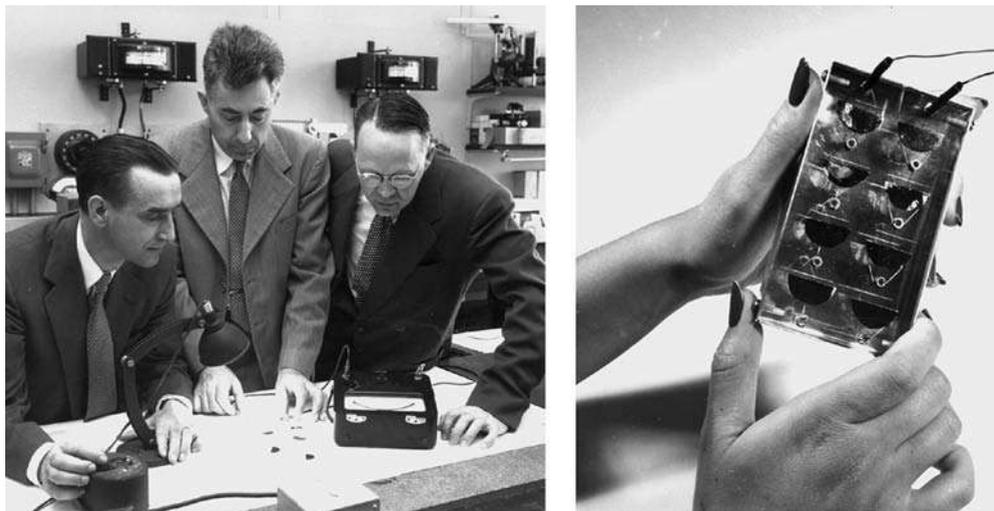
Figure 1.11   The inventors of the first "real" solar cell: Chapin, Fuller and Pearson. The right hand figure shows the first "solar module" in the world, a mini module of 8 solar cells (Courtesy of AT&T Archives and History Center)

The Bell cell **combined** for the first time the concept of the **p-n junction with the internal photo effect**. In this, the p-n junction serves as conveyor that removes the released electrons. Thus this effect can be more accurately described as the **depletion layer photo-effect** or also as the *photovoltaic effect*.

In the following years the efficiency was raised to 10%. Because of the high prices of the solar modules (the price per Watt was around 1000 times more than today's price) they were only used for special applications. On the March 17, 1958 the first **satellite with solar cells** on board was launched: the American satellite **Vanguard 1** with two transmitters on board (Figure 1.12). Transmitter 1 was operated by mercury batteries and ceased operation after 20 days. Transmitter No 2 drew its energy from six solar cells attached to the outer skin of the satellite and operated till 1964.

Figure 1.12   View of the *Vanguard I* satellite: Because of the diameter of 16 cm it was also called "Grapefruit" (photo: NASA)
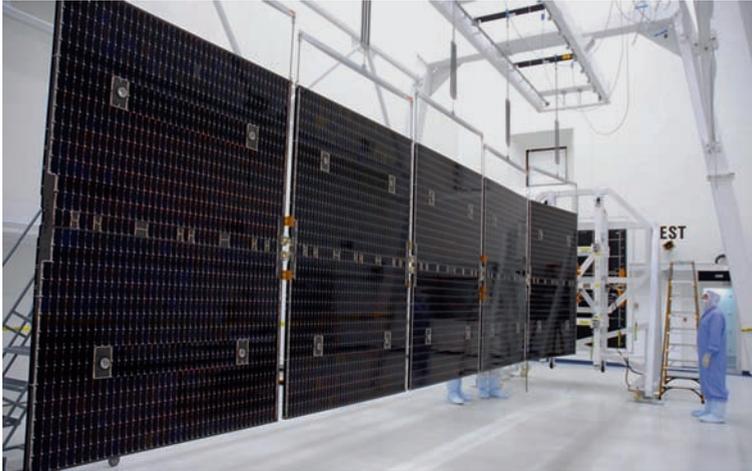
Figure 1.13   Modern solar array of the space probe *Dawn* with a power of 5 kW (photo: NASA)

The success of this project led to **photovoltaics** being used as the **energy source for satellites**. The developments in the 1960s were thus advanced by space flight. Besides the silicon cells the first solar cells of gallium arsenide (GaAs) and other alternative materials were presented.

As a comparison to **Vanguard I**, the Figure 1.13 shows one of the two solar arrays of the 2007 **spacecraft Dawn**. The probe is meant to reach the dwarf planet Ceres in February 2015. The array of 5 kW power is built up of high capacity three-layer stacked cells of InGaP/InGaAs/ Ge (see Chapter 5) that achieve an **efficiency of 27.5%** in space [13].

1.6.3   From Space to Earth

The terrestrial use of photovoltaics limited itself first to applications in which the nearest electrical grid was very far away: transmitter stations, signal systems, remote mountain huts, and so on (Figure 1.14). However, a change in thinking was brought about with the oil crisis in 1973. Suddenly alternative sources of energy became the center of interest. In 1977 in the Sandia Laboratories in New Mexico, a **solar module** was developed with the aim of producing a standard product for **economical mass production**.

The accident in the nuclear power plant in Harrisburg (1979) and especially the reactor catastrophe in **Tschernobyl** (1986) increased the pressure on governments to find new solutions in energy supply.

1.6.4   From Toy to Energy Source

From the end of the 1980s research in the field of photovoltaics intensified especially in the USA, Japan and Germany. In addition, research programs were started in the construction of grid-coupled photovoltaic plants that could be installed on single-family homes. In Germany this was first the **1000-roof program** of 1990–1995 that provided valuable knowledge on the reliability of modules and inverters as well as on questions of grid-feeding [14].
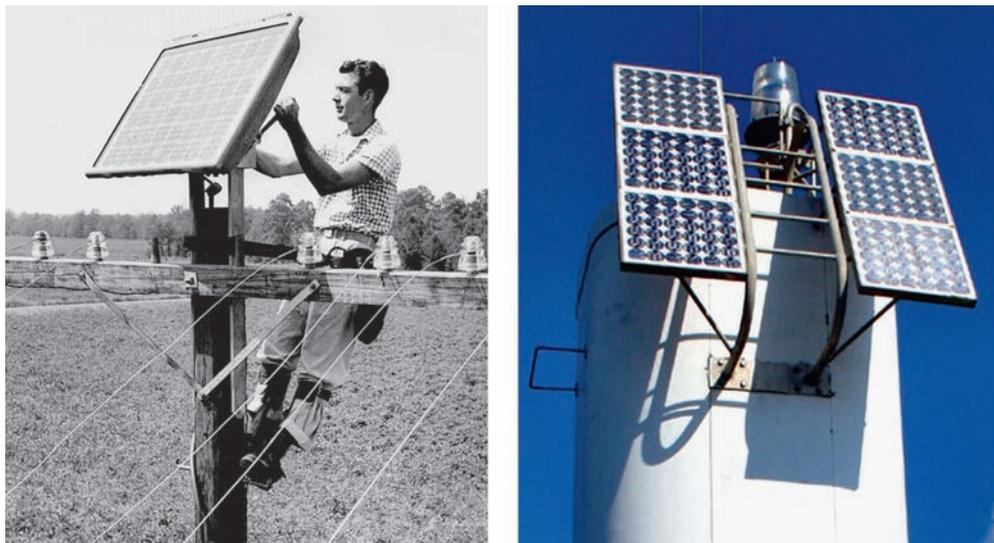
Figure 1.14 Examples of photovoltaic island plants: Telephone booster of 1955 with the legendary Bell Solar Battery and modern solar-driven lighting tower in Australia (photos: Courtesy of AT&T Archives and History Center, Erika Johnson)

The **Energy Feed-in Law** of 1991 obligated energy suppliers to accept power from small renewable power stations (wind, photovoltaics, etc.). Whereas the wind industry developed in a storm of activity, the subsidy of 17 Pfennigs per kWh was not nearly enough for an economical operation of photovoltaic plants. For this reason, environmentalists demanded a higher subsidy for solar power. A key role in this was played by the **Aachen Association for the Promotion of Solar Power (SFV)**. This association achieved that in 1995 the **cost-covering subsidy** at a rate of 2 DM per kWh for power from photovoltaic was introduced, which throughout the Federal Republic became known as the **Aachen Model**.

The 2000 promulgated **Renewable Energy Law** was introduced on the basis of this model. This successor law of the Energy Feed Law defined cost-covering subsidies for various renewable energy sources and led to an unexpected boom in photovoltaics (see Figure 1.15).

Figure 1.15 shows the photovoltaic capacities installed in the various countries over the years. In Germany the total installed photovoltaic capacity increased from 76 MWp in 2000 to approximately 32 GWp in 2012. Thus, up to now, around a third of all worldwide produced modules have been installed in Germany. In second place is Italy with a PV capacity of 16 GWp, which, as in Germany, has been achieved by energy subsidies for solar energy. The USA has installed more than 3 GWp in 2012 resulting in a total installed power of 7.2 GWp. Just behind is Japan with 7 GWp which enforced its PV program after the catastrophe in Fukushima. Spain had relatively high feed-in tariffs some years ago, that led to a short PV boom. This was suddenly stopped by cutting the subsidies; therefore the total installed power of 5 GWp has remained almost the same in the past years. The strongest growth is shown by China, which increased its installed PV capacity in a single year from 3.3 to 7 GWp.

All the other countries not shown individually in Figure 1.15 (Rest of World – ROW) have a total PV capacity of 15 GWp.
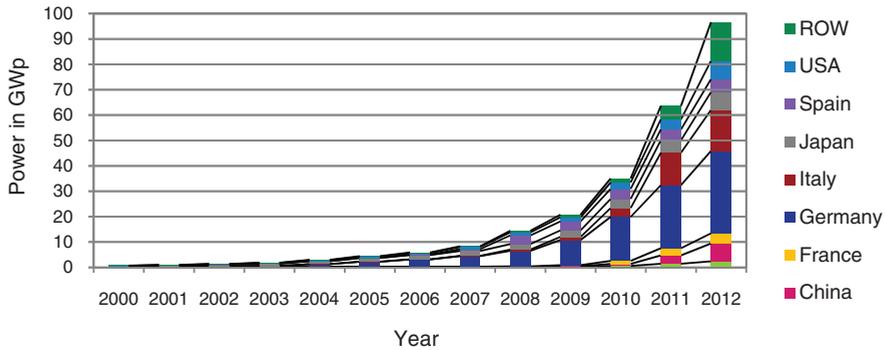
Figure 1.15 Development of the world-wide photovoltaic market (cumulative installed capacity) [15]

Independently of the view of the individual countries, Figure 1.15 emphasizes the **fast growth of photovoltaics in the past years**. The annual installed PV capacity has grown from 217 MWp in 2000 to 25 GWp in 2012, which corresponds to an average annual growth of about 48%!

The possible future development in photovoltaics and its contribution to electric energy consumption is dealt with in Chapter 10.

2

Solar Radiation

The basis of all life on Earth is the radiation from the Sun. The utilization of photovoltaics also depends on the availability of sunlight. For this reason we will devote this chapter to the characteristics and possibilities of solar radiation.

2.1 Properties of Solar Radiation

2.1.1 Solar Constant

The Sun represents a gigantic fusion reactor in whose inside each four hydrogen atoms are melted into one helium atom. In this atomic fusion temperatures of around 15 million degrees Celsius are created. The energy freed is released into Space in the form of radiation.

Figure 2.1 shows the Sun–Earth system more or less to scale. The distance between the two space bodies is approximately 150 million km and other dimensions can be taken from Table 2.1.

The Sun continuously radiates an amount of $P_{\mathrm{Sun}} = 3.845 \cdot 10^{26}$ W in all directions of which the Earth only receives a small fraction.

In order to calculate this value, we assume there is a sphere around the Sun that has a radius of $r = r_{\mathrm{SE}}$. At this distance the amount of radiation from the Sun has already spread over the whole area of the sphere. Thus at the position of the Earth we get the following power density or **irradiance**.

$$Es = \frac{\text{Radiation power}}{\text{Area of sphere}} = \frac{P_{\mathrm{Sun}}}{4 \cdot \pi \cdot r_{\mathrm{SE}}^2} = \frac{3.845 \cdot 10^{26}\,\mathrm{W}}{4 \cdot \pi \cdot (1.496 \cdot 10^{11}\,\mathrm{m})^2} = 1367\ \mathrm{W/m^2} \qquad (2.1)$$

The result of 1367 W/m^2 is called the **solar constant**.

The solar constant is 1367 W/m^2. It denotes the irradiance outside the Earth's atmosphere.

Table 2.1 Characteristics of the Sun and the Earth

Properties	Sun	Earth
Diameter	$d_{Sun} = 1\,392\,520\,km$	$d_{Earth} = 12\,756\,km$
Surface temperature	$T_{Sun} = 5778\,K$	$T_{Earth} = 288\,K$
Temperature at center	$15\,000\,000\,K$	$6700\,K$
Radiated power	$P_{Sun} = 3.845 \cdot 10^{26}\,W$	–
Distance Sun–Earth	$r_{SE} = 149.6$ Mio. km	
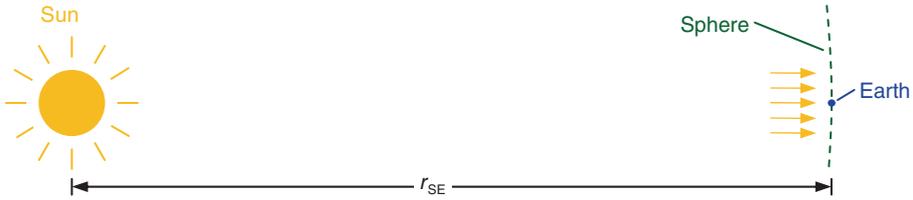
Figure 2.1 Determination of the solar constants

2.1.2 Spectrum of the Sun

Every hot body gives off radiation to its surroundings. According to **Planck's Law of Radiation** the surface temperature determines the spectrum of the radiation. In the case of the Sun the surface temperature is 5778 K, which leads to the idealized **Black Body Spectrum** shown in Figure 2.2 (dashed line). The actual spectrum measured outside the Earth's atmosphere (AM 0) approximately follows this idealized line. The term AM 0 stands for **Air Mass 0** and means that this light has not passed through the atmosphere. If the individual
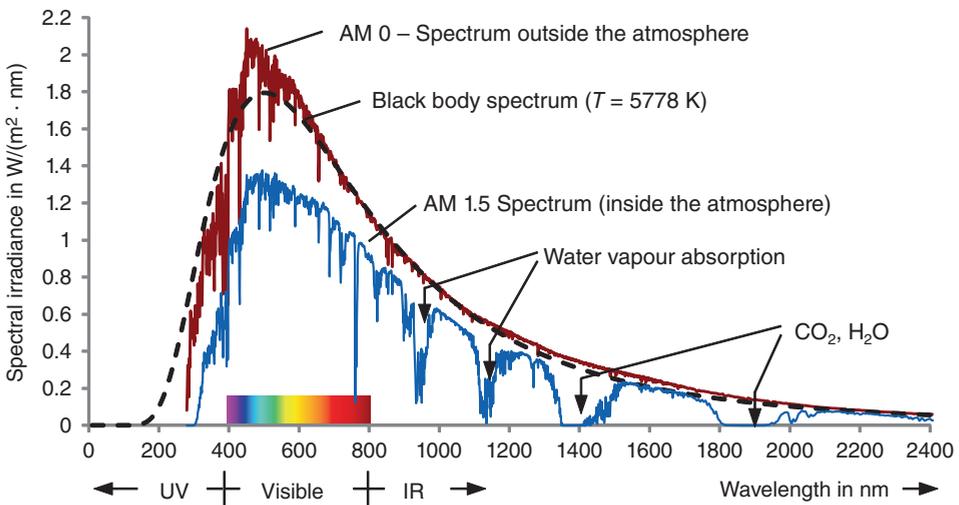
Figure 2.2 Spectrum outside and inside the atmosphere

amounts of this spectrum are added together in Figure 2.2, then the result is an irradiance of 1367 W/m^2, which is the already-mentioned solar constant.

However, the spectrum changes when sunlight passes through the atmosphere. There are various reasons for this:

1. *Reflection of light*:
   Sunlight is reflected in the atmosphere and this reduces the radiation reaching the Earth.
2. *Absorption of light*:
   Molecules (O_2, O_3, H_2O, CO_2 . . .) are excited at certain wavelengths and absorb a part of the radiation causing "gaps" in the spectrum especially in the infrared region (see, for instance, Figure 2.2 at $\lambda = 1400$ nm).
3. *Rayleigh scattering*:
   If light falls on particles that are smaller than the wavelength, then **Raleigh scattering** occurs. This is strongly dependent on wavelength ($\sim 1/\lambda^4$) so shorter wavelengths are scattered particularly strongly.
4. *Scattering of aerosols and dust particles*:
   This concerns particles that are large compared to the wavelength of light. In this case one speaks of **Mie scattering**. The strength of Mie scattering depends greatly on the location; it is greatest in industrial and densely populated areas.

2.1.3 Air Mass

As we have seen, the spectrum changes when passing through the atmosphere. The effect is greater, the longer the path of the light. For this reason one designates the different spectra according to the path of the rays through the atmosphere. Figure 2.3 shows the principle: the term AM 1.5 means for example that the light has travelled 1.5 times the distance in comparison to the vertical path through the atmosphere.

At a known **Sun height angle** γ_S of the Sun, the AM value x gives:

$$x = \frac{1}{\sin \gamma_S} \tag{2.2}$$

The Sun has different heights depending on the time of day and year. Figure 2.3 shows on which days in Münster in Germany the respective AM values are reached (always a noon Sun position).
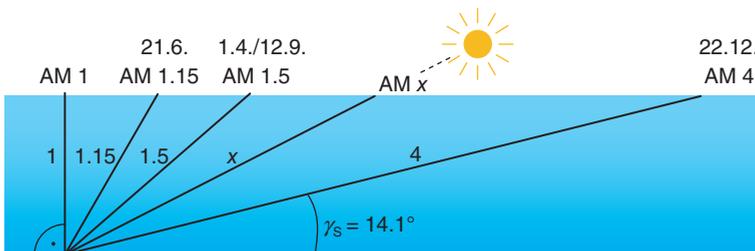
Figure 2.3 Explanation of the term *Air Mass*: The number x represents the extension of the path compared to the vertical distance through the atmosphere [138]

The **standard spectrum** for measuring solar modules has established itself at the **AM 1.5 spectrum** as it arrives in spring and autumn and can be viewed as an **average year's spectrum**.

2.2 Global Radiation

2.2.1 Origin of Global Radiation

The various effects such as scattering and absorption cause a weakening of the AM 0 spectrum from Space. In the summation of the AM 1.5 spectrum in Figure 2.2 we receive only 835 W/m^2. Thus, of the originally available 1367 W/m^2, the Earth receives just 61% as so-called **direct radiation**. However, due to the scattering of light in the atmosphere there exists a further portion: the **diffuse radiation** (see Figure 2.4).

Weak radiation portions arrive from all directions of the sky and are added to diffuse radiation. The sum of both types of radiation is called **global radiation**.

$$E_G = E_{Direct} + E_{Diffuse} \tag{2.3}$$

On a nice, clear summer's day it is possible to measure on a surface vertical to the radiation of the Sun a global radiation value of $E_G = E_{STC} = 1000$ W/m^2. This is the reason why, in the definition of the **standard test conditions for solar modules** (see Section 1.5), one uses an **enhanced AM 1.5 spectrum** by the factor $1000/835 = 1.198$. This, then, has a total irradiance of exactly $E_{STC} = 1000$ W/m^2 and is thus suitable for determining the peak power of a solar module.

In reality, why don't radiation strengths higher than 1000 W/m^2 occur?

In individual cases higher global radiation can occur. This is mostly the case in mountainous regions such as the Alps. Besides the reduced atmospheric density, reflection from snow and ice can occur. However, one also sometimes measures
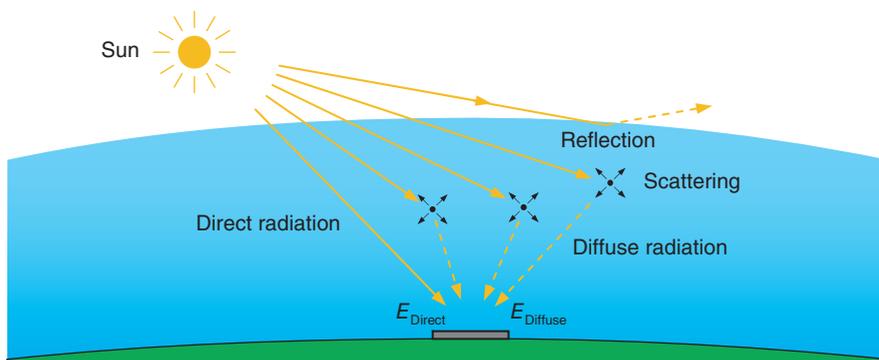
Figure 2.4 Origin of global radiation: It is the sum of the direct and diffuse radiation

radiation values up to $1300\,\mathrm{W/m^2}$ in the flat country. This occurs in sunny weather and bright light clouds around the Sun that increase the diffuse portion. This effect is called **cloud enhancement**.

2.2.2 Contributions of Diffuse and Direct Radiation

The contribution of diffuse radiation to the global radiation is often underrated. In Germany, when viewed over the whole year, the diffuse radiation makes a greater contribution than direct radiation. For proof of this see Table 2.2. This shows the **average monthly radiation H** (irradiated energy) on a flat surface at various places.

In **Hamburg** the average diffuse radiation H_{Diffuse} is $1.52\,\mathrm{kWh/(m^2\cdot d)}$ against a H_{Direct} of $1.08\,\mathrm{kWh/(m^2\cdot d)}$. Thus, the **diffuse radiation contributes almost 60% to the yearly global radiation**. In **Munich** the position is somewhat changed. The diffuse radiation here **only contributes 54%**.

Thus, to summarize:

In Germany, diffuse radiation makes a slightly higher contribution to global radiation than direct radiation.

In places south of Germany, the position is different: In **Marseille and Cairo** the direct radiation of **65** and **71%** respectively, contributes to the main portion of global radiation.

In Figure 2.5 the data for Hamburg and Munich are shown again graphically. What can be derived from this? First it is obvious that it is more worthwhile to operate a photovoltaic plant in Munich than in Hamburg. The average global radiation of $H = 3.15\,\mathrm{kWh/(m^2\cdot d)}$ provides over a whole year (365 days) a yearly total of:

$$H = 3.15\ \mathrm{kWh/(m^2 \cdot d)} \cdot 365\ \mathrm{d/a} = 1150\ \mathrm{kWh/(m^2 \cdot a)}.$$

The corresponding year's total in Hamburg is only $949\,\mathrm{kWh}$ per $\mathrm{m^2}$ per annum.

Furthermore, it can be seen that the diffuse radiation in Munich is only slightly higher than in Hamburg. The higher global radiation in Munich is achieved mainly due to greater direct radiation. The reason for this is easy to guess: the higher position of the Sun in Munich. But obviously the height of the Sun has hardly any influence on the diffuse radiation.

How different the daily courses of direct and diffuse radiation can be is shown in Figure 2.6. Here the radiation for a sunny day and a cloud-covered summer's day are shown.

On a sunny day the direct radiation clearly dominates whereas on the cloud covered day it plays practically no role compared to diffuse radiation. Yet the cloud-covered day with $3.7\,\mathrm{kWh/m^2}$ still brings more than half the radiation of the sunny day. This shows how profitable even cloud-covered days can be for photovoltaic usage.

2.2.3 Global Radiation Maps

In order to be able to estimate the yield of a photovoltaic plant already in the planning stage, it is necessary to obtain the data of the global radiation at the planned site. The most important

Table 2.2 Total radiation over the year on a horizontal level for various places in kWh/(m²·d) [18]

Place		Jan	Feb	Mar	Apr	May	Jun	Jul	Aug	Sep	Oct	Nov	Dec	Σ
Glasgow	H_{Direct}	0.06	0.23	0.49	1.18	1.66	1.60	1.38	1.03	0.60	0.25	0.10	0.03	0.71
55.7°N	$H_{Diffuse}$	0.39	0.81	1.45	2.23	2.83	3.11	2.97	2.46	1.73	1.00	0.51	0.29	1.65
4.5°W	H	**0.45**	**1.04**	**1.94**	**3.41**	**4.49**	**4.71**	**4.35**	**3.49**	**2.33**	**1.25**	**0.61**	**0.32**	**2.36**
Hamburg	H_{Direct}	0.13	0.37	0.74	1.49	2.18	2.32	2.01	1.82	1.10	0.52	0.18	0.10	1.08
53.6°N	$H_{Diffuse}$	0.40	0.78	1.35	2.04	2.55	2.79	2.67	2.26	1.63	0.99	0.51	0.31	1.52
10.0°E	H	**0.53**	**1.15**	**2.09**	**3.53**	**4.73**	**5.11**	**4.68**	**4.08**	**2.73**	**1.51**	**0.69**	**0.41**	**2.60**
London	H_{Direct}	0.17	0.36	0.82	1.36	1.88	2.08	1.91	1.72	1.24	0.61	0.26	0.12	1.04
51.6°N	$H_{Diffuse}$	0.48	0.84	1.43	2.06	2.56	2.79	2.68	2.28	1.70	1.08	0.61	0.38	1.57
0.0°W	H	**0.65**	**1.20**	**2.25**	**3.42**	**4.44**	**4.87**	**4.59**	**4.00**	**2.94**	**1.69**	**0.87**	**0.50**	**2.61**
Munich	H_{Direct}	0.36	0.75	1.28	1.83	2.43	2.62	2.69	2.26	1.71	0.89	0.38	0.24	1.45
48.4°N	$H_{Diffuse}$	0.67	1.05	1.60	2.18	2.61	2.81	2.71	2.35	1.82	1.24	0.75	0.55	1.70
11.7°E	H	**1.03**	**1.80**	**2.88**	**4.01**	**5.04**	**5.43**	**5.40**	**4.61**	**3.53**	**2.13**	**1.13**	**0.79**	**3.15**
Marseille	H_{Direct}	1.01	1.34	2.40	3.24	4.03	4.78	5.03	4.24	3.05	1.76	1.05	0.79	2.72
43.3°N	$H_{Diffuse}$	0.79	1.11	1.49	1.90	2.16	2.18	2.02	1.85	1.58	1.24	0.87	0.70	1.49
5.4°E	H	**1.80**	**2.45**	**3.89**	**5.14**	**6.19**	**6.96**	**7.05**	**6.09**	**4.63**	**3.00**	**1.92**	**1.49**	**4.21**
New York	H_{Direct}	0.84	1.35	1.88	2.43	3.04	3.25	3.17	3.03	2.34	1.68	0.74	0.57	2.03
40.8°N	$H_{Diffuse}$	1.03	1.37	1.85	2.31	2.62	2.74	2.68	2.37	1.98	1.51	1.12	0.91	1.87
74.0°W	H	**1.87**	**2.72**	**3.73**	**4.74**	**5.66**	**5.99**	**5.85**	**5.40**	**4.32**	**3.19**	**1.86**	**1.48**	**3.90**
Cairo	H_{Direct}	2.16	2.94	3.80	4.60	5.41	5.95	5.82	5.34	4.50	3.56	2.48	1.92	4.04
30.1°N	$H_{Diffuse}$	1.26	1.47	1.76	1.99	2.05	2.01	1.99	1.89	1.73	1.50	1.30	1.18	1.68
31.2°E	H	**3.42**	**4.41**	**5.56**	**6.59**	**7.46**	**7.96**	**7.81**	**7.23**	**6.23**	**5.06**	**3.78**	**3.10**	**5.72**
Miami	H_{Direct}	2.03	2.50	3.16	3.82	3.54	3.07	3.36	3.23	2.72	2.50	2.10	1.90	2.82
25.9°N	$H_{Diffuse}$	1.46	1.71	1.96	2.17	2.42	2.54	2.47	2.36	2.17	1.83	1.53	1.37	2.00
80.1°W	H	**3.49**	**4.21**	**5.12**	**5.99**	**5.96**	**5.61**	**5.83**	**5.59**	**4.89**	**4.33**	**3.63**	**3.27**	**4.82**
Quito	H_{Direct}	1.97	2.07	2.20	2.10	2.06	2.05	2.27	2.33	1.98	1.96	2.12	1.87	2.08
0.2°S	$H_{Diffuse}$	2.16	2.27	2.35	2.23	2.06	1.96	1.99	2.13	2.28	2.28	2.18	2.11	2.17
78.5°W	H	**4.13**	**4.34**	**4.55**	**4.33**	**4.12**	**4.01**	**4.26**	**4.46**	**4.26**	**4.24**	**4.30**	**3.98**	**4.25**
Sidney	H_{Direct}	3.38	3.01	2.74	2.25	1.81	1.72	1.86	2.54	3.17	3.57	3.48	3.67	2.76
33.9°S	$H_{Diffuse}$	2.56	2.27	1.81	1.34	0.98	0.80	0.86	1.07	1.48	1.97	2.43	2.61	1.68
151.2°E	H	**5.94**	**5.28**	**4.55**	**3.59**	**2.79**	**2.52**	**2.72**	**3.61**	**4.65**	**5.54**	**5.91**	**6.28**	**4.44**
Buenos Aires	H_{Direct}	4.38	3.57	2.99	2.20	1.68	1.26	1.41	1.88	2.62	3.11	3.93	4.32	2.77
34.6°S	$H_{Diffuse}$	2.39	2.17	1.74	1.31	0.97	0.84	0.90	1.17	1.56	2.03	2.35	2.50	1.66
53.4°W	H	**6.77**	**5.74**	**4.73**	**3.51**	**2.65**	**2.10**	**2.31**	**3.05**	**4.18**	**5.14**	**6.28**	**6.82**	**4.43**
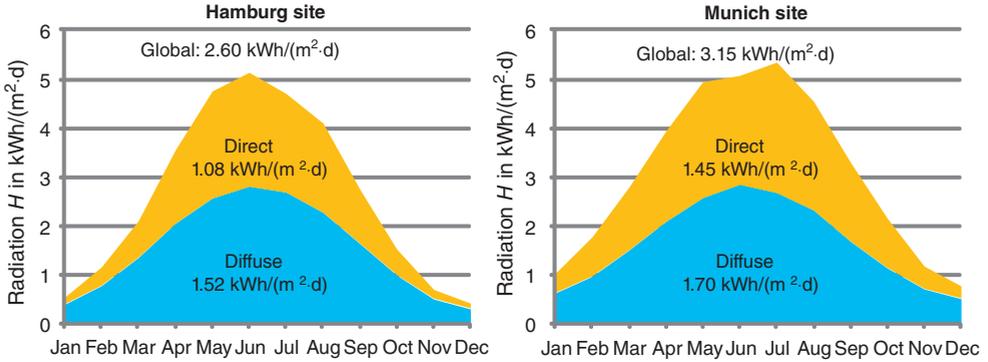
Figure 2.5 Radiation for a year on a horizontal level for the sites of Hamburg and Munich

characteristic for this is the year's total H of the global radiation on a horizontal level. Nowadays global radiation maps are available that show this characteristic in high resolution. The basis of these is many years of measurements by a dense network of measuring stations, satellite pictures and simulation tools. Figure 2.7 shows this type of map from the German Weather Services.

It is clearly seen that the year's radiation energy increases from the north to the south. The values range from 900 to 1150 kWh/(m² a). On average one can assume 1000 kWh/(m² a) for Germany. This unusual unit can be bypassed by means of a very clear model, the **Model of Sun full load hours**:

We assume that the Sun can only have two conditions:

1. It shines with "Full load": $E = E_{STC} = 1000$ W/m².
2. It is fully "Switched off": $E = 0$.
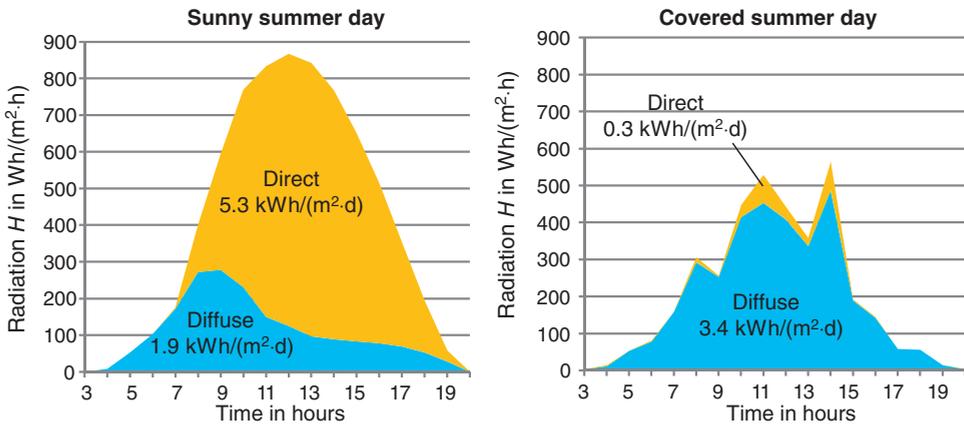
Figure 2.6 Radiation on two summer days in Braunschweig: the cloud-covered day provides a good half of the radiation energy of the sunny day [19]
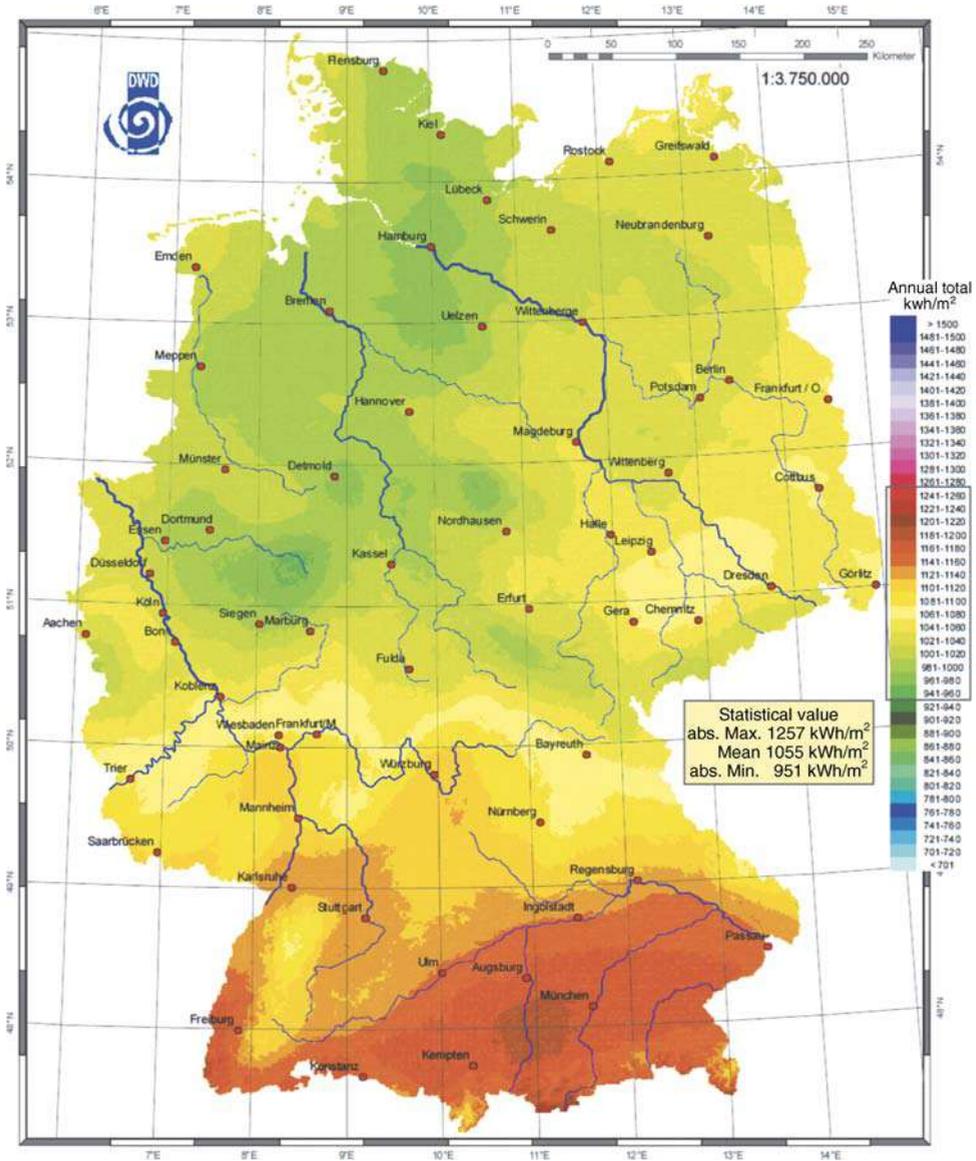
Figure 2.7 Global horizontal radiation in Germany [20]

For how long must the Sun shine with full load for it to provide an radiation of $H = 1000$ kWh/(m^2 a) on the Earth's surface, for instance?

$$\frac{H}{E_{\text{STC}}} = \frac{1000 \dfrac{\text{kWh}}{\text{m}^2 \cdot \text{a}}}{1000 \dfrac{\text{W}}{\text{m}^2}} = 1000 \frac{\text{h}}{\text{a}} \tag{2.4}$$

The Sun would need 1000 full load hours to provide the same optical energy as it actually provides in a year (8760 h).

In Germany, the Sun provides approximately 1000 full load hours.

In other countries the situation in part is much better. Figure 2.8 shows the radiation situation in Europe. The radiation is mostly in the region of 1000–1500 kWh/(m^2·a). Extreme values are found in Scotland with only 700 and in Southern Spain with 1800 kWh/(m^2·a).

An overall picture is provided in Figure 2.9 in a world map of radiation. The highest radiation is naturally found in the region of the equator with values of up to 2500 full load hours.

2.3 Calculation of the Position of the Sun

2.3.1 Declination of the Sun

Within a year the Earth travels around the Sun in an almost perfect circle. Because the axis of the Earth is tilted, the height of the Sun changes in the course of a year. Figure 2.10 shows this connection for the summer and winter changes.
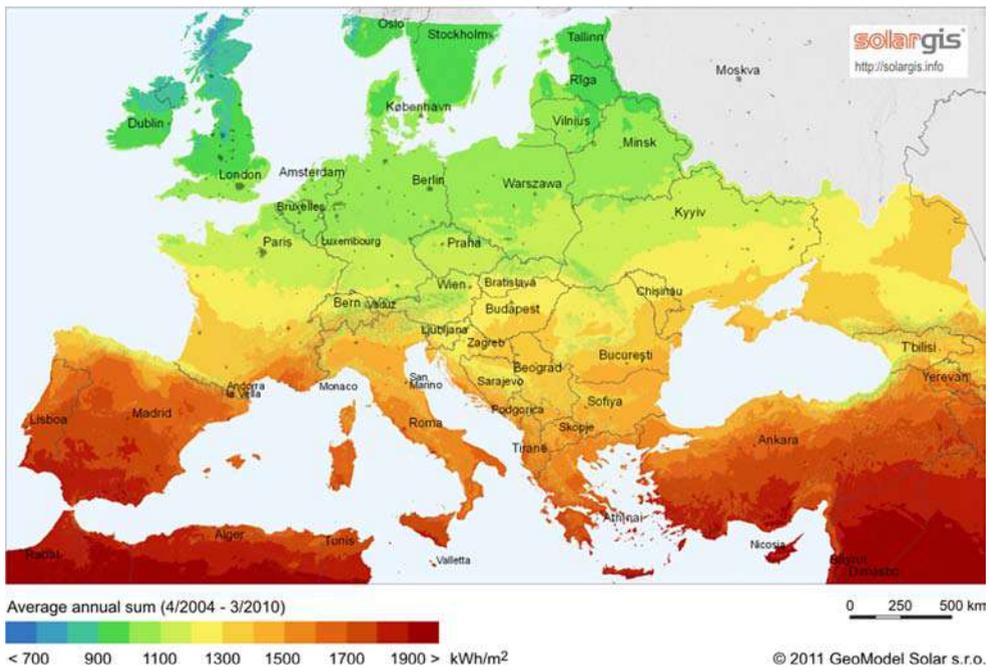
Figure 2.8 Global radiation map of Europe. The radiation is between 700 kWh/m^2 in Scotland and 1800 kWh/m^2 per year in southern Spain [source: solargis.info]
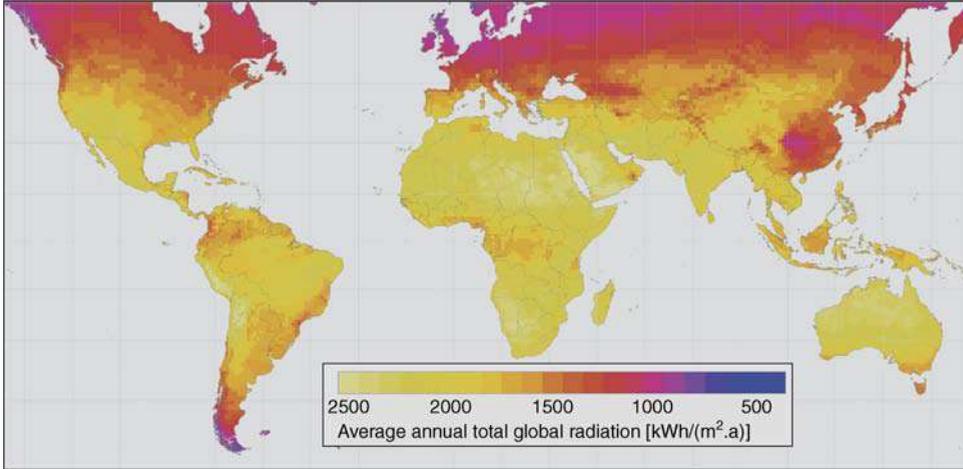
Figure 2.9 World map of the global radiation [created by Meteonorm, www.meteonorm.com]

In **summer** the North Pole is tilted towards the Sun so that large angles of the sun (often also called the **solar altitude**) exist. The maximum solar altitude γ_{S_Max} (noon) can be determined with simple angle consideration:

$$\gamma_{S\_Max} = 113.4° - \varphi. \tag{2.5}$$

The **angle** φ is the **geographic width** (latitude) of the site being considered. It is exactly the opposite for the **winter solstice**, the axis of the Earth slants away from the sun, and therefore there is only a noonday solar altitude of:

$$\gamma_{S\_Min} = 66.6° - \varphi. \tag{2.6}$$
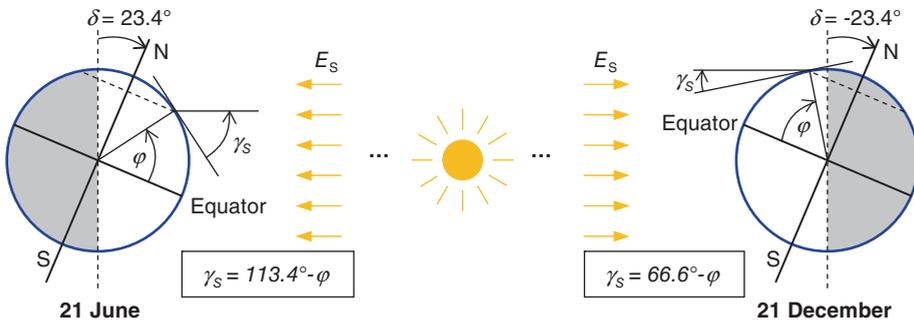
Figure 2.10 Influence of the Earth's axis tilt on the noonday solar altitude γ_{S_Max} for summer and winter solstice. There is a different value depending on the latitude φ

Example 2.1   Solar altitude at Münster

A PV plant is to be erected at Münster (latitude $\varphi = 52°$). In the middle of June the solar altitude is $113.4–52° = 61.4°$. In the middle of December the value is $66.6–52° = 14.6°$.
∎

The solar altitude of the winter solstice is especially important in planning photovoltaic plants.

> A photovoltaic plant should be structured if possible so that there are no shadows at noon even on the shortest day of the year (21.12).

Figure 2.10 shows only the two extreme cases of the **Sun declination** δ. This is understood to be the respective tilt of the Earth's axis in the direction of the Sun. This changes continuously over the year as can be seen in Figure 2.11. With the aid of this picture the Sun declination can be determined for each day of the year.

2.3.2 Calculating the Path of the Sun

In the case of possible shadows it is of help in the detail planning of the plant to know the path of the Sun on certain days. In order to make the calculation simple, use is made of the so-called **local solar time (*LST*)** or **solar time**. This is the time in which at noon the Sun is exactly in the south and has thus reached its highest point of the day. In principle, it is therefore the time that a sun dial would show at the site.

The **Coordinated Universal Time (*UTC*)** would, however, be referenced to the zero meridian at Greenwich. Thus it would only be correct with the local solar time at those places that are situated on 0° latitude.

The difference between both times can be roughly determined from the respective **geographic location** Λ as the Earth rotates once in 24 h (360°) and thus 1 h corresponds to just 15°.

$$LST = UTC + 1\text{h} \cdot \frac{\Lambda}{15°} \qquad (2.7)$$
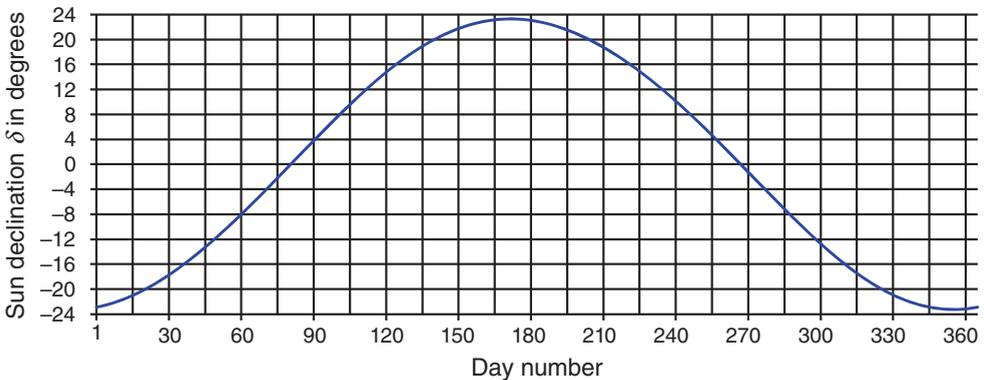
Figure 2.11   Sun declination for the year (365 days)
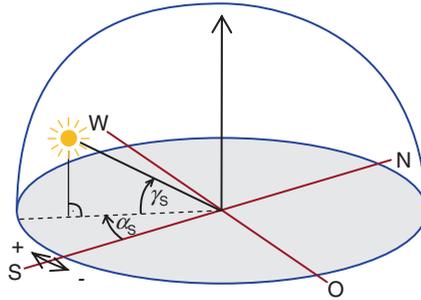
Figure 2.12 Calculation of the Sun's position with the dimension of solar altitude γ_S and Sun's azimuth α_S

What is ignored here is that the local solar time does not only depend on the rotation of the Earth but also on the Sun declination and the elliptical path of the Earth around the Sun.

Example 2.2   Local solar time in Belfast

You are in Belfast and would like to find out the local solar time. Your wristwatch shows noon. Belfast has a latitude of $\Lambda = -6.0°$.

$$LST = 12\,\text{h} + 1\,\text{h} \cdot \frac{-6°}{15°} = 12\,\text{h} - 60\,\text{min} \cdot 0.4 = 11\!:\!36\,\text{h} \tag{2.8}$$

Thus the local solar time is 11:36 h: You will have to wait almost another half hour until the Sun reaches its highest point.

In the case of other time zones, the respective clock time must first be converted to world time in order to use Equation 2.7. Thus, for instance, noon **Middle European Time (*MET*)** would correspond to a World Time of 11:00.

∎

We will now calculate the path of the Sun for certain days. For this purpose, Figure 2.12 shows the sizes for describing the position of the Sun. This shows the **Sun's azimuth α_S** as well as the solar altitude γ_S and depicts the **displacement of the Sun from the south**. **Positive values** show **western deviations** and **negative values** the **eastern displacements**.

Remarks: This definition of the Sun's azimuth is the most common one in the field of photovoltaics. However, some simulations make use of the **definition according to DIN**. There, **North is defined with 0°** and then added in a clockwise direction (east; 90°, south; 180°, etc.).We will also insert the **hour angle ω** as an abbreviation: This calculates the local solar time into the respective rotation position of the Earth:

$$\omega = (LST - 12) \cdot 15° \tag{2.9}$$

Now the position of the Sun can be determined from the latitude φ and the Sun declination δ:

$$\sin \gamma_S = \sin \varphi \cdot \sin \delta + \cos \varphi \cdot \cos \delta \cdot \cos \omega \tag{2.10}$$

$$\sin \alpha_S = \frac{\cos \delta \cdot \sin \omega}{\cos \gamma_S} \tag{2.11}$$
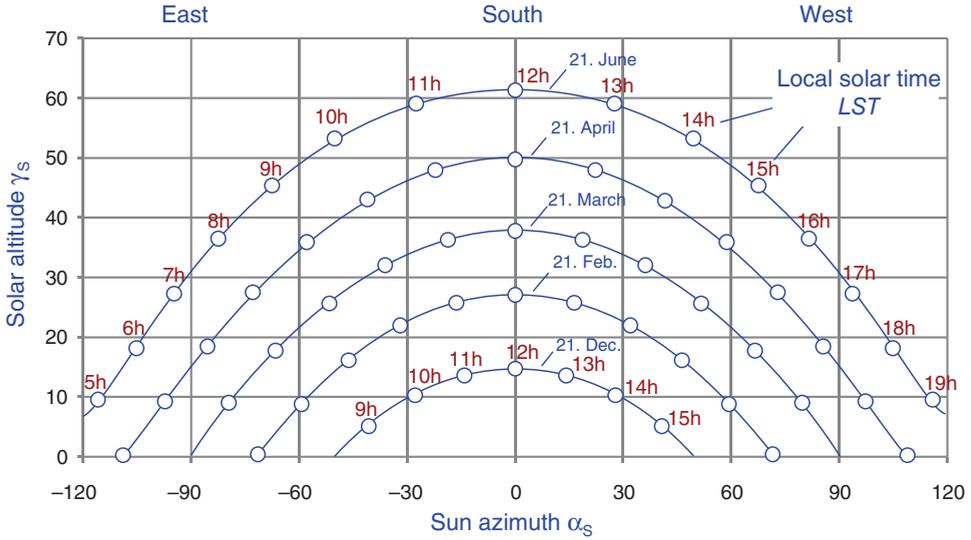
Figure 2.13 Sun path diagram for the town of Münster (geographic latitude $\varphi = 52°$); the time used is the local solar time (*LST*)

Figure 2.13 shows a **Sun path diagram** calculated according to this equation. It shows the path of the Sun for the town of Münster on different days of the year. On June 21 and December 21 the determined maximum and minimum solar altitudes already shown in Example 2.1 are reached. The time entered is the *LST* so the Sun reaches its highest position at noon.

These types of diagrams help to show up possible shadows caused by trees, houses or similar and to estimate their effects on the yield of the plant (see Chapter 9).

The web site *www.textbook-pv.org* contains an Excel file with which the Sun path diagram for any desired latitude can be determined and printed out.

2.4 Radiation on Tilted Surfaces

Photovoltaic plants are mostly installed on pitched roofs so that the module is at an angle of attack β to the horizontal. Also in the case of flat roofs or open air plants it is usual to tilt the modules in order to achieve a higher annual yield.

2.4.1 Radiation Calculation with the Three-Component Model

Figure 2.14 shows the radiation relationships in the case of a suitable solar module surface (or more generally, a **solar generator**). Besides the direct and diffuse radiation there is still a further radiation component: the radiation reflected from the ground. These add themselves to an overall radiation E_{Gen} on the tilted generator.

$$E_{\text{Gen}} = E_{\text{Direct\_Gen}} + E_{\text{Diffuse\_Gen}} + E_{\text{Refl\_Gen}} \tag{2.12}$$
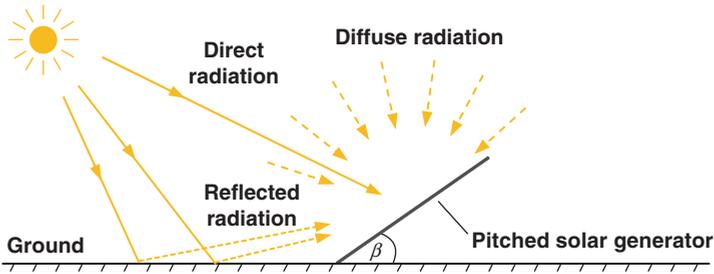
Figure 2.14 Radiation situation with tilted surfaces: The radiation is made up of the direct, diffused and reflected radiation

We will now look at the calculation of the individual components in more detail.

2.4.1.1 Direct Radiation

Let us consider the case that direct sunlight shines on a tilted solar module. For this case the left sketch of Figure 2.15 shows how solar radiation impinges on a horizontal surface A_H. The optical power P_{Opt} of the impinging radiation is:

$$P_{Opt} = E_{Direct\_H} \cdot A_H \qquad (2.13)$$

If a solar generator were arranged exactly vertically to the solar radiation, then it would be possible to take up the same power on a smaller surface $A_{Vertical}$:

$$P_{Opt} = E_{Direct\_H} \cdot A_H = E_{Direct\_Vertical} \cdot A_{Vertical} \qquad (2.14)$$

The strength of the radiation $E_{Direct\_Vertical}$ is therefore increased by the factor $A_H/A_{Vertical}$ compared to the horizontal strength of radiation. This increase can be seen in Figure 2.15 in that the light rays are closer together on the vertical surface in comparison to the horizontal surface.

A_H:	Horizontal surface	γ_S:	Solar altitude angle
$A_{Vertical}$:	Surface vertical to the incidental direction	β:	Elevation angle of the solar generator
A_{Gen}:	Surface in generator level	χ:	Complementary angle
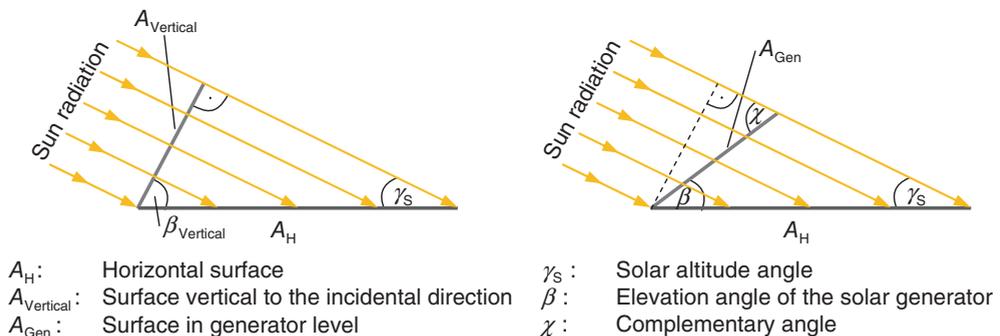
Figure 2.15 Influence of the solar generator tilt on direct radiation

The right-hand sketch in Figure 2.15 shows the general case: a solar generator tilted by the angle β. For determining the strength of the radiation in the generator level use is made of a pair of trigonometric equations:

$$A_{\text{Vertical}} = A_{\text{H}} \cdot \sin \gamma_{\text{S}} \tag{2.15}$$

$$A_{\text{Vertical}} = A_{\text{Gen}} \cdot \sin \chi \tag{2.16}$$

The complementary angle χ can be calculated by the sum of the angles in the triangle and as subsidiary angle:

$$\chi = \gamma_{\text{S}} + \beta \tag{2.17}$$

Using the Equations 2.14–2.17 we then derive:

$$E_{\text{Direct\_Gen}} = E_{\text{Direct\_H}} \cdot \frac{\sin(y_s + \beta)}{\sin y_s} \tag{2.18}$$

It must be noted that this equation applies only for direct radiation.

Example 2.3   Radiation on a tilted solar module

Assume that on a clear summer's day the Sun is at a solar altitude of $40°$ in the sky. On flat ground the irradiance is measured at $E_{\text{Direct\_H}} = 700 \, \text{W/m}^2$. What angle of attack is ideal for a solar module and what yield can be expected when the diffuse radiation and reflection of the ground is ignored?

Figure 2.16 shows for this case the Equation 2.18 as a diagram. With an increasing angle of the solar module the irradiance increases continuously up to an angle of $\beta = 50°$ (thus an angle $90° - \gamma_{\text{S}}$). Here the irradiance reaches a maximum value of $E_{\text{Direct\_Gen}} = 1089 \, \text{W/m}^2$. The solar module power can thus be increased by more than 50%.

∎
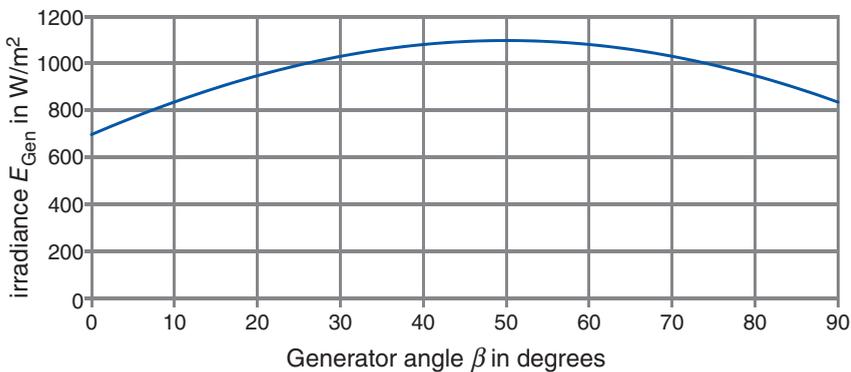
Figure 2.16   Example of dependency of the irradiance (direct radiation) on a tilted solar module for a solar altitude of $\gamma_{\text{S}} = 40°$
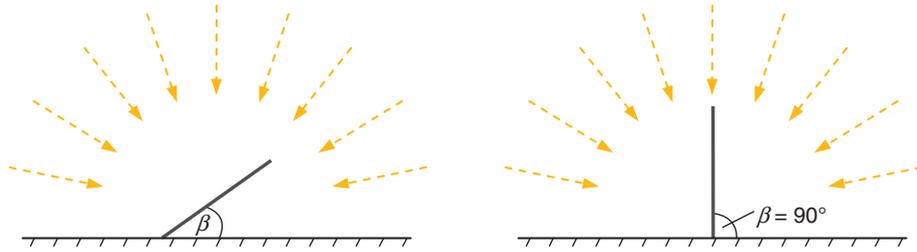
Figure 2.17   Isotropic assumption for diffuse radiation on a tilted surface. Only half the radiation can be used in the case of a vertically standing solar generator

2.4.1.2   Diffuse Radiation

The calculation of the diffuse radiation of tilted surface can be much simplified. For this purpose we make a simple assumption that the diffuse radiation from the whole sky is approximately of the same strength (the **isotropic assumption**: Figure 2.17, left). Thus the strength of radiation of a solar generator at an angle β is calculated as:

$$E_{\text{Diffus\_Gen}} = E_{\text{Diffus\_H}} \cdot \frac{1}{2} \cdot (1 + \cos\beta) \tag{2.19}$$

Starting with a horizontal generator ($\beta = 0°$) the radiation is reduced until at ($\beta = 90°$) it is:

$$E_{\text{Diffus\_Gen}} = \frac{E_{\text{Diffus\_H}}}{2} \tag{2.20}$$

In this case the solar generator is vertical so that only the left hand side of the sky can be used (Figure 2.17, right).

The isotropic assumption is only to be understood as a coarse approximation. Thus, the sky around the Sun is mostly brighter than in the region of the horizon. More refined models are used in modern simulation programs in order to achieve greater degrees of accuracy.

2.4.1.3   Reflected Radiation

As shown in Figure 2.14 a part of the global radiation is reflected from the ground and can act as an additional radiation contribution to the solar generator.

In the calculation of this portion the main problem is that every ground material reflects (or more exactly: scatters) differently. The so-called **albedo value (*ALB*)** describes the resulting reflection factor. Table 2.3 lists the albedo value of some types of ground.

The large range of the given values shows that the simulation of the reflected radiation is accompanied by large uncertainties. If the ground is not known then the standard value of $ALB = 0.20$ is often entered into the simulation program.

Table 2.3 Albedo value of different types of ground [21]

Material	Albedo (ALB)	Material	Albedo (ALB)
Grass (July, August)	0.25	Asphalt	0.15
Lawn	0.18 . . . 0.23	Concrete, clean	0.30
Unmown fields	0.26	Concrete, weathered	0.20
Woods	0.05 . . . 0.18	Snow cover, new	0.80 . . . 0.90
Heath surfaces	0.10 . . . 0.25	Snow cover, old	0.45 . . . 0.70

An isotropic assumption is again made for the calculation of the reflected radiation on the tilted generator.

$$E_{\text{Refl\_Gen}} = E_{\text{G}} \cdot \frac{1}{2} \cdot (1 - \cos \beta) \cdot ALB \tag{2.21}$$

Figure 2.18 shows the results for the case of ground covered with **lawn and fresh snow**. In the case of flat solar modules ($\beta = 0$) the portion of the radiation reflected by the ground is zero and then rises continuously. At $\beta = 90°$ half the available reflective radiation reaches the solar generator. This is the case of façade plants where solar modules are fixed to the vertical house walls. If one goes beyond 90° then the part of the reflection radiation continues to rise but the top face of the solar module now faces down, which obviously is not the optimum for overall radiation.

2.4.2 Radiation Estimates with Diagrams and Tables

The equations and characteristic values described are meant as an aid to understanding the features and limits of the use of solar radiation. However, simulation programs are always used today for detail planning of photovoltaic plants, and they work with refined models and detailed weather information in order to create very exact yield forecasts (see Chapter 9).
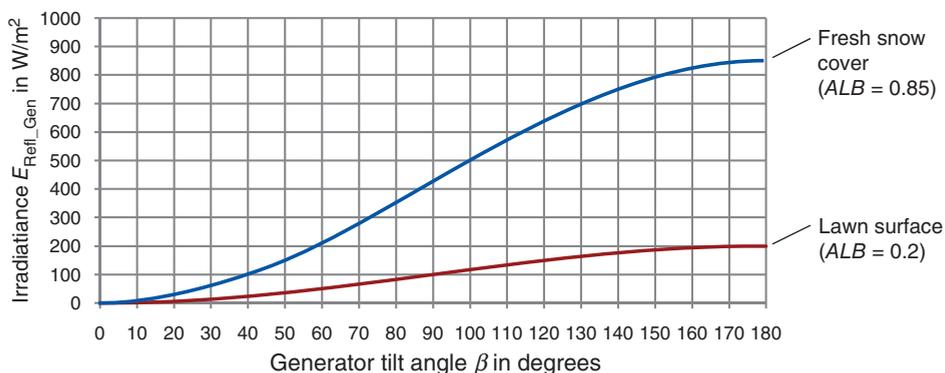
Figure 2.18 Reflected radiation as an example of lawn and fresh snow for various degrees of tilt of the solar module ($E_{\text{G}} = 1000\,\text{W/m}^2$)
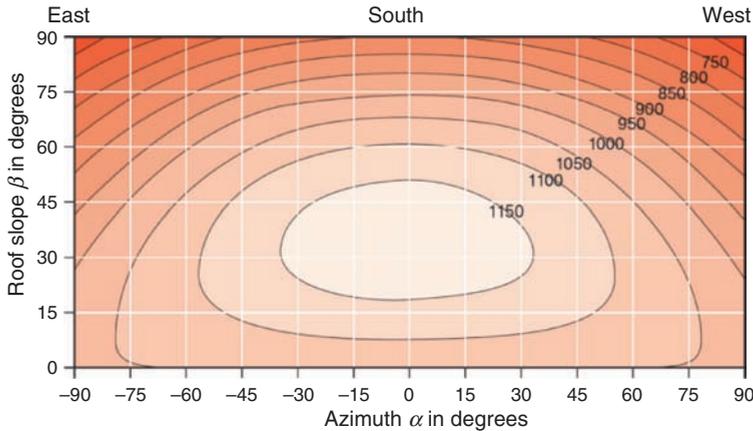
Figure 2.19 Radiation diagram for estimating the suitability of a roof for the city of Berlin given as the radiation sum H in kWh/(m²·a) [22]

Radiation diagrams and tables are of help for a coarse estimate of the radiation on a pitched roof. Figure 2.9 shows such a diagram for the city of Berlin.

Clearly to be seen is a relatively broad maximum of the radiation total for a south facing roof (azimuth $\alpha = 0°$) and a roof slope of approximately 35°. The direction does not make much difference in the case of a lesser slope (e.g., $= 15°$). If, however, the roof is relatively steep (e.g., $= 60°$) then a south-west direction leads to a reduction of the radiation to less than 1050 kWh/(m²·a).

A somewhat more accurate estimate of the deviation of the roof slope and direction from the optimum can be found in Table 2.4 for the example of the town of Münster (the same geographic latitude as Berlin). The radiation amount here was standardized on the maximum values $\alpha = 0°$ and $\beta = 35°$ so that the deviations can be read directly in percentages.

For instance the yield of a façade plant ($\beta = 90°$) that is aligned directly south is only 71% of the optimum. A horizontal surface, however, still yields 88% of the optimum.

Figure 2.19 and Table 2.4 show the different incidental radiation in dependence of the alignment and the roof pitch. In reality, though, **soiling** also plays a certain role. Thus, the soiling of the solar module is reduced with increasing inclination angle. Added to this is the fact that a larger angle of attack ensures that snow in winter can slide off more easily and thus more solar energy can be harvested. In the case of façade plants, shading by trees and houses also plays a large role.

2.4.3 Yield Gain through Tracking

Basically, it is possible to increase the yield of a photovoltaic plant in that the solar generator actively tracks the Sun (see Chapter 6). The tracking, however, only increases the direct radiation portion whereas the diffuse radiation remains almost the same. An example of this is shown in Figure 2.20 of the daily yield of a tracking and a fixed photovoltaic plant on two different days. On the sunny day the tracking brings an energy yield of almost 60%. In the case of the overcast day the yield of the tracking plant provides approximately 10% less than the fixed plant. The reason is that the tracking modules are relatively steep in the morning and afternoons, and therefore receive less diffuse radiation.

Table 2.4 Effect of the direction and slope of a roof on the incidental annual global radiation (data from PV-SOL Expert 4.0 for the town of Munster)

Azimuth α	Angle of slope β																		
	0°	5°	10°	15°	20°	25°	30°	35°	40°	45°	50°	55°	60°	65°	70°	75°	80°	85°	90°
−90°	88.3	88.0	87.5	86.7	85.8	84.6	83.4	81.9	80.3	78.4	76.4	74.3	72.0	69.6	66.9	64.2	61.4	58.4	55.3
−85°	88.3	88.4	88.0	87.6	86.8	86.0	84.9	83.6	82.0	80.4	78.5	76.4	74.0	71.6	69.0	66.0	63.2	60.2	57.0
−80°	88.3	88.5	88.5	88.4	87.9	87.3	86.3	85.2	83.8	82.2	80.4	78.3	76.0	73.5	70.8	68.0	64.9	61.8	58.6
−75°	88.3	88.9	89.2	89.2	89.0	88.5	87.8	86.8	85.5	84.1	82.2	80.3	78.0	75.4	72.7	69.9	66.7	63.4	60.0
−70°	88.3	89.2	89.7	90.0	90.0	89.8	89.2	88.4	87.2	85.8	84.0	82.0	79.8	77.2	74.4	71.6	68.4	64.9	61.4
−65°	88.3	89.4	90.2	90.8	90.9	91.1	90.6	89.9	88.8	87.5	85.8	83.8	81.6	79.0	76.2	73.2	70.0	66.5	62.8
−60°	88.3	89.7	90.7	91.5	91.9	92.0	91.8	91.3	90.3	89.1	87.5	85.4	83.2	80.7	77.9	74.7	71.4	67.8	64.1
−55°	88.3	89.9	91.2	92.2	92.8	93.1	93.0	92.5	91.7	90.5	89.1	87.1	84.7	82.2	79.4	76.2	72.7	69.1	65.3
−50°	88.3	90.1	91.6	92.8	93.6	94.0	94.1	93.8	93.1	91.9	90.5	88.6	86.3	83.6	80.8	77.6	74.0	70.3	66.4
−45°	88.3	90.3	92.1	93.4	94.4	95.0	95.2	94.9	94.3	93.2	91.7	90.0	87.7	85.1	82.0	78.8	75.3	71.4	67.4
−40°	88.3	90.6	92.4	94.0	95.1	95.8	96.1	96.0	95.5	94.5	93.0	91.1	88.9	86.3	83.3	79.9	76.3	72.4	68.2
−35°	88.3	90.8	92.8	94.5	95.7	96.5	97.0	96.9	96.4	95.6	94.1	92.3	90.0	87.4	84.4	81.0	77.2	73.2	69.0
−30°	88.3	90.9	93.1	94.9	96.3	97.2	97.7	97.7	97.2	96.4	95.0	93.2	90.9	88.3	85.2	81.8	78.0	74.0	69.6
−25°	88.3	91.0	93.3	95.3	96.7	97.8	98.3	98.4	98.0	97.1	95.8	94.0	91.7	89.1	86.0	82.5	78.7	74.5	70.0
−20°	88.3	91.1	93.6	95.6	97.2	98.2	98.8	99.0	98.7	97.8	96.4	94.6	92.4	89.7	86.6	83.0	79.1	75.0	70.5
−15°	88.3	91.2	93.8	95.8	97.4	98.6	99.2	99.4	99.1	98.2	96.9	95.1	92.8	90.1	87.0	83.5	79.6	75.3	70.8
−10°	88.3	91.3	93.9	96.0	97.7	98.8	99.5	99.6	99.4	98.7	97.3	95.6	93.2	90.5	87.3	83.7	79.8	75.6	70.9
−5°	88.3	91.3	94.0	96.1	97.8	99.0	99.7	99.9	99.6	98.7	97.5	95.7	93.4	90.7	87.6	84.0	80.0	75.7	71.1
0°	88.3	91.4	94.0	96.2	97.9	99.1	99.8	100.0	99.7	98.8	97.5	95.7	93.5	90.8	87.6	84.1	80.1	75.8	71.2
5°	88.3	91.3	94.0	96.1	97.8	99.0	99.7	99.9	99.6	98.8	97.5	95.7	93.4	90.7	87.6	84.0	80.0	75.7	71.1
10°	88.3	91.3	93.9	96.0	97.7	98.8	99.5	99.6	99.4	98.7	97.3	95.6	93.2	90.5	87.3	83.7	79.8	75.6	70.9
15°	88.3	91.2	93.8	95.8	97.4	98.6	99.2	99.4	99.1	98.2	96.9	95.1	92.8	90.1	87.0	83.5	79.6	75.3	70.8
20°	88.3	91.1	93.6	95.6	97.2	98.2	98.8	99.0	98.7	97.8	96.4	94.6	92.4	89.7	86.6	83.0	79.1	75.0	70.5
25°	88.3	91.0	93.3	95.3	96.7	97.8	98.3	98.4	98.0	97.1	95.8	94.0	91.7	89.1	86.0	82.5	78.7	74.5	70.0
30°	88.3	90.9	93.1	94.9	96.3	97.2	97.7	97.7	97.2	96.4	95.0	93.2	90.9	88.3	85.2	81.8	78.0	74.0	69.6
35°	88.3	90.8	92.8	94.5	95.7	96.5	97.0	96.9	96.4	95.6	94.1	92.3	90.0	87.4	84.4	81.0	77.2	73.2	69.0
40°	88.3	90.6	92.4	94.0	95.1	95.8	96.1	96.0	95.5	94.5	93.0	91.1	88.9	86.3	83.3	79.9	76.3	72.4	68.2
45°	88.3	90.3	92.1	93.4	94.4	95.0	95.2	94.9	94.3	93.2	91.7	90.0	87.7	85.1	82.0	78.8	75.3	71.4	67.4
50°	88.3	90.1	91.6	92.8	93.6	94.0	94.1	93.8	93.1	91.9	90.5	88.6	86.3	83.6	80.8	77.6	74.0	70.3	66.4
55°	88.3	89.9	91.2	92.2	92.8	93.1	93.0	92.5	91.7	90.5	89.1	87.1	84.7	82.2	79.4	76.2	72.7	69.1	65.3
60°	88.3	89.7	90.7	91.5	91.9	92.0	91.8	91.3	90.3	89.1	87.5	85.4	83.2	80.7	77.9	74.7	71.4	67.8	64.1
65°	88.3	89.4	90.2	90.8	90.9	91.1	90.6	89.9	88.7	87.5	85.8	83.8	81.6	79.0	76.2	73.2	70.0	66.5	62.8
70°	88.3	89.2	89.7	90.0	90.0	89.8	89.2	88.4	87.2	85.8	84.0	82.0	79.8	77.2	74.4	71.6	68.4	64.9	61.4
75°	88.3	88.9	89.2	89.2	89.0	88.5	87.8	86.8	85.5	84.1	82.2	80.3	78.0	75.4	72.7	69.9	66.7	63.4	60.0
80°	88.3	88.5	88.5	88.4	87.9	87.3	86.3	85.2	83.8	82.2	80.4	78.3	76.0	73.5	70.8	68.0	64.9	61.8	58.6
85°	88.3	88.4	88.0	87.6	86.8	86.0	84.9	83.6	82.0	80.4	78.5	76.4	74.0	71.6	69.0	66.0	63.2	60.2	57.0
90°	88.3	88.0	87.5	86.7	85.8	84.6	83.4	81.9	80.3	78.4	76.4	74.3	72.0	69.6	66.9	64.2	61.4	58.4	55.3
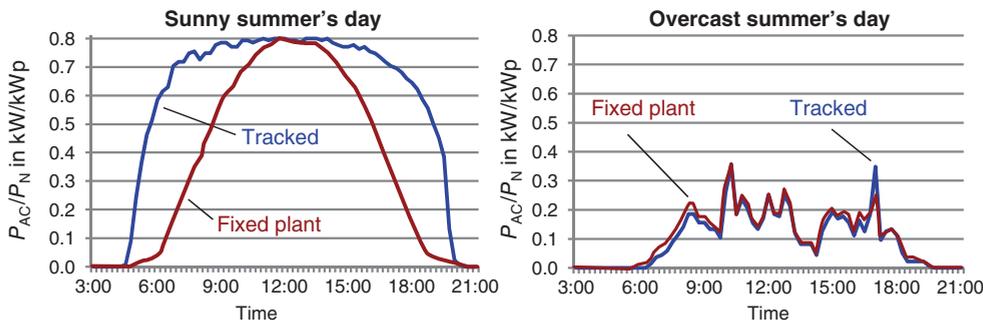
Figure 2.20 Yields of fixed and tracked photovoltaic plant on two different days (source: IBC Solar AG)

As we have seen, the portion of the diffuse radiation of the yearly global radiation in **Germany** is more than half. For this reason the **yield** of tracking in our latitude of approximately **30%** is limited. For this reason the utilization of tracking should be well thought through because of the substantial mechanical and electrical effort required. A compromise may be a single-axis tracking plant that can easily achieve a yield of 20% (see Chapter 6). In **southern countries** with a high degree of direct radiation the situation is much better: Here two-axis tracking plants can achieve **more than 50%** increase in yield.

2.5 Radiation Availability and World Energy Consumption

In concluding this chapter we will also consider the potential of solar radiation.

2.5.1 The Solar Radiation Energy Cube

As we have seen in Section 2.1, the sun shines continuously on the earth with a power density of 1367 W/m^2. Approximately 1000 W/m^2 of this arrives inside the atmosphere. We can simply roughly calculate the energy arriving on Earth W_{Earth}. For this we calculate the cross sectional area A_{Earth} of the Earth's sphere as shown in Figure 2.21.

The total optical power P_{Earth} radiated by the Sun on the Earth is then:

$$P_{Earth} = E_{STC} \cdot A_{Earth} = E_{STC} \cdot \frac{\pi \cdot d_{Earth}^2}{4} = 1.278 \cdot 10^{17} \text{ W} \tag{2.22}$$

Over the whole year the Earth receives radiation energy of:

$$W_{Earth} = P_{Earth} \cdot t = 1.278 \cdot 10^{17} W \cdot 8760 \, h = 1.119 \cdot 10^{18} \text{ kWh} \tag{2.23}$$

This number only tells us something if, for instance, we use it in relationship to the current yearly world energy consumption. From Figure 1.3 in Chapter 1 we can see that this is approximately 12.5 billion tons of oil equivalent. After conversion into kWh (Table 1.2) we get:

$$\frac{W_{Earth}}{W_{World}} = \frac{1.119 \cdot 10^{18} \text{ kWh}}{1.454 \cdot 10^{14} \text{ kWh}} = 7969 \tag{2.24}$$

The Sun sends us more than 7000 times the energy than we use in a year.
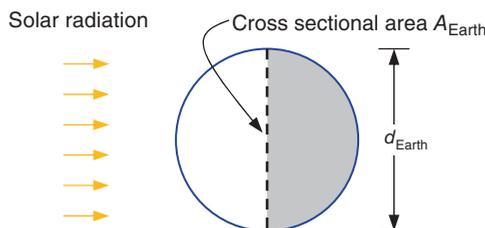
Figure 2.21 Cross sectional area of Earth for determining the total incidental radiation energy
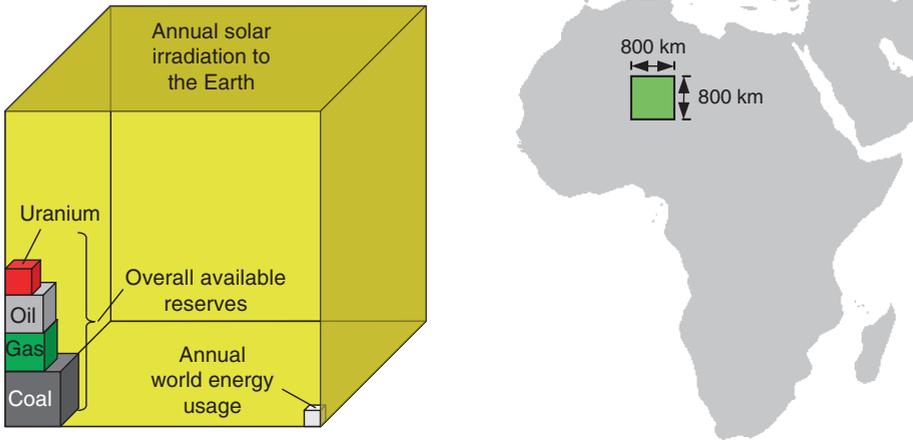
Figure 2.22   Estimate of the potential of solar energy: Energy cube and the "Sahara Miracle" [138]

This relationship is clearly seen in the energy cube as depicted in the left side of Figure 2.22. The yearly solar incidental radiation is represented by the large cube; the small blocks of world energy usage at the bottom-right look tiny compared with the large solar cube. Interesting is also in the same figure the comparison of the annual solar radiation with the reserves of fossil and nuclear energy carriers. It must be mentioned here that with these cubes at the bottom-left, the reserves still available are included whereas the large solar radiation cube is available again every new year.

2.5.2   The Sahara Miracle

Now we will not be able to make use of all the energy radiating on to the Earth. Therefore we will look at the case from another point of view and ask ourselves:

What area would be necessary in order to supply the whole primary consumption of the world with photovoltaics?

To find a solution, let us assume that the solar modules would be erected in the Sahara. The best solar modules available on the market have an efficiency of 20%. As a precautionary measure we will take a total system efficiency of $\eta_{Total} = 10\%$. In this way the losses from cables, inverters, transmission lines as well as the distance between module rows are more than covered.

According to Figure 2.9 the Sahara annually supplies approximately 2500 kWh/m^2 radiation energy. With an efficiency of 10% it is thus possible to obtain electrical energy of approximately 250 kWh/m^2.

For covering the worldwide primary energy consumption W_{World} we would thus need an area of:

$$A = \frac{W_{World}}{250\,\text{kWh/m}^2} = \frac{1.454 \cdot 10^{14}\,\text{kWh}}{250\,\text{kWh/m}^2} = 5.816 \cdot 10^{11}\,\text{m}^2 = 5.816 \cdot 10^5\,\text{km}^2 \qquad (2.25)$$

This would result, for instance, in a square of approximately 763 km per side. In order to estimate the size, the right-hand side of Figure 2.22 shows a square of 800 km × 800 km,

which is about 7% of the size of the Sahara's surface. Thus, this area is sufficient to cover the Earth's primary energy consumption with photovoltaics. In this way one could really speak of a "Sahara Miracle". In practice, of course, it would make no sense to concentrate the photovoltaic power stations at one site in the world. The power generated would have to be distributed expensively over the whole world, besides which humanity would have energy available only in daylight. More sensible would be the distribution of the PV plants over the whole Earth. In Chapter 10 we will consider the future role of photovoltaics in more detail.

3

Fundamentals of Semiconductor Physics

Typically, solar cells consist of semiconductors. In order to understand how solar cells work we will first deal with the structure and properties of semiconductors. This is associated with the consideration of the p-n junction and the optical features of semiconductors.

3.1 Structure of Semiconductors

3.1.1 Bohr's Atomic Model

To start off we will consider an individual atom. According to Bohr's atomic model, an atom consists of a nucleus and a shell. The **nucleus** contains **protons and neutrons** whereas the **shell** contains **electrons**, which orbit the nucleus. The protons are positively electrically charged with an elementary charge of $+q$ and the **electrons** are **negatively charged** with a charge of $-\mathbf{q}$. The size of the **elementary charge** is $1.6 \cdot 10^{-19}$ As. As the number of protons in the nucleus is equal to the number of electrons (the so-called atomic number) an atom is electrically neutral to the outside.

The simplest atom we know of is the hydrogen atom (Figure 3.1). It has the atomic number 1 and thus has only one proton in the nucleus and one electron in the shell.

Nils Bohr recognized that electrons can only circulate in very particular paths (so-called "shells") about the nucleus and defined this in his First postulate.

> Bohr's First Postulate:
>   There are only certain discrete shells permitted for an electron.

Each of these shells stands for a particular path radius that represents the respective energy state of the electron. The shells are designated with the letters of K, L, M, and so on. In Figure 3.1 the possible energy states for the hydrogen atom are shown. In the basic state the electron is situated on the K shell. If the electron is moved to the L shell then energy of 10.2 eV (electron volts) is necessary. In order to separate the electron completely from the

---
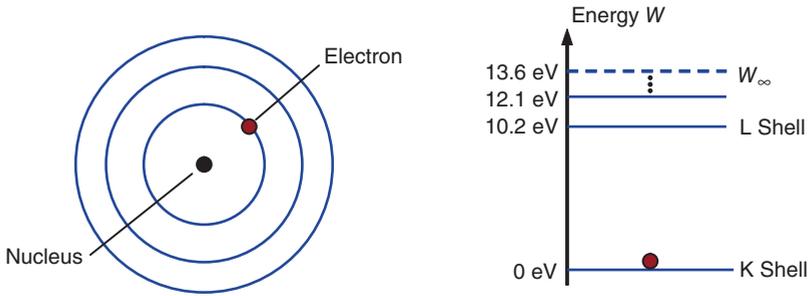
Figure 3.1 Structure and energy model of the hydrogen atom

atom (thus to transport it into "infinity") the so-called **ionizing energy W_∞** of 13.6 eV must be used.

What happens in the transfer from one shell to another? This is described in the following postulate:

Bohr's Second Postulate:
    The transfer of an electron from one shell to another occurs under the emission or absorption of electromagnetic radiation.

The **frequency f** of this radiation is thus determined by the following equation:

$$\Delta W = |W_2 - W_1| = h \cdot f \tag{3.1}$$

with

W_1: energy before the transfer
W_2: energy after the transfer
  h: Planck's constant; $h = 6.6 \cdot 10^{-34}\ \mathrm{Ws}^2$

In order to determine the **wavelength λ** from the frequency f the following equation is used:

$$\lambda = \frac{c_0}{f} \tag{3.2}$$

with

c_0: speed of light in a vacuum, $c_0 = 299.792$ km/s $\approx 3 \cdot 10^8$ m/s

In order to better understand Bohr's Second Postulate, consider Figure 3.2: The left part shows how the electron from the L shell falls onto the K shell. The energy released by this is radiated in the form of light as a photon. This process is called **light emission**. A light packet of a particular wavelength ("light particle") is known as a **photon**.
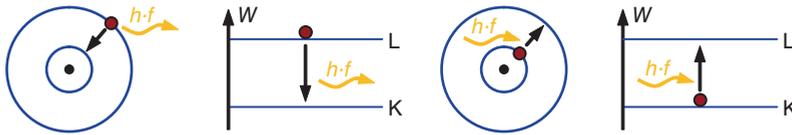
Figure 3.2   Schematic depiction of the emission (left) and absorption (right) of light

The opposite case is shown in the right-hand part of Figure 3.2: A light particle hits an electron and is "swallowed." The energy released in this lifts the electron from the K to the L shell. This process is called the **absorption of light**.

Example 3.1   Light emission

An electron of a hydrogen atom falls from the M to the L shell. What will be the wavelength of the radiated light?

Calculation:

$$\Delta W = W_1 - W_2 = 12.1\,\text{eV} - 10.2\,\text{eV} = 1.9\,\text{eV} = h \cdot f$$

$$\Rightarrow f = \frac{1.9\,\text{eV}}{h} = \frac{1.9\,\text{V} \cdot 1.6 \cdot 10^{-19}\text{As}}{6.6 \cdot 10^{-34}\text{Ws}^2} = 0.461 \cdot 10^{15}/\text{s} = 461 \cdot 10^{12}\text{Hz}$$

The wavelength is calculated again by:

$$\lambda = \frac{c_o}{f} = \frac{3 \cdot 10^8\,\text{m/s}}{461 \cdot 10^{12}\,\text{Hz}} = 6.508 \cdot 10^{-7}\,\text{m} = 650.8 \cdot 10^{-9}\,\text{m} \approx 651\,\text{nm}$$

The light radiates at 651 nm and thus in the red region.

∎

3.1.2   Periodic Table of the Elements

Table 3.1 shows a section of the Periodic Table of the elements. The rows of the table provide the highest shells that are occupied by electrons. The **value** is also obtained from the respective column of an element. This is understood to be the number of electrons in the outer shell and is often called the **valence**. For instance, we recognize that the noble gas helium (He) has two electrons and thus fully occupies the K-Shell. In the following lithium (Li), the K-shell is also occupied; the third electron is situated on the L-shell. The electrons of the outermost shell are called **valence electrons** as they are decisive in the bonding of atoms.

Example 3.2   Valence electrons of silicon

The element silicon (Si), extremely important for photovoltaics, has the atomic number 14 and is situated in the fourth main group. The K and L shells are full, there are four electrons in the topmost shell. The Si atom thus possesses four valence electrons.

∎

Table 3.1 Extract from the Periodic Table of Elements. The number under the element name is the atomic number

Main group/valence								Shell
I	II	III	IV	V	VI	VII	VIII	
H Hydrogen 1							He Helium 2	K
Li Lithium 3	Be Beryllium 4	B Boron 5	C Carbon 6	N Nitrogen 7	O Oxygen 8	F Fluorine 9	Ne Neon 10	L
Na Sodium 11	Mg Magnesium 12	Al Aluminum 13	Si Silicon 14	P Phosphorous 15	S Sulfur 16	Cl Chlorine 17	Ar Argon 18	M
K Potassium 19	Ca Calcium 20	Ga Gallium 31	Ge Germanium 32	As Arsenic 33	Se Selenium 34	Br Bromine 35	Kr Krypton 36	N
Rb Rubidium 37	Sr Strontium 38	In Indium 49	Sn Tin 50	Sb Antimony 51	Te Telluride 52	J Iodine 53	Xe Xenon 54	O

3.1.3 Structure of the Silicon Crystal

When the electrons of neighboring atoms make fixed connections, then a regular lattice structure can be formed. Such a structure is called a **crystal**. With silicon, each valence electron makes a connection with an electron of the neighboring atom. The lattice formed in this way is shown in Figure 3.3 as a sphere and as a two-dimensional depiction.

In this, the **atomic nucleus** together with all internal shells is drawn as a circle. The correct designation is Si^{4+}, as the 14 protons in the nucleus together with the 10 electrons on the inner shells result in $4\times$ positive charge. At the same time one recognizes that each Si atomic nucleus is surrounded by eight valence electrons. This is called the **noble gas configuration** as they are comparable with the noble gas argon that also has eight electrons in the outer shell (see Table 3.1).
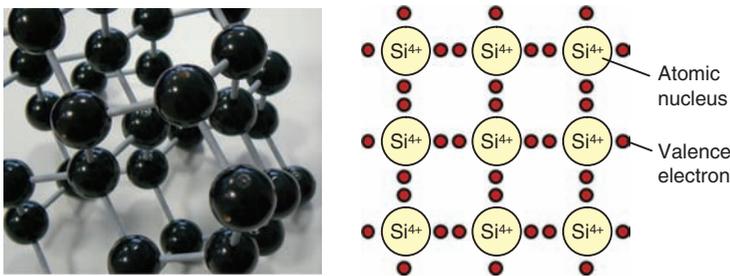
Figure 3.3 Structure of a silicon crystal: The left-hand figure shows the spherical model and the right the two-dimensional depiction
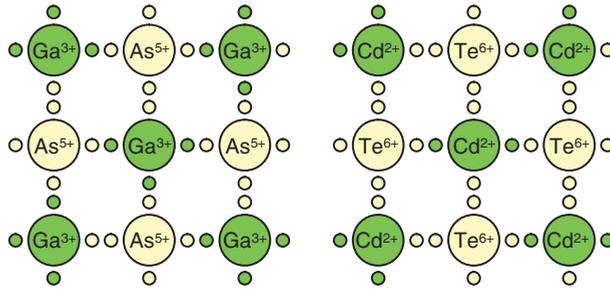
Figure 3.4   Lattice of compound semiconductors of the example GaAs and CdTe

3.1.4 Compound Semiconductors

The lattice considered up to now is made up exclusively of silicon, an element in Group IV. It is possible, however, to combine elements of different main groups. A well-known representative is the material connection **gallium-arsenide (GaAs)** that can ensure high efficiencies in solar cells. It consists of trivalent gallium and pentavalent arsenic atoms and is thus called a ***III/V-semiconductor***. Figure 3.4 shows the structure: The crystal contains at the same time particles of gallium and arsenic atoms that always include their valence electrons in the connection so that the result is again the especially stable noble gas configuration. Besides the III/V-semiconductor, the II/VI-semiconductors are also of interest; Figure 3.4 shows this in the example of cadmium-telluride (CdTe).

3.2 Band Model of the Semiconductor

3.2.1 Origin of Energy Bands

Meanwhile we know that there are defined, discrete levels of energy for the electrons of an individual atom. What happens if we make a thought experiment and bring two atoms close together? There occurs a mutual coupling of the atoms. The result is that the energy conditions change and each state divides into two individual states (see Figure 3.5). An analogy to this phenomenon can be seen from classical mechanics. If one couples two harmonic oscillators (e.g., two guitar strings) then the result are two new resonance frequencies. In the case of three coupled atoms the result is always three new levels, and so on. If one views a semiconductor crystal then a practically infinite number of atoms can be coupled together. Individual levels will hardly still be recognized and in this case one
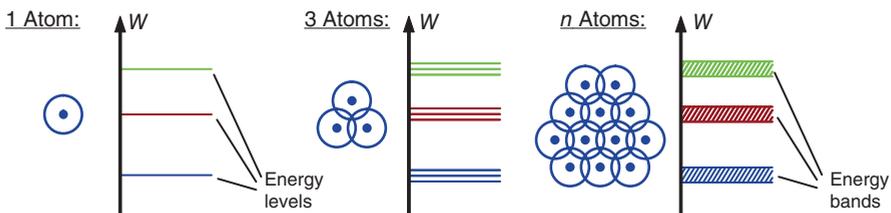
Figure 3.5   Origin of the energy bands in a semiconductor crystal: the coupling of the atoms leads to a spreading of the energy levels. For $n \to \infty$ this results in continuous energy bands
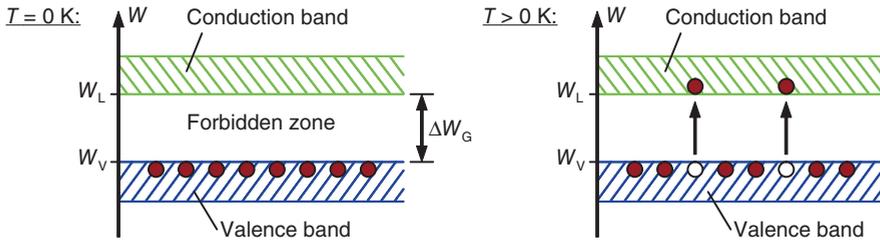
Figure 3.6 Valence and conduction bands for silicon: With rising temperatures individual electrons rise into the conduction band

speaks of **energy bands**. The energy bands show all the energy states that are permitted for an electron.

The highest band still occupied by electrons is decisive for the electrical relationship of a solid-state body. As this is occupied by the valence electrons it is called the **valence band** (see Figure 3.6). The first unoccupied band is called the *conduction band*. In order to enter into the **conduction band**, an electron must first overcome the **forbidden zone**. The width of the forbidden zone decides the amount of energy needed to move out of the valence band into the conduction band. This is also called the **bandgap** ΔW_G. It is the result of the difference of the underside of the conduction band W_L and the upper side of the valence band W_V. In the case of silicon, the bandgap is at $\Delta W_G = 1.12\,\text{eV}$. The index "G" stands for the term *bandgap*.

What does this mean for the electrical behavior of the crystals? In the case of the zero absolute temperature ($T = 0\,\text{K}$) the valence electrons remain fixed in their bonds. In this case the crystal is unable to conduct electrical current as no free charge carriers are available.

> The absolute zero temperature of $T = 0\,\text{K}$ (Kelvin) corresponds to a temperature of $\vartheta = -273.15\,°\text{C}$.

If the temperature is now increased then the electrons start to move due to heat oscillations. If the temperature is increased further, then individual electrons can loosen from their bonds and become available in the crystal as free electrons. In the band model this corresponds to the case where these electrons are lifted out of the valence band, overcome the forbidden zone and arrive in the conduction band. They become **conductor electrons** and increase the conductivity of the crystal.

3.2.2 Differences in Isolators, Semiconductors and Conductors

After we have made the acquaintance of the semiconductor, we will expand to other materials. For this purpose, Figure 3.7 shows the comparison of the band scheme of insulators, semiconductors and metals. In the case of **insulators**, the forbidden zone is very big. Insulators are typically materials whose bandgap is greater than about 3 eV. This means that almost no free electrons are available even at high temperatures. **Semiconductors** at low temperatures also act as insulators. At medium temperatures, however, the conductivity is increased until at very high temperatures (e.g., over 200 °C) they become good conductors (thus the term *semiconductor*).
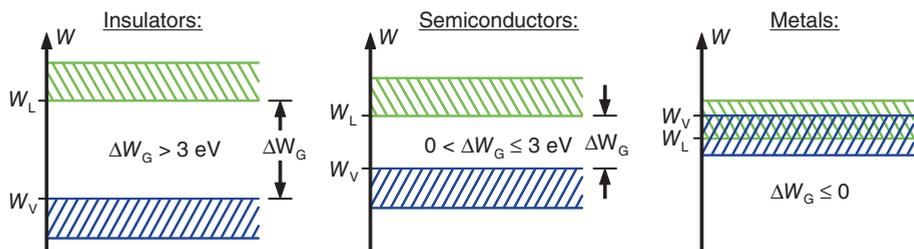
Figure 3.7 Depiction of energy bands of insulators, semiconductors and metals

Table 3.2 Comparison of the bandgaps of various materials

Material	Type of material	Bandgap ΔW_G (eV)
Diamond	Insulator	7.3
Gallium arsenide	Semiconductor	1,42
Silicon	Semiconductor	1.12
Germanium	Semiconductor	0.7

Metals are a special case. With these we can say in simplified terms that their valence and conduction bands overlap so that they possess a high degree of conductivity even at low temperatures.

Table 3.2 shows the bandgaps of various materials.

3.2.3 Intrinsic Carrier Concentration

We will now study the processes in the semiconductor crystal more closely. Figure 3.8 shows the generation of a free electron in the crystal as well as in the band model. As soon as an electron is released from its bonds, there is a gap in the crystal called a **hole**. The whole process is called **electron-hole pair generation**. The reverse process can be seen in the right-hand picture of Figure 3.8: The free electron falls back into the hole and this is called **electron-hole pair recombination**.

The generation and recombination of electron-hole pairs occurs continuously in the crystal. Depending on the semiconductor material and the current temperature there is an average number of free electrons as well as holes, known as the **intrinsic carrier concentration n_i**.
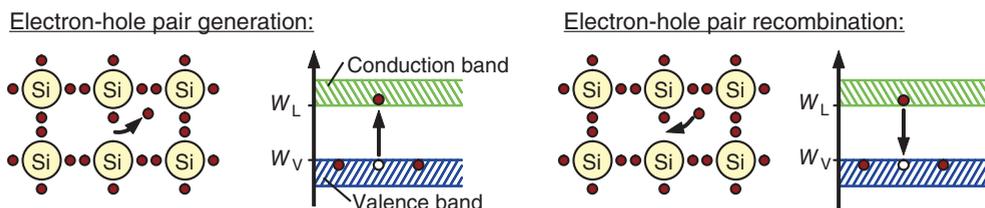
Figure 3.8 Thermal generation and recombination of electron-hole pairs: In a time average there is an average number of free electrons as well as holes, the intrinsic carrier concentration

The index i stands for *intrinsic*. It indicates that this is an **undoped** semiconductor (see Section 3.4).

The intrinsic carrier concentration can be determined by means of the following equation:

$$n_i = N_0 \cdot e^{-\frac{\Delta W_G}{2 \cdot k \cdot T}} \tag{3.3}$$

with

N_0: effective density of states; for silicon: $N_0 \approx 3 \cdot 10^{19}/cm^3$
 k: Boltzmann constant; $k = 1.38 \cdot 10^{-23}$ Ws/K $= 8.62 \cdot 10^{-5}$ eV/K

To a certain extent the **effective density of states N_0** gives the number of free electrons that can be generated in the extreme case (at extreme high temperature). In this, for the sake of simplicity, we have assumed that the effective density of states of the electrons is the same as one of the holes. Each generated free electron leaves a hole in the crystal lattice. Therefore n_i describes the number of free electrons as well as the number of holes.

Example 3.3   Intrinsic carrier concentration

We calculate the intrinsic carrier concentration of silicon at room temperature ($\vartheta = 25°C$) First we calculate the absolute temperature T in Kelvin:

$$T = 273.15 \text{ K} + 25 \text{ K} = 298.15 \text{ K}.$$

Now we insert all values into Equation 3.3:

$$n_i = N_0 \cdot e - \frac{1.12 \text{ eV}}{2 \cdot 8.62 \cdot 10^{-5} \text{ eV/K} \cdot 298.15 \text{ K}} = 1.06 \cdot 10^{10}/cm^3 \approx 10^{10}/cm^3$$

■

3.3   Charge Transport in Semiconductors

3.3.1 Field Currents

Figure 3.9 shows a crystal of silicon that has an electric voltage V applied to it. As in a plate capacitor this voltage leads to an electrical field F in the crystal:

$$F = \frac{V}{l} \tag{3.4}$$

By means of this field the negatively charged electrons are accelerated in the direction of the positive pole of the voltage source. There is thus a flow of current through the semiconductor, which is called **field current** (sometimes **drift current**). However, the electrons in the crystal repeatedly collide against the atomic nucleus, are decelerated and accelerated again by the field. In a timed average they achieve a certain average **drift velocity v_D**.
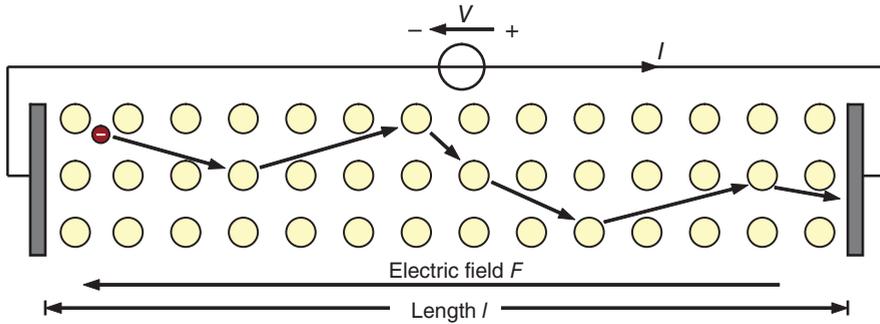
Figure 3.9   Current transport through the silicon crystal: the electrons are repeatedly decelerated by collisions with the atomic nucleus and then accelerated again

The quotient from these achieved drift velocities v_D for an applied field F is called the **mobility μ_N of the electrons**:

$$\mu_N = \frac{v_D}{F} \tag{3.5}$$

It is easy to understand how an **increase in temperature affects the crystal**: The greater the temperature the stronger the oscillations of the crystal lattice. This increases the probability that the accelerated electrons collide with the atomic nuclei.

The average **drift velocity** and thus the mobility of the electrons decrease.

The number of electrons in the volumes of the crystal from Figure 3.9 is N:

$$N = n \cdot \text{volume} = n \cdot A \cdot l \tag{3.6}$$

with

n: electron concentration
A: cross sectional area of the crystal
l: length of the crystal

These electrons are pushed by the electrical field through the crystal in the time $\Delta t = v_D \cdot l$, with the Equation 3.5 for the **field current I_F** this results in:

$$I_F = \frac{\text{Charge}}{\text{Time}} = \frac{q \cdot N}{\Delta t} = q \cdot n \cdot A \cdot \frac{l}{\Delta t} = q \cdot n \cdot A \cdot v_D = q \cdot A \cdot n \cdot \mu_N \cdot F \tag{3.7}$$

with

n: carrier concentration

If the current is now divided by the cross sectional area, the result is the **current density j_F**:

$$j_F = \frac{I_F}{A} = q \cdot n \cdot \mu_N \cdot F \tag{3.8}$$

Besides the current transport by the electrons, there is also **current transport through holes** in the semiconductor. Consider Figure 3.10 for better understanding: because of the applied
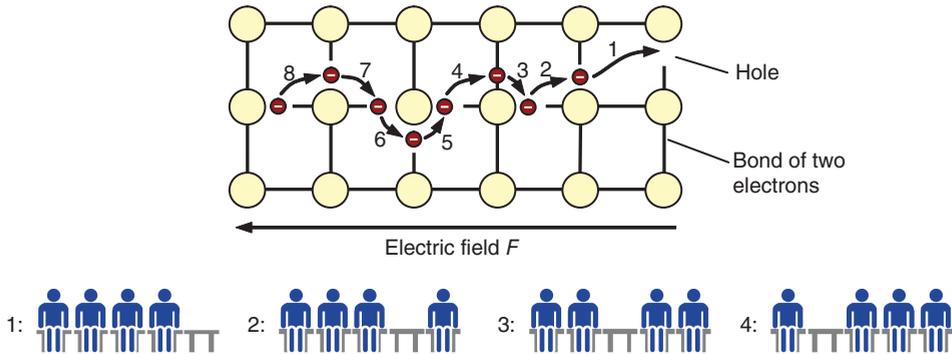
Figure 3.10 Transport of current by means of holes. The electrons move to the right one after the other. Therefore there is a "hole movement" in the opposite direction. The situation is comparable to the movement of people along a row of seats

electrical field, an electron jumps into a neighboring free space. In this way the hole is basically moved in the opposite direction. A similar comparison, for instance, is a soccer stadium. If there is an empty seat at the end of a row and one spectator after the other moves to the next empty seat, then the empty seat "moves" in the opposite direction.

It is obvious that the **hole mobility is lower than that of the electron**. For the mobility of the hole it is necessary that electrons must move one after the other to free spaces, which occurs much slower than the movement of a free electron in the crystal. In silicon, hole mobility μ_P with approximately $450\,cm^2/Vs$ is therefore only a third of the electron mobility μ_N of $1400\,cm^2/Vs$.

3.3.2 Diffusion Currents

Besides the field current there is also a **second type of current** in semiconductors: the **diffusion current**. This comes from the **differences in concentration** in which the necessary energy is provided by the thermal lattice movement. As soon as there is an increased concentration of charge in a place in the crystal (e.g., generated by light, see Section 3.6) then a diffusion current flows until the increased charge carrier concentration is equalized again. The height of the diffusion current is proportional to the gradient (thus the equalization) of the **particle concentration $n(x)$**:

$$j_D = -q \cdot D \cdot \frac{dn(x)}{dx} \tag{3.9}$$

with

j_D: diffusion current density
q: elementary charge
D: diffusion constant

For better understanding we will consider the **analogy** of a **sand heap** (Figure 3.11). This lies on a board that is shaken by a vibrator. The sand flows apart due to the vibration. The
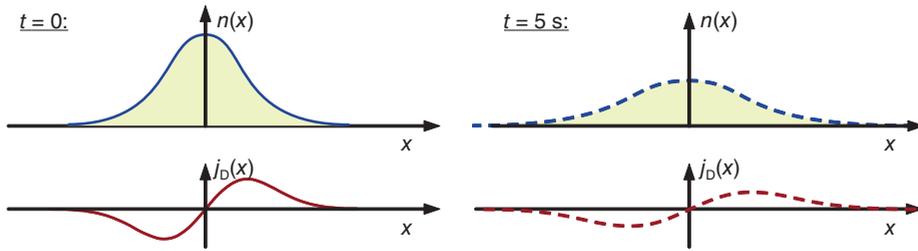
Figure 3.11 Explanation of the diffusion current on a heap of sand. If the vibrator is switched on at a time $t = 0$, then the sand heap flows apart. The highest "sand particle flows" occur at the steepest places of the heap

largest flows of sand will be on the steep sides, whereas the sand particles in the middle practically sink straight to the bottom.

Thus, the slope of the sand heap height $n(x)$ gives the amount of the "sand heap flow." After 5 s the sand heap has already become wider and flatter and consequently the particle flows are less. The process continues until the "sand concentration differences" have been fully reduced, the sand is therefore fully evenly distributed.

3.4 Doping of Semiconductors

As we have seen, to start off with, **semiconductors** are **poor electrical conductors**. They have achieved their particular importance in that their conductivity can be influenced in a targeted manner. For this purpose one introduces foreign atoms into the semiconductor crystal (**doping**).

3.4.1 n-Doping

One speaks of **n-doping** when, instead of the original atom, one installs an atom from Group V (see the Periodic Table in Table 3.1). An example is phosphorous. This atom has one valence electron more than silicon and at the same time an additional proton in the nucleus. If this is inserted into a silicon lattice – as shown in Figure 3.12 – then the result is like the "Journey to Jerusalem." **Four valence electrons** enter into a **bond** with the neighboring atom: The **fifth** finds **no open bond**. Instead it is so weakly connected to the atomic nucleus that it is available as a **free electron** at room temperature. This becomes quite clear when viewing the band diagram: the doping atom generates an additional energy level just below the conduction band edge. Only a very low energy (e.g., 1/50 eV) is required to lift the affected electron into the conduction band. The built-in foreign atom is called a **donor atom** from the Latin *donare*: To give or present. The donor atom more or less "presents" the crystal lattice with a free electron. As the donor atom is only bound to four electrons and at the same time has five protons at the nucleus, in total this is a site-fixed positive charge.

Due to the n-doping, the concentration n of the free electrons rises drastically. At the same time many of these electrons possess free bonds so that there are almost no holes left. In the case of the n-semiconductor the electrons are therefore designated as **majority carriers** and the holes as **minority carriers**. The concentration of the free electrons in n-doped semiconductors is practically only determined by the **density N_D of the donor atoms**: $n \approx N_D$. These increase the conductivity of the crystal and almost turn the semiconductor into a conductor.
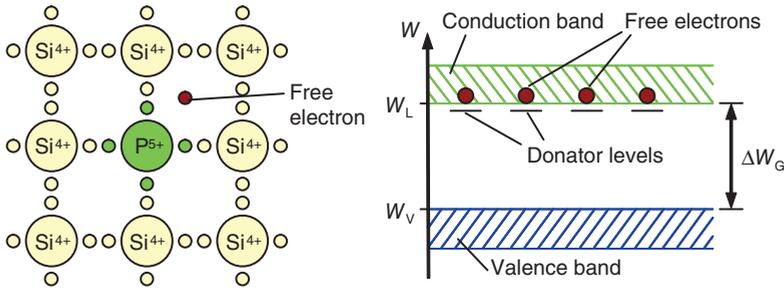
Figure 3.12 n-Doping of semiconductors; one of the five valence electrons of the phosphorous atom is not necessary for the bond and is therefore available as a free electron. Because of the doping there is a new energy level in the band diagram just below the conduction band edge
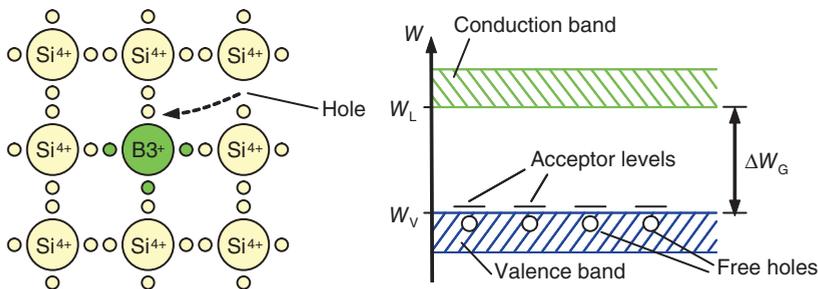
Figure 3.13 Example of p-doping of a silicon crystal with a boron atom: one of the four links remains open as the boron atom can only offer three valence electrons. A neighboring electron moves into this binding and thus "generates" a hole

3.4.2 p-Doping

The second possibility of changing the conductivity of the semiconductor is by **p-doping**: Here, for instance, **trivalent boron atoms** are inserted (Figure 3.13). In this case there are only three valence electrons available so that one bond remains incomplete. A neighboring electron moves into this open bond so that again a noble gas configuration is available for this boron atom. Now there is a missing electron on a neighboring place and thus a hole is formed. In this hole, conductance becomes possible. The trivalent atom is also designated as **acceptor atom**, after the Latin *acceptare*: acceptance. In a certain sense this atom accepts an electron of the crystal. Then the acceptor atom represents a fixed negative charge as it only possesses three protons in its nucleus.

In practice the **doping densities** (donor density N_D and acceptor density N_A) are very low: For instance, only every hundred-thousandth silicon atom is replaced by a doping atom. Yet the conductivity of the material can be increased by many factors of 10.

3.5 The p-n Junction

> **?** Why are we going into such details of semiconductors? They conduct electrical current so poorly and must be doped in order to conduct as well as simple metals!

> In fact the main reason for the victory march of semiconductor electronics is that the combination on n- and p-doping can create components with very special features. An important fundamental of almost all components is the p-n junction that represents a diode in its technical realization.

3.5.1 Principle of Method of Operation

Figure 3.14 shows the principle processes in a p-n junction. The left crystal is n-doped and the right one p-doped. Both **regions** are **electrically neutral**. Thus, on the left side, the number of free electrons is equal to the number of fixed positive donor atoms. The right side corresponds to this where the positively charged holes compensate for the negative charge of the acceptor atoms.

Let us now assume that both regions have just been combined. On the n-side there is a surplus of free electrons. These diffuse due to the **concentration gradient** from the **diffusion current** to the right into the p-doped region, and there they recombine with the holes. In reverse, holes diffuse from the right to the left into the n-region where they recombine with the electrons. Thus there are almost no free electrons and holes in the neighborhood of the junction that the fixed charges could compensate for. Because of the rising number of **superfluous fixed charges** in the junction region, an **electrical field** eventually comes into existence. This field again leads to the electrons being pushed to the left and the holes to the right. Finally a new balance is built up in which **diffusion and field current cancel each other** and a **space charge region** exists at the p-n junction.

This space charge region causes a **potential difference** between the right and left borders of the space charge region that is called the **diffusion voltage V_D**.

In Figure 3.14 we make use of a new drawing convention: Free charge carriers are shown with a border and fixed charges without a border.

> We have already made the acquaintance of a good model for the diffusion current, the sand heap. If we vibrate this long enough the sand becomes fully flat. This should really be the same with the p-n junction: if we wait long enough after
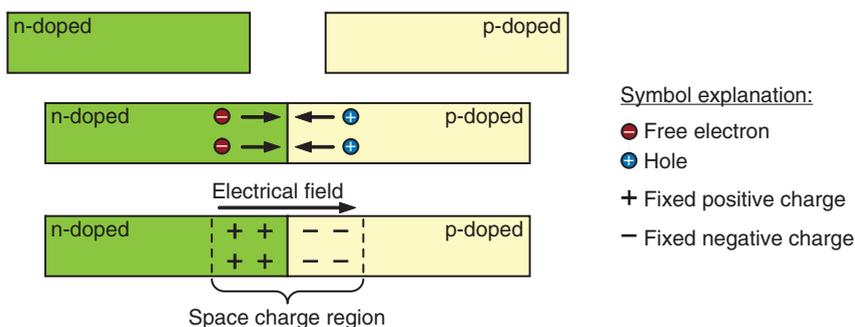
Figure 3.14 The p-n junction: Electrons flow from the n-side to the p-side and there occupy the holes. On the n-side, fixed positive charges remain behind; on the p-side fixed negative charges are generated

> combining the two regions then the electrons should distribute themselves throughout the crystal evenly, or is it not so?

> **[!]** Here it must be noted that there is a decisive difference between the sand particles and the electrons: Sand particles have no charge! The electrons are subjected to the influence of the field of the space charge region and are "pulled back". In this way the flowing apart is slowed down and finally comes to a stop.

In the example shown, the left- and right-hand sides of the space charge region are the same size. This is because each electron that wanders from the left to the right side leaves a fixed positive charge behind on the left side and generates a negative fixed charge on the right (**neutrality condition**). The doping in technical diodes is often carried out asymmetrically. Figure 3.15 shows this on the example $N_D = 2 N_A$: the negative region extends twice as far as the p-region because the individual doping atoms are further apart there. The designation n^+ denotes a **strong n-doping**.

3.5.2 Band Diagram of the p-n Junction

We will now determine the size of the diffusion voltage. One possibility for this is through *Fermi energy*, the maximum energy occupied by an electron at $0\,K$, named after the Italian Physicist and Nobel Prize winner Enrico Fermi (1901–1954).

> **Fermi energy W_F** is generally defined so that the probability for the occupation of this energy level is exactly 50%.

Somewhat clearer (if not physically quite correct) we can describe Fermi energy such that it tells us the average energy of the electrons of a crystal. Thus, for instance, the Fermi energy of an undoped semiconductor is in the middle of the forbidden region as every electron in the conduction band generates a hole in the valence band, and the quantity of possible energy conditions in the conduction and valence bands is the same. However, as soon as the semiconductor is n-doped, then the number of electrons in the conduction band rises and with this so does the Fermi energy W_F (see Figure 3.16(a)).

The reverse case occurs in p-doping: there are hardly any free electrons, most of the electrons are situated in the valence band so that W_F is just above the valence band edge.
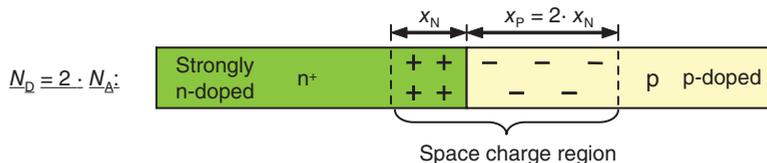
Figure 3.15 Asymmetric doping of the p-n junction: The space charge region extends mainly into the low doping region
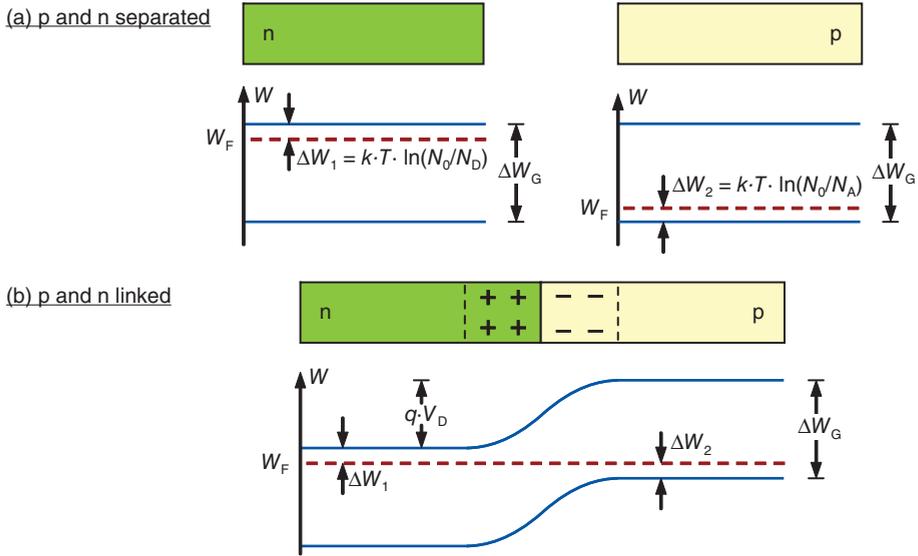
Figure 3.16   Determination of the diffusion voltage V_D of a p-n junction by means of the Fermi energies of n- and p-doped sides [23]

If the p- and n-regions are now brought together, then the Fermi energy in thermal equilibrium must be at the same level in both regions. As shown in Figure 3.16(b), a **potential step q · V_D** builds up that corresponds to the band distance but is reduced about both the **Fermi differences** ΔW_1 and ΔW_2:

$$q \cdot V_D = \Delta W_G - \Delta W_1 - \Delta W_2 \tag{3.10}$$

The Fermi differences are calculated by:

$$\Delta W_1 = k \cdot T \cdot \ln\left(\frac{N_0}{N_D}\right) \tag{3.11}$$

$$\Delta W_2 = k \cdot T \cdot \ln\left(\frac{N_0}{N_A}\right) \tag{3.12}$$

Here the dimension N_0 is the **effective density of states** of the electrons and holes as they have already been applied in Equation 3.3.

Thus the result is:

$$q \cdot V_D = \Delta W_G - k \cdot T \cdot \ln\left(\frac{N_0}{N_D}\right) - k \cdot T \cdot \ln\left(\frac{N_0}{N_A}\right) = \Delta W_G - k \cdot T \cdot \ln\left(\frac{N_0^2}{N_D \cdot N_A}\right) \quad (3.13)$$

$$\Rightarrow$$

$$q \cdot V_D = \Delta W_G - k \cdot T \cdot \ln\left(\frac{N_0^2}{N_D \cdot N_A}\right) \tag{3.14}$$

Example 3.4   Diffusion voltage of a p-n junction

We consider an asymmetric p-n junction with $N_D = 10^{17}/cm^3$ and $N_A = 10^{15}/cm^3$. The result for the diffusion voltage is:

$$q \cdot V_D = 1.12\,eV - 8.62 \cdot 10^{-5}\,eV/K \cdot 298.15\,K \cdot \ln\left(\frac{(3 \cdot 10^{19}\,cm^3)^2}{10^{17}/cm^3 \cdot 10^{15}/cm^3}\right)$$

$$= 1.12\,eV - 0.41\,eV = 0.71\,eV$$

Therefore we obtain a diffusion voltage of approximately 0.7 V.   ∎

3.5.3 Behavior with Applied Voltage

If we apply a **voltage V in the forward direction**, then the electrons are driven by the voltage source into the n-region (Figure 3.17(a)). However, in the region of the junction they are hindered by the field of the space charge region to move into the p-region. They back up at the left border of the space charge region and reduce this by the **neutralization** of the positive fixed charges. The same occurs on the right side with the interlinkage of the holes and fixed negative charges. If we increase V then the space charge region is further reduced until finally it completely disappears. From this point on the current can flow, the "**diode**" **becomes a conductor**. The voltage required for this corresponds to the **diffusion voltage V_D**.

The case of backwards polarity is shown in Figure 3.17(b). Because of the external voltage, the space charge region is enlarged somewhat as free charge carriers are taken out at the borders. Only a minimal reverse current flows in the nA region.
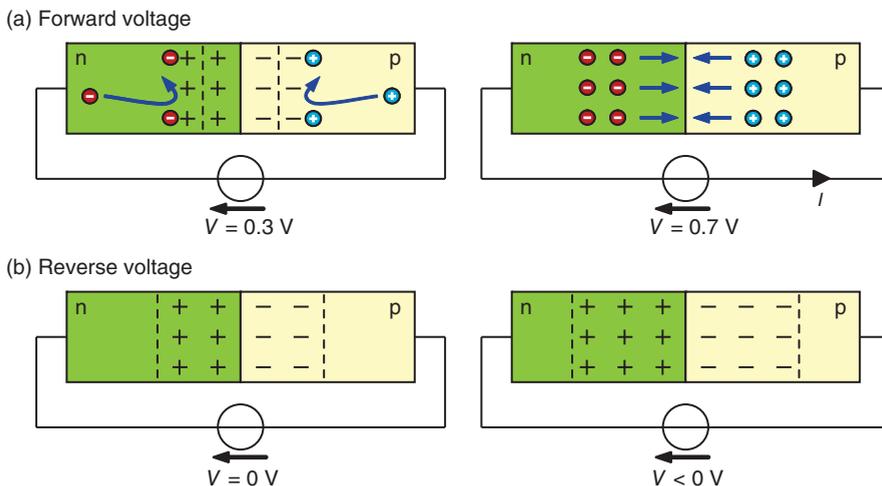
Figure 3.17   Behavior of the p-n junction with applied voltage: when V rises the space charge region is reduced until it finally disappears completely and a current can flow. In the case of reverse voltage the diode blocks and the space charge region is enlarged

3.5.4 Diode Characteristics

For deriving the characteristics, use is made of the knowledge that field and diffusion currents at the p-n junction are the same size. With the Equations 3.8 and 3.9 there is given:

$$j_F = j_D \Rightarrow q \cdot n(x) \cdot \mu \cdot F(x) = -q \cdot D \cdot \frac{dn(x)}{dx} \tag{3.15}$$

This equation is valid for the electrons as well as the holes. A solution for this system of differential equations can be found by means of a longer calculation and simplified assumptions (for instance, see [24]). The result is the so-called **diode** or **Shockley equation**.

$$I = I_S \cdot \left(e^{\frac{V}{V_T}} - 1 \right) \tag{3.16}$$

with

I_S: saturation current of the diode
V_T: thermal voltage

The *saturation current I_S* is determined by:

$$I_S = A \cdot \left(\frac{q \cdot D_N \cdot n_i^2}{L_N \cdot N_A} + \frac{q \cdot D_P \cdot n_i^2}{L_P \cdot N_D} \right) \tag{3.17}$$

with

L_N, L_P: diffusion lengths of the electrons or holes

Therefore it depends on the concrete structure (doping, area of the junction, etc.) of the p-n junction and is typically in the nA to µA region. The **diffusion lengths** L_N and L_P define what distance a free particle travels on average in the foreign region until it recombines. This dimension will be discussed in greater detail in Section 4.2. The size of **thermal voltage V_T** used in Equation 3.16 can be determined by means of the following equation:

$$V_T = \frac{k \cdot T}{q} \tag{3.18}$$

Example 3.5 Thermal voltage at room temperature

The following thermal voltage occurs at room temperature ($T \approx 300\,\text{K}$):

$$V_T = \frac{k \cdot T}{q} = \frac{8.62 \cdot 10^{-5}\,\text{eV/K} \cdot 300\,\text{K}}{q} = 25.89\,\text{mV} = 26\,\text{mV}$$

∎

At room temperature ($T \approx 300\,\text{K}$) the thermal voltage is approximately $26\,\text{mV}$.

Figure 3.18 Symbol and *I*/*V* characteristic curve of a p-n diode: in the forward direction the diode only conducts from the threshold voltage V_{Th}, in reverse direction, there are high currents in the case of exceeding the breakthrough voltage V_{Br}

The typical characteristic curve of a p-n diode that is shown in Figure 3.18 can be taken from the Shockley equation. The exponential function results in a seeming kink in the characteristic after which the current rises drastically. This occurs at the **threshold voltage V_{Th}** that corresponds in amount approximately to that of the diffusion voltage V_{D}.

If one applies a **strongly negative voltage** to the semiconductor diode, then the **electrical field** is increased in the space charge region. This accelerates the available free electrons.

If the negative voltage is increased further, then at some point the electrons reach such a high speed that they knock further electrons out of the crystal bonds. These, in turn are also accelerated and increase the effect. Thus we speak of an **avalanche effect** or **avalanche breakthrough**. At a later point we will return to our knowledge of the p-n junction when dealing with solar cells.

3.6 Interaction of Light and Semiconductors

3.6.1 Phenomenon of Light Absorption

We learned of the effect of light absorption on individual atoms when discussing the Bohr's atomic model (see Section 3.1.1). The behavior of the semiconductor is similar. In place of the individual energy levels, however, the bandgap ΔW_{G} is decisive here for the absorption behavior.

3.6.1.1 Absorption Coefficient

Figure 3.19 shows the effect of the light absorption in the semiconductor crystal. Incident light photons lift individual electrons from the valence into the conduction band. In order to trigger this effect, the energy W_{Ph} of the photons must be greater than the bandgap:

$$W_{\text{Ph}} = h \cdot f = \Delta W_{\text{G}} \tag{3.19}$$

What is the effect of the light absorption in the solid-state body? Figure 3.19 shows the incidence of a light ray in a semiconductor crystal. In passing through the crystal the irradiance *E* sinks continuously due to absorption. The **course of the irradiance** in the absorbing material
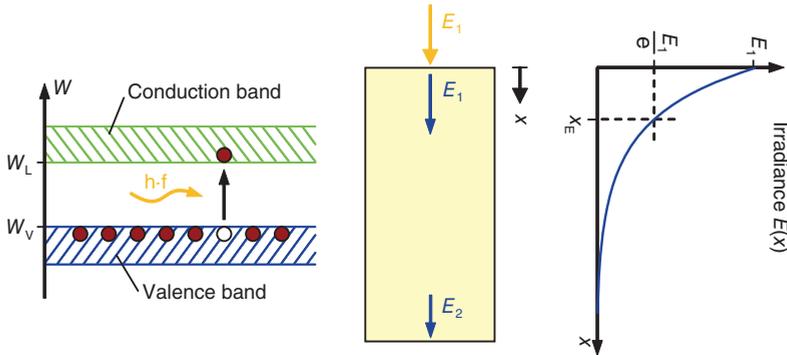
Figure 3.19 Principle of light absorption in the semiconductor. (Left); the photon is absorbed only with sufficient light energy and an electron is raised into the conduction band. (Right); incidental light radiation into a semiconductor crystal: Due to absorption in the material the light intensity sinks with increasing penetration depth

can be described by means of a **decaying exponential function**:

$$E(x) = E_1 \cdot e^{-\alpha \cdot x} \tag{3.20}$$

with

E_1: irradiance at $x = 0$
α: absorption coefficient

The **absorption coefficient** α indicates the absorption "ability" of the respective material. Occasionally use is made of the **penetration depth x_p**. This describes according to which light path the intensity has decayed by the 1/e times (thus approximately 37%). The connection between the two quantities is given by the following equation (see Exercise 3.3):

$$x_P = \frac{1}{\alpha} \tag{3.21}$$

Example 3.6   Penetration depth of silicon

In the visible spectrum ($\lambda = 600$ nm), crystalline silicon (c-Si) has an absorption coefficient of approximately 4000/cm. From this the result with Equation 3.21 is a penetration depth of 2.5 μm. ∎

3.6.1.2   Direct and Indirect Semiconductors

In order to understand why different materials possess greatly different absorption coefficients we must study the interactions between light and the semiconductor crystal more closely. A semiconductor crystal is a system of coupled oscillating lattice particles and for this reason the energy of the lattice oscillations cannot take on every desired state. Similar to a photon, these lattice oscillations can also be allocated to a particle character. Such a particle is called a **phonon**. With this model we can describe the optical generation of an electron-hole pair as an impact process for which both energy as well *as conservation of momentum* must apply. An incidental **photon** has a relatively **high energy** but only a **low momentum**. In contrast a **phonon** has **low energy** but at the same time **high momentum**.
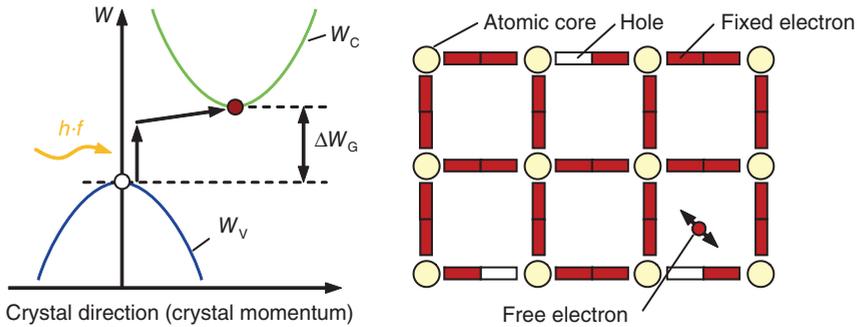
Figure 3.20 Simple model for understanding an indirect semiconductor: In order for it to absorb the photon, the electron must change its energy as well as its direction of oscillation

Semiconductor materials are divided into **two groups**: indirect and direct semiconductors. With an **indirect semiconductor** (e.g., Si) the minimum of the conduction band edge is situated at a different crystal momentum to the maximum of the valence band edge (Figure 3.20).

This means that an electron-hole pair can only be formed with the participation of a phonon. In the case of a **direct semiconductor**, however, no phonon is necessary as here the minimum of the conduction band and the maximum of the valence band exist with the same crystal momentum (Figure 3.21).

In order to really understand these processes we should go into the details of solid-state physics (see, for instance, [25]). Instead, we will select a **simple mechanical model** for description. Let us view Figure 3.20 again. The x axis now shows the oscillation direction of an electron. We see that the minimum of the conduction band is positioned in a different oscillation direction to the maximum of the valence band. If a photon with energy $W_{Ph} \geq \Delta W_G$ is to lift an electron into the conduction band then the electron must not only change its energy, but also its oscillation direction at the same time.

In the crystal model on one hand, we show this in that the holes here are not shown as circles but as slots. On the other hand we represent a free electron as a to-and-fro swinging sphere that can only exist when it achieves a **diagonal oscillation direction**. This only occurs when the electron collides with the nucleus of an atom (more or less when it takes up an additional momentum from the lattice).
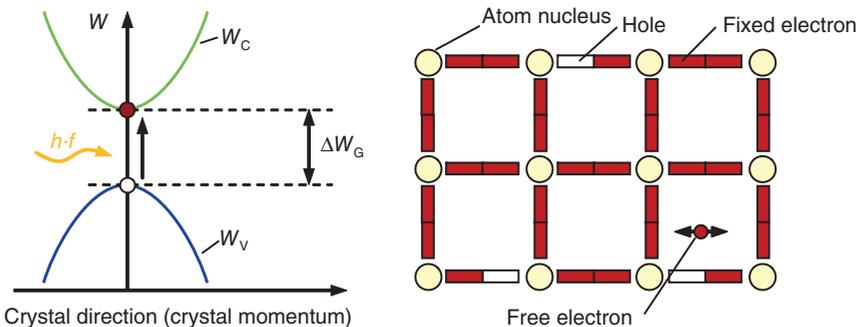
Figure 3.21 Situation in the direct semiconductor: A free electron can be generated by means of absorption in that it changes only its energy but not its direction of oscillation

Table 3.3 Comparison of the absorption coefficients of different materials for light of the wavelength 600 nm [26–28]

Material	Type	Bandgap ΔW_G (eV)	Absorption coefficient α (cm^{-1})	Penetration depth x_p (μm)
c-Si	Indirect	1.12	4000	2.5
a-Si	Direct	1.7	40 000	0.25
CdTe	Direct	1.45	37 000	0.3
GaAs	Direct	1.42	47 000	0.2

As this coincidence is relatively unlikely, a photon moves comparatively far into an indirect semiconductor crystal before it is absorbed. For this reason **indirect semiconductors** like silicon or germanium only possess a **low absorption coefficient**.

The position is different with a **direct semiconductor** (Figure 3.21). The absorption of a photon can take place in that the electron is torn out of its bond without the direction of oscillation being changed. The result is that absorption is relatively probable and thus a **high absorption coefficient** is given. Table 3.3 lists the absorption properties of various direct and indirect semiconductors.

The strongly differing absorption behavior of individual semiconductors is shown even more clearly in Figure 3.22. In the case of direct semiconductors the absorption coefficient rises steeply above the bandgap energy. In crystalline silicon, however, the rise is much more moderate, resulting overall in an relatively low absorption coefficient.
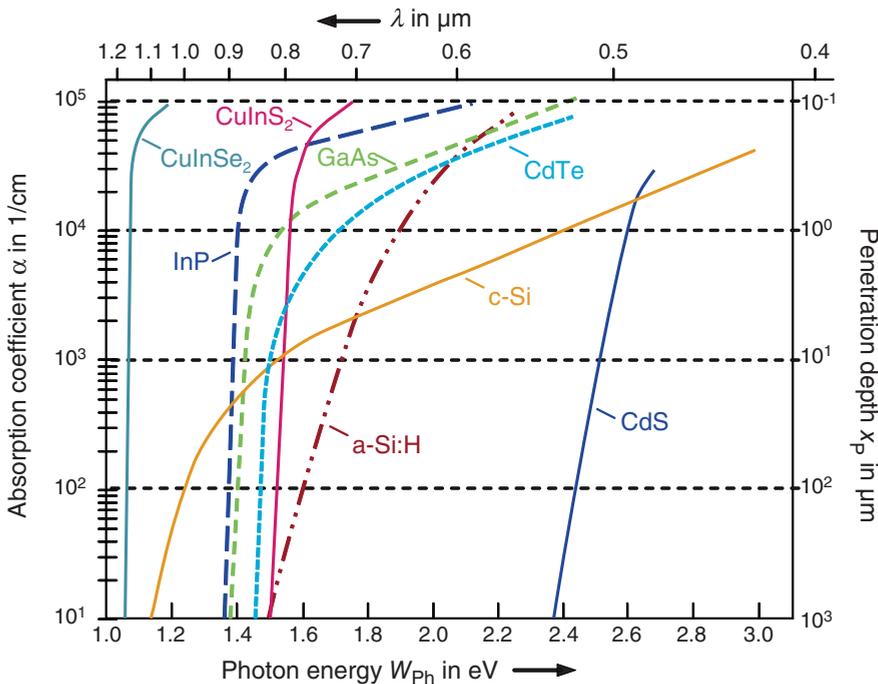
Figure 3.22 Absorption coefficient of different semiconductor materials in dependence of the photon energy: The direct semiconductors show a steep rise in the absorption above the bandgap energy [26–28]

3.6.2 Light Reflection on Surfaces

3.6.2.1 Reflection Factor

We will consider two materials with different *refractive indices* n_1 and n_2 (see Figure 3.23 left). The **refractive index n** of a material indicates by which factor the speed of light is reduced compared to its speed in a vacuum: $n = c_0/c$. If the ray of light falls on an interface between two materials then *reflection* is the result. The strength of the reflection is given by the **reflection factor R** [29]:

$$R = \frac{E_R}{E_0} \tag{3.22}$$

with

E_0: incident irradiance
E_R: reflected irradiance

For vertical incidental radiation the reflection factor is calculated according to the following equation:

$$R = \left(\frac{n_1 - n_2}{n_1 + n_2}\right)^2 \tag{3.23}$$

Example 3.7   Reflection on a silicon surface

In the case of silicon the refractive index is in the visible spectrum at approximately $n = 3.9$ [30]. If a ray of light ($n = 1$) impinges vertically on the silicon surface, this results in a reflection factor of:

$$R = \left(\frac{1 - 3.9}{1 + 3.9}\right)^2 = \left(\frac{-2.9}{4.9}\right)^2 = 0.35 = 35\%$$

Thus, approximately one third of the light is reflected.

∎

If, instead of a vertical, one selects a flat incidence of radiation, then the reflection factor rises further. This effect can be seen well on a pane of glass: The more we turn a pane of glass to look at it as flat, the more it acts as a mirror.
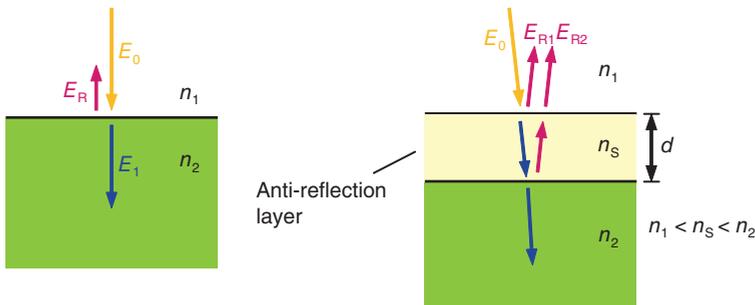
Figure 3.23   Reflection of light on the interface between two media: The reflection can be reduced with the use of an anti-reflection layer (right)

3.6.2.2 Anti-Reflection Coating

The incidental reflection must be reduced in order to achieve a high degree of efficiency in a solar cell. A standard means of doing this is **anti-reflection coating**. Figure 3.23 shows the principle in the right-hand picture: a material of thickness d is inserted between the two media. At the interface there is a reflective ray E_{R1}. There is also a reflection at the transition from n_S to n_2 that appears at the surface with the strength E_{R2}. The trick is to make the layer d so thick that the ray 2 is displaced by $180°$ phase compared to ray 1 so that the reflective radiations cancel each other out due to interference.

> **[?]** I can just imagine that the two reflecting rays could cancel each other out. This doesn't bring anything useful, as in this way no more light penetrates the semiconductor, or is this not the case?

> **[!]** First of all we must admit that the right-hand sketch of Figure 3.23 does not mirror the actual case accurately enough. In fact the ray reflected at the border layer n_S/n_2 is partly reflected again at the front border layer n_S/n_1. This results in an infinite number of continuously weakening to-and-fro reflections. The rays moving downwards have a phase displacement of $360°$ to each other and superimpose themselves constructively (for details see [29]). As a result in the optimum case actually the whole of the incidental light penetrates into the semiconductor.

The conditions for the optimal layer thickness can be determined as follows:

$$d = \frac{\lambda}{4 \cdot n_s} \cdot (2 \cdot m + 1) \tag{3.24}$$

with

m: 0, 1, 2, 3, . . .

In matter the speed of light c and thus the wavelength compared to that in a vacuum is reduced: $\lambda_{\text{Mat}} = \lambda/n_S$. The layer thickness must therefore correspond to an uneven multiple of a quarter wavelength:

$$d = \frac{\lambda_{\text{Mat}}}{4} \cdot (2 \cdot m + 1) \tag{3.25}$$

The remaining reflection factor can now be calculated according to the **Fresnel equations** [29]:

$$R = \left(\frac{n_S^2 - n_1 \cdot n_2}{n_S^2 + n_1 \cdot n_2} \right)^2 \tag{3.26}$$

From Equation 3.26 can be seen that the reflection factor even reaches to zero, when the refractive index n_S is at the geometric average of the two other indices:

$$n_S = \sqrt{n_1 \cdot n_2} \tag{3.27}$$
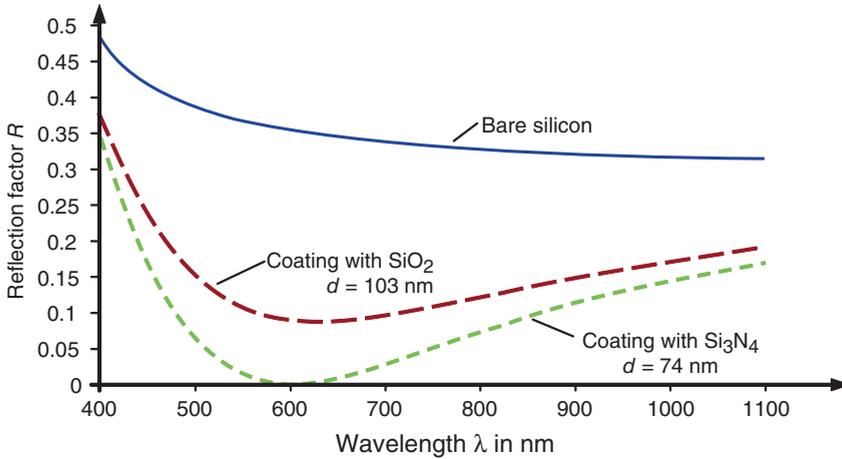
Figure 3.24 Spectral progression of reflection for uncoated and, for silicon oxide or silicon nitride, coated silicon: For both materials the reflection factor can be clearly reduced compared with bare silicon

In reality, however, a complete prevention of reflection is not achievable. Thus, Equation 3.27 cannot be fulfilled optimally as only few suitable materials are available for anti-reflection coatings.

Example 3.8   Anti-reflection coating with SiO$_2$

In the case of silicon the refractive index of $n_S = \sqrt{3.9} = 1.97$ is optimum. The easy-to-use material silicon oxide (SiO$_2$) has a refractive index of 1.46. With Equation 3.26 this gives a reflection factor of $R = \left(\frac{1.46^2 - 1 \cdot 3.9}{1.46^2 + 1 \cdot 3.9}\right)^2 = 8.6\%$

∎

Silicon nitride (Si$_3$N$_4$) is much better and is used today as the **standard material for anti-reflective coatings** of solar cells. It possesses a refractive index of 2.0, which again leads to a remaining reflection factor of less than 1%.

However, it has to be kept in mind that a selected layer thickness can always function only as the optimum for one single wavelength. But with solar cells we want to utilize the largest possible region of the Sun's spectrum. Mostly the layer thickness is defined for minimal reflection at $\lambda = 600$ nm. Figure 3.24 shows the result: With the use of a Si$_3$N$_4$ layer the reflection disappears almost completely at 600 nm and rises at the borders of the viewed spectral region by up to 34%.

A third limitation must be noted, that the considerations made here apply only for vertical incidence. In a flat incidence the path difference changes between the two reflected rays so that an increased reflection also applies here. In Chapter 4 we will discuss further possibilities for reducing the reflection.

4

Structure and Method of Operation of Solar Cells

The basis of photovoltaic power generation is the solar cell. For this reason this chapter will deal with its structure and function in greater detail. We will pay special attention to the question of how to achieve a higher degree of efficiency and will present the current efficiency record of solar cells.

4.1 Consideration of the Photodiode

A good foundation for understanding the solar cell is the photo diode.

4.1.1 Structure and Characteristics

We can represent a photodiode in the simplest case as a p-n junction that is illuminated from the side (Figure 4.1).

Penetrating photons are absorbed and generate free electron-hole pairs. These are separated again by the electrical field prevailing in the space charge region and "brought home": The electrons to the n-side and the holes to the p-side. There they are majority carriers, which reduce the probability of undesired recombinations. Now the generated power can be drawn off at the contacts. As it is generated by photons, it is called **photocurrent I_{Ph}.**

We will assume that every absorbed photon also leads to an electron-hole pair and therefore makes a contribution to the photocurrent. Thus the **photocurrent I_{Ph} is proportional to the irradiance E**:

$$I_{Ph} = \text{const} \cdot E \tag{4.1}$$

The resulting characteristic curve is shown in Figure 4.2.

As long as no light shines on the photodiode it behaves like a normal p-n junction. With a reverse voltage only a small reverse current flows, which is called **dark current**. As soon as light shines on the diode a photocurrent that is independent of the voltage V is added to the

---
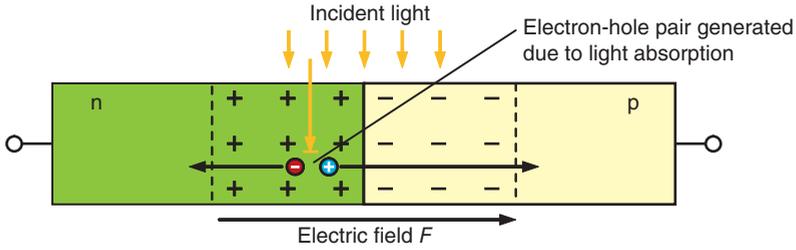
Figure 4.1 Lighted p-n junction: The free electrons and holes generated by light absorption are separated from the field of the space charge region and "brought home"
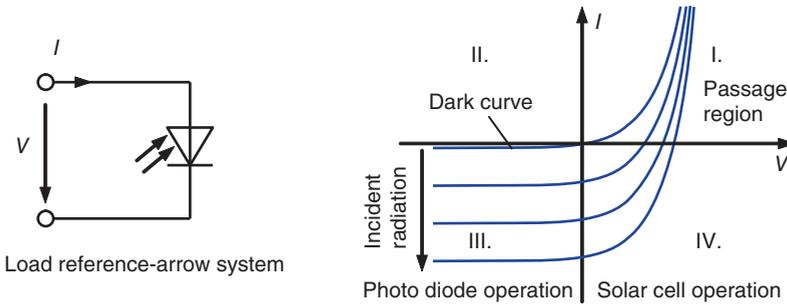
Figure 4.2 Symbol and curves of a photodiode

diode characteristic curve. Because it flows in the reverse direction it displaces the depicted *I/V* curve downwards. The use of the photodiode in quadrant III is called **photodiode operation** as photodiodes are typically operated with applied reverse voltage in order, for instance, to serve as detectors for optical data receivers. In quadrant IV the photodiode is operated as a solar cell: with positively applied voltage the result is a negative current. In the depicted **load reference-arrow system** this means that energy is not used from the device but that energy is generated.

In the user reference-arrow system, the voltage *V* is applied to the device and then the current *I* flowing from the voltage source to the component is counted as positive.

In principle one could also dispense with the p-n junction in the diode. Also in an undoped silicon crystal the absorption of light would lead to the generation of electron-hole pairs. Could one also use this external generation of electrical energy?

Actually electron-hole pairs are generated in an illuminated undoped semi-conductor. This increases the carrier concentration and therefore the conductivity

> of the crystal. Thus, we have an LDR (Light Dependent Resistor). Although this can be used for the measurement of light (e.g., in a twilight switch), it cannot be used for the generation of electrical energy.

4.1.2 Equivalent Circuit

The electrical behavior of the photodiode can be expressed by the Shockley equation (3.16) in combination with the photocurrent.

$$I = I_D - I_{Ph} = I_S \cdot \left(e^{\frac{V}{V_T}} - 1 \right) - I_{Ph} \qquad (4.2)$$

In this the dimension I_S is the **saturation current** already mentioned in the previous chapter:

$$I_S = A \cdot q \cdot n_i^2 \cdot \left(\frac{D_N}{L_N \cdot N_A} + \frac{D_P}{L_P \cdot N_D} \right) \qquad (4.3)$$

Equation 4.2 can be shown by an electrical equivalent circuit (Figure 4.3). In this a current source with the strength I_{Ph} is combined with a passive diode. We will return to this equivalent circuit in the consideration of the solar cell.

4.2 Method of Function of the Solar Cell

4.2.1 Principle of the Structure

What is the structure of a solar cell? Figure 4.4 provides information on this. Basically, like the photodiode it consists of a p-n junction. This is asymmetrically doped, at the bottom is the **p-base** and at the top the heavily doped **n$^+$-emitter**. The terms *base* and *emitter* come from the starting times of the bipolar transistors and have been taken over for the solar cells. If light penetrates the cell, then every absorbed photon generates an electron-hole pair. The particles are separated from the field of the space charge region and moved to the contacts: the holes through the base to the bottom back contact, the electrons through the emitter to the front contacts.

These are small metal strips that transport the generated electrons to the **current collector rail (busbar)**. If a load is connected to the two poles of the solar cell then this can draw off the generated electrical energy.
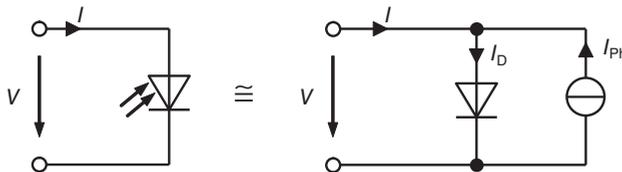
Figure 4.3 Equivalent circuit of the photodiode
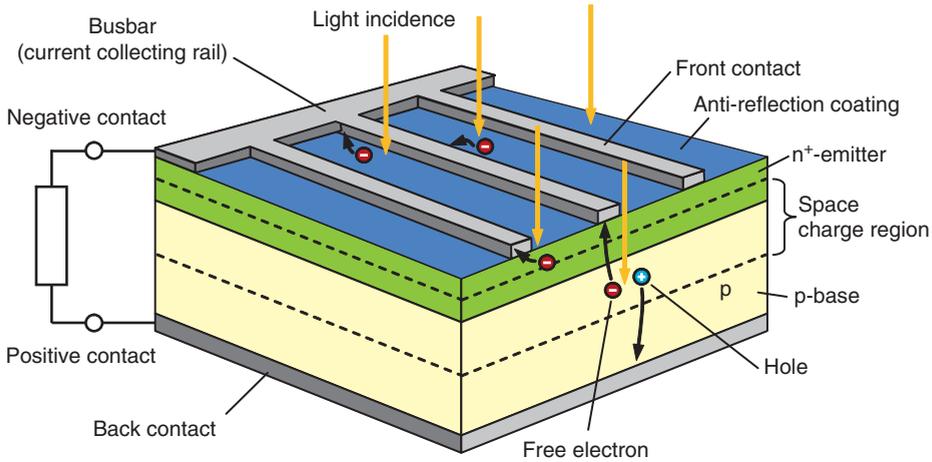
Figure 4.4   Typical silicon solar cell

4.2.2 Recombination and Diffusion Length

Before we consider the method of operation of the cell in greater detail we must acquaint ourselves with the behavior of the minority charge carriers. With incident light, electron-hole pairs are generated by the absorption of photons and these are then available as "surplus" charge carriers. When the source of light is switched off, the particles **recombine** after a short time in order to recreate the starting condition.

The mechanism of greatest importance to us is **imperfection recombination**. It occurs when the theoretically ideal crystal is impure due to **foreign atoms, crystal structure errors** or similar. In this case the forbidden zone is no longer empty but has additional levels (Figure 4.5). Thus, an iron atom in a silicon crystal, for instance, leads to a level in the middle of the forbidden zone but a sulphur atom is situated only 0.18 eV below the conduction band. For an electron, additional levels represent something like **step levels** over which a descent into the valence band becomes simpler and thus more probable. The level of the sulphur atom is easy
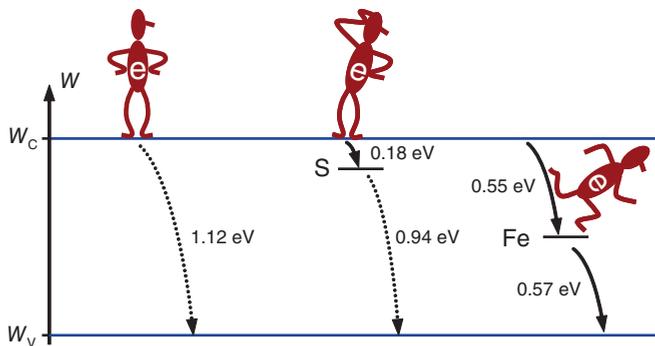
Figure 4.5   Recombination of electron-hole pairs in the case of impurities: the energy level of the foreign atoms form "step levels" with which the transfer of an electron from the conduction to the valence band increases in probability

for the electron to reach from the conduction band, but then it must still bridge almost the whole of the bandgap of $1.12\,\text{eV} - 0.18\,\text{eV} = 0.94\,\text{eV}$. With an iron atom, however, the step height is reduced to $0.56\,\text{eV}$ so that here the recombination probability is extremely large. The **recombination centers** caused by the foreign atoms are also called **traps**. Besides foreign atoms, also crystal errors such as **empty lattice places** or **crystal displacements** lead to increased recombination.

A **crystal surface** is also a disturbance of the ideal, infinitely extended crystal. The electrons of the outer atoms do not find bonding partners and remain as **open bonds**. These then lead to undesired **surface recombinations**.

From this consideration it becomes clear that a crystal used for solar cells should be single crystalline as far as possible and of a high degree of purity. In order to compare various materials one measures the carrier lifetime of a particular material sample. The **carrier lifetime τ_N** defines how long a generated electron exists on average until it recombines again. Depending on the quality of the silicon and the doping concentrations, it lies in the range from ms down to μs.

More useful is the use of the **diffusion length L_N**. This describes the distance a generated electron travels in the semiconductor until it recombines again. It can be calculated from the lifetime of the carrier:

$$L_N = \sqrt{D_N \cdot \tau_N} \tag{4.4}$$

with

D_N: diffusion constant of the electron; $D_N = 35\,\text{cm}^2/\text{s}$ for c-Si

Typical numerical values for silicon, for instance, are between 50 and 500 μm.

4.2.3 What Happens in the Individual Cell Regions?

The situation in the interior of the solar cells is shown in greater detail in Figure 4.6. As we have already seen in Section 3.6.1, light is absorbed differently for different wavelengths. Blue light has the highest absorption coefficient with penetration depths of less than 1 μm, infrared, in comparison, has penetration depths of more than 100 μm. For this reason we will look more closely at the situation of the photocurrent generation at the different depths of the cell.

4.2.3.1 Absorption in the Emitter

Now consider **Photon ①**. It is absorbed in the highly doped emitter. Because of the high degree of doping, the diffusion length is extremely small so that the generated hole probably recombines before reaching the space charge region. The particularly highly doped upper edge of the emitter is also occasionally called the **dead layer** in order to emphasize that this is where the highest recombination probability is situated.

4.2.3.2 Absorption in the Space Charge Region

What happens to **Photon ②**? Absorption takes place within the space charge region. The **field** prevailing in the space charge region separates the generated electron-hole pair and **drives** the two charge **carriers in different directions**. The electron is moved to the n-region and from there further to the minus contact of the solar cell. The hole is moved in the opposite direction. It
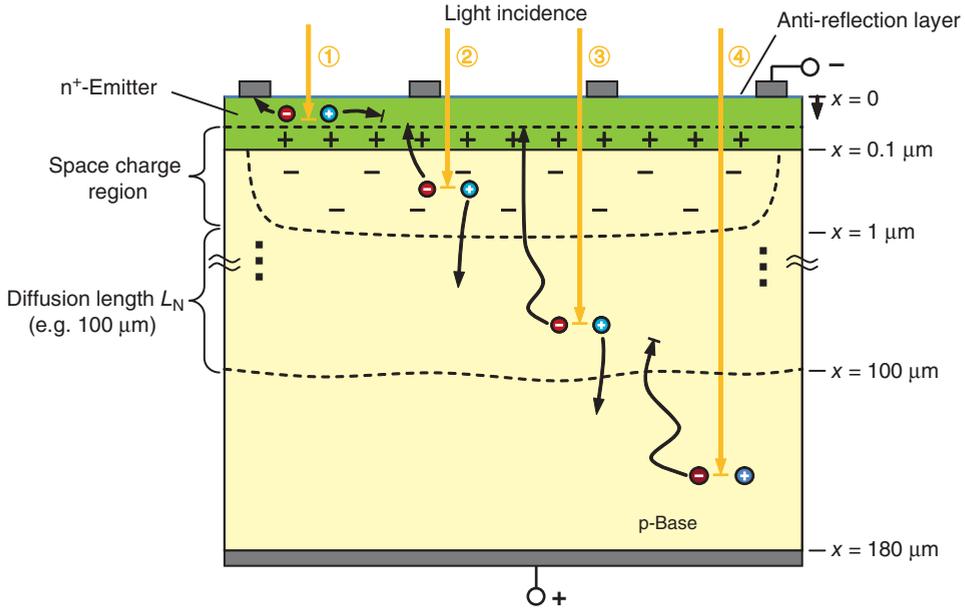
Figure 4.6 Cross section of a solar cell: The individually generated electron-hole pairs have different good chances of making a contribution to the photocurrent

must travel a relatively long way through the base to the plus contact. As it is in the p-region during this movement, the probability of a recombination is slight. Thus, practically all generated electron-hole pairs can be used for the photocurrent.

4.2.3.3 Absorption within the Diffusion Length of the Electrons

Photon ③ is only absorbed deep in the solar cell. The generated **electron** is not situated in an electrical field but **diffuses** as a minority charge carrier that is somewhat motivation-less throughout the crystal. If, by chance, it arrives at the edge of the space charge region then it is pulled to the n-side by the prevailing field where it can flow as a majority carrier to the contact. As the electron was still generated within the diffusion length, the probability that it can save itself up to the space charge region is relatively high.

4.2.3.4 Absorption outside the Diffusion Length of the Electrons

Photon ④ is a **true loser**, and is only absorbed in the lower region of the solar cell. Although the electron diffuses through the p-base, it **recombines** with a hole before it can reach the space charge region. Thus, although an electron-hole pair is formed due to light absorption, an electron and a hole are "eliminated." This has contributed nothing to the photocurrent and with this conversion process the crystal has only become slightly warmer. This consideration has made clear the importance of good crystal quality for a high degree of efficiency. Only in this way is a high diffusion length achieved so that absorbed infrared light rays can even be used deep in the cell.

> [?] Figure 4.6 shows how the generated electrons flow outwards via the upper contacts and the holes downwards. Would the available electrons and holes in cells be used up at some stage?

> [!] This is a misunderstanding regarding the thought model of the holes. In fact the holes are only positions in which the electrons are missing, see Section 3.3.1. In the solar cell it means that electrons flow away at the upper contact through the outer current circuit and then return into the cell at the lower contact. The holes that come to meet them mean the electrons "slip" in the opposite direction. An electron flowing from the bottom of the cell fills a hole so that this electron-hole pair can then be "regenerated" by means of light absorption. Therefore electrons and holes are not "used up".

4.2.4 Back-Surface Field

A special danger for the electrons that are generated in the lower region of the solar cell is the metal semiconductor interface, as massive surface recombinations can occur there. A normal trick for containment of this danger is the application of a highly doped p^+-layer between metal and semiconductor. This is achieved, for instance, by doping with boron or aluminum atoms.

How does this trick work? Because of the concentration gradient, holes flow out of this highly doped p^+-layer into the p-region and leave site-fixed negatively charged acceptor atoms behind. The generated electrical field is called ***Back-Surface-Field*** **(BSF)**. It acts like an electric mirror that returns the electrons generated by means of absorption in the direction of the space charge region. The probability of an undesired recombination at the rear of the cell is thus greatly reduced.

An alternative way of viewing in order to understand this effect is shown in the band diagram (Figure 4.7). Analogous to Figure 3.16, we first give thought to which Fermi energy the individual regions of the cells possess. After the merge, the result is the depicted band process. At the transition of the p^+ to the p-layer the resulting small **potential step** that prevents the electrons from moving further up to the back contact can be seen. Besides being an **electric mirror**, the BSF function has a further advantage. The whole of the voltage drop at the cell is now divided in the potential level at the actual p-n junction and the additional level at the pp^+ interface. The thus reduced voltage at the p-n junction leads to a reduced dark current and then finally to an **increase in the open circuit voltage** V_{OC} [31].

4.3 Photocurrent

On the one hand, the amount of the photocurrent depends on the number of incident photons that are absorbed by the solar cell. On the other hand, the electron-hole pairs generated by light absorption must be separated and brought home safely. We will look at the conditions for this more closely.
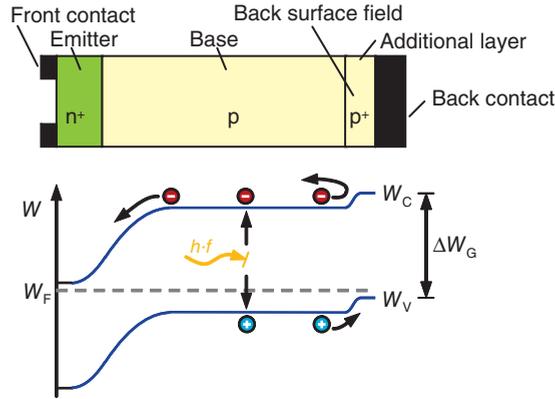
Figure 4.7 Effect of the *Back Surface Field*: The generated electrons are stopped by the layer-forming potential step at the pp$^+$-interface and driven back into the p-region [11]

4.3.1 Absorption Efficiency

Figure 4.8 shows the light absorption of a solar cell similar to Figure 3.19. One part E_R of the overall irradiance E_0 is reflected at the surface (see Section 3.6.2). Thus the portion $E_1 = (1 - R) \cdot E_0$ penetrates into the cell. The intensity of the light is now weakened by absorption by passing through the cell according to Equation 3.20. At the bottom end $E_2 = E(x = d) = E_1 e^{-\alpha \cdot d}$ still remains. The difference $E_{Abs} = E_1 - E_2$ gives the portion of the light absorbed in the cell.

We define the **absorption efficiency** η_{Abs} as the relationship between the number of absorbed photons and the number of photons incident from outside.

$$\eta_{Abs} = \frac{\text{Number of absorbed photons}}{\text{Number of incident photons}} = \frac{N_{Ph\_Abs}}{N_{Ph}} = \frac{E_{Abs}}{E_0} = \frac{E_1 - E_2}{E_0} \tag{4.5}$$
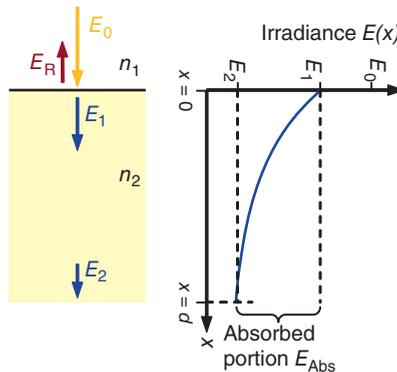
Figure 4.8 Light absorption in the solar cell

After inserting the above equations we get:

$$\eta_{Abs} = (1 - R) \cdot (1 - e^{-\alpha \cdot d}) \tag{4.6}$$

with

R: reflection factor
α: absorption coefficient

η_{Abs} can reach values almost to 100%. For this, on the one hand, the reflection on the surface must be reduced (e.g., by means of an anti-reflection layer, see Section 3.6.2). On the other hand, the cell should be made thick enough that for $x = d$ almost no photons are left over. The problem here is that the absorption coefficient is strongly dependent on the wavelength. Light in the near infrared region is absorbed relatively weakly.

Example 4.1   Absorption of infrared light

Infrared light with a wavelength $\lambda = 1000$ nm has an absorption coefficient of approximately 50/cm; according to Equation 3.21, this, corresponds to a penetration depth of 200 μm. For a cell thickness of 200 μm a portion of $1/e \approx 37\%$ is lost as unused (assume: $R = 0$). If one wishes to make the cell thick enough that a maximum of 1% of the light is lost then the minimum thickness according to Equation 4.6 is:

$$0.99 = 1 - e^{-\alpha \cdot d} \rightarrow e^{-\alpha \cdot d} = 1 - 0.99 \rightarrow d = \frac{\ln(1 - 0.99)}{-\alpha} = 921 \, \mu m$$

The cell in the example would therefore be approximately 900 μm thick. Besides the high costs in the production of such a cell there would still be the problem that the electrons generated in the depth of the cell would recombine on the way to the space charge region. A better solution, for instance, is to provide the back of the cell with an optical reflector. In this way the optical path distance can be doubled for the same thickness of cell.

■

4.3.2   Quantum Efficiency

Even if it is successful in driving the absorption efficiency up to 100%, not all electron-hole pairs generated would contribute to the photocurrent. For this reason one defines the **external quantum efficiency η_{Ext}** as the relationship between the electron-hole pairs usable for the photocurrent and the overall incident photons:

$$\eta = \frac{Number\ of\ usable\ electron\text{-}hole\ pairs}{Number\ of\ impinging\ photons} = \frac{N_{EHP}}{N_{Ph}} \tag{4.7}$$

In addition to the external, we also define the **internal quantum efficiency η_{Int}**, where the losses caused by reflections are not considered:

$$\eta_{Int} = \frac{\eta_{Ext}}{1 - R} \tag{4.8}$$

Naturally, its value is always greater than the external quantum efficiency.

4.3.3 Spectral Sensitivity

The **spectral sensitivity** $S(\lambda)$ shows which photocurrent is generated with the incidence of a particular optical power:

$$S(\lambda) = \frac{I_{Ph}}{P_{Opt}} \tag{4.9}$$

The connection between the two quantities can be easily found when the current is interpreted as a charge Q per time and the optical power as optical energy W_{Opt} per time:

$$S(\lambda) = \frac{I_{Ph}}{P_{Opt}} = \frac{\dfrac{Q}{\Delta t}}{\dfrac{W_{Opt}}{\Delta t}} = \frac{N_{EHP} \cdot q}{N_{Ph} \cdot (h \cdot f)} = \frac{N_{EHP}}{N_{Ph}} \cdot \frac{q}{\dfrac{h \cdot c}{\lambda}} = \frac{q}{h \cdot c} \cdot \lambda \cdot \eta_{Ext}(\lambda) \tag{4.10}$$

The pre-factor $q/(h \cdot c)$ consists only of natural constants and can be combined to:

$$\frac{q}{h \cdot c} = \frac{1.6 \cdot 10^{-19}\,\text{As}}{3.6 \cdot 10^{-34}\,\text{Ws} \cdot 3 \cdot 10^{8}\,\text{m/s}} = 0.808 \cdot \frac{\text{A}}{\text{W} \cdot \mu\text{m}} = \frac{1}{1.24\,\mu\text{m}} \cdot \frac{\text{A}}{\text{W}} \tag{4.11}$$

Thus, finally for spectral sensitivity:

$$S(\lambda) = \frac{\lambda}{1.24\,\mu\text{m}} \cdot \frac{\text{A}}{\text{W}} \cdot \eta_{Ext}(\lambda) \tag{4.12}$$

Figure 4.9 shows the measured curve of the spectral sensitivity of a c-Si standard solar cell as well as a high efficiency cell (see Section 4.7). At the same time the ideal curve for the case of $\eta_{Ext} = 100\%$ is shown. It is noticeable that the **quantum efficiency** in the region of **blue light** (400–500 nm) is relatively **poor**. This is because blue light is absorbed mostly
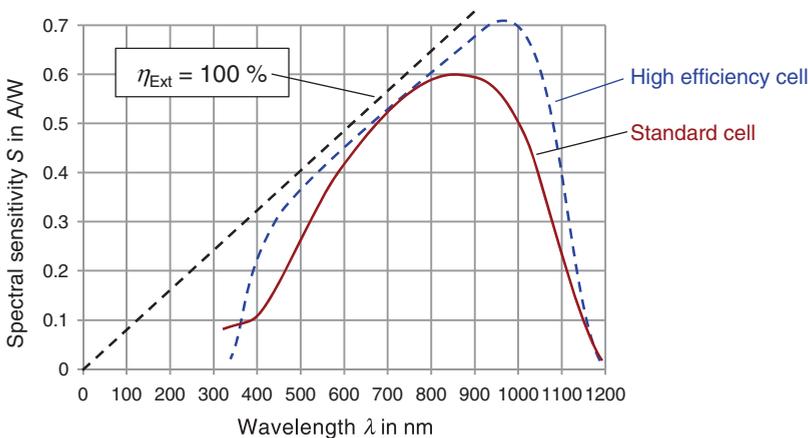
Figure 4.9   Spectral sensitivity of two solar cells: in the blue and infrared regions the measured curves deviate especially strongly from the ideal line [33,34]

in the n$^+$-emitter and a large part of the holes generated recombine there without contributing to the photocurrent. In the infrared spectral region, the η_{Ext} is reduced again as the absorption occurs only in the lower region of the solar cell. **Above 1100 nm** the energy of the light photons becomes too small to overcome the bandgap of the silicon and for this reason $S(\lambda)$ **collapses** relatively suddenly.

4.4   Characteristic Curve and Characteristic Dimensions

The characteristic curve of a solar cell corresponds to the principle of a photodiode. However with the solar cell, the **generator reference-arrow system** is mostly selected (see Figure 4.10).

In the generator reference-arrow system, the voltage V is measured at the energy source and counts the current I flowing from the energy source to the load as positive.

Compared to Figure 4.2 the voltage is maintained, only the prefix of the current is reversed. The generation of energy now takes place in the first quadrant and for this reason mostly only the characteristic curve of the first quadrant of the solar cell is shown. Instead of the symbol for the photodiode, the special **solar cell symbol** has become standard (see Figure 4.10) and we will use it in the following as well.

A typical solar cell characteristic curve is shown in Figure 4.11 including the equivalent circuit that we have become acquainted with from the photodiode. We will call this the **simplified equivalent circuit** as it describes the behavior of the real solar cells only approximately (see Section 4.5).

The characteristic curve equation, similar to Equation 4.2, is:

$$I = I_{\text{Ph}} - I_{\text{D}} = I_{\text{Ph}} - I_{\text{S}} \cdot \left(e^{\frac{V}{m \cdot V_{\text{T}}}} - 1 \right) \tag{4.13}$$

However, we have introduced an **ideality factor m** into the exponent that permits us to better model real solar cell curves. The ideality factor is usually between 1 and 2.
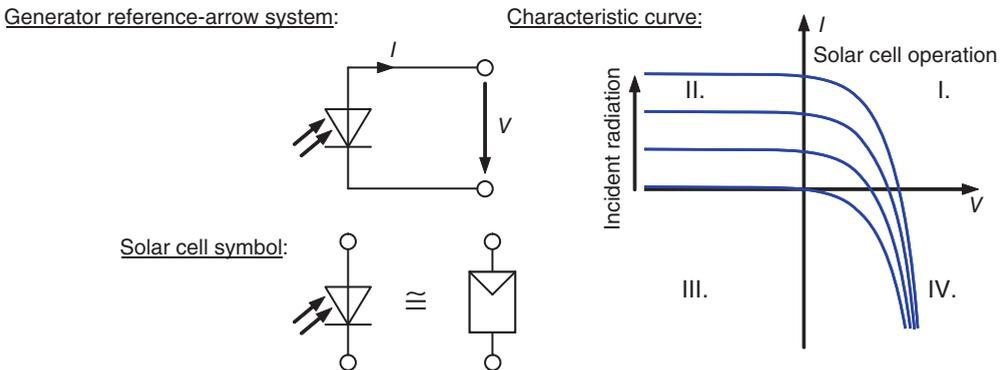
Figure 4.10   Characteristic curves of a solar cell in the generator reference-arrow system
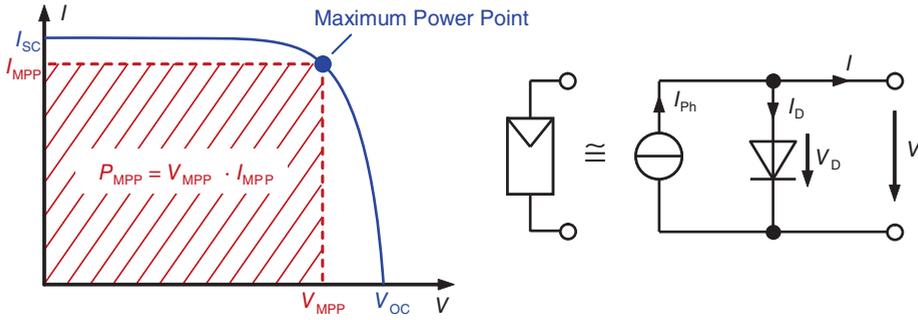
Figure 4.11 Characteristic curve of a solar cell and its associated simplified equivalent circuit

We will consider the individual points of the characteristic curve in Figure 4.11 in more detail in order to derive various parameters of solar cells from them.

4.4.1 Short Circuit Current I_{SC}

The **short circuit current I_{SC}** is delivered by the solar cells when it is short circuited at its connections; the voltage V is thus 0.

With Equation 4.13 this results in:

$$I_{SC} = I(V=0) = I_{Ph} - I_S \cdot (e^0 - 1) = I_{Ph} \tag{4.14}$$

We can thus define:

The short circuit current I_{SC} is equal to the photocurrent I_{Ph}.

This is also immediately clear from the equivalent circuit: an external short circuit also short circuits the internal diode, so that $I_D = 0$ applies. In this way the whole photocurrent I_{Ph} can be taken off outside. From Equation 4.1 we already know that the photon current is proportional to the irradiance E. Therefore we can immediately derive:

The short circuit current I_{SC} of a solar cell is proportional to the irradiance E.

4.4.2 Open Circuit Voltage V_{OC}

The second extreme case occurs when the current becomes zero. In this case the resulting voltage is called **Open Circuit Voltage V_{OC}**.

In order to determine the open circuit voltage we resolve Equation 4.13 according to V and set $I = 0$. The result is $I_{Ph} = I_{SC}$:

$$V_{OC} = V(I=0) = m \cdot V_T \cdot ln\left(\frac{I_{SC}}{I_S} + 1\right) \tag{4.15}$$

Already with very small currents the value of 1 for I_{SC}/I_S can be ignored so that, in a simplified manner the equation becomes:

$$V_{OC} = m \cdot V_T \cdot ln\left(\frac{I_{SC}}{I_S}\right) \tag{4.16}$$

The dependency of the open circuit voltage is thus much lower than that of the short circuit current:

> The open circuit voltage V_{OC} of a solar cell only changes with the natural logarithm of the irradiance E.

4.4.3 Maximum Power Point (MPP)

The solar cell provides different capacities depending on the actual working point in which it is operated. The operating point at which the maximum power is provided is called the **Maximum Power Point** (**MPP**). As the power of a working point always corresponds to the surface $V \cdot I$, this **area** must be the **maximum** in the case of the MPP. This case is shown in Figure 4.11. The current and voltage values associated with the MPP are called I_{MPP} and V_{MPP}.

4.4.4 Fill Factor FF

The *fill factor FF*, describes the relationship of MPP power and the product from open circuit voltage and short circuit current (see Figure 4.12). As depicted, *FF* shows the size of the area under the MPP working point compared to the area $V_{OC} \cdot I_{SC}$:

$$FF = \frac{V_{MPP} \cdot I_{MPP}}{V_{OC} \cdot I_{SC}} = \frac{P_{MPP}}{V_{OC} \cdot I_{SC}} \tag{4.17}$$

The fill factor is a measure for the quality of a cell; typical values for silicon cells are between 0.75–0.85 and in the region of thin film materials they are between 0.6–0.75.
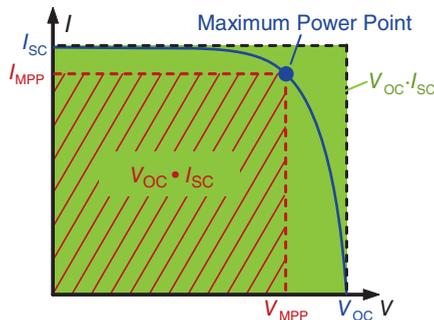
Figure 4.12 The fill factor gives the relationship of the shaded to the gray background surface

For the fill factor, an approximation equation for the dependence of the open circuit voltage is used ("idealized fill factor") [35]:

$$FF = \frac{1 + ln\left(\dfrac{V_{OC}}{V_T} + 0.72\right)}{\dfrac{V_{OC}}{V_T} + 1} \tag{4.18}$$

4.4.5 Efficiency η

The efficiency of a solar cell describes what portion of the optical power P_{Opt} incident on the cell is output as electrical energy P_{MPP} again.

$$\eta = \frac{P_{MPP}}{P_{Opt}} = \frac{P_{MPP}}{E \cdot A} = \frac{FF \cdot V_{OC} \cdot I_{SC}}{E \cdot A} \tag{4.19}$$

with

A: cell area

Typical efficiencies of crystalline silicon cells are **between 15 and 22%**. The calculation of the efficiency is described in Section 4.6 in greater detail.

4.4.6 Temperature Dependency of Solar Cells

A rise in temperature of a semiconductor brings with it an increase in thermal movement of the electrons built into the crystal lattice. From Section 3.2, we know that in this case more and more electrons are torn from their bonds and move into the conduction band and that therefore the **intrinsic carrier concentration n_i rises.**

Higher intrinsic carrier concentration again leads to an **increase in saturation current I_S.**

How does this affect the solar cell? According to Equation 4.16 the increased saturation current leads to a **reduction in open circuit voltage**. For calculating this we use Equations 3.3 and 4.3 in 4.16 and the result is:

$$V_{OC} = m \cdot V_T \cdot ln\left(\frac{I_{SC}}{I_S}\right) = m \cdot V_T \cdot ln\left(\frac{I_{SC}}{B}\right) + m \cdot \frac{\Delta W_G}{q} \tag{4.20}$$

The constant B collates the following expression:

$$B = A \cdot q \cdot N_0^2 \cdot \left(\frac{D_N}{L_N \cdot N_A} + \frac{D_P}{L_P \cdot N_D}\right) \tag{4.21}$$

If the Equation 4.20 is differentiated to T, then, applying Equation 4.20 again, the result is:

$$\frac{V_{OC}}{dT} = \frac{m \cdot k}{q} \cdot ln\left(\frac{I_{SC}}{B}\right) = \frac{V_{OC} - m \cdot \Delta W_G/q}{T} \tag{4.22}$$

For a typical solar cell we obtain ($m = 1$):

$$\frac{\Delta V_{OC}}{\Delta \vartheta} = \frac{0.6\,V - 1.12\,V}{300\,K} = 1.7\,mV/K \tag{4.23}$$

In this derivation we have not yet taken into account that the **bandgap** and the intrinsic carrier concentration of the semiconductor are also **temperature dependent**. A more accurate consideration gives [36]:

$$\frac{\Delta V_{OC}}{\Delta \vartheta} = \frac{V_{OC} - \Delta W_{G0}/q - \gamma \cdot V_T}{T} \tag{4.24}$$

with:

ΔW_{G0}: Bandgap at $T = 0$; for silicon: $\Delta W_{G0} = 1.2$ eV
  γ : Temperature parameter, typically $\gamma = 1 \ldots 4$

Thus, for the Si cell we obtain ($\gamma = 3$):

$$\frac{\Delta V_{OC}}{\Delta \vartheta} = -2.3 \text{ mV/K} \tag{4.25}$$

For a typical open circuit voltage of 600 mV there is thus a temperature coefficient $TC(V_{OC})$ of approx. 0.4%/K.

> The open circuit voltage V_{OC} of a Si solar cell is reduced by 2.3 mV per Kelvin, which corresponds to a temperature coefficient of approximately -0.4% per Kelvin.

The position is different in the case of a **short circuit current I_{SC}**. The **reduction of the bandgap** has the effect that even energy-poor photons still have enough energy in order to be absorbed and to generate an electron-hole pair. For this reason the **short circuit current I_{SC} increases slightly** with increasing temperature, for instance by 0.06%/K.

Figure 4.13 shows the temperature dependency of a monocrystalline cell as an example of the Bosch Solar Cell M-3BB. With rising temperature, the open circuit voltage and thus also the MPP is clearly displaced to the left.

> **[?]** How can I imagine in a descriptive way why the bandgap of the semiconductor is reduced with increasing temperature?

> **[!]** The crystal expands with a rise in temperature. This also increases the mean spacing between the atoms (lattice constant). As a result the attractive force of the positively charged atom nuclei on the negative electrons is reduced, which practically corresponds to a reduction of the bandgap. Although this explanation does not quite cover the physical causes it is still quite descriptive.

The question of how the temperature changes the power is of interest especially for the user of solar cells and solar modules. As the decay of the open circuit voltage is much
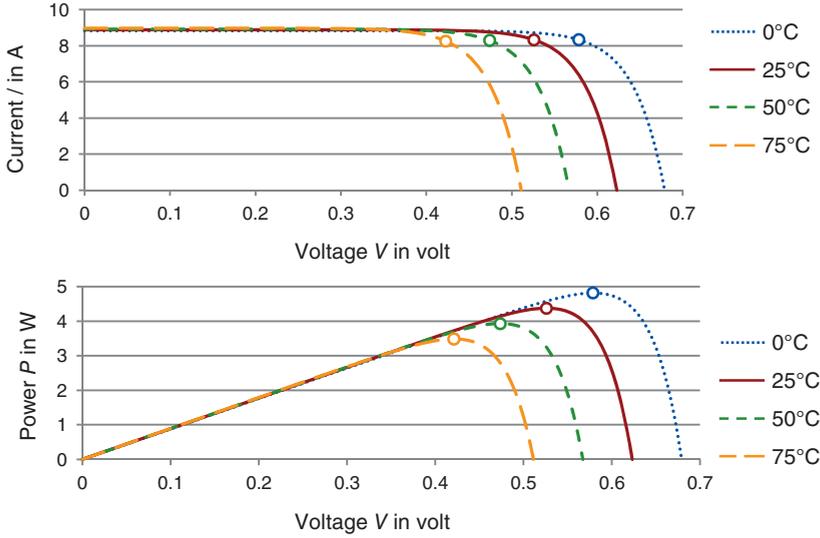
Figure 4.13 Temperature-dependency of a Si solar cell as an example of the Bosch Solar Cell M-3BB: The circles indicate the position of the MPP [37]

stronger than the slight rise of I_{SC}, the power P_{MPP} also sinks. Added to this is the fact that according to Equation 4.18 the **fill factor** is dependent on V_{OC}/V_T: an increase in temperature increases V_T and thus reduces the fill factor. All three effects finally result in a **temperature coefficient TC_P** of the power of:

$$TC(P_{MPP}) = \frac{\Delta P_{MPP}}{\Delta \vartheta \cdot P_{MPP}} = 0.\dot{4} \ldots 0.5\%/\text{K} \tag{4.26}$$

The **power** of a Si solar cell sinks by 0.4 to 0.5% per Kelvin.

Roughly one can say that the power of a solar cell is reduced by approximately 5% with an increase of temperature of 10 K. As solar modules with full sunlight can easily reach a temperature of 60°C, this means a clear loss of power compared to the assumed 25°C given in the data sheet.

4.5 Electrical Description of Real Solar Cells

4.5.1 Simplified Model

This model is already known from Figure 4.11 and Equation 4.13:

$$I = I_{Ph} - I_D = I_{Ph} - I_S \cdot \left(e^{\frac{V}{m \cdot V_T}} - 1 \right) \tag{4.27}$$
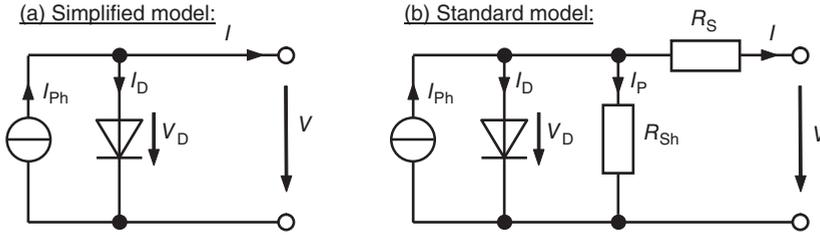
Figure 4.14 Simplified and standard equivalent circuit for electrical description of solar cells and solar modules

4.5.2 Standard Model (Single-Diode Model)

The **standard model**, also called the **single-diode model** goes deeper into electrical losses in the solar cell (Figure 4.14(b)). The **series resistance R_S** describes especially the ohmic losses in the front contacts of the solar cell and at the metal-semiconductor interface. In contrast, leak currents at the edges of the solar cell as well as any point short circuits of the p-n junction are modeled by the **shunt resistance R_{Sh}**.

For deriving the characteristic curves of the standard model the current I becomes $I = I_{Ph} - I_D - I_{Sh}$ and we find I_{Sh} as:

$$I_{Sh} = \frac{V_D}{R_{Sh}} = \frac{V + I \cdot R_S}{R_{Sh}} \tag{4.28}$$

This gives the **characteristic curve equation of the standard model**:

$$I = I_{Ph} - I_S \cdot \left(e^{\frac{V + I \cdot R_S}{m \cdot V_T}} - 1 \right) - \frac{V + I \cdot R_S}{R_{Sh}} \tag{4.29}$$

This equation can only be solved numerically as the current I appears on the left as well as the right hand of the equal sign. The program **PV-Teach** can be found at *www.textbook-pv.org* and characteristic curves according to various equivalent circuits can be calculated with it (see also Figure 4.17).

The influence of the series resistance on the *I/V* characteristic curve is shown in the upper diagram of Figure 4.15. With a **rising value of R_S** the curve flattens and the **fill factor sinks** significantly. The situation is **similar** in the case of **falling values of** the shunt resistance R_{Sh} (lower diagram of Figure 4.15). Here even the open circuit voltage is affected as the rising shunt current I_P causes the diode voltage V_D to drop.

4.5.3 Two-Diode Model

In the derivation of the Shockley equation 3.16 it was assumed for the sake of simplicity that there would be no recombination in the space charge region. Especially for semiconductors with larger bandgaps this leads to deviations between actual and simulated characteristic curves.

In these cases one makes use of the **two-diode model** in which the **diffusion current** is modeled by means of a diode with an **ideality factor of 1** and a **recombination current** through an additional diode with an **ideality factor of 2** (Figure 4.16).
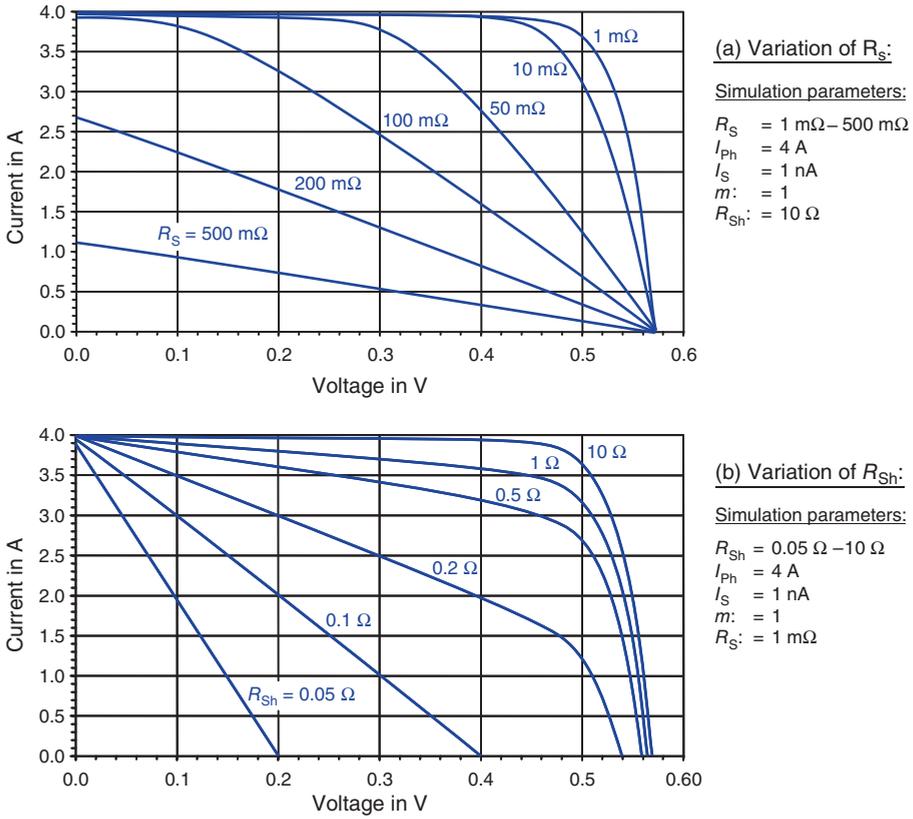
Figure 4.15 Influence of series resistance R_S and shunt resistance R_{Sh} on the solar cell characteristic curve: The fill factor decreases significantly with rising R_S and falling R_{Sh}

The characteristic curve equation can be determined in a similar manner to Equation 4.29:

$$I = I_{Ph} - I_{S1} \cdot \left(e^{\frac{V + I \cdot R_S}{V_T}} - 1 \right) - I_{S2} \cdot \left(e^{\frac{V + I \cdot R_S}{2 \cdot V_T}} - 1 \right) - \frac{V + I \cdot R_S}{R_{Sh}} \qquad (4.30)$$
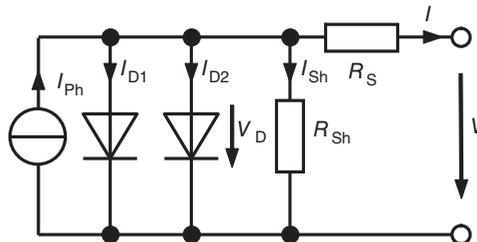
Figure 4.16 The two-diode model for possible exact modeling of the solar cell characteristic curve

Besides the three equivalent circuits presented, use is also occasionally **made of the effective characteristic curve model**. This corresponds to the standard model but without the use of shunt resistance R_{Sh}. Also negative values are permitted for the variable of the series resistance in this model in order to be able to achieve a good approximation quality of measured curves. Details of this can be found in [11].

4.5.4 Determining the Parameters of the Equivalent Circuit

If the measured I/V characteristic curve of a solar cell is available, then the parameters of the simplified equivalent circuit can be derived from it. As described in Section 4.4.1, the photocurrent I_{Ph} may be set as equal to the short circuit current I_{SC}. Besides this, one first takes the diode ideality factor m as 1. The saturation current I_S can then be determined from Equation 4.16:

$$I_S = I_{SC} \cdot e^{-V_{OC}/V_T} \tag{4.31}$$

However, the **agreement** of the curve calculated from these parameters with the original measured curve is **usually poor**. The reason for this is that the ideality factor of real solar cells is greater than 1. Here the only help is a **simulation of the progression of the curve** (e.g., with Excel, Mathematica, etc.) with variations of the two parameters m and I_S until the best possible agreement between simulation and measured curve is reached. Figure 4.17 gives an example of the measured curve of a solar module. The left picture also shows a simulated curve based on the simplified equivalent circuit. Here, there is still a clear deviation between measurement and simulation even after the optimization of the parameters.

The approximation quality with the use of the **standard equivalent circuit** is much better. In the example of Figure 4.17 (right diagram) there is practically **no deviation** between measurement and simulation anymore.

Really **good starting values** for the two resistances R_S and R_{Sh} are obtained from the **curve gradient in the short circuit and open circuit points**. For this purpose we will now consider the **short circuit point**: Here the largest part of the I_{Ph} flows to the outside so that the voltage V_D in Figure 4.14(b) becomes small.
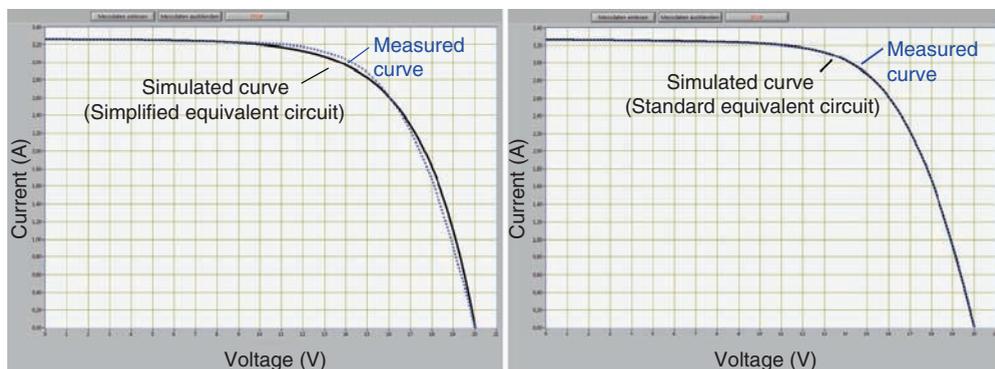
Figure 4.17 Simulation of the curve of a solar module with PV-Teach: The simplified equivalent circuit achieves only an insufficient agreement with the measured curve whereas the standard equivalent circuit shows an almost perfect fit

The current I_D over the diode can therefore be ignored. The remaining characteristic curve equation compared to Equation 4.29 is:

$$I = I_{Ph} - \frac{V + I \cdot R_S}{R_{Sh}} \qquad (4.32)$$

The slope of the curve is found from the derivation:

$$\frac{dI}{dV} = 0 - \frac{1}{R_{Sh}} - \frac{R_S}{R_{Sh}} \cdot \frac{dI}{dV} \qquad (4.33)$$

Resolving the equation according to dI/dV gives:

$$\frac{dI}{dV} = \frac{1}{R_S + R_{Sh}} \qquad (4.34)$$

In general applies $R_S \ll R_{Sh}$ so that we finally write:

$$R_{Sh} = - \frac{dV}{dI}\Big|_{V=0} \qquad (4.35)$$

Thus the **shunt resistance R_{Sh}** can be determined **directly from the slope of the tangent in the short circuit point** (Figure 4.18).

A similar consideration is made for the **open circuit case**: here the voltage V_D is quite large but the diode becomes very low resistant, so that in Figure 4.14(b) the current I_D can be ignored compared to I_{Sh}. The remaining equation from Equation 4.29 is now:

$$I = I_{Ph} - I_S \cdot \left(e^{\frac{V + I \cdot R_S}{m \cdot V_T}} - 1 \right) \qquad (4.36)$$

We differentiate this with respect to the current and rearrange it for dV/dI. In this we take into account that V is dependent on the current I:

$$\frac{d(I)}{dI} = 1 = 0 - I_S \cdot e^{\frac{V + I \cdot R_S}{m \cdot V_T}} \cdot \frac{1}{m \cdot V_T} \cdot \left(\frac{dV}{dI} + R_S \right) \qquad (4.37)$$
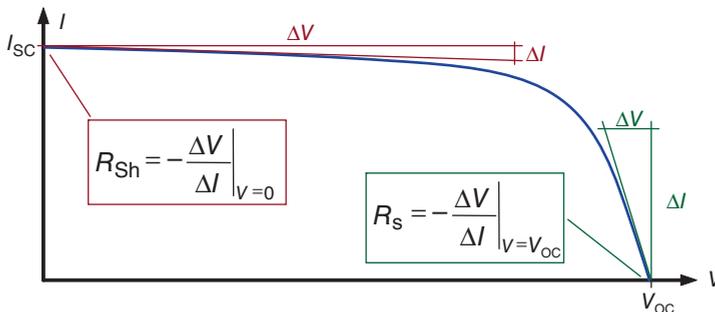
Figure 4.18 Determination of R_S and R_{Sh} from the solar cell characteristic curve: The two resistances can be determined from the gradient in the short circuit or open circuit point

$$\frac{dV}{dI} = -R_S - \frac{m \cdot V_T}{I_S} \cdot e^{-\frac{V+I \cdot R_S}{m \cdot V_T}} \tag{4.38}$$

In the open circuit point there applies $V = V_{OC}$ and $I = 0$, thus the equation simplifies to:

$$\frac{dV}{dI}\bigg|_{V=V_{OC}} = R_S + \frac{m \cdot V_T}{I_S} \cdot e^{-\frac{V_{OC}}{m \cdot V_T}} \approx R_S \tag{4.39}$$

The second term of the sum has been ignored here. This represents the forward resistance of the diode that at the open circuit point is typically significantly lower than R_S. The **series resistance** can thus be determined in that the **gradient of the open circuit point** is measured (see Figure 4.18). In Section 8.2 we will get to know a somewhat more accurate method of determining R_S.

Instead of the ideality factor, a second saturation current as a second unknown variable will be placed in the case of the **two-diode equivalent circuit**. A practical proposal for determining the parameters of the equivalent circuit is shown in [38].

4.6 Considering Efficiency

The efficiency of solar cells is a deciding parameter for using solar energy efficiently and economically. We will now consider, on the one hand, what upper limits physics places on the efficiency and, on the other hand, will learn technologies for approaching these upper limits.

4.6.1 Spectral Efficiency

A fundamental limit of the efficiency of a solar cell is the fact that every semiconductor material has a bandgap ΔW_G. The wavelength at which light is just absorbed is called the **bandgap wavelength λ_G** with

$$\lambda_G = \frac{h \cdot c}{\Delta W_G} \tag{4.40}$$

The portion of the solar spectrum that lies above λ_G thus cannot be used for providing electrical energy. We call this portion **transmission losses** (see Figure 4.19).
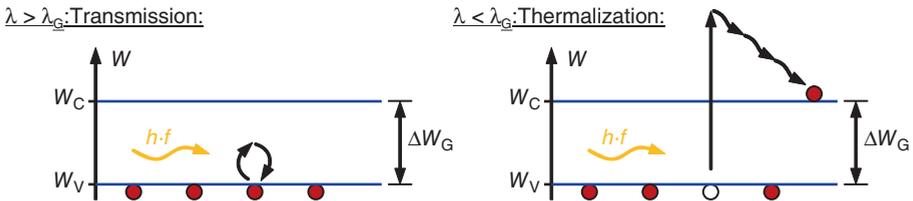
Figure 4.19 Loss mechanisms due to unsuitable energy of the photons: in the case of too little photon energy the electron cannot be raised to the conduction band; if the energy is too great, then a portion of it is given up to the lattice as heat energy

On the other hand, the radiation below λ_G represents photon energies that are larger than the bandgap necessary for absorption. This surplus energy is given up by impacts on the crystal lattice; we call these **thermalization losses**.

It is now interesting to find out what electrical energy can theoretically be won from the solar spectrum with a semiconductor of the bandgap ΔW_G. First we will consider the maximum possible current density j_{Max}, that an ideal solar cell with a radiation of an AM 1.5 spectrum can generate.

N_{Ph} is the number of photons that can impinge within a time interval Δt on an area A. It can be determined from the spectral irradiance $E_\lambda(\lambda)$ in that we divide the optical energy W_λ of the radiation at a given wavelength with the energy of a single photon W_{Ph} of this wavelength. Then we have to integrate over all wavelengths.

$$N_{Ph} = \int_0^\infty \frac{W_\lambda(\lambda)}{W_{Ph}(\lambda)} \cdot d\lambda = \int_0^\infty \frac{A \cdot E_\lambda(\lambda) \cdot \Delta t}{\frac{h \cdot c}{\lambda}} \cdot d\lambda = \frac{A \cdot \Delta t}{h \cdot c} \int_0^\infty E_\lambda(\lambda) \cdot \lambda \cdot d\lambda \qquad (4.41)$$

We assume as an idealized case that every photon in the cell is absorbed and an electron-hole pair is generated that contributes to the current density. This, however, does not apply to photons whose energy is less than the bandgap so that we only integrate up to the bandgap wavelength λ_G:

$$j_{Max} = \frac{\text{Charge}}{\Delta t \cdot A} = \frac{q \cdot N_{Ph}}{\Delta t \cdot A} = \frac{q}{h \cdot c} \int_0^{\lambda_G} E_\lambda(\lambda) \cdot \lambda \cdot d\lambda \qquad (4.42)$$

As a standard spectrum AM 1.5 we use a spectrum, which is enhanced about the factor $1000/850 = 1.1976$ with respect to the curve shown in Figure 2.2 (see Figure 4.20). Thus it possesses an overall power density of $1000 \, \text{W/m}^2$ as is required for STC conditions.
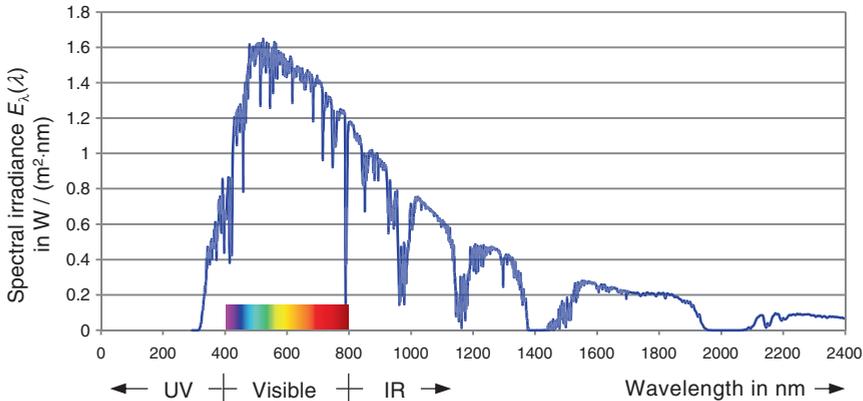
Figure 4.20 Standard spectrum with an irradiance of $1000 \, \text{W/m}^2$ based on STC [39]
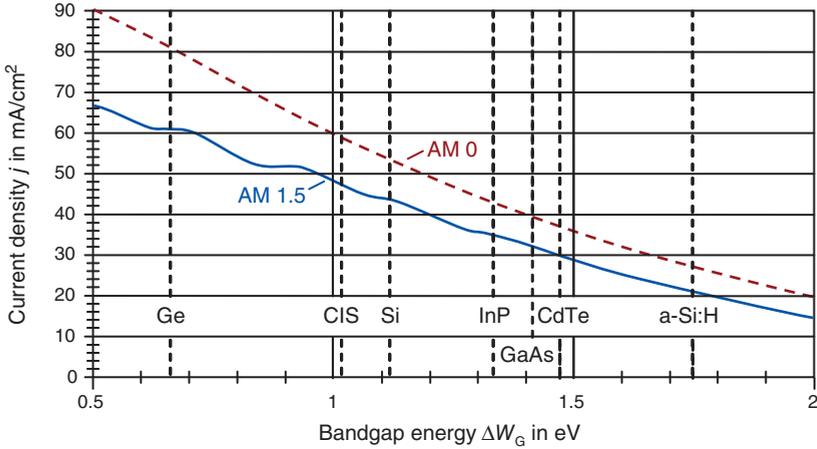
Figure 4.21 Maximum possible current density j_{Max} depending on the bandgap

Figure 4.21 shows a diagram[1] created with Equation 4.42. It shows the maximum possible current density in dependence of bandgap ΔW_G for the two spectra AM 0 and AM 1.5.

Naturally j_{Max} rises for semiconductors with small bandgaps as these can also make use of light in the deep infrared region.

It is noticeable that the AM 1.5 curve has kinks and flat parts at some places. This is due to the irregular course of the AM 1.5 spectrum, in which whole wavelength regions are filtered out in the atmosphere. For silicon there is a maximum current density of $j_{Max} = 44.1 \, \text{mA/cm}^2$ for an AM 1.5 spectrum.

After knowing what the maximum current is, we need to find out the dimension of the maximum possible voltage in dependence of the bandgap. We assume that our ideal solar cell manages to give up the full energy of each photon to the outer electric circuit. The maximum possible voltage is then:

$$V_{Max} = \Delta W_G / q \tag{4.43}$$

The **maximum electrical power P_{El}** of the cell is then:

$$P_{El} = V_{Max} \cdot I_{Max} = V_{Max} \cdot j_{Max} \cdot A \tag{4.44}$$

With this we are in a position to calculate the so-called **spectral efficiency η_S** of the ideal solar cell [40]:

$$\eta_S = \frac{P_{El}}{P_{Opt}} = \frac{V_{Max} \cdot j_{Max}}{E} \tag{4.45}$$

---

[1] The calculations for this and the following diagrams were carried out with the finely resolved solar spectra of the American standard ASTM-G173-03 [ASTM]. These correspond to the new international standard Norm IEC 60904-3, Edition 2 of 2008.
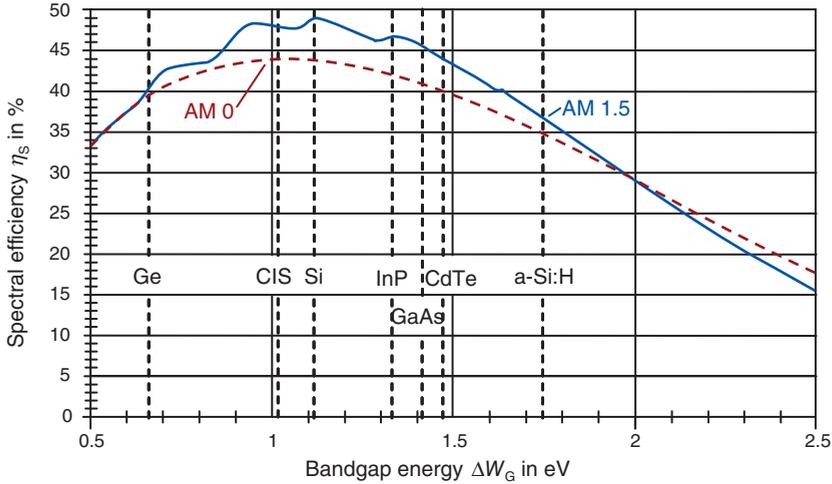
Figure 4.22   Spectral efficiency of the ideal solar cell

With Equation 4.42 this results in:

$$\eta_S = \frac{\Delta W_G}{E} \cdot \frac{1}{h \cdot c} \cdot \int\limits_{0}^{\lambda_G} E_\lambda(\lambda) \cdot \lambda \cdot d\lambda \qquad (4.46)$$

Figure 4.22 shows the spectral efficiency for AM 0 and AM 1.5 calculated with this equation. For falling values of ΔW_G we can again see a rise called up by the rising current density from Figure 4.21. However, below 1 eV this rise is overcompensated by the falling voltage $\Delta W_G/q$. We thus have an optimum that reaches a value of almost $\eta_S = 49\%$ at the AM 1.5 spectrum. With a bandgap of 1.12 eV, silicon is placed almost exactly at this optimum.

For the sake of clarity, Figure 4.23 shows the losses due to transmission and thermalization in an ideal Si solar cell. Photons above 1.12 µm have too little energy to be absorbed. Because the AM spectrum above this wavelength has an irradiance of 193 W/m^2, there are **transmission losses of 19.3%**. In the short-wave region things are different: here, only a maximum energy in the amount of the bandgap can be used by the energy-rich photons. The calculation shows **losses due to thermalization of 31.7%**. The sum of both types of losses is 51% and thus **a maximum of 49% of the solar radiation can be used**. This corresponds exactly to the previously-calculated spectral efficiency.

4.6.2 Theoretical Efficiency

There are two things that have not yet been considered in the discussion of the efficiency:

1. In a real solar cell it is not possible to use the full voltage $V_{Max} = \Delta W_G/q$.
2. Because of a fill factor <100%, the current I_{MPP} is smaller than I_{SC} and the voltage V_{MPP} is smaller than V_{OC} (see Figure 4.12).
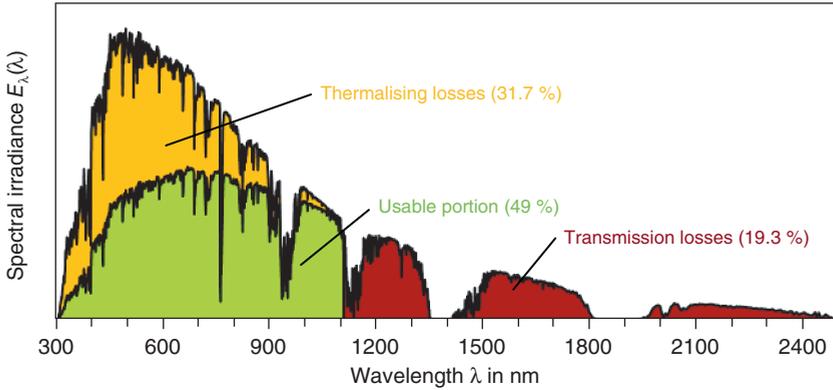
Figure 4.23 Spectral losses in a c-Si solar cell

Both limitations refer to the fact that a real solar cell also has a p-n junction. All other properties of the cell are meant to remain as ideal (especially: each incident photon with $W_{Ph} > \Delta W_G$ is absorbed and leads to a contribution to the photocurrent). Under these conditions we define the **theoretical efficiency** $\boldsymbol{\eta_T}$ [40]:

$$\eta_T = \frac{P_{MPP}}{E \cdot A} \tag{4.47}$$

With Equation 4.17 this results in:

$$\eta_T = \frac{FF \cdot V_{OC} \cdot I_{SC}}{E \cdot A} = FF \cdot \frac{V_{OC}}{V_{Max}} \cdot \frac{V_{Max}}{E} \cdot \frac{I_{SC}}{A} = FF \cdot \frac{V_{OC}}{V_{Max}} \cdot \frac{V_{Max}}{E} \cdot j_{Max} \tag{4.48}$$

With the use of Equation 4.45 we can directly determine a connection with the already calculated spectral efficiency η_S.

$$\eta_T = FF \cdot \frac{V_{OC}}{V_{Max}} \cdot \eta_s \tag{4.49}$$

We therefore require a high open circuit voltage and a large fill factor. By way of Equation 4.16 the open circuit voltage depends on the saturation current I_S; the smaller this is, the higher is the achievable open circuit voltage. The saturation current depends again on the bandgap. This can easily be proved when we consider Equation 4.3: the determining dimension is the intrinsic carrier concentration n_i, which, according to Equation 3.3, is determined exponentially on the bandgap. The result is the dependency:

$$j_S = K_S \cdot e^{-\frac{\Delta W_G}{k \cdot T}} \tag{4.50}$$

with

j_S: saturation current density

In the literature, the lower limit for the constant K_S a value of 40 000 A/cm^2 is given [40, 41].
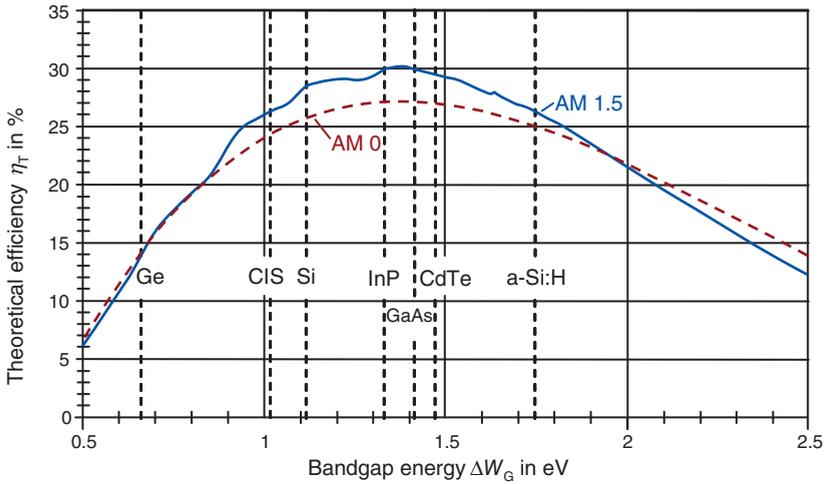
Figure 4.24 Theoretical efficiency in dependency of the bandgap

Figure 4.24 shows the calculated theoretic efficiency calculated with Equations 4.18, 4.49 and 4.50 in dependency of the bandgap energy. A noticeable deterioration of the efficiency can be seen in comparison to Figure 4.22. A maximum value of $\eta_T = 30.02\%$ is given for an energy of 1.38 eV; thus InP and GaAs are very near to the optimum. For **silicon** there is still a good value of **28.6%**.

> The theoretical efficiency of 28.6% is the upper limit of the achievable efficiency of a cell of crystalline silicon (assumption: only one p-n junction).

4.6.3 Losses in Real Solar Cells

After we have determined the theoretical limits of the maximum achievable efficiency in the previous section, we will now find out how we can come as near as possible to these limits. For this purpose we will first consider the optical and electrical losses that occur. An overview of this is shown in Figure 4.25.
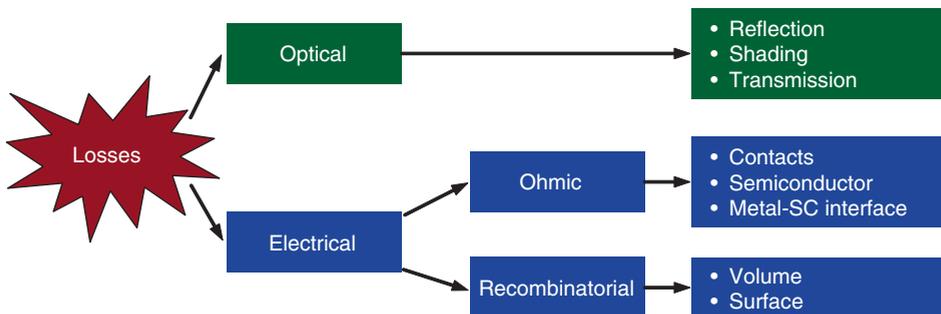
Figure 4.25 Types of losses in a solar cell
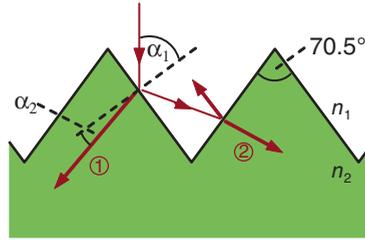
Figure 4.26 Reduction of overall reflection by means of texturing: giving light "a second chance"

4.6.3.1 Optical Losses, Reflection on the Surface

As we have already seen in Chapter 3, the refractive index step of air on silicon causes a reflection of approximately 35%. Help is obtained by an **anti-reflective coating** that lowers the average reflection of an AM 1.5 spectrum to around 10%. A further measure is **texturing** the cell surface. The surface is etched with an acid in order to roughen it up. In the case of monocrystalline silicon with anisotropic etching processes (e.g., with potassium hydroxide, KOH) pyramid structures can also be fabricated. The results are pyramids with an angle at the top of 70.5° (Figure 4.26).

What does this texturization yield? Figure 4.26 shows how incident rays partly penetrate the cell and are partly reflected. According to the **Fresnel equations** the strength of the reflection factor R can be determined from the **angle of incidence α_1** [29]:

$$R(\alpha) = \left(\frac{\sin(\alpha_1 - \alpha_2)}{\sin(\alpha_1 + \alpha_2)} \right)^2 \tag{4.51}$$

In this, the **exit angle α_2** can be determined by the *law of refraction:*

$$n_1 \cdot \sin \alpha_1 = n_2 \cdot \sin \alpha_2 \tag{4.52}$$

However, the reflected ray is not lost; it impinges on the surface of the cell again where once again a part of the light is reflected. The light is therefore given a "second chance" in a way. In total more light penetrates the cell and in the case shown the improvement is more than 20% compared to the simple vertical incidence. As a result the short circuit current is increased and thus the efficiency of the cell. Table 4.1 shows the remaining reflection factor in the combination of anti-reflection layer and texturization.

Table 4.1 Remaining reflection losses for anti-reflection layer and texturization [23,36]

Anti-reflection coating	Texturization	Average reflection factor (%)
No	No	30
Yes	No	10
No	Yes	10
Yes	Yes	3
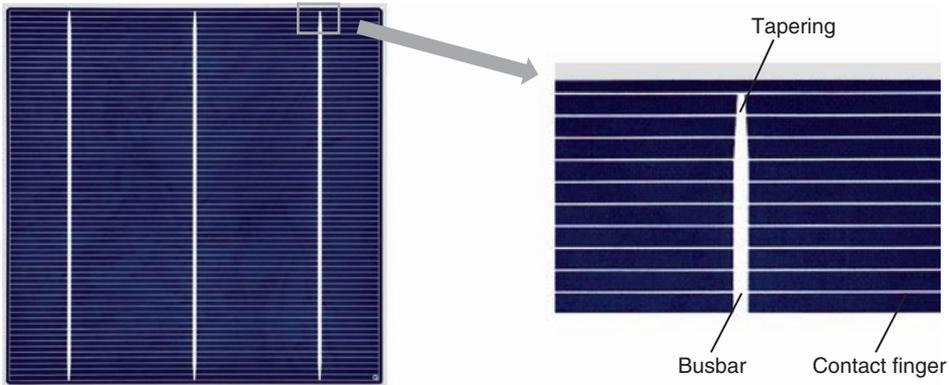
Figure 4.27 Front contacts of a solar cell with contact fingers and current collector rails (busbars) (source: Q-Cells)

Shading by Means of Contact Finger

The current generated by the solar cell must be led via the contact fingers to the connection wires. The cross section must not be too low in order that they possess a low ohmic resistance.

At the same time the shading losses increase with greater finger width, the usual widths are at 100–200 μm. Broader strips serve as current collectors, the so-called **busbars**. These are tapered at the ends as that is where the current density is at its lowest (see Figure 4.27).

A further possibility for optimizing is making the contact fingers narrow and high instead of broad and flat. The contacts are "buried" in the semiconductor material so as not to create additional shadows in case of an oblique incidence. To accommodate these **buried contacts**, small grooves are first cut in the cell surface by means of lasers and these are then filled with a Ni-Cu mixture (Figure 4.28). The shading losses can be reduced by approximately 30% [35].

Losses through Transmission

Long-wave light only possesses little absorption. Thus, for instance, the penetration depth of light with a wavelength of 1000 nm already lies in the range of the currently normal cell thickness of 150–200 μm. Without further measures this leads to transmission losses.
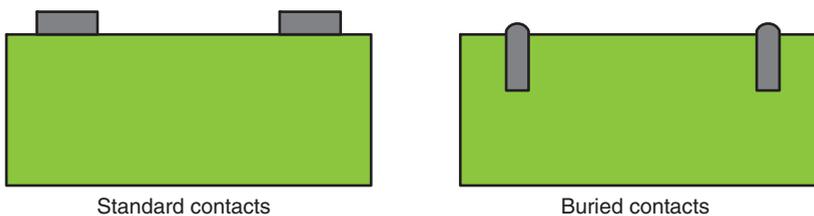
Figure 4.28 Comparison of standard contacts with the buried contact technology: the shading losses can be significantly reduced
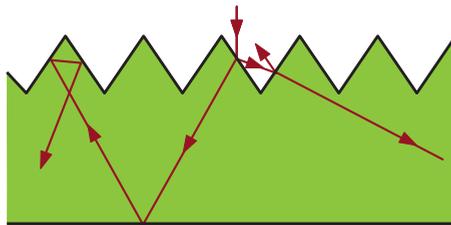
Figure 4.29 Depiction of light trapping: the obliquely refracted rays are reflected on the rear side and thus travel a longer path through the semiconductor

A further improvement can be achieved by means of the texturization shown in Figure 4.26. As can be seen from Figure 4.29, the vertical incident light rays are refracted in an oblique path to the bottom and thus travel a longer way through the cell. A further improvement is by means of a reflecting material at the bottom of the cell for which the normal aluminum bottom contact layer is well suited as it provides a reflection factor of more than 80% [42].

4.6.3.2 Electrical Losses and Ohmic Losses

There are electrical losses in the **contact fingers** on the top side of the cell. Narrow and high contacts (in the optimum case as buried contacts) help in this. In addition, ohmic losses can occur in the **semiconductor material** as the conductivity of the doping material is limited. High currents must be led to the front contacts especially with thin **emitters**. An increase in the n-doping brings an improvement but also leads to stronger recombination in the doped area. Finally there are also losses at the **metal-semiconductor junction**. The reason for this is that in bringing metal and semiconductor together a potential step is caused (so-called *Schottky contact*). This acts like a p-n junction and thus reduces the achievable cell voltage. Here an extremely high doping is of help (e.g., $N_D = 10^{20}/cm^3$) leaving such a narrow space charge region that it can be tunneled through by the electrons [23,36]. Figure 4.30 shows one such structure. The **n^{++}-doping** is only applied in the immediate surroundings of the metal contact in order to reduce recombination losses.

Recombination Losses
The various reasons for recombination of generated charge carriers in the **semiconductor volume** have already been discussed in Section 4.2.2. Added to this in real cells are recombinations at surfaces that are created by the open bonds at the **border** of the crystal lattice. A measure for reducing the recombination at the bottom is the **back surface field** discussed in Section 4.2.4. At the top one attempts to cover the largest possible area with an oxide that saturates the open bonds and thus **passifies** them. As is shown in Figure 4.30 the anti-reflection layer (e.g., of Si_3N_4) is used for this. At the same time the n^{++}-n$^+$-layer at the front contact leads to a "front surface field" that keeps the holes away from the contacts.

4.7 High Efficiency Cells

In the following we will consider some examples of current high efficiency cells.
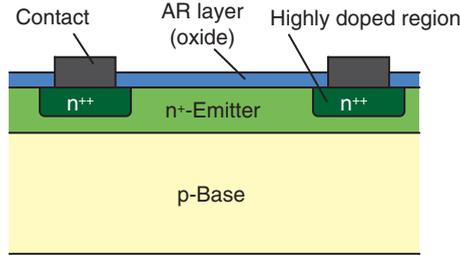
Figure 4.30   Structure for preventing a Schottky contact: The high doping permits tunneling of the electrons from the semiconductor to the metal contact

4.7.1   Buried-Contact Cells

The best known high efficiency cell is the buried contact cell that was developed in the 1980s by **Professor Martin Green** at the University of New South Wales (UNSW) in Australia. Martin Green is a true luminary in the field of cell development and has repeatedly achieved world records for efficiency. Figure 4.31 shows the structure of the buried contact cell. The pits cut by laser in which the front contacts have been inserted are clearly visible. About the contacts can be seen the n^{++}-regions for preventing the Schottky contact. At the bottom is the p^+-layer for forming the back surface field. A feature is that the cell was also texturized at the bottom. The light rays arriving there are thus reflected back and travel a particularly long way through the cell (**Light-Trapping**).

The cell concept was developed by the BP Solar Company under license and subsequently released for mass production under the name of **Saturn Cell**. This possesses an efficiency of 17.5% on a surface area of $150\,cm^2$ [43].

4.7.2   Point-Contact Cell

Figure 4.32 shows a point contact cell developed at the Stanford University.
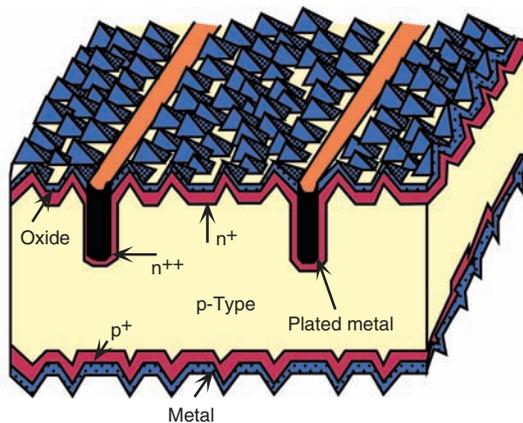
Figure 4.31   Buried contact cell (more accurately: Laser Grooved Buried Contact: LGBC cell) (reprinted with the kind permission of Martin Green)
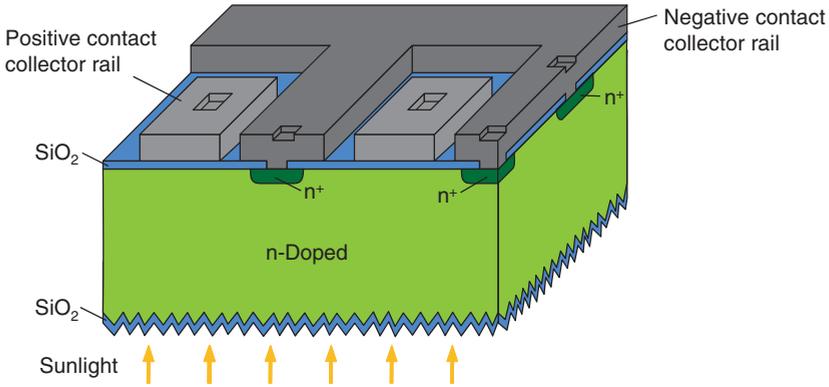
Figure 4.32   View of the point-contact cell: all contacts are positioned on the rear side of the cell and can thus be made as thick as desired [44]

A noticeable feature is that both the negative as well as the positive **contacts** are positioned **on the rear side of the cell** and that therefore **no shading** occurs. This is possible as a good quality of silicon is used. Thus the diffusion length is so long that almost all charge carriers find their way to the rear side without recombining. The whole of the front side is passivated and therefore there is hardly any recombination there. A special trick is used on the rear side: also an oxide layer is inserted between the contacts and the silicon. This is drilled through by laser only at particular points and then **a local emitter** is diffused in. Thus, the surface recombination can be reduced to a minimum. In 1988, the laboratory cell achieved a record efficiency of 22.3%. The technology is now marketed by the SunPower Company under the name **A-300** and developed further. A **record cell** of $150 \, cm^2$ has meanwhile achieved an efficiency of **more than 24%**.

4.7.3 PERL Cell

The current **efficiency champion** is again from the UNSW in Australia. As shown in Figure 4.33 the PERL cell (Passivated Emitter Rear Locally diffused) also uses the principle
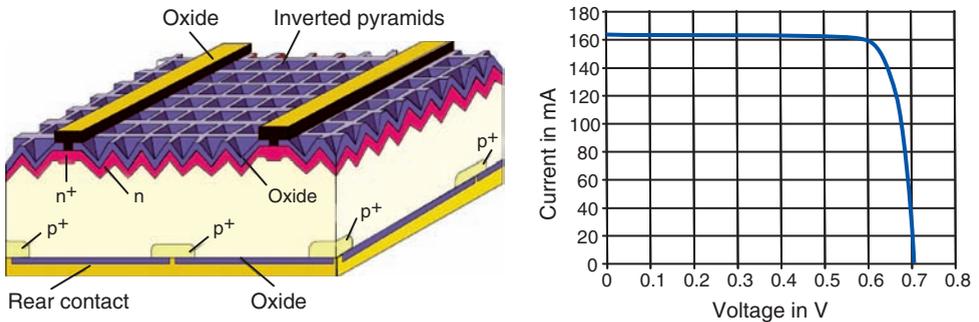
Figure 4.33   PERL cell together with *I/V* characteristic curve, characteristic curve to [35] (reprinted with the kind permission of Martin Green)

of the rear-side point contacts. The front side contains regular texturization in the form of inverted pyramids – a very effective measure of efficient light trapping. The upper passivating layer is made up of two layers of silicon oxide and silicon nitride and acts as an anti-reflective double layer.

The cell achieves a short circuit current of $42 \, \text{mA/cm}^2$ and an open circuit voltage of $714 \, \text{mV}$. With the fill factor of 83% this results in a **record efficiency of 25%** [45,46].

Approximately 100 process steps were required for the manufacture of the record cell, which is an unacceptable effort for industrial production. Meanwhile, the Suntech Company produces a much simplified cell on the principle of the PERL concept under the name "**Pluto**". At present the cells are produced with "normal" rear sides (flat surface aluminum with back surface field). The low reflection factor of the front side of only 1% is notable, even though it possesses only one simple anti-reflection shield. Current cells achieve efficiencies of 19%; increases to 21% are announced [46,47].

Finally the spectral sensitivity of a high efficiency cell should be discussed (similar to PERL cell) (dashed line in Figure 4.9). In a wide wavelength region it achieves almost the ideal value that corresponds to an external quantum efficiency of 100%. In the short-wave region this is much better than the standard cell as there is no **dead layer** due to the surface passivation and very small n^{++}-areas. Above $800 \, \text{nm}$ it works especially effectively as the infrared light travels several times through the cell by means of *light trapping* and is thus also absorbed.

5

Cell Technologies

Now that we have become experts in the method of operation of solar cells we will look in more detail at how solar cells are produced out of crystalline silicon. Then we will make the acquaintance of cells of alternative materials such as amorphous silicon or gallium arsenide. Finally, ecological aspects of individual technologies will be handled.

5.1 Production of Crystalline Silicon Cells

The workhorse of photovoltaics is the silicon solar cell. For this reason we will deal in detail with its production from sand via the silicon, the wafer and cell processing up to the finished solar module.

5.1.1 From Sand to Silicon

The first step is the conversion of quartz sand into high-grade silicon for the production of wafers.

5.1.1.1 Production of Polysilicon

The starting point of the solar cell is silicon (from the Latin *silicia*: gravel earth). After oxygen it is the second most common element on Earth. However, it almost never comes in its pure form in nature but mostly in the form of silicon oxide (quartz sand). Therefore in the truest sense silicon is like the sand at the beach.

First the silicon is reduced in an electric arc furnace with the addition of coal and electrical energy at approximately 1800 °C (Figure 5.1):

$$SiO_2 + 2C \rightarrow Si + 2CO$$
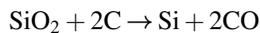
Thus, we obtain **metallurgical silicon (Metallurgical Grade: MG-SI)** with a purity of approximately 98%. The designation is because this type of silicon is also used in the production of steel. For use in solar cells the MG-Si must still go through complex cleaning. In the so-called **silane process**, the finely-ground silicon is mixed in a fluidized bed reactor

1. Production of metallurgical silicon:

Sand (SiO$_2$)   Coal (C)   Electric arc oven   MG-silicon
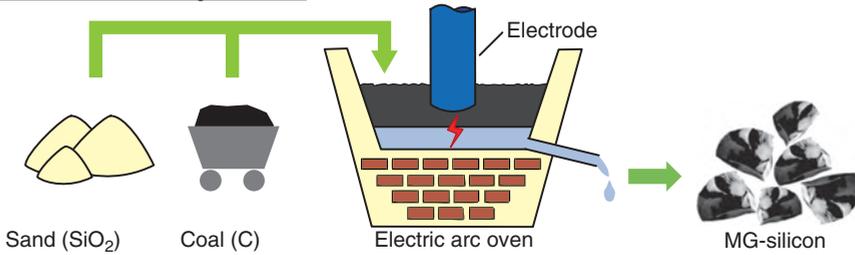
2. Processing to highly purified polysilicon (Solar Grade):

Polysilicon   Siemens   Repeated   Fluidised bed
(SG silicon)   reactor   distillation   reactor
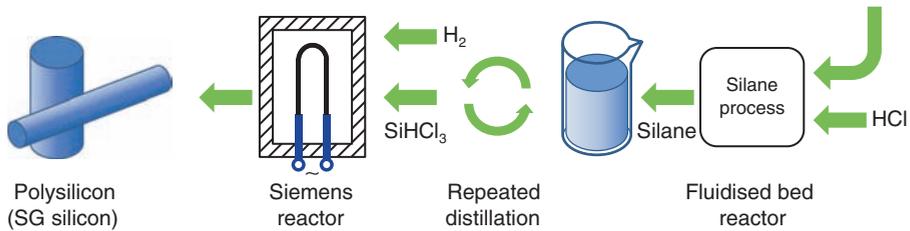
Figure 5.1   Production of polysilicon from quartz sand

with hydrochloric acid (hydrogen chloride, HCl). In an exothermic reaction this results in trichlorosilane (SiHCl$_3$) and hydrogen.

$$Si + 3HCl \rightarrow SiHCl_3 + Si + H_2$$

Now the trichlorosilane can be further cleaned by means of repeated distillation. Fortunately the boiling point is only at 31.8 °C. The reclamation of the silicon takes place in a reactor (**Siemens Reactor**), in which the gaseous trichlorosilane with hydrogen is fed past a 1350 °C hot thin silicon rod. The silicon separates out at the rod as **highly purified polysilicon**. This results in rods for instance of length 2 m with a diameter of approximately 30 cm (Figure 5.1).

The polysilicon should have a purity of at least 99.999% (5 nines, designation **5N**) in order to be called **Solar Grade Silicon** (**SG-Si**). However, for normal semiconductor technology used in the production of computer chips and so on, this degree of purity would be insufficient; here a purity of 99.9999999% (**9N, Electronic Grade: EG-Si**) is normal. As the Siemens process is relatively energy-intensive, the search has been on for years for alternatives to cleaning silicon. One possibility is the use of **fluidized reactors** in which the purest silicon is continually separated. These have higher production rates and a 70% lesser energy usage than the Siemens reactor [48]. However, processing is difficult and requires much skill and experience.

Very promising is the production of **directly purified silicon (Upgraded Metallurgical Grade: UMG-Si)**, for which there are now different versions. For instance, the process of the 6N-Silicon Company consists in that MG-silicon is melted in liquid aluminum. This is already possible in practice at 800 °C in contrast to the much higher "normal" **melting point of silicon at 1414 °C**. Then one allows the melt to cool so that silicon crystals are formed. The foreign atoms such as boron or phosphorous are taken up by the aluminum. However, after cooling the silicon is contaminated with aluminum that must be extracted in further steps. The production
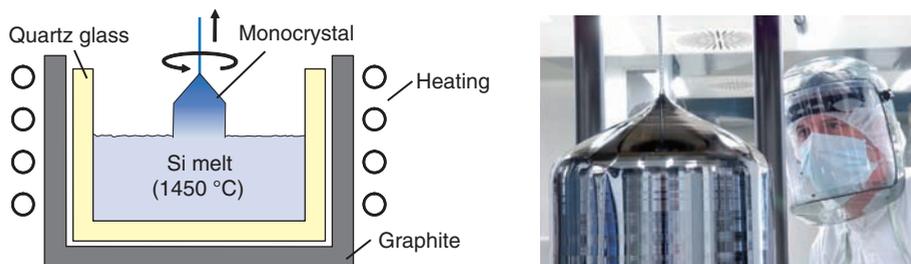
Figure 5.2 Production of monocrystalline silicon rods by means of the Czochralski process (photo: Wacker Chemie AG)

of UMG silicon requires only approximately **half the energy effort** of the Siemens process. However, the desired purity does not yet approach that attained by the Siemens process [49].

The structure of the polycrystalline silicon is too poor for it to be used directly in solar cells. Therefore, in the following we will consider the two most important processes for improving the properties of the crystal.

5.1.1.2 Production of Monocrystalline Silicon

The *Czochralski process* (**CZ process**) is the process that has been used most for production of monocrystalline silicon (see also 1.6.1). For this purpose, pieces of polysilicon are melted in a crucible at 1450 °C and a seed crystal, fixed to a metal rod, is dipped into the melt from above. Then, with light rotation, it is slowly withdrawn upwards whereby fluid silicon attaches to it and crystallizes (Figure 5.2). Thus, eventually a monocrystalline silicon rod (**ingot**) is formed whose thickness can be adjusted by the variation of temperature and withdrawal speed. Rods with a diameter of up to 30 cm and a length of up to 2 m can be produced with this method. For photovoltaics the diameter is typically 5–6 inches (12.5–15 cm).

If the crystal quality still needs to be improved, then the **Float-Zone (FZ or Zone Melt) process** can be used instead of the CZ process. Here a seed crystal is placed under a vertical hanging polysilicon rod (Figure 5.3). Then an induction coil is slowly pushed from below
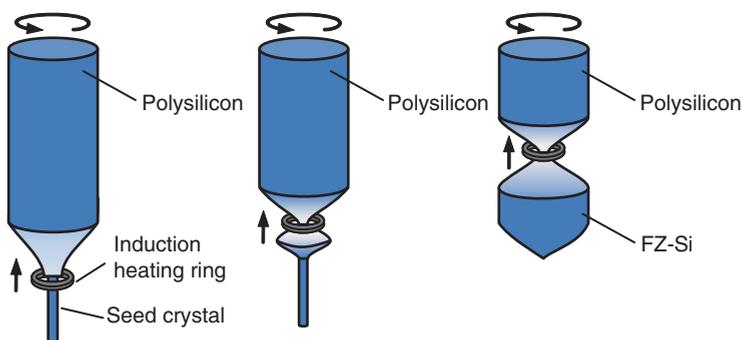
Figure 5.3 Principle of the float-zone process: the upwards moving heating ring melts the polysilicon only locally so that impurities are driven upwards during crystallization
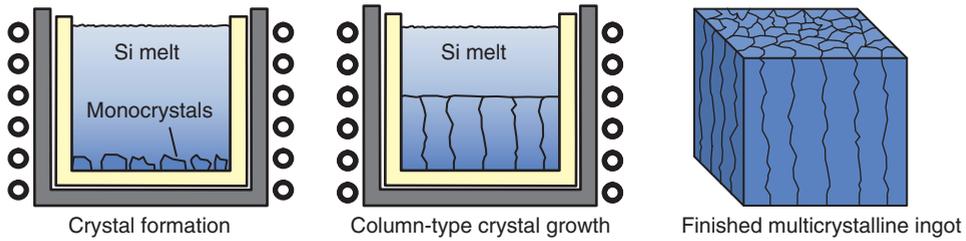
Figure 5.4   Production of multicrystalline ingots

upwards over the rod. In this the silicon is only melted in the induction zone so that the monocrystal forms from the bottom upwards. Because any existing contaminants are driven upwards with the melt in the crystallization, the zone process achieves a particularly **high crystal quality**. However, FZ-Si is significantly **more expensive than CZ-Si** and for this reason it is used for photovoltaics only in exceptional circumstances. The PERL world record cell mentioned in Section 4.7, for instance, was established with float-zone silicon.

5.1.1.3   Production of Multicrystalline Silicon

The production of **multicrystalline silicon** is much simpler. Figure 5.4 shows the principle: Pieces of polysilicon are poured into a graphite crucible and brought to a melt, for instance, using induction heating. Then the crucible is allowed to cool from the bottom by the heating ring slowly pulled upwards. At various places on the bottom of the crucible small monocrystals are formed that grow sideways until they touch each other. With the vertical cooling process the crystals grow upwards in a column (**columnar growth**). At the boundary layers crystal displacements are formed that later become centers of recombination in the cell. For this reason one tries to let the monocrystals become as large as possible. The column structure also has the advantage that minority carriers generated by light do not have to cross over a crystal boundary in the vertical direction.

> Because of the poorer material quality of multicrystalline silicon the efficiency of solar cells made from this material is typically 2–3% below that of monocrystalline solar cells.

After the crystallization of the whole melt, the silicon block is divided into cubes (**ingots**) of 5 or 6 inches along the edges.

> **[?]**   What exactly is the difference between multicrystalline and polycrystalline silicon?

> **[!]**   Polycrystalline silicon is of poorer crystal quality than multicrystalline material; the diameter of the monocrystals contained is in the micro to millimeter region. With multicrystalline material one speaks of monocrystals in the order of millimeters to 10 cm [50]. If the monocrystals are larger than 10 cm then monocrystalline silicon is present. However, this clear difference is not always reflected in the literature.

Multicrystalline ingot   Fragmentated ingot   Cutting the wafers with a wire saw
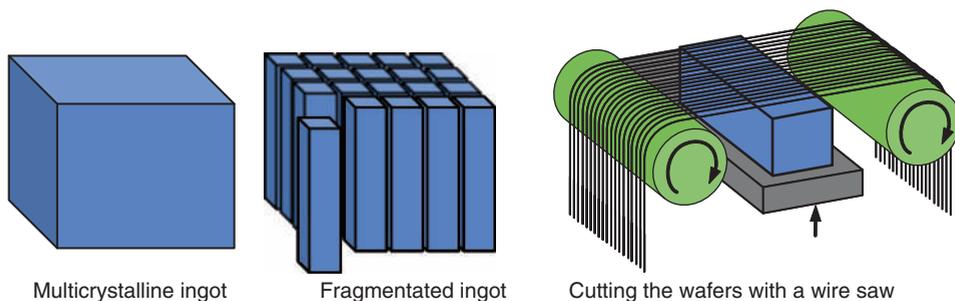
Figure 5.5 Production of multicrystalline wafers: after the fragmentation of the ingots into individual blocks they are cut into wafers with the wire saw

5.1.2 From Silicon to Wafer

5.1.2.1 Wafer Production

After production, the ingots must be sawed into individual sheets (**wafers**). This is mostly done with **wire saws** that remind one of an egg cutter (Figure 5.5). A wire with the **thickness of 100–140 μm** moves at high speed through a paste (**slurry**) of glycol and extremely hard silicon-carbide particles and carries these with it into the saw gap of the silicon. This is more a grinding or lapping process rather than sawing. The **saw gap** is at least **120 μm**.

Unfortunately the silicon chips cannot be recycled with sufficient purity. With the current wafer thicknesses of 180 μm there are **saw losses** that are almost as large as the used parts. First producers use saw wires encrusted with diamond particles in order to refrain from the use of silicon carbide particles. In this case it should be possible to clean the silicon chips and to use them for new wafers [51].

5.1.2.2 Wafers from Ribbon Silicon

If pulling the wafers directly from the melt is successful, then the saw losses can be completely prevented. This is the idea of the **ribbon silicon**. In the so-called **Edge-Defined-Film-Fed-Growth process (EFG process)** from the Schott Solar Company, a former of graphite is dipped into the silicon melt (Figure 5.6). The fluid silicon rises in the gap by means of capillary force and can be "docked" on a longitudinal seed crystal and pulled upwards as a thin sheet.

In the real process an octagon-shaped gap is used and eight-cornered tubes of 6 m with a diameter of 30 cm and **silver-thin** wall thickness of only 300 μm are pulled. The production of a tube takes about 5 h. These tubes are then cut into individual wafers of 12.5 cm by means of lasers.

Although the EFG process with the elimination of the saw losses promises clear advantages, the Schott Solar decided in 2009 to shut down the production of EFG wafers. Apparently the company could not follow the industry trend to larger and thinner wafers. Added to this was a relatively slow pulling speed in order to achieve a sufficient crystal quality.

A second process for producing silicon film has been developed by the Evergreen Solar Company under the name **String-Ribbon** which resembles on the principle of the soap bubble. Two parallel heated wires are pulled upward through the Si melt. In doing so a "soap skin" of silicon forms between the two and hardens as multicrystalline silicon in the air. Evergreen states that their process has the lowest use of energy of all wafer production processes [53].
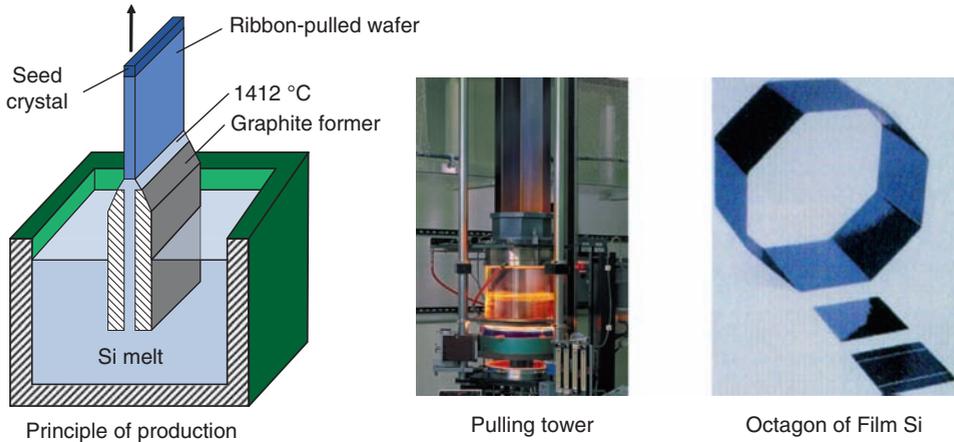
Figure 5.6 Production of wafers according to the EFG process: the wafers are pulled without sawing directly from the melt (photos: Schott Solar AG)

5.1.3 Production of Standard Solar Cells

In the following we will consider the typical steps for producing a modern silicon cell (see Figure 5.7). First the already-doped wafers are dipped into an etching bath in order to remove contaminants or crystal damage on the surface (**damage-etching**). Then follows **texturizing** of the surface (e.g., by means of etching with potassium solvent). The formation of the **p-n junction** is then achieved by the formation of the n^+-emitter by means of phosphorous diffusion. This is a relatively energy-intensive process as temperatures of 800–900 °C are required. In the next step the deposition of the **anti-reflection coating** of silicon nitride (Si_3N_4) is carried out which causes a passivation of the surface at the same time.

The application of the contacts occurs in the **screen printing process**. For this purpose a mask with slits is placed on the cell and metal paste is brushed on. In this way it is placed on the wafer only at particular positions. The formation of the **rear side contacts** occurs in two steps. First the **soldering contact surfaces** of silver paste are applied in order later to solder the connection wires to them. Then the rest of the rear side is fully covered with aluminum. The **front side contacts** are applied in the next step. Here, too a silver paste is used in order to achieve a low series resistance.
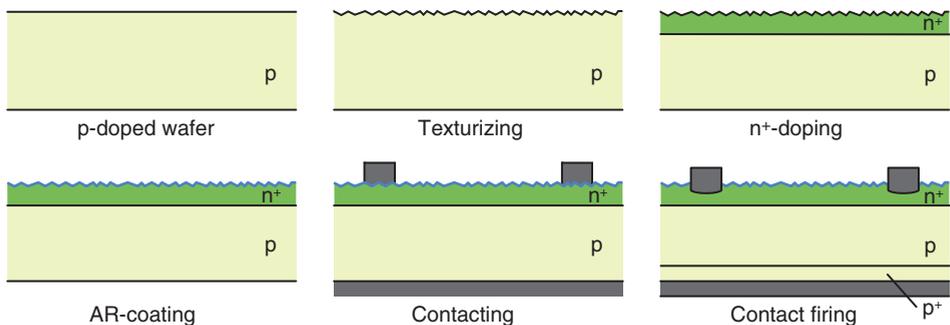
Figure 5.7 Process steps for producing standard cells

The subsequent **contact firing** of the cells (approximately 800 °C) ensures the hardening of the pastes and the "firing" of the anti-reflection layer between the front contact and emitter. Besides this the firing achieves a diffusion of the Al atoms from the rear contact into the base in order to generate the required p$^+$-layer for the **back-surface-field** (see Section 4.2.4). Because of the phosphorous diffusion the border regions of the cell are also n-doped whereby the p-n junction is basically short-circuited. Thus, as a last step, an **edge insulation** of the cell is carried out (etching or laser cutting process). The production process of the solar cell is completed with the **measurement** of the *I/V* characteristic curve under standard test conditions in order to allocate the cell to a **quality class**. Figure 5.8 shows the views of a monocristalline cell after the respective production steps.

> [?] The use of silver for solar cell contacts is certainly quite expensive. Are there alternatives to this?

> [!] In fact the cost of the silver is a real hurdle in the further reduction of production costs. Meanwhile there are many promising attempts to do without silver. One of the many attempts by producers is to use copper. However, copper diffuses into the cell already at room temperature and generates traps there (see also Section 4.2.2). Attempts are now being made to use nickel which acts as a barrier between copper and the Si emitter [54].
>
> Silver is also used on the rear side. Normally this is coated with aluminum over the whole surface for the back-surface-field. Unfortunately the zinc-covered cell-connector strips cannot be soldered directly to aluminum, which is the reason why silver has been used up to now. A new process makes use of zinc contact strips that are connected directly with the aluminum. Thus, besides the silver paste a screen printing step also falls away in the production [52].

> [?] The solar cell in the earlier figures always has a p-doped base and an n-doped emitter. Could one not do this just as well the other way around?

> [!] Nowadays it is common practice that cell producers purchase p-doped wafers and then dope them in a well-known process with phosphor for the emitter. However, these p-type cells have an important disadvantage: together with contaminants (e.g., chrome or iron), boron forms complexes that again form additional recombination centers. Added to this is the problem of the oxygen that enters the melt during the production of the wafer. The metastable boron-oxygen complexes that form from this lead to additional recombination centers with the incidence of light. In this way, depending on the quality of the material, the efficiency is reduced by about 7% for example, within a month of operation (degradation) [55].

p-doped raw wafer	Texturization	Phosphor diffusion
Anti-Reflection coating	Rear side screen printing	Front side screen printing
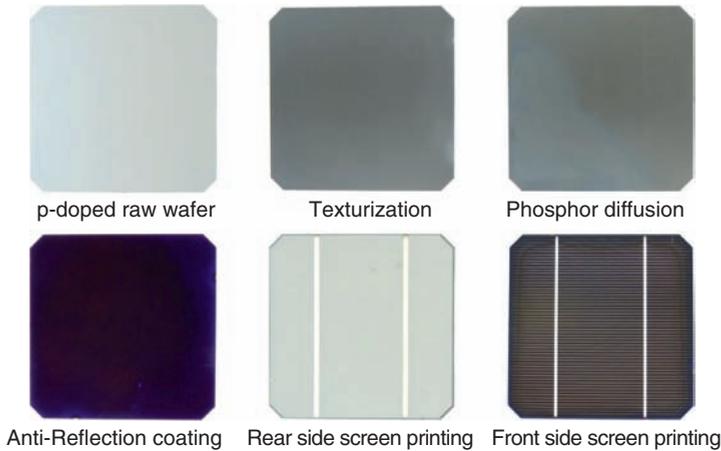
Figure 5.8   View of a monocrystalline cell after the respective production steps

Meanwhile an increasing number of producers are changing to n-type cells as these problems do not occur there. For instance, aluminum or boron can be used as the doping material for the emitter. However, special measures must be taken in order to passivate the surfaces [56]. For instance, cells that use n-type wafers are the point-contact cell (see Section 4.7.2) and the HIT cell (see Section 5.4.1)

The next production step is the integration of the solar cells into the solar module and we will consider this in the following sections.

5.1.4 Production of Solar Modules

In order to make solar cells manageable for power supply, they are integrated into solar modules. Figure 5.9 shows the principle of the structure of a **glass-foil solar module**. The individual cells are connected electrically in series into a **cell string** by means of galvanized copper strips. This string is bedded between two sheets of **Ethyl-Vinyl-Acetate (EVA)**, a transparent plastic. To finish off, a **glass sheet** is placed on the front side and a **rear-side foil** on the rear side. This sandwich is then heated in a laminator under vacuum up to 150 °C. The EVA material softens and flows around the cells and then hardens again.

The rear side foil is for protection from moisture and is also an electric insulator. It is made up of a layered film of polyvinyl fluoride and polyester and is mostly designated a **Tedlar foil**, a trade name of the DuPont Company. The edge of the module must be sealed (e.g., by means of adhesive tape) before being inserted into the aluminum **module frame**.

An alternative to the glass-foil module is the **glass-glass module** (Figure 5.9). For architectural reasons this is often used on façades or for integration in roofs. The second
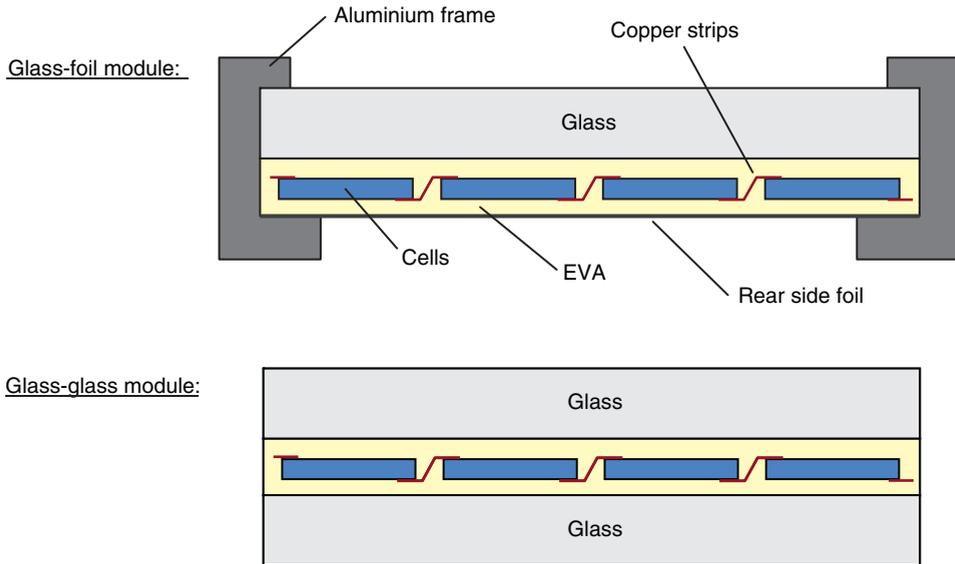
Figure 5.9 Structure of a glass-foil as well as a glass-glass module
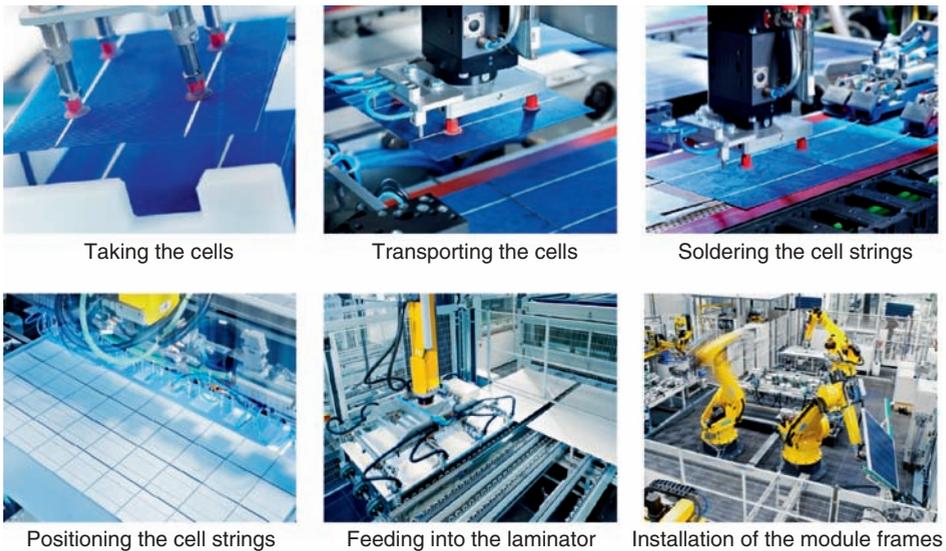
Figure 5.10 Steps for producing a solar module (photos: Solar-Fabrik AG)

sheet of glass is for increasing mechanical stability as there is no metal frame. Figure 5.10 shows the individual steps in the production of a solar module.

The features of solar modules are described in Chapter 6 and questions on optimum cell circuitry are discussed in greater detail. In the following we will look at alternative cell technologies.
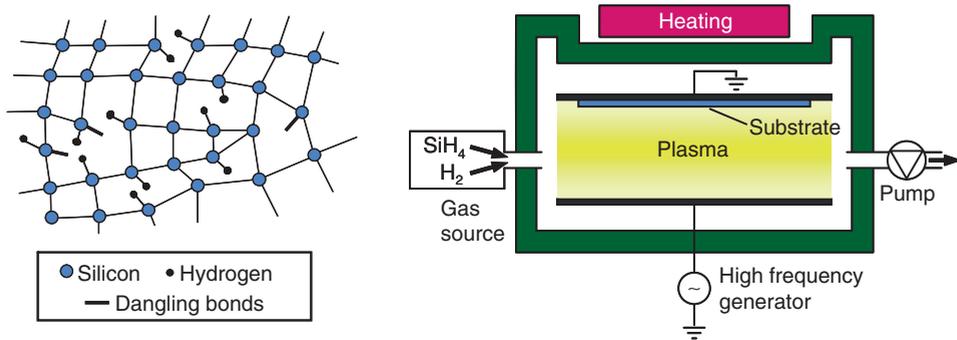
Figure 5.11 Structure of the a-Si lattice and depiction of the Plasma-Enhanced Chemical Vapor Deposition (PECVD) for producing a-Si thin film cells [59]

5.2 Cells of Amorphous Silicon

As we have learnt in Chapter 3, direct semiconductors possess an extremely high absorption coefficient. With them it is possible to absorb sunlight in a "**thin film cell**" of one micrometer. The best-known thin film material is amorphous silicon, which we will now examine.

5.2.1 Properties of Amorphous Silicon

If one deposits silicon out of the gas phase onto a carrier material then an extremely irregular structure of silicon atoms is formed (*amorph*: Greek: without structure). It consists of a multitude of open bonds that are called **dangling bonds**. They form recombination centers for electron-hole pairs and make the material unsuitable for solar cells. The trick is to add hydrogen for passivation during the deposition in order to saturate the dangling bonds.

The structure of the material designated as **a-Si:H** is shown in Figure 5.11 in the left-hand sketch. Unfortunately not all bonds can be saturated as this would require the hydrogen portion to be increased to such an extent that the optical properties of the material would be impaired [57]. Depending on the hydrogen portion, the crystal structure of a-Si:H possesses a **direct bandgap** in the region **of $\Delta W_G = 1.7$ to 1.8 eV** [58]. As can be seen in Figure 3.22 the absorption coefficient is one or two factors above that of c-Si. At a wavelength of 600 nm the penetration depth is only 0.25 μm. Thus **cell thicknesses of 0.5 μm** are sufficient to absorb a large part of sunlight!

5.2.2 Production Process

For the production of a-Si thin film cells use is mainly made of **Plasma Enhanced Chemical Vapor Deposition – PECVD**, see Figure 5.11. The starting gases silane (SiH_4) and hydrogen (H_2) flow into the approximately 200 °C hot process chamber and there enter into a strong **high-frequency field**. This accelerates individual electrons that in their turn separate the molecules of the starting gases by means of impact ionization into their constituent parts (SiH_3^+ etc.). The charged particles form **plasma** that contains highly reactive ions, which react with the substrate surface and settle there. This layer of a-Si:H continues to grow with further addition of the two process gases. The process would also function without the plasma enhancement (normal gas phase deposition – CVD) but then one
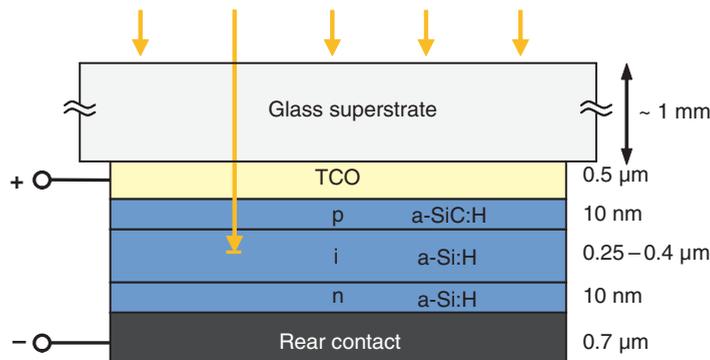
Figure 5.12 Structure of the thin film cell: the overall thickness of the deposed material is less than $2\,\mu m$

would require temperatures of more than $450\,°C$ for breaking up the starting gases and this would strongly limit the selection of substrate materials.

Typical deposition rates are in the region of $0.2\,nm/s$. The production of a $0.5\,\mu m$ thick a-Si-H layer takes about 40 min. This time is actually too long for mass production; desirable would be a reduction by a factor of 10. Many promising new processes are available for this (for instance, **Very-High-Frequency-PECVD** as well as **Hot-Wire-CVD**) with high deposition rates, which, however, often increase the number of defects in the a-Si:H [57].

5.2.3 Structure of the pin Cell

The typical structure of an a-Si thin film cell produced with the PECVD process in shown in Figure 5.12.

A glass sheet is coated over its whole area with a transparent electrode of conducting oxide called **Transparent Conducting Oxide – TCO**; a technology that is also used in the production of flat screens. Typical materials are **indium-tin oxide (ITO)** or zinc oxide (ZnO). Connected to this is a sandwich of p-doped, intrinsic (undoped) and n-doped amorphous silicon. The final coat is a thin rear contact of aluminum or silver. The surprising thing is the **low material usage** for the cell: The layers applied to the glass have a combined thickness of less than $2\,\mu m$! The structure shown in Figure 5.12 is called a ***superstrate cell***, as the glass sheet on which the layers are deposited lie above the rest of the cell in sunlight (*super*: Latin for over).

As far as possible the light absorption should occur in the intrinsic layer as the electron-hole pairs in doped materials recombine within a few nanometers. For this reason one adds **carbon** to the p-region and this increases the bandgap to approximately $2\,eV$ so that the **a-SiC:H** layer is almost transparent.

The probability of recombination is also very large in the undoped a-Si. The generated minority carriers must be "brought home" as quickly as possible (see Section 4.2). This is achieved by building up **pin cells** that generate a large electric field, which separates the particles as soon as they are generated and transports them to their home area.

For a better understanding of the operating method of the pin cell, Figure 5.13 shows the space charge region (compare with Figure 3.14). Analogous to the normal p-n junction, the electrons diffuse out of the n-region into the intrinsic region and leave positive donor atoms behind.
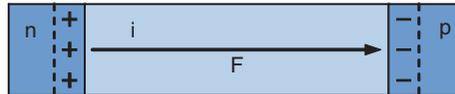
Figure 5.13   Results of the build-up as a pin cell: The space charge region extends practically over the whole of the intrinsic region

As they can find no holes for recombination there, they "roll" further until they drop into holes in the p-region and there form negative space charges. The result is the formation of a **constant electric field** over the whole i-area.

The thin film cells are also called a **drift cells** or **field cells** as the optically generated minority carriers flow here as pure field current. However, we had named the **c-Si cells**, **diffusion cells**: there the particles diffuse into the space charge region where they then flow as field current into the home region.

> **[?]**   Could one interchange the layer sequence of an a-Si cell just as well? A nip instead of a pin?

> **[!]**   Basically yes. However in a-Si:H, the mobility of the holes and therefore the drift velocity is smaller by one order of magnitude than the electrons [60]. After generation they take longer to arrive in the p-region and are in special danger of recombination. This is the reason for the advantage of the pin structure. As the absorption of light occurs mainly in the upper half of the i-layer (see Figure 4.8) the generated holes so do not have far to go to the p-layer.

5.2.4   Staebler–Wronski Effect

The large bandgap of 1.75 eV has the result that light above approximately 700 nm can no longer be absorbed. Because of these transmission losses, the theoretically possible efficiency is 26% (see Figure 4.24). In fact the record efficiency of real cells is only around 10% [61]. Standard cells achieve approximately 7–8%. Besides the high concentration of defects of the a-Si and the shunt resistance of the TCO layer, an important reason is that newly produced cells degrade under the influence of light. Figure 5.14 shows this in the example of two pin cells that were exposed to full sun radiation for more than 10 000 h at AM 1.5 (*light soaking*) after production. After approximately 3000 h the power reduction was 29%, then 37%, and then stabilized.

The cause of the degradation is the **Staebler–Wronski effect**, named after the two scientists who first described it in detail [63]. The reason is in the **strained Si–Si crystal bonds** that are caused by the irregular crystal structure. In the recombination of the electron-hole pairs generated by light, these weak bonds are "split open" and, as **new dangling bonds**, form new recombination centers for the minority carriers (see Figure 5.15). The split-open bonds also represent additional space charge regions that can weaken the built-in field in the pin cells.

After a certain light radiation time, all the weak bonds are split open so that the efficiency of the cell stabilizes itself.

The exact method of operation of the effect is not yet fully understood. However, a method for reducing this has been found. Thus, the additional crystal defects can be healed by means of
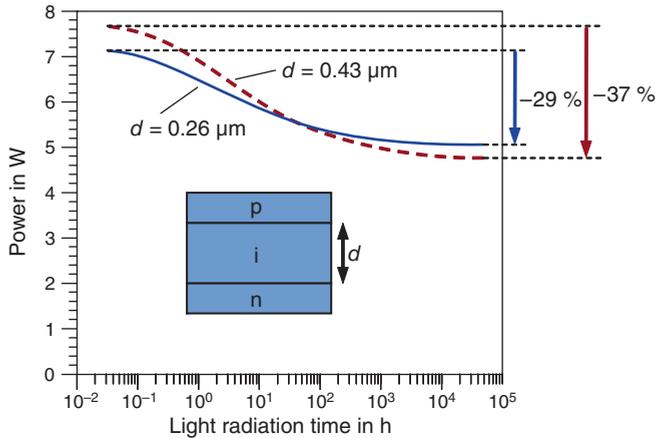
Figure 5.14 Light degradation measurement of two s-Si pin cells on different thicknesses: within 3000 h with full light radiation the power is reduced by up to 37% [62]

tempering (from 150 °C) and the Stabler–Wronski effect can be reversed [64]. In addition, Figure 5.14 shows that **thinner i-layers** are subject to **less degradation** than thick layers. The reason for this is in the larger electric field that brings the electron-hole pairs safely home even in the case of the existence of disturbing space charge regions [59].

> ? When the layers are made ever thinner, don't you think that then not enough sunlight would be absorbed? Or do you think otherwise?

> ! Of course transmission losses rise with thinner i-layers. However, there is a trick we have seen in Chapter 4 that helps: Light trapping by means of texturizing. For this purpose both the TCO layers as well as the rear side electrode are roughed so that the light path is significantly lengthened and layer thicknesses of 250 nm become possible.
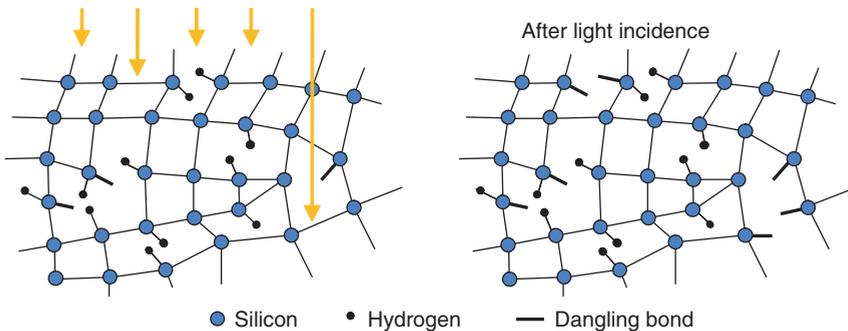
Figure 5.15 Depiction of the Staebler–Wronski effect: with incident light the weak bonds in the crystal are split open [57]
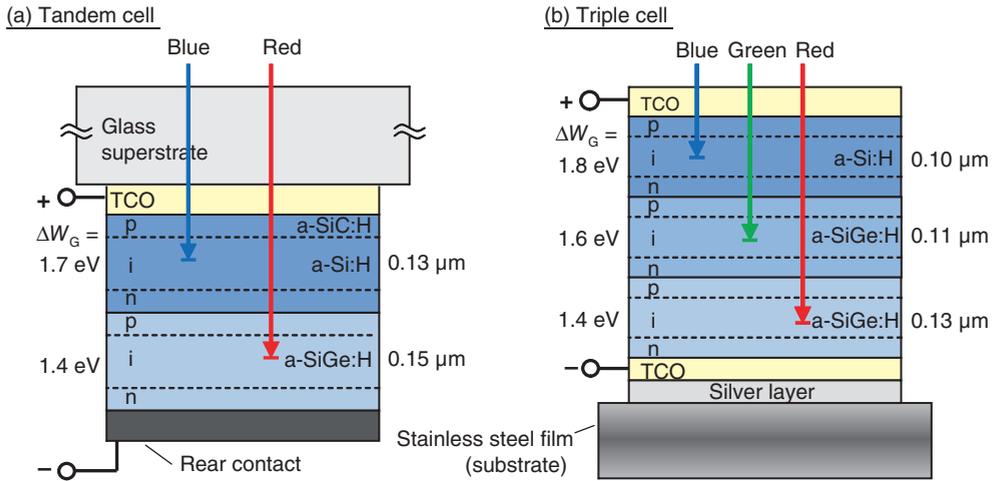
Figure 5.16 Examples of superstrate tandem and substrate triple cells [59,65]

5.2.5 Stacked Cells

In order to significantly increase the efficiency, the Sun's spectrum must be used more effectively. For this purpose two pin cells of materials of different bandgaps are stacked into a **tandem cell** optimized to a particular spectral range. Figure 5.16 shows this by means of two examples.

In the case of the tandem cell an additional a-SiGe layer is applied on top of the a-Si absorber layer. Depending on the portion of germanium atoms, this alloy can possess a bandgap between 1.4 and 1.7 eV. Also depending on the wavelength, incident light is absorbed at different depths: short-wavelength light ("blue") above 1.7 eV only manages to reach the first pin cell. The upper pin cell is transparent for long-wavelength ("red") light; it is therefore only absorbed in the lower cell. As both cells are switched in series, the weaker cell determines the overall current. For this reason the thickness of the individual absorber layers must be selected so that the two cells achieve approximately the same current **(current matching)**.

Even better is the light separation in the case of the **triple cell**: Here a further a-SiGe layer with a bandgap of 1.6 eV is used (Figure 5.16(b)). A feature of this cell produced by the **United Solar** Company is that it is applied to a flexible stainless steel film. It thus represents a **substrate cell** (*sub*: Latin for "under"). The layer of silver between the film and TCO is for reflecting the light upwards. Figure 5.17 shows the external quantum efficiency (see Section 4.3) of the whole cell with the contributions of the respective individual cells. The given short circuit currents show clearly that the Current Matching has been quite successful. The cell possesses a starting efficiency of 14.6% and a **stabilized efficiency of 13%**. As the individual pin cells are switched in series the result is a relatively high **open circuit voltage of 2.3 V** [65].

> The stabilized efficiency of the record tripel cell lies only about 10% below that of the initial efficiency. Why do we have so little degradation in this case?
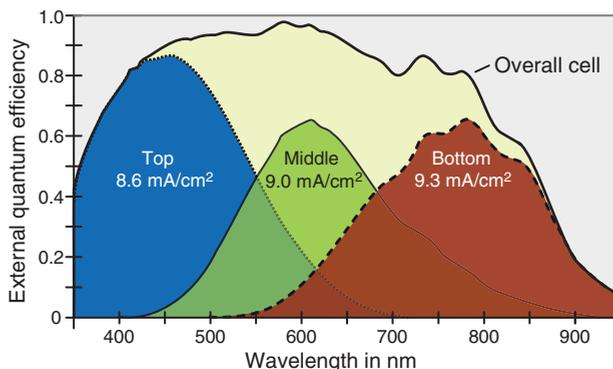
Figure 5.17 External quantum efficiency of the triple cell in Figure 5.16: the individual pin cells are responsible for different wavelength regions [65]

> [!] The example emphasizes another advantage of the stacked cells. The individual pin cells are optimized for the respective spectral regions and can therefore be made thinner. However, a thin cell leads to a high electrical field. As was seen in Figure 5.14 this also leads to a reduction of the degradation.

At this point it should be mentioned that the upper limit of the theoretical efficiency η_T discussed in Section 4.6 applies only for simple cells. Stacked cells of different materials can exceed this limit without problems (see also Section 5.4)

5.2.6 Combined Cells of Micromorphous Material

A relatively new development is the combination of amorphous and microcrystalline silicon (**μc-Si**). This technology was developed in the 1990s at the University of Neuchâtel and has meanwhile reached industrial maturity. The term **microcrystalline** designates a material that contains silicon particles (**nanocrystals**) in a size significantly less than $1\,\mu m$. These nanocrystals occur by PECVD deposition at certain silane concentrations. The result is a conglomerate of nanocrystals that is embedded in an a-Si:H environment (see Figure 5.18).

The material behaves similarly to crystalline silicon with a bandgap of $1.12\,eV$. Thus it is very well suited for a combination with a-Si in order to cover a large part of the solar spectrum. Besides this, the material shows practically no degradation. However, like c-Si, it has a low absorption coefficient. In order to still use it in the thin film region, one needs **relatively large layer thicknesses** and must also significantly lengthen the light path by means of effective light trapping. Figure 5.18(b)) shows the example of a **micromorphous tandem cell** (*micromorph*: an artificial word made up of **microcrystalline** and **amorph**).

Micromorphous laboratory cells have reached stable efficiencies of 12.1% and large-area modules are already available with 10% efficiency. A number of companies have now changed their production from pure a-Si cells to the micromorphous technology.

An important producer of machines for production of these types of cells and modules is the Oerlikon Company in Switzerland, which has commercialized the technology of the University of Neuchâtel. However, a number of companies throughout the world have ceased production

(a)

a-Si:H

Nanocrystals of
crystalline silicon

(b)

Glass

TCO

a-Si:H   0.25 µm

µc-Si:H   1 – 3 µm

ZnO

Ag

+

−
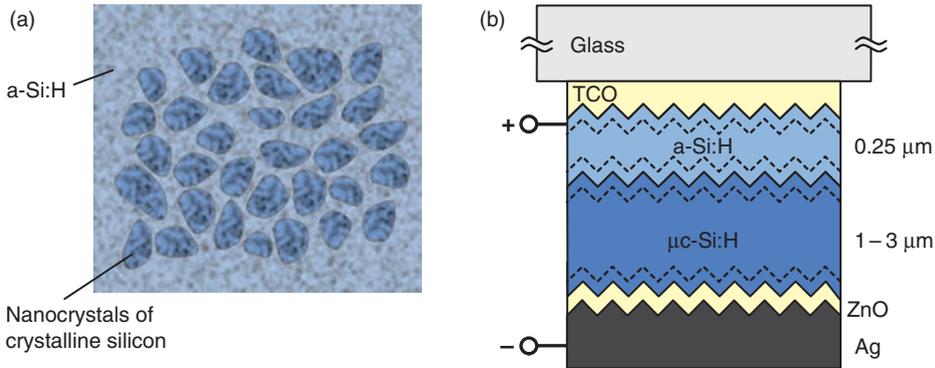
Figure 5.18 Structure of microcrystalline silicon and build-up of the a-Si:H/µ-Si:H tandem cell [31,57]

of this thin film technology as CdTe and especially CIS offer much higher efficiencies (see Section 5.3) [66].

5.2.7 Integrated Series Connection

A big advantage of the thin film technology is that the cells can be **connected to a whole module during production**. Figure 5.19 shows the individual process steps for this. After applying the TCO it is divided by means of laser into individual partitions on which the pin cells are then deposited. These cells must then again be separated and provided with a rear contact. After this has been structured as well, the electric connection is complete. Important for a small series resistance is a sufficient width of the pit in the semiconductor structuring, as, after filling with the rear contact, the cells are connected in series through this.

The last picture in Figure 5.19 shows the portion of the unusable area caused by this series connection. The depiction is not to scale. Depending on the technology, the unused portion is

(1) Applying the TCO

TCO

Glass

(2) TCO structuring (Laser)

TCO

Glass

(3) Deposition of the pin structure

pin

TCO

Glass

(4) Si structuring

pin

TCO

Glass

(5) Applying the rear contacts

pin

TCO

Glass

(6) Structuring the rear contacts

Current flow

pin

TCO

Glass

Cell Unused   Cell   Unused Cell
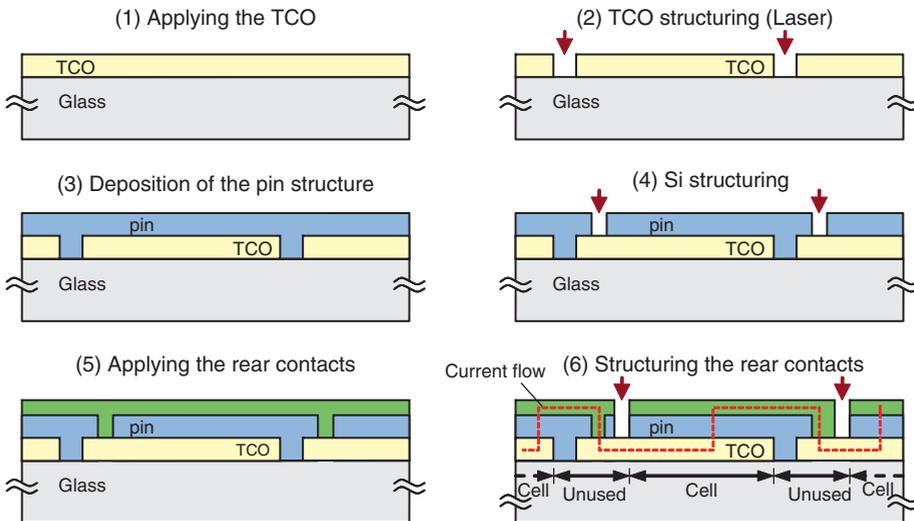
Figure 5.19 Production steps for integrated series connection of the individual pin cells

Figure 5.20 View of a-Si modules: Semi-transparent module (photo: Taiyo Kogyo Corporation) and flexible laminate for roof membranes (photo: United Solar)

only approximately 5–10% of the active cell surface. The encapsulation of the module is carried out as for normal c-Si glass-glass modules by means of EVA and a rear pane (see Section 5.1.4). The **integrated series connection** leads to a very homogeneous looking strip design so that this type of module is appreciated for architecturally demanding solutions such as façades or semitransparent glazing (see Figure 5.20(a)).

There is however also a **great disadvantage** with this process: the **deposition** of the silicon layers **must be fully homogenous** over the whole of the module area (e.g., 2 m^2). If this is not the case then every inferior cell lowers the current through all the others. For this reason the efficiencies of thin film modules are often more than 10% below those of individual cells. This is not so in the case of the crystalline wafer technology, as the produced cells are first divided into quality classes and only then are the cells of the same class combined into a module.

The United Solar Company follows a middle path in its a-Si module production. It generates integrated connected solar cells of DIN A4 size on a narrow long roll (see Figure 5.20(b)). In order to make a module out of this, two strips each with 10 cells are placed next to each other and then electrically connected and encapsulated into a module frame.

Cells of amorphous silicon also have an **important advantage compared** to their **c-Si** representatives: the temperature dependency of the efficiency is much less. Whereas the power of a c-Si cell typically falls off by 0.5% per Kelvin (see Section 4.4) the **temperature coefficient of a-Si** is **less than half** of that.

5.3 Further Thin Film Cells

After the detailed discussion on the thin film technology from the example of the amorphous silicon, we will now consider other materials. This deals primarily with getting to know the differences between them and a-Si cells.

5.3.1 Cells of Cadmium-Telluride

Cadmium-telluride (CdTe) is a compound semiconductor of the IInd and VIth Groups (see Figure 3.4) This is a direct semiconductor with a bandgap of $\Delta W_{G} = 1.45$ eV. According to Figure 4.24, this bandgap leads to a theoretical efficiency of 29.7% and is therefore very near to the optimum. A great advantage of this material is that it can be deposited in various ways with good quality as a thin film. The usual method is thermal evaporation over a short distance
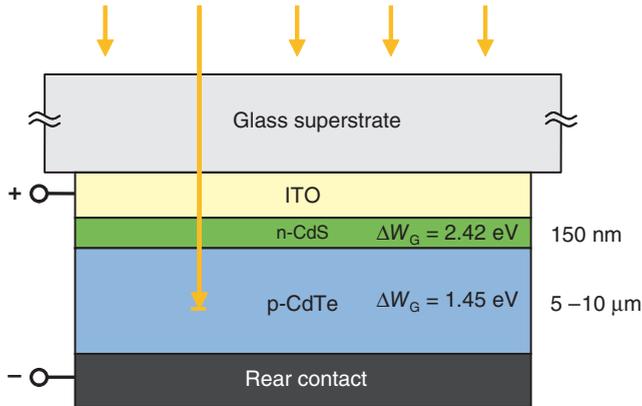
Figure 5.21 Structure of the CdTe superstrate cell: The cadmium-sulfide layer serves at the same time as n-region and as a window layer [67]

(CSS – Close-Spaced-Sublimation). In this process the semiconductor sources are heated to approximately 500 °C. At this temperature the semiconductors vaporize and deposit on the somewhat lower temperature substrate. Figure 5.21 shows a typical cell structure. As the CdTe can only be badly n-doped, a **window layer** of n-doped cadmium sulfide (CdS) is grown on after applying the transparent electrode of ITO. Then the actual **absorber layer** of poly-crystalline CdTe is followed. The two materials form a so-called **hetero junction** as the bandgaps of n- and p-doped regions are different (*hetero*: Greek for "other").

The properties of absorber and junction are at first relatively poor but can be much improved with **cadmium-chloride treatment**. For this purpose $CdCl_2$ is applied and diffused into the absorber layer by means of tempering. In a certain manner this is **applied alchemy** as the positive effect of this step is not yet fully understood.

In Figure 5.21 it can be seen that the absorber layer is relatively thick with 5–10 μm, although CdTe has a very high absorption coefficient. The reason is the difficulty of generating thin films with high crystal quality on large surfaces. A reduction of the layer thickness is thus still the subject of research [68].

The **record efficiency** of CdTe cells is **18.3 %** and modules with efficiencies of 13% can be found on the market [[61], www.firstsolar.com]. In the past few years, the First Solar Company has massively extended its cell production to an annual capacity of 2 GWp. According to its own statement, the company has the lowest manufacturing costs of all solar companies.

We will deal with the question of the environmental aspects of CdTe in Section 5.7.

5.3.2   CIS Cells

The final thin film technology we will deal with consist of materials of the Chalkopyrite group that are generally summarized under the abbreviation of **CIS** or **CIGS**. What they have in common is that they have the lattice structures of Chalkopyrite (copper pyrites – $CuFeS_2$). As shown in Table 5.1, there are different ternary (consisting of three elements) compound semiconductors.

Research on CIS cells has been carried out since the 1970s. In the year **1978 ARCO Solar** was successful in the production of CIS cells with **14.1 %** [69]. But disappointment soon

Table 5.1 Material combination of the CIS family

Material combination	Name	Bandgap (eV)	Abbreviation
$CuInSe_2$	Copper-indium-diselenide	1	CISe
$CuInS_2$	Copper-indium-disulfide	1.5	CIS
$CuGaSe_2$	Copper-indium-gallium-diselenide	1.7	CIGSe
			CIGS

followed: the efficiency sank drastically in the transfer to larger areas. Only in the 1990, with better knowledge of the properties of the material was it possible to produce solar modules with an efficiency of 10%.

The most promising material is $\mathbf{CuIn_xGa_{(1-x)}Se_2}$. Here x is the portion of indium in the material combination. With $x = 1$, $CuInSe_2$ with a bandgap of 1 eV is obtained, and with $x = 0$ the result is a corresponding $CuGaSe_2$ with 1.7 eV. By changing the indium portion, the bandgap can therefore be varied between the two extreme values and thus the efficiency can be optimized.

A **typical cell structure** is shown in Figure 5.22. This is a **substrate configuration**. The bottom glass is merely a supporting material; molybdenum acts as the rear electrode. Between the two is a layer of silicon nitride that acts as a barrier for foreign atoms which could diffuse during the manufacturing process from the glass into the absorber layer. The p-n junction is formed, as with CdTe, from the absorber layer and a thin CdS layer. For a long time there have been attempts to **replace** the **unpopular cadmium** from the CIS cells but this has only been achieved at the **expense of efficiency**.

Co-vaporization is mostly used as the method of deposition, where the individual elements are vaporized at temperatures of around 500 °C and deposit themselves on the substrate. Here, too, a bit of "magic" is used: With the addition of sodium and additional tempering, there is an improvement of the crystal structure and the electronic properties of the polycrystalline CIGS.
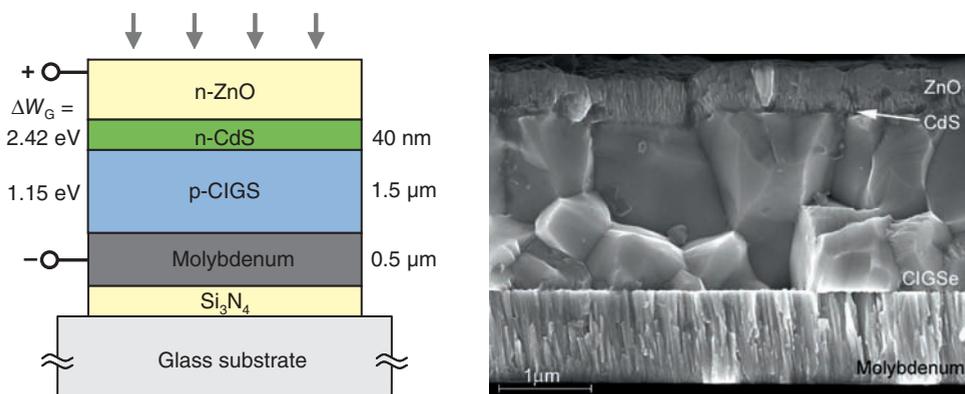
Figure 5.22 Principle of the structure of a CIGS cell and photo of a CIGS cell: the polycrystalline structure of the absorber material can be clearly seen (photo: Hahn–Meitner Institut; with kind permission of John Wiley & Sons, Ltd. [70])

The record efficiency for laboratory cells is 19.6%, which is by far the **highest efficiency of all thin film technologies** [61]. Miasolé is already offering modules with 15% efficiency on the market.

A technology that can dispense with vacuum and higher temperatures would be desirable for economical mass production. An enticing idea is to place the semiconductors as nanocrystals into a watery solution and then to print them out as normal ink. The **Nanosolar Company** is following such a concept and has reported achieved efficiencies of 14.5% [71]. However, it is unclear whether the reported conversion to module mass production has really been carried out in the factory in Luckenwalde in Germany [72]. Independently of this, it is to be expected that **CIGS technology** will make **substantial progress** in the coming years in economic production of thin film modules.

5.4 Hybrid Wafer Cells

After considering the thin film cells we will now turn to two technologies that combine different materials on the basis of wafer cells in order to achieve high degrees of efficiency.

5.4.1 Combination of c-Si and a-Si (HIT Cell)

An interesting hybrid form of c-Si and a-Si material has been developed by the Sanyo Company, which meanwhile belongs to the Panasonic Corporation. Figure 5.23 shows the structure of these so-called **HIT cells** (**HIT: Heterojunction with Intrinsic Thin-Layer**).

On the wafer, which is n-doped on both sides, there are deposited an intrinsic and then a doped layer of a-Si material. A transparent electrode (TCO) is deposited on this. As the TCO is relatively high-resistive, additional normal metal contact strips must be used.

What is the advantage of this cell concept? The a-Si layers act as very **effective passivating layers** for the c-Si wafer cell, resulting in an open circuit voltage of more than 700 mV. Panasonic is meanwhile producing cells with dimensions of $100\,cm^2$ with **efficiencies of 23%** [74]. At the same time the high open circuit voltage results in an **improved temperature dependency** of $TC(P) = -0.23\%/K$ compared to $-0.5\%/K$ for a normal c-Si cell. In addition, in the production of the cell there is the advantage that one can dispense with the energy-intensive diffusion step for emitter production. Temperatures of below $200\,°C$ are sufficient
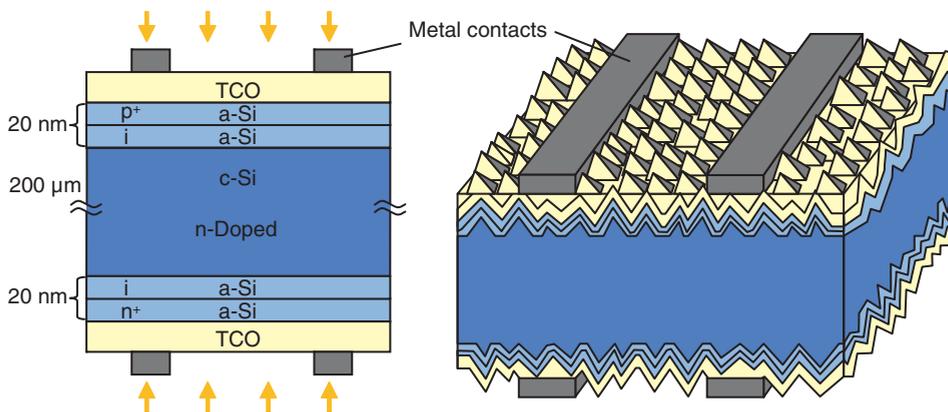
Figure 5.23   Structure and cross section of the HIT cell from Panasonic: the a-Si layers serve primarily for very efficient surface passivation [73]

because the a-Si layers are applied in the PECD process. The structure shown in Figure 5.23 also permits light from the bottom of the cell. In particular applications, these types of **bifacial cells** can result in an **increased yield of 10%** [74]. Since important patents for the HIT cell expired in 2010, a number of companies are now adopting the cell concept.

5.4.2 Stacked Cells of III/V Semiconductors

For particular applications, for example, space use or concentrator cells (see Section 5.6), maximum efficiency is required and costs play a subsidiary role. Thus, for instance, use can be made of relatively expensive GaAs wafers as this material with a bandgap of 1.42 eV lies very near to the theoretical optimum (see Figure 4.24). The best cells of GaAs thus achieve an **efficiency of 29%** [61].

It is even better to combine several materials in a cell as already seen in the triple cell. For instance the Spectrolab Company has specialized in this technology. The structure of such **monolithic stacked cells** of III/V semiconductors is shown in the left-hand sketch of Figure 5.24. **Monolithic** means that the middle and upper cell are grown onto the bottom cell. For this purpose these materials must possess approximately the same lattice constants as the germanium wafer in order to achieve a sufficient crystal quality. Window layers are placed between the cells to reduce recombination and highly doped **tunneling layers** are inserted in order to improve the charge transport between individual cells. This results in a very complex production. These types of cells achieve efficiencies of more than 32%.

A second method is to **stack different cells mechanically on top of each other** (so-called **mechanically stacked multijunction cells**). On the one hand, this has the advantage that the individual materials can possess **different lattice constants**. Added to this is that the cells need not necessarily be connected in series as the connecting wires can be led to the outside. In this way
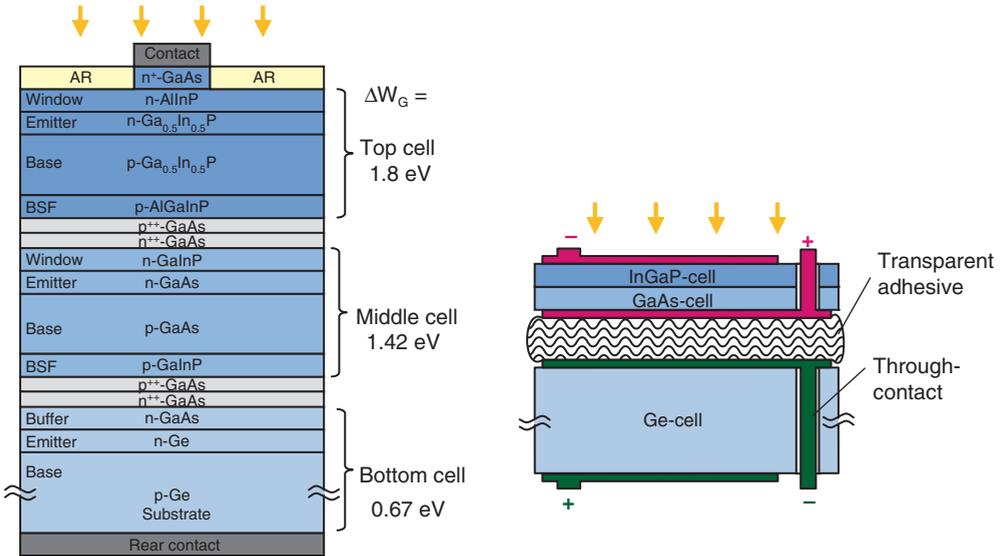
Figure 5.24 Structure of a monolithic GaInP/GaAs/Ge stacked cell of the Spectrolab Company (left) and a depiction of the principle of a mechanically stacked triple cell [75,76]

the **losses fall away** because of the **current matching** (see Section 5.2.5) and higher overall efficiencies can be achieved. The right hand sketch of Figure 5.24 shows a concept of the Belgian research institute IMEC. The top cell, which again consists of a monolithic tandem cell, is connected to the bottom cell by means of a transparent adhesive. The rear contacts are connected to the surface by means of a through-contact in order to connect the respective cells from outside.

5.5   Other Cell Concepts

Besides the cell technologies already discussed there is still a series of other materials and cell concepts that can be of importance in the future.

The **Dye Sensitized Cell (DSC)** was discovered at the start of the 1990s by Professor Michael Grätzel at the Ecole Polytechnique in Lausanne and is therefore called the **Grätzel Cell**. This cell has long played the role of "Everlasting Talent." The specialty of this concept is a relatively simple manufacturing process and the use of cheap materials. Meanwhile laboratory cells have efficiencies of more than 12% and small modules have up to 10% [61]. A hindrance for commercialization has hitherto been the lack of stability. High temperatures lead to the formation of gas and leaks due to the fact that the cell contains a liquid electrolyte. An exact description for the build-up and method of operation of the dye sensitized cells can be found in [77].

A further candidate is the **organic solar cell** that uses **polymers** in place of semiconductor materials. As with the dye sensitized cells, here too there is hope in the future of producing much cheaper electric energy than with the presently available technologies. The record efficiency for mini-laboratory cells is held by the Mitsubishi Chemical Company with 10.7%; small sub-modules achieve an efficiency of about 7% [61]. Further success can be expected in the coming years as there are a number of companies worldwide researching in the field of polymer electronics. Further information on organic solar cells can be found, for instance, in [78].

5.6   Concentrator Systems

The idea of concentrator systems is to concentrate sunlight by means of mirrors or lenses and then to divert it to a solar cell. We will look at this technology in more detail in the following.

5.6.1   Principle of Radiation Bundling

The two most important principles of concentration of light radiation are shown in Figure 5.25. In the case of lens systems, use is made of **Fresnel lenses** that were discovered by the French Physicist Augustin Jean Fresnel (1788–1827). With these lenses that were originally developed for lighthouses, one can achieve a relatively small focal length without the lens becoming too thick. This occurs with the use of circular steps on the lens surface. The resulting picture errors would be catastrophic for cameras but for photovoltaics the only concern is to be able to concentrate radiation on the solar cell.

Another principle is the use of mirror systems. Here the light is reflected by a curved mirror surface and concentrated on the solar cell. In the optimum case, use is made of parabolic mirrors as they concentrate incident rays on a focal point.

5.6.2   What is the Advantage of Concentration?

The purpose of light concentration on solar cells is the **reduction of production costs**. If the lenses or mirrors can be produced cheaply, then an actual cost advantage can accrue due to the
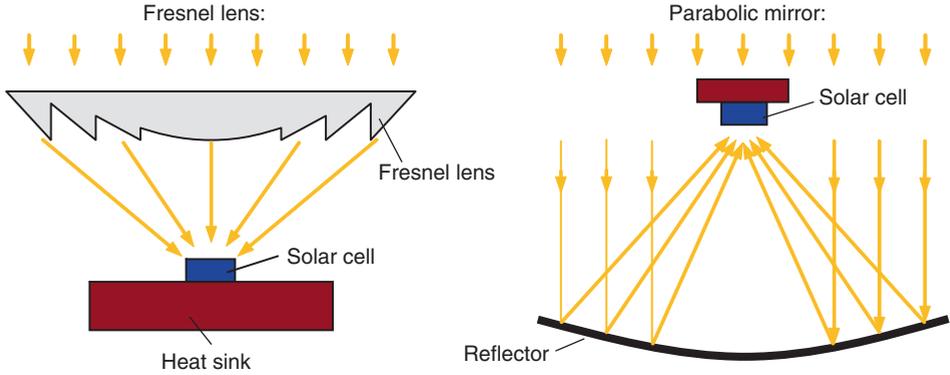
Figure 5.25 Principle of light concentration by means of a Fresnel lens (left) and parabolic mirror (right)

drastic reduction of the required solar cell area. But there is still a **further advantage**: The **efficiency** of the solar cell **increases with** the **irradiance**. How is this to be explained? This can be seen in Figure 5.26. The cell curve moves upwards with the increase in radiation. As the short circuit current behaves proportionally to irradiance, an increase, for instance, by a factor of $X = 2$ effects a doubling of the short circuit current. However, this does not result in a change in efficiency as double the optical power also hits the cell. But it is known that the open circuit voltage increases at the same time by the logarithm of the irradiance. With the resulting increase of the MPP voltage, this leads to an over-proportional rise in power and thus to an increase in efficiency.

In order to calculate the effects more accurately, we make use of Equation 4.16 for the open circuit voltage. The increase in the irradiance by the factor X leads to a changed voltage V'_{OC}:

$$V'_{OC} = m \cdot V_T \cdot \ln\left(\frac{I_{SC} \cdot X}{I_S}\right) = m \cdot V_T \cdot \ln\left(\frac{I_{SC}}{I_S}\right) + m \cdot V_T \cdot \ln(X) \tag{5.1}$$

$$V'_{OC} = V_{OC} + m \cdot V_T \cdot ln(X) \tag{5.2}$$
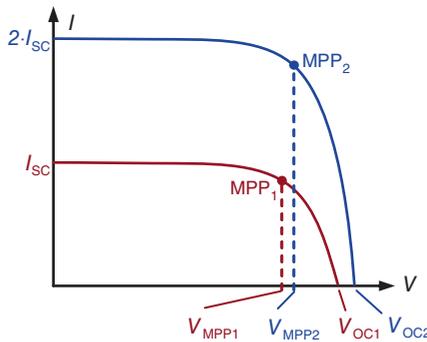
Figure 5.26 Displacement of the solar cell characteristic curve for double irradiance: besides the short circuit current there is also an increase in the open circuit voltage and thus the MPP voltage

Thus, for instance, a **concentration of the sunlight** by the **factor $X = 100$** results in an increase in the open circuit voltage by 120 mV (assumption: $m = 1$). Referenced to a typical c-Si voltage of 600 mV this means an **increase of 20%**.

The increase in efficiency can be verified for particular cell types. This is shown by the stacked cell presented in Section 5.4.2 of the Spectrolab Company; under standard conditions an efficiency of 29.1% is achieved and under 66 times concentrated sunlight this increases to 35.2% [79].

The worldwide highest efficiency is from a cell from Solar Junction: Under a light concentration of $X = 418$ there is a **record efficiency of 43.5%**! However, **the efficiency does not climb continuously**: For one thing the cell heats up with high irradiance and even an active cooling cannot prevent this. On the other hand, the electrical losses of the series resistances rise with the square of the operating current.

5.6.3 Examples of Concentrator Systems

In the two left-hand pictures, Figure 5.27 shows the application of the lens principle by the Concentrix Company, which now belongs to the French company Soitec. This installs a multitude of extremely small cells (3 mm^2) into a box-shaped module (product name ***Flatcon***). The Fresnel lenses imprinted on the upper glass sheet concentrate the light up to 500 times on these cells. The cells used are monolithic stacked cells of GaInP/GaInAs/Ge. Under concentrated radiation the cells achieve an efficiency of up to 41% and the module efficiency is more than 30% [80].

An example of **parabolic mirror collectors** is shown on the right in Figure 5.27. The reflector is made up of 112 individual curved mirrors, which feed the sunlight with 500 times concentration onto the receiver. This, again, consists of an array of III/V stacked cells that are kept to a maximum of 60 °C by means of active cooling. The size of the reflector is gigantic with **a diameter of 12 m**. In this way the system achieves an electric **power of 35 kWp**.

Besides the highly efficient cells of III/V semiconductors, **cells of crystalline silicon** can also be used. For instance, there is the Point-Contact cell from the SunPower Company (see Figure 4.32). As the **contacts are only on the rear side**, they can be as thick as desired and can thus conduct extremely high currents without noticeable losses.

Figure 5.27   Examples of concentrator systems: path of rays and photo of a Flatcon concentrator module (left) and parabolic mirror system (right)

5.6.4 *Advantages and Disadvantages of Concentrator Systems*

Whether concentrator systems are more economical than conventional solar modules depends greatly on the costs of the concentrating elements. They can only be competitive when, despite the high requirements (mechanically and optical stability over more than 20 years) of the used surface, they are significantly cheaper than the standard modules. Added to this is the important disadvantage that concentrator systems can **only** use the **direct portion** of the global radiation. As diffuse radiation from many directions arrives at the mirror or reflector it cannot be bundled on the solar cell. Added to this is that concentrator systems almost always require a **Sun-tracking system**, which adds further cost. It must therefore always be weighed up as to whether the utilization of concentrator technology is really worthwhile.

5.7 **Ecological Questions on Cell and Module Production**

5.7.1 *Environmental Effects of Production and Operation*

Various materials are used in the production of solar cells and modules and their environmental friendliness will be discussed.

5.7.1.1 **Example of Cadmium-Telluride**

The CdTe cells presented in Section 5.3.1 pose a special hazard for the environment. Cadmium is a **poisonous heavy metal** that is classed as carcinogenic. Thus it should not be released into the environment. However, cadmium combined with tellurium is a very stable water-insoluble compound that only melts above 1000 °C. In normal operation of a photovoltaic plant it presents almost no danger for the environment. The quantities used are astonishingly small due to the thinness of the active layer in the cell. Only 7 g are used per **square meter**, which represents approximately the cadmium content of **two Mignon-type NiCd batteries** [81].

However, there could be a hazard in the case of a **fire**. The temperature reached could be so high that gaseous cadmium would be released into the surroundings. On the other hand, in the case of a house fire, many other poisonous substances (dioxins, etc.) are released so that cadmium would only be one problem among many. At the same time we note in comparison that e.g., the **German coal fired power stations** emit more than 1.4 t of cadmium into the air every year and at the same time they produce approximately 100 t of cadmium in slag form [82].

Special attention is paid to **recycling** solar modules. This is indispensable in order to justify the use of CdTe modules. The First Solar Company has instituted a free return system for all sold modules. The recycling process developed by the company achieves a **recycling rate of 95% of cadmium** [139].

5.7.1.2 **Example of Silicon**

Silicon looks much better regarding environmental friendliness. It is **non-poisonous** and available in unlimited amounts in the form of quartz sand. However, in its production a series of **etching chemicals** such as trichlorosilane are used for the silane process (see Section 5.1). Potassium hydroxide and hydrofluoric acid are used in the cleaning of the mono- and polycrystalline wafers. Also phosphoric and boric acids are used for doping the wafer. An increasing number of chemical companies are offering **reprocessing plants** for these materials in order to increase recycling quotas [83]. In the ideal case integrated multi-industry companies can make use of the wastes
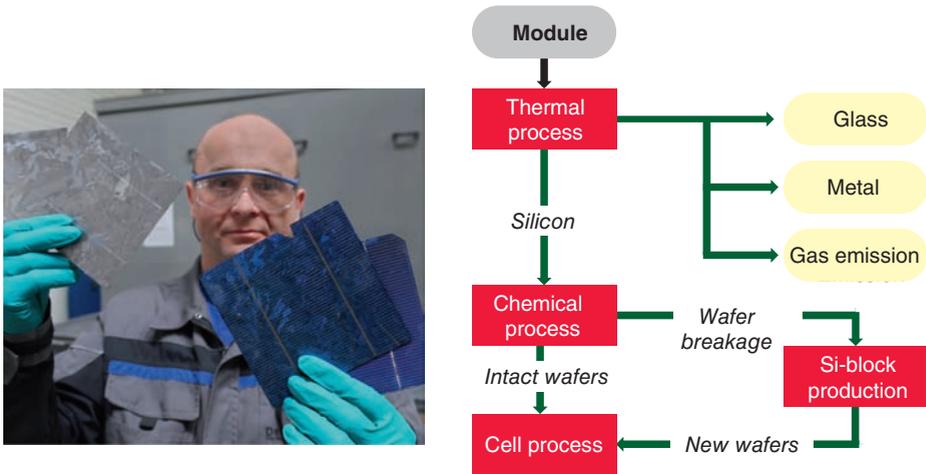
Figure 5.28 Recycling solar modules: besides the recycling of glass and metal, the solar cells are chemically cleaned and made into "new" wafers again (photo: Solarworld AG; sketch is from [86])

produced in their own companies. Thus, for instance at Wacker; the used tetrachlorosilane is converted into silicon dioxide and is then used for wall paints or even toothpaste [84].

Recycling of c-Si modules is also possible and has been carried out by the Deutsche Solar AG in Freiberg, a daughter of the Solarworld Company (Figure 5.28). For this the module is heated to 500 °C so that the EVA laminate is dissolved. The cells are then separated manually and cleaned of the doping substances by means of etching. Originally the plan was to reuse mostly wafers. However, the cells of older modules often have sizes and thicknesses that are no longer in use today. Besides, the thin wafers used today break easily when being separated. For this reason currently wafer pieces are melted into ingots again and new wafers are produced in the block casting process. The remaining materials such as glass, aluminum, copper and silver can also be reused. In total a **recycling quota of 90%** was achieved [85]. However, the Deutsche Solar GmbH ceased recycling solar modules after the prices for solar silicon fell sharply.

Meanwhile the solar industry has founded the Association PV CYCLE that has the aim of the Europe-wide return and subsequent recycling of solar modules. The members obligate themselves to free return of photovoltaic waste (see *www.pvcycle.org*).

5.7.2 Availability of Materials

Besides the environmental relevance of the substances used, their availability plays an important role. If photovoltaics are to be a support in the worldwide supply of energy then the materials necessary for the production of solar modules must be available in sufficient quantities.

5.7.2.1 Silicon

In the case of silicon solar cells the situation is very relaxed. Silicon is the **second most common element** on the Earth's surface and can be produced fairly easily from quartz sand (see Section 5.1). In recent years, however, there has been talk of a "scarcity of silicon". This, though, always referred to the already produced and highly refined polysilicon. The producers had underestimated

the demand so that the price rose to more than 200 €/kg. Since massive capacity was added there is now sufficient polysilicon available, which has reduced prices to below 20 €/kg.

5.7.2.2 Cadmium-Telluride

As regards the availability of CdTe, **tellurium** is a critical material, as on Earth it is almost as scarce as gold. The estimate of the total available quantities is 21 000 t worldwide. Annually about 130 t are extracted mainly as a by-product in the extraction of copper and nickel, which is used primarily in steel production. Some studies assume that the extraction of tellurium could be increased to 600 t/a [87]. Let us assume that at best 500 t/a would be available for photovoltaics. How much photovoltaic power could be generated with this?

One needs approximately 7 g of tellurium for a square meter of module area. If in the future a module efficiency of 15% is achieved, then the result is a requirement of 50 g tellurium per kWp. With the assumed extraction of 500 t/a, we would have a possible PV production of

$$(500 \, \text{t/a})/(50 \, \text{g/kWp}) = 10 \, \text{GWp/a}$$

Is that a lot or little? The quantity corresponds approximately to one third of the solar module production of the year 2012. But what would the situation be in **2030**? If we assume an annual growth of the PV market of 20%, then yearly production would have increased to approximately 840 GWp. **CdTe modules** would contribute to this world market only a **maximum of 1.2%** (see Figure 5.29).

With **cadmium** the situation regarding **availability is unproblematic**. The annual production is 20 000 t/a, moreover, the use of cadmium is generally being reduced.

5.7.2.3 CIS

With the CIS modules it is mainly the **indium** that has limited availability as it occurs almost as rarely as silver [88]. The estimate of the total extraction is 6000–11 000 t but actually about 950 t are extracted of which 800 t/a are required by other industries. The market for flat screens especially takes up a large part as indium is used there in indium oxide as a transparent electrode.

Since the triumphal development of the flat screen, the price of indium has risen 10-fold to 1000 €/kg. If one uses the remaining 150 t/a for **CIS modules**, then for a demand of 30 g/kWp one arrives at a **installable power of 5 GWp/a** [87].
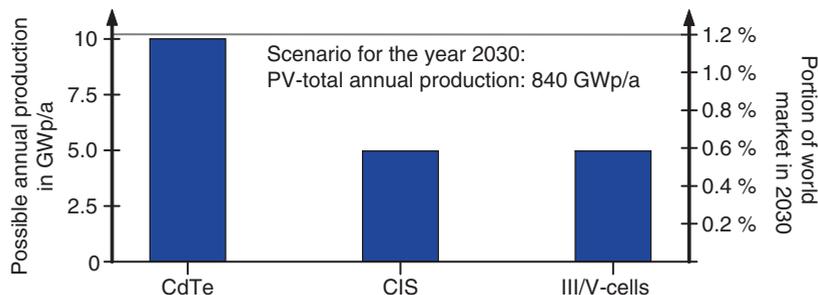
Figure 5.29   Maximum possible annual production of various PV technologies: they will only be able to make up a small portion for the assumed world market in 2030

The selenium required, like tellurium, is also a byproduct of copper and nickel production. The current annual production of 1500 t/a can easily be increased so that here there are no bottlenecks for PV production.

5.7.2.4   III/V Semiconductors

With the stacked cells discussed in Section 5.4.2 there is a **problem with the availability of germanium**. It occurs in relatively small concentrations in the rare earths and can only be extracted with much effort. The extracted quantities are about 90 t/a. Prices have risen in recent years as germanium is used in modern optical components. Assume that, despite this, half of the annual extraction could be used for photovoltaics. With the utilization of cells in concentrator systems we can assume a future efficiency of 45%. For a concentration factor of 500, the demand for germanium is 9 g/kWp. [87]. The possible annual production is then:

$$(45\,\text{t/a})/(9\,\text{g/kWp}) = 5\,\text{GWp/a}$$

In summary one can say that **no availability problems** are foreseen **up to 2020**. **After that** one should expect **raw material bottlenecks for CdTe, CIS and III/V semiconductors**.

5.7.3   Energy Amortization Time and Yield Factor

There is a persistent rumor that more energy is required for the production of photovoltaic plants than the energy generated by the plant in the course of its life. If this were actually the case then one could hardly call photovoltaics an option for the solution of energy problems. It would then only be suitable for providing power for areas far from an electric grid (space, rural areas in the developing world).

In order to discover the amount of energy required for the production of a photovoltaic plant, let us assume a **rooftop installation in Germany**. This consists of multicrystalline solar modules, support structure, cables and inverters. In a study by Erik Anselm in 2006 it was shown that the **primary energy demand w_{Prod}** for producing the installation was **7830 kWh/ kWp**. The cells under consideration had an efficiency of 13.2% and a wafer thickness of 285 μm, which corresponded to the state of production of 2004. Figure 5.30 shows that approximately **three-quarters of the energy was required for the production of the cells**. Of this, again, the largest part was for production of polysilicon.

The **energy amortization time** is more informative than the primary energy demand.

> The **energy amortization time T_A** is the time that a solar power plant must work until it has generated as much energy as was required for its production.

If a photovoltaic plant is feeding into the public grid then it replaces power from conventional power stations. Thus every kwH that is fed-in is included in the number of kWh of primary energy it replaces. The **primary energy factor F_{PE}** describes this relationship. For the typical Middle-European electric grid we assume a value of $F_{\text{PE}} \approx 3$ (see also Chapter 1).

$$T_A = \frac{w_{\text{Prod}}}{w_{\text{Year}} \cdot F_{\text{PE}}} \tag{5.3}$$
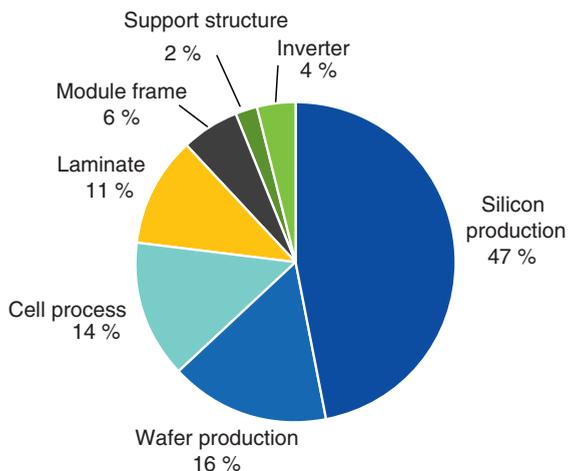
Figure 5.30 Portion of the primary energy demand for the production of a PV plant with multicrystalline modules in the year 2004

with

w_{Prod}: specific production effort (primary energy)
w_{Year}: specific annual yield per PV plant

In Germany the specific annual yield of a plant is $w_{Year} = 900 \, \text{kWh}/(\text{kWp·a})$. For the example of the rooftop installation with multicrystalline cells the result is then:

$$T_A = \frac{w_{Prod}}{w_{Year} \cdot F_{PE}} = \frac{7830 \, \text{kWh}/\text{kWp}}{900 \, \text{kWp}/(\text{kWp} \cdot \text{a}) \cdot 3} = 2.9a \tag{5.4}$$

In Germany, the installation must be **in use** for almost **3 years** in order to produce as much energy as was required for its production. This is a very good result in view of the plant lifetime of about 25 years.

This consideration immediately leads to the definition of the **Energy Returned on Energy Invested**, *ERoEI*.

> The **Energy Returned on Energy Invested**, *ERoEI* is the amount of energy that a solar power plant generates in its lifetime T_L in comparison to the required production energy (always referenced to primary energy).

$$ERoEI = \frac{Total \; generated \; energy}{w_{Prod}} = \frac{T_L \cdot w_{Year} \cdot F_{PE}}{T_A \cdot w_{Year} \cdot F_{PE}} = \frac{T_L}{T_A} \tag{5.5}$$

In our example this results in:

$$ERoEI = \frac{T_L}{T_A} = \frac{25a}{2.9s} = 8.6 \tag{5.6}$$
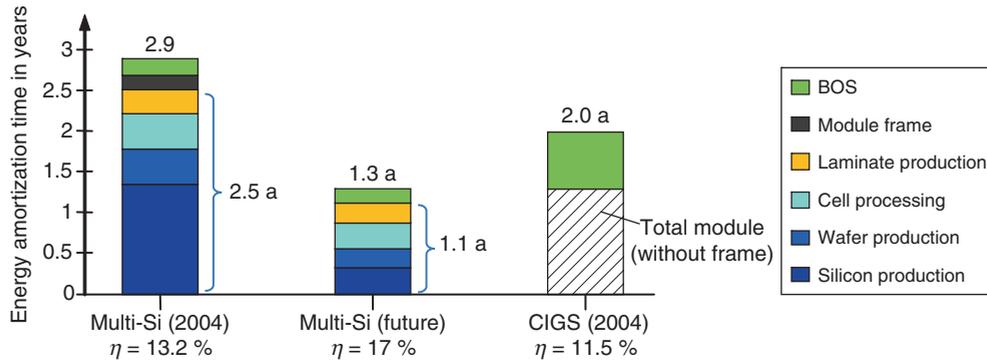
Figure 5.31 Energy amortization times of various types of plants: modern production techniques substantially reduce the energy demand for plant production [48]

Thus, in the course of its period of operation, the **plant generates** more than **eight times** the energy required for its production.

However, development does not stand still. Figure 5.31 shows the energy amortization times of three different technologies. The left bar shows the situation in the already considered multi-Si plant of 2004. Besides this, is an analysis of a **modern plant**. Compared to the old plant, use was made of **thinner wafers** (150 μm) and **higher efficiencies** (17%). Also this the silicon production of solar grade silicon was carried out with the aid of a **fluidized reactor** instead of the older Siemens reactor. These framework conditions are largely normal practice in modern plants.

The result is a **reduction of the energy amortization time from 2.9 years to 1.3 years**, which corresponds to an *ERoEI* of 19!

Figure 5.31 shows the results of a third plant with CIGS thin film modules from the year 2004. Here an amortization time of 2 years has already been achieved. Because of the relatively low efficiency, the area-dependent material portions (glass of the modules, support structure, etc.) have a strong influence. In the region of thin film technology, future improvements in energy amortization time will be achieved mainly by means of higher efficiency.

Remarks: the term BOS (Balance of System) combines the components of the system technology (support structure, cables, inverter, etc.).

Up to now we have always considered Germany as the site of photovoltaic plants. **Operation** of a plant in **southern Europe** (e.g., Spain) would reduce the energy amortization time **by a factor of 1.7** again.

> **?** Would the energy amortization time be reduced further if recycled material is used in production?

> **!** At present, module recycling is not a part of the calculation of the energy amortization time. In fact it would effect a further improvement of the environmental balance of photovoltaic plants in the future. The materials silicon, glass and aluminum can be reused very efficiently. A saving of more than 95% can be achieved especially with aluminum.

> **?** What is the actual energy amortization of other power generating plants such as wind turbines or coal fired power stations?

> **!** Depending on their location, wind turbines have an energy amortization of only 3–5 months for a typical life of 15 years [89]. Conventional power plants never produce more energy than is used for their production and operation as ever more primary energy in the form of coal or gas or uranium must be provided. Their energy amortization is therefore infinite to a certain extent.

SUMMARY

After having considered the individual cell technologies in great detail, it is now time for a summary. Table 5.2 shows the efficiencies of the types of cells together with their most

Table 5.2 Comparison of the various cell technologies

Cell technology	η_{Cell_Lab} (%)	η_{Module} (%)	Important advantages and disadvantages
Mono c-Si	25	20	+ Very high efficiencies + Unlimited availability − Presently high energy amortization time
Multi c-Si	20.4	17	+ High efficiencies + Unlimited availability + Acceptable energy amortization time
a-Si (single)	10.1	7	+ Low temperature coefficient
a-Si (tandem)		8	− Efficiency too low
a-Si (triple)	13	8.2	
a-Si/μc-Si	11.7	10	+ Potential for improvements − Low efficiencies
CdTe	16.7	11	+ Medium efficiencies − Availability problem + Potential for improvements − Image problem + Low energy amortization time
CIS	19.4	15	+ Acceptable efficiencies + Potential for improvements + Low energy amortization time − Availability problem
Mono c-Si/a-Si (HIT cell)	23	19	+ Very high efficiencies + Great potential for improvements
III/V semiconductors	32	n.a.	+ Extremely high efficiencies (with concentration over 40%) − Possible availability problem − Only sensible in concentrator systems
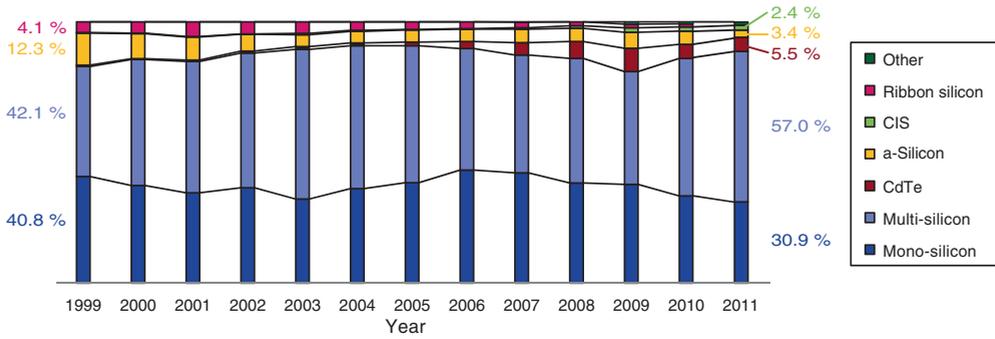
Figure 5.32 Portion of various cell technologies in percent over the years. Crystalline silicon continues to dominate the world market with a share of more than 85% [90]

important advantages and disadvantages. In the second column the respective peak efficiencies of laboratory cells are shown and the third column shows the greatest efficiency of the modules delivered on the market.

Figure 5.32 shows the **development** of the worldwide photovoltaic market with reference of the various **cell technologies**. The two crystalline technologies have for years dominated photovoltaic production with a market share between 80 and 90%. Meanwhile thin film technology has made up ground again especially driven with the CdTe production of First Solar. However, in 2011 the portion of c-Si cell installations was again at 88%. It can be assumed that especially the CIS technology will make up in percentage points.
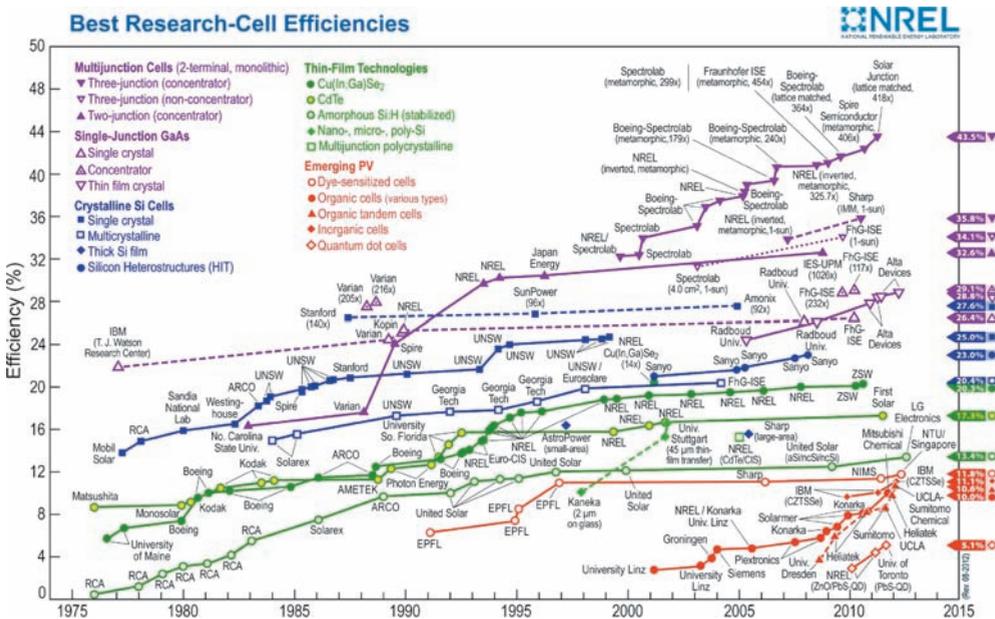
Figure 5.33 Development of record cell efficiencies in the past 40 years: Practically all technologies continue to show increasing efficiencies (source: NREL)

Finally let us look at Figure 5.33. This presents the development of the best cell efficiencies over the past 40 years. It shows the great advances that have been made since then.

In the upper part we naturally find the stacked cells of III/V semiconductors under concentrated sunlight. The winner is the already well-known cell from the **Solar Junction** described in Section 5.2 with an efficiency of **43.5%**.

With the crystalline cells we find the **PERL cell** with an efficiency of **25%** developed by Martin Green at the UNSW in Australia (see Section 4.7). Also noticeable are the rapid advances in **organic cells**: Within only 10 years the **efficiencies** have increased almost **fourfold** from 3% to nearly 12% today.

As we are now very well acquainted with the principles and production of solar cells, we will now turn our attention in the next chapter to the application of solar generators.

6

Solar Modules and Solar Generators

In this chapter we will become acquainted with the buildup of solar generators. This is understood to be the interconnection of solar modules in series and parallel, connected into a direct current source. First we will deal with the features of solar modules and the problems that can arise in the connection of modules. Then we will consider the special components of direct current technology and then look at different structural variations of photovoltaic systems.

6.1 Properties of Solar Modules

The properties of solar modules (temperature coefficient, efficiency, etc.) are mainly determined by the solar cells used in those modules and, in addition to this, the type of interconnection in the module. Here parallel and series connections have different effects, especially in the case of partial shading.

6.1.1 Solar Cell Characteristic Curve in All Four Quadrants

If several cells are interconnected, then reverse voltages or reverse currents can easily occur in individual cells. The result of this is that these cells operate not only in the first but also in the second or fourth quadrant. As a reminder, Figure 6.1 shows the characteristic curves of a solar cell in all quadrants. Here the generator reference-arrow system has been used again.

The first quadrant is called the **active region** as this is where normal operation occurs and in which power is generated. The **diode reverse region** is situated in the second quadrant: with rising reverse voltages, the starting **avalanche breakthrough** of the p-n junction (see also Section 3.5.4) can clearly be seen. The **diode pass region** is situated in the fourth quadrant. It is sometimes called the **reverse current region** as the current flows in reverse direction to the normally flowing photocurrent.
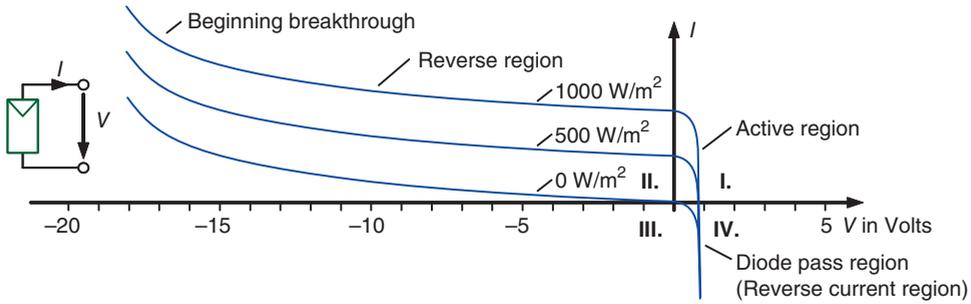
Figure 6.1 Solar cell characteristic curves in all quadrants in the generator reference-arrow system

6.1.2 Parallel Connection of Cells

We will first consider the parallel connection of cells in a solar module. Figure 6.2 shows a mini-module that will consist of three parallel-connected solar cells. The **parallel connection** forces all the cells to have the **same voltage**. At the same time the **individual currents are added up**:

$$V = V_1 = V_2 = V_3 \tag{6.1}$$

$$I = I_1 + I_2 + I_3 \tag{6.2}$$

The simplest method drawing the overall characteristic curve (module characteristic curve) is to prescribe voltage values and then add the individual currents.

What happens when one of the cells is partly shaded? In the following we will call this cell **"Shady"** (see Figure 6.3). We will assume that Shady is three-quarters shaded. We know from Chapter 4 that the open circuit voltage of Shady only alters slightly but that the short circuit current will decay by about three-quarters.

Figure 6.3 shows the effect on the overall characteristic curve of the solar module: it also decays by approximately the amount of the current loss of Shady whereas the open circuit voltage hardly changes. The power loss of the solar module is thus approximately one quarter and corresponds to the portion of the area of the module that was shaded. Therefore the **parallel connection reacts** in a relatively **good-natured** way to the partial shading. When considering the series connection we will see that this behaves in a very much worse fashion.
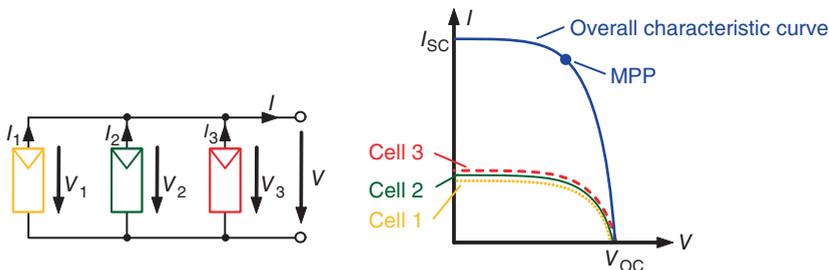
Figure 6.2 Parallel connection of solar cells: The voltage is the same in all cells while the currents add up
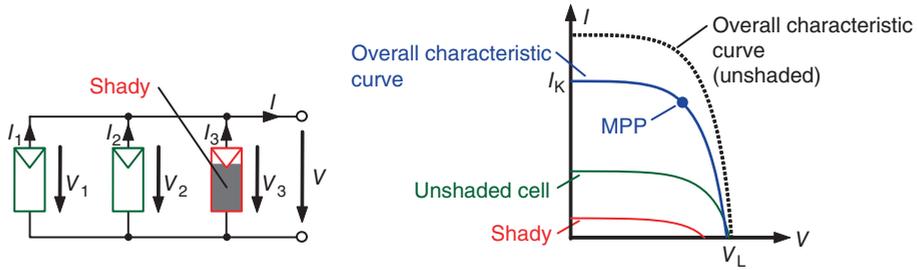
Figure 6.3 Shading one of the three cells: The current of the overall characteristic curve decays by the same amount as the current of Shady

Why don't we connect all cells in parallel?

If all cells were connected in parallel then the module would have an open circuit voltage of only 0.6 V and a short circuit current of, for instance, 100 A. To transport this current we would need an extremely thick cable. Besides this, typical photovoltaic plants (especially solar plants connected to the grid) would need much higher voltages that could only be generated from the 0.5 V with much effort.

6.1.3 Series Connection of Cells

As already described, one connects many cells in a module in series in order to achieve "decent" voltages. Figure 6.4 shows the effect of **series connection** on an example of a three-cell mini-module: the **current** in all cells is **the same** and the **overall voltage** is made up of the **sum of the individual voltages**.

$$I = I_1 = I_2 = I_3 \tag{6.3}$$
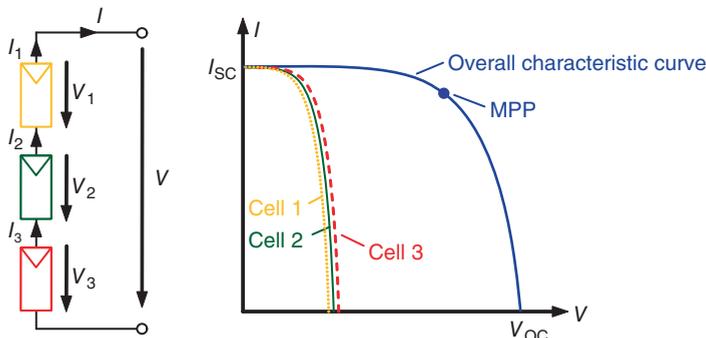
Figure 6.4 Series connection of solar cells: The voltages of individual cells are added together
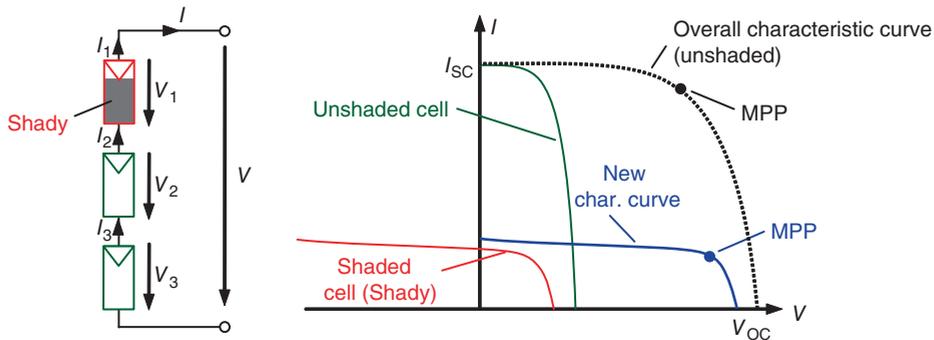
Figure 6.5 Partial shading of a cell with series connection: As Shady acts as the bottleneck, the overall current sinks strongly

$$V = V_1 + V_2 + V_3 \tag{6.4}$$

The overall characteristic curve of a series connection can be graphically determined in that one adds the individual voltages for fixed current values.

What happens when one of the cells is partly shaded? For this we will assume that we connect three equal cells in series of which again one is shaded by three-quarters (see Figure 6.5).

The two fully irradiated cells attempt to press their current through Shady. This causes a negative voltage at the shaded cell and it is therefore operated partly in the II_{nd} quadrant.

If we again add all the cell voltages at prescribed currents, then we obtain the new overall characteristic curve shown in Figure 6.5. The **current** is almost completely **determined by Shady**. The MPP power of the module has been reduced by approximately three quarters compared to the unshaded case, although just one single cell was shaded by three-quarters.

6.1.4 Use of Bypass Diodes

6.1.4.1 Reducing Shading Losses

The cells in modern modules are usually connected in series; this normally involves cell quantities of 36, 48, 60 or 72 leading to MPP voltages of between 18 and 36 V. Figure 6.6 shows a **typical solar module** with 36 cells and the resulting characteristic curve. Here, too, **one shaded cell** leads to a **drastic power reduction** from MPP_1 to MPP_2. Such a loss is unacceptable, which is the reason that so-called **bypass diodes** are included as additional components.

This is shown in Figure 6.7 in the example of Figure 6.6: a bypass diode is connected anti-parallel to every solar cell. As long as there is **no shading**, all cells have a positive voltage. This voltage acts as reverse voltage for the **diodes**; they conduct no current and **create no disturbance**. If Shady is now again three-quarters covered by shade, then this cell has a negative voltage. This means that the diode conducts and Shady is bridged. The remaining 35 cells can therefore conduct their full current. However, the bypass diode has a **threshold voltage V_{Th}** of approximately 0.7 V, which is approximately the open circuit voltage of a solar cell. Only when the current drawn off outside the module is as small as the current still deliverable by Shady, will Shady's voltage become positive again. As a result, the bypass diode blocks and Shady can still deliver a portion of the voltage (see characteristic curve at bottom right of Figure 6.7).
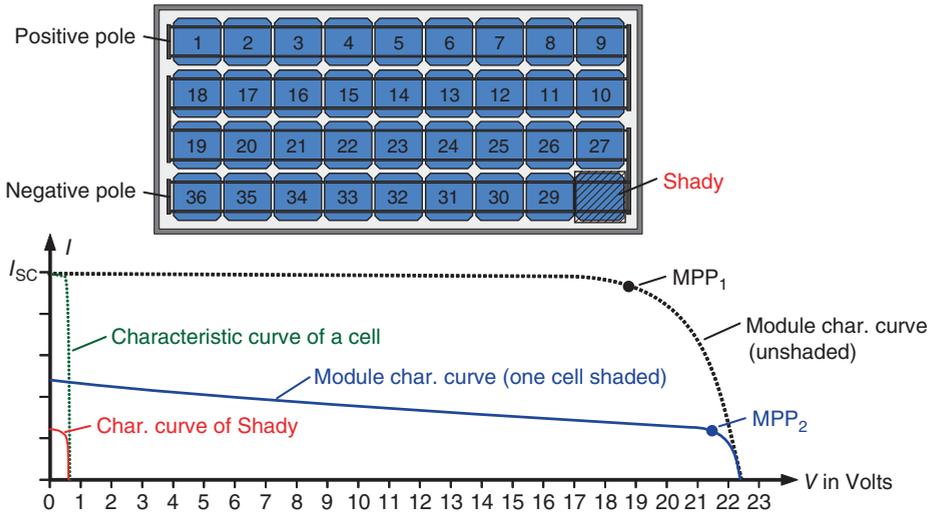
Figure 6.6 Solar module with 36 cells: The module power sinks drastically in the case of shading of a single cell

The adjusting MPP$_2$ in the case of shading is approximately two cell voltages lower than MPP$_1$. The power loss due to shading is:

$$\frac{P_{\mathrm{MPP2}} - P_{\mathrm{MPP1}}}{P_{\mathrm{MPP1}}} \approx \frac{I_{\mathrm{MPP}} \cdot 34 \cdot V_{\mathrm{Cell}} - I_{\mathrm{MPP}} \cdot 36 \cdot V_{\mathrm{Cell}}}{I_{\mathrm{MPP}} \cdot 36 \cdot V_{\mathrm{Cell}}} - \frac{-2}{36} = \frac{-1}{18} = -5.6\% \qquad (6.5)$$

The **losses** have been **drastically reduced due to** the **bypass diodes**.
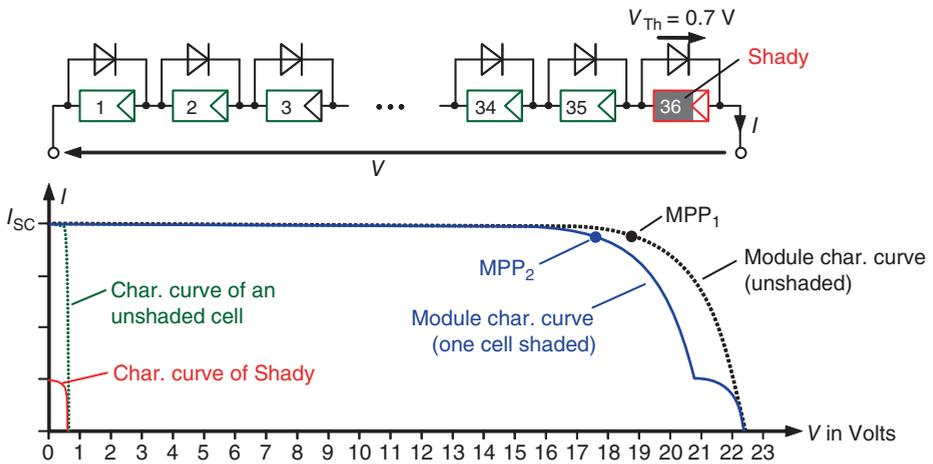
Figure 6.7 Solar module with 36 cells and bypass diode over each cell: The power loss is a minimum in the case of shading of any cell
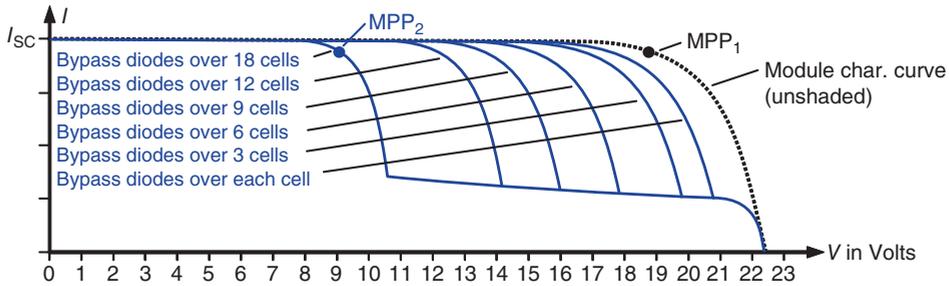
Figure 6.8 Characteristic curve of the solar module of Figure 6.7 with a different number of bypass diodes: With only a few diodes the shading has a particularly strong effect

However, only a **few bypass diodes are used** in **real solar modules**. If one wished to equip all cells with their own diodes they would have to be accommodated in the very thin EVA encapsulation. The heat created in the diodes in the case of shading would hardly be possible to dissipate there. Added to this is the fact that they could not be replaced in the case of a defect.

For this reason the bypass diodes are situated in the module connection box. Typically only one **bypass diode** is provided **for 12, 18 or 24 cells**.

The disadvantage of this solution is that the shading of a cell has a much stronger effect than is the case shown in, for instance, Figure 6.7. This is seen in Figure 6.8. Depending on the number of bypass diodes, a more or less large cell string falls away with shading. In the case of only two diodes per module, the module power-fall with the shading of only one cell is approximately half.

6.1.4.2 Prevention of Hotspots

The bypass diodes are used for another reason besides the reduction of shading losses: to prevent the existence of **hotspots**. This is understood to be the massive heating of a shaded cell caused by the other series-connected cells. An explanation is given in Figure 6.9. It again shows a solar module with 36 cells of which one is shaded.

Let us assume that the module is being operated in the short circuit mode. In this case the 35 cells attempt to push their power through Shady. The current in Shady is still positive but the voltage is negative. In order to find the operating point we mirror the original characteristic curve of Shady at the axis of the current. This results in an operating point with a transferred
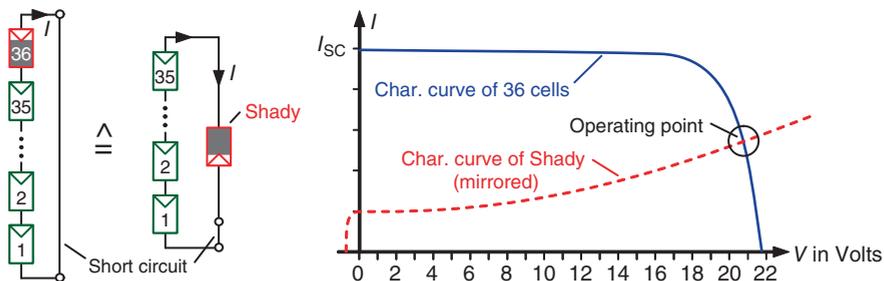
Figure 6.9 Solar module with 36 cells without bypass diodes: Shady acts as a load that is massively heated by the remaining 35 cells
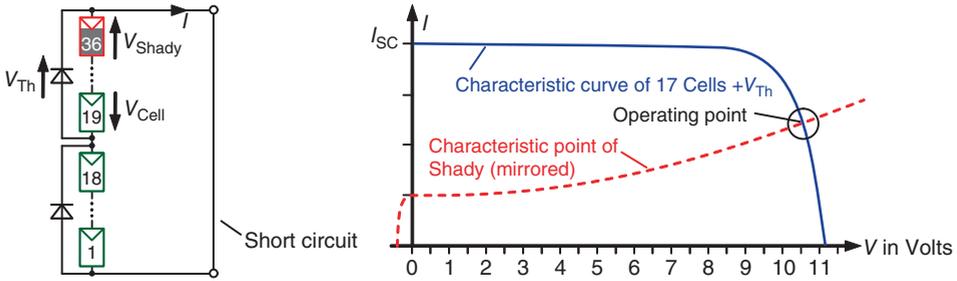
Figure 6.10 Solar module with 36 cells and two bypass diodes: The voltage at Shady clearly sinks compared with Figure 6.9 so that the heating is reduced

power, which is a multiple of the normal MPP power of a cell. The result is **massive heating of Shady**. The temperatures thus obtained can cause **damage to the EVA encapsulation** or even lead to the **destruction of the cell**.

If a maximum of 24 cells is used per diode, then experience has shown that in this case the heat power generated will not damage the module. Figure 6.10 once again shows the module of Figure 6.9, which is now equipped with a bypass diode over each of the 18 cells. Because of the high internal resistance of Shady, the current of the lower 18 cells is pressed through the upper bypass diode. A loop in the upper mesh provides the existing voltage V_{Shady} at Shady:

$$V_{Shady} = (z - 1) \cdot V_{Cell} + V_{Th} \tag{6.6}$$

with

z: number of cells under a bypass diode.

Thus Shady has a voltage of 17 cells and additionally, threshold voltage V_{Th} of the bypass diode.

The new operating point is approximately at half the voltage compared to Figure 6.9; thus the transmitted heat power is halved.

> **[?]** The short circuit case is always used in the last two figures. But a short circuit only occurs in the case of an error. Does the assumed heating also occur without a short circuit?

> **[!]** Normally the modules are connected in series with other modules and connected to an inverter. This operates the modules in the MPP. The MPP current of a module is only slightly below the short circuit current. Thus, the actual heating of Shady is actually almost as great as in the short circuit case.

> **[?]** In which case does Shady heat up most? With greater or with lesser shading?
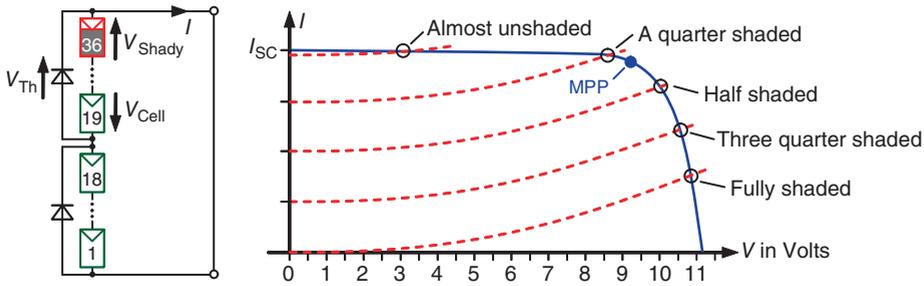
Figure 6.11 View of various degrees of shading: The transferred heat power reaches a maximum for degrees of shading between a quarter and half of the cell

> 【!】 In general this is hard to say. For this we must check where the operating point sets with the respective shading. Figure 6.11 shows the characteristic curve for Shady in various degrees of shading. It can be clearly seen that the maximum power occurs for degrees of shading between one quarter and half. However, different cell types have greatly different reverse characteristics that also depend on the temperature. One can generally only say that maximum heating occurs with medium shading.

> 【?】 Is there also a hotspot by Shady in the partial shading of parallel connected cells (Figure 6.3)?

> 【!】 We will have to look at this in greater detail. The worst case for Shady is certainly the open circuit point of the module. In this case the two unshaded cells will try to press their current through Shady (Figure 6.12). The direction of the current through Shady is thus negative whereas the voltage remains positive and this corresponds to the load reference-arrow system. We will thus find the self-adjusting operating point when we mirror the characteristic curve of Shady about the x axis. The power imparted at this operating point to Shady is within the range of the MPP power of an unshaded cell. Therefore no hotspot will arise at Shady.

> 【?】 This may not be critical for two parallel connected cells. But what happens when many cells are connected in parallel?
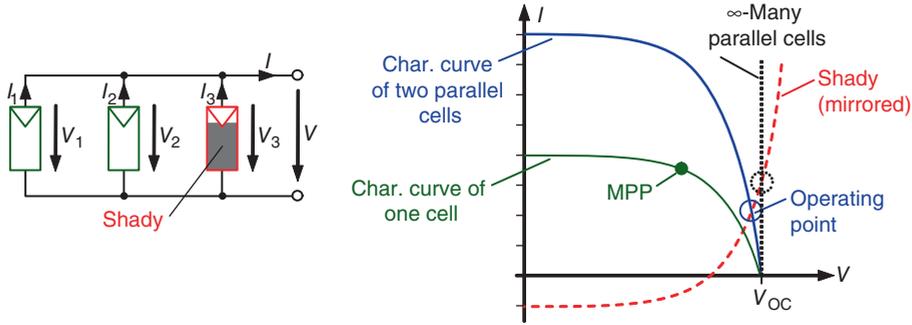
Figure 6.12 Characteristic curve of Shady and the two unshaded cells connected in parallel: In the case of an open circuit in the module, the resulting operating point shown receives little heat from Shady

> [!] In this case, too, we can make an estimate based on Figure 6.12. Further parallel cells lead us to add many cell characteristic curves to the shown characteristic curve of the two cells. It becomes ever steeper at the right edge and the operating point wanders upwards. In the extreme case of an infinite number of parallel cells there will arise an intersection point of Shady with a vertical line through V_{OC}. Even this operating point is not critical as regards the power.

6.1.5 Typical Characteristic Curves of Solar Modules

6.1.5.1 Variation of the Irradiance

Figure 6.13 shows the typical characteristic curve of the solar module of Solarworld SW-165 at a cell temperature of $\vartheta = 25\,°C$ and various irradiances. As already mentioned for the characteristic curve in Chapter 4, the short circuit current increases linearly with the irradiance, whereas the open circuit voltage alters little.

The purchaser of the solar modules is not interested only in the nominal power of the module at STC. Because of the high contribution of the diffuse radiation to the annual yield, the **weak-light behavior** of the solar module should also be taken into account. In the example of the SW-165 the MPP power for an irradiance of 200 W/m² is only almost 31 W. The efficiency has been reduced by:

$$\frac{\eta_{200} - \eta_{1000}}{\eta_{1000}} = \frac{31\,\text{W}/(200\,\text{W}/\text{m}^2) - 165\,\text{W}/(1000\,\text{W}/\text{m}^2)}{165\,\text{W}/(1000\,\text{W}/\text{m}^2)} = -6\%. \tag{6.7}$$

This relatively small degradation of the efficiency is also shown in many module data sheets. The **cause** of this degradation, is due to the **dependency of the open circuit voltage** on the incident light described in the Sections 4.4.2 and 5.6.2. For very small irradiances the **shunt resistance R_{Sh}** of the standard equivalent circuit is also noticeable (Section 4.5). For a small photocurrent there is only a small voltage V_D at the diode of the equivalent circuit so that it
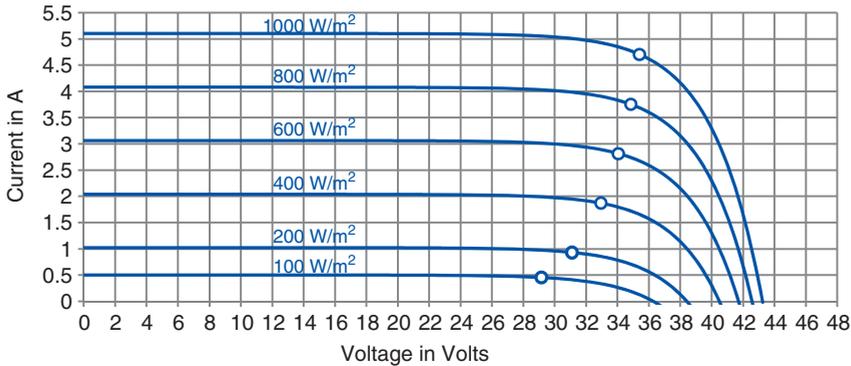
Figure 6.13 Characteristic curve of the SW-165 module at various irradiances and constant module temperature of 25 °C (Spectrum: AM 1.5)

hardly conducts. Instead of this, the photocurrent is converted partly in the shunt resistance R_{Sh} into heat.

6.1.5.2 Temperature Behavior

Beside the irradiance, also the temperature behavior of solar modules is of interest. As an example, Figure 6.14 shows the characteristic curve of the SW-165 at constant irradiance and different temperatures. The characteristic values from the data sheets are used here: $TC(V_{OC}) = -0.39\%/K$ and $TC(I_{SC}) = 0.04\%/K$. Starting from 25 °C, the open circuit voltage sinks from 43.2 V to only 35.6 V at 75 °C. At the same time the MPP power is reduced from 175 to 131 W.

> In the data sheets of solar modules the temperature coefficients $TC(V_{OC})$, $TC(I_{SC})$ and $TC(P_{MPP})$ are often designated by α, β and γ.
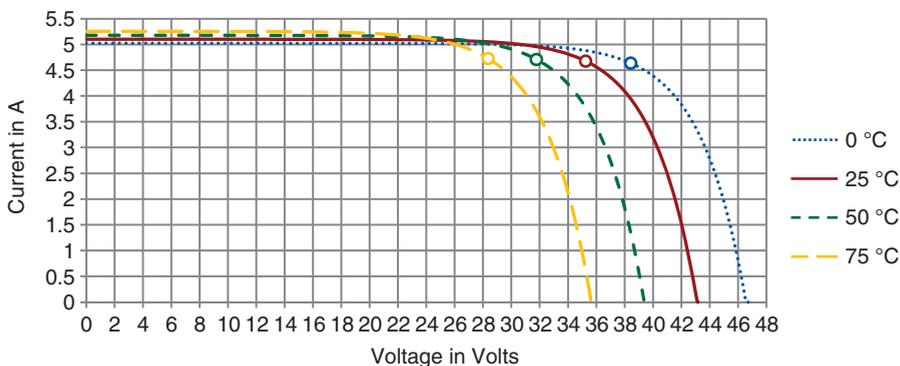
Figure 6.14 Characteristic curve of the SW-165 module from Solarworld at various module temperatures (Irradiance: 1000 W/m², spectrum: AM 1.5)

In Figure 6.13 the irradiance was varied and the temperature was kept constant at the same time. These types of characteristic curves can be obtained in the laboratory with a **module flasher** that irradiates the module for only a few milliseconds with an AM 1.5 spectrum and measures the characteristic curve at the same time (see Chapter 8). The module can barely heat up in this short period of time. However, things look quite different in the operation of a solar module in a PV plant. The solar module heats up differently with various irradiances. Added to this are influences such as types of construction and assembly of the modules, ambient temperature, wind velocities, and so on.

The data sheet gives the **nominal operating cell temperature (NOCT)** for estimating the self-heating of a particular module. NOCT is defined as the temperature that is arrived at for the following conditions:

- Irradiance $E = E_{NOCT} = 800\,\text{W/m}^2$
- Ambient temperature $\vartheta_A = 20\,°\text{C}$
- Wind velocity $v = 1\,\text{m/s}$

The **typical NOCT temperature** of c-Si modules is in the region of **45–50 °C**.

If the NOCT temperature is known then one can calculate approximately the expected cell temperature ϑ_{Cell} for a given irradiance and ambient temperature ϑ_A:

$$\vartheta_{Cell} = \vartheta_A + (NOCT - 20\,°\text{C}) \cdot \frac{E}{E_{NOCT}} \tag{6.8}$$

Here, for the sake of simplicity we assume that the temperature increase against the ambient temperature is proportional to the irradiance.

Example 6.1   Actual module power on a summer's day

The 200 W *Bosch c-Si M48-200* solar module has a NOCT temperature of 48.6 °C. What module power can be expected on a nice summer's day ($E = 1000\,\text{W/m}^2$, $\vartheta_A = 30\,°\text{C}$)?

The actual cell temperature is:

$$\vartheta_{Cell} = 30\,°\text{C} + \left(48.6\,°\text{C} - 20\,°\text{C} \cdot \frac{1000\,\text{W/m}^2}{800\,\text{W/m}^2} \right) = 30\,°\text{C} + 35.75\,\text{K} = 65.75\,°\text{C}$$

With the temperature coefficient $TC(P_{MPP})$ we obtain as actual power:

$$P = P_{STC} \cdot [1 + TC(P_{MPP}) \cdot (\vartheta_{Cell} - 25\,°\text{C})] = 200\,\text{W} \cdot (1 - 0.47\%/\text{K} \cdot 40.75\,\text{K}) = 161.7\,\text{W}$$

The **200 W module** thus **generates only** a power of **161.7 W**.   ■

6.1.6 Special Case Thin Film Modules

As already comprehensively described in Chapter 5, modules of thin film materials often possess properties that deviate strongly from c-Si modules. Of special interest to us are the characteristic curve and the shading tolerance. As an example, Figure 6.15 shows the characteristic curve of
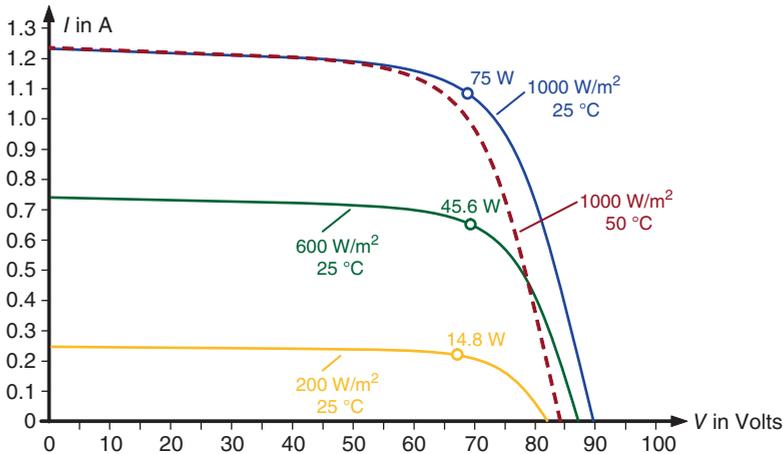
Figure 6.15 Characteristic curve of the CdTe module FS-275 from First Solar: A disadvantage is the low fill factor of 68%, but the power decay is relatively small at high temperatures

the **CdTe module** FS-275 of First Solar. Noticeable when compared to c-Si modules is the **low fill factor** of 68%. This results mainly from the relatively **high series resistances** that are a consequence **of the integrated series connection** of cells. The power reduction at 50 °C is only 6.25% due to the **low power temperature coefficient** of −0.25%K.

Thin film modules also differentiate themselves clearly from c-Si modules as regards the **shading tolerance**. As the individual cells are long and narrow they are often only partly shaded.

Figure 6.16 first shows the case where one module is shaded in the **longitudinal direction** (crosswise to the cell strips) by 25%. The current through all the cells is reduced by 25% so that also approximately only **25%** of the module power **is lost**. This is substantially different with the **lateral shading** (parallel to the cell strips). The left cells are fully shaded so that their current collapses. As no bypass diodes are connected, even the remaining cells are hardly effective. The **module power** in the example **sinks by** approximately **75%**.

> **?** Are bypass diodes used in thin film modules? Also, could hotspots occur besides shading losses?

> **!** Only a single bypass diode is installed in most thin film modules. This is meant to prevent the shading of a module from reducing the power of the whole string. Hotspots do not occur as the thin film cells have a relatively low breakdown voltage of 3–12 V. If a negative voltage occurs in a cell due to shading, then its reverse current increases until the breakdown voltage is reached. Thus, even without bypass diodes no voltages higher than 12 V occur.
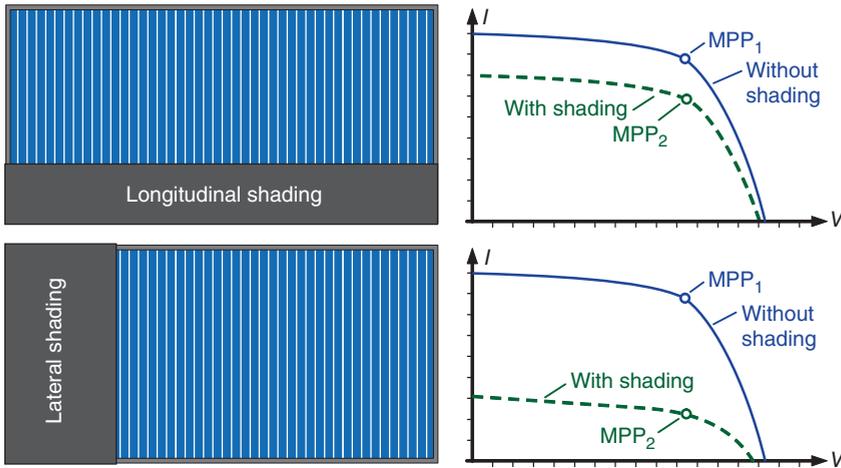
Figure 6.16 Comparison of longitudinal and lateral shading: In the case of lateral shading the module power declines drastically as complete cells fail (own measurements [21])

6.1.7 Examples of Data Sheet Information

Finally Table 6.1 lists the most important technical data of some solar modules.

6.2 Connecting Solar Modules

6.2.1 Parallel Connection of Strings

To construct a solar generator, firstly a row of modules are connected in a string in series. This string can again be parallel-connected to further strings. Figure 6.17 shows a typical structure for this.

The **string diodes** shown are meant to prevent that with the appearance of a short circuit or an earth fault in a string all the other parallel-connected strings drive a reverse current through the defective string. A disadvantage of the string diodes, however, is the voltage drop associated with them: This causes a continuous power loss also in normal operation of the plant. For this reason string diodes are seldomly used nowadays and are replaced by **string fuses**.

String fuses are special sand-filled DC fuses that safely extinguish the electric arc when fuses burn through. They are typically **dimensioned with double the nominal string current** as solar modules can easily accommodate reverse currents of double or triple the nominal current. However, this means that generators with up to three parallel strings do not need string fuses as in this case a maximum of two strings would feed their current through the defective string. At the same time it must be ensured that the cables are designed to handle the increased strength of current.

Table 6.1 Technical data of some solar modules [www.photon.info/]

Designation	SW-245 poly	c-Si M M200	SPR245 NE-WHT	HIT N240 SE10	US-64	U-EA120	FS-380	Q.Smart UF 95
Producer	Solarworld	Bosch Solar	SunPower	Sanyo	United Solar	Kaneka	First Solar	Q-Cells
Type of cell	multi-Si	mono-Si	mono-Si	HIT	a-Si	µc-Si/a-Si	CdTe	CIGS
Nominal power P_N	240 Wp	200 Wp	245 Wp	240 Wp	64 Wp	120 Wp	80 Wp	95 Wp
Nominal current I_N	7.96 A	8.10 A	6.05 A	5.51 A	3.88 A	2.18 A	1.58 A	1.55 A
Nominal voltage V_N	30.2 V	24.4 V	40.5 V	43.7 V	16.5 V	55 V	50.7 V	61.3 V
Short circuit current I_{SC}	8.44 A	8.70 A	6.3 A	5.85 A	4.8 A	2.6 A	1.76 A	1.7 A
Open circuit voltage V_{OC}	37.2 V	29.7 V	48.5 V	52.4 V	23.8 V	71 V	61.7 V	77.2 V
Temp.-coeff. TC (I_{SC})	0.034%/K	0.035%/K	0.033%/K	0.03%/K	0.1%/K	0.055%/K	0.04%/K	0.01%/K
Temp.-coeff. TC (V_{OC})	−0.34%/K	−0.34%/K	−0.27%/K	−0.25%/K	−0.31%/K	−0.39%/K	−0.27%/K	−0.3%/K
Temp.-coeff. TC (P_{MPP})	−0.48%/K	−0.47%/K	−0.38%/K	−0.30%/K	−0.21%/K	−0.35%/K	−0.25%/K	−0.38%/K
NOCT	46 °C	48.4 °C	45 °C	44 °C	46 °C	45 °C	45 °C	51 °C
Module efficiency η_M	14.3%	15.1%	19.7%	19.0%	7.5%	9.8%	11.1%	12.7%
Number of cells	60	48	72	72	11	106	154	118
Number of bypass diodes	3	3	3	3	11	1	1	1
Length L in mm	1675	1343	1559	1580	1366	1210	1200	1190
Width W in mm	1001	994	798	798	741	1008	600	630
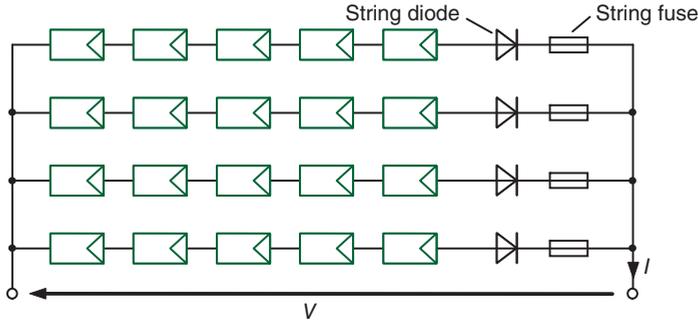
Figure 6.17 Structure of a solar generator with several strings

6.2.2 What Happens in Case of Cabling Errors?

Assume that during the cabling of a solar generator an unequal number of modules per string are interconnected. For an example of this see the generator in Figure 6.18: it contains two strings with each four modules and one string with only two modules.

What current will flow in the right hand string? The **worst case** is certainly the **open circuit case** in which both the left hand strings press their current through the right hand string. Thus, in a manner similar to Figure 6.12, we could depict the right-hand string in the load reference-arrow system. There arises an operating point at which a reverse current in the right-hand string is set to almost the double module short circuit current. **This operating condition** is **not critical** for both modules.

At the generator connections, in this example, in the open circuit case one would measure a voltage of approximately 90 V instead of the expected 160 V.

This type of cabling error would be discovered by a simple measurement with the multimeter.
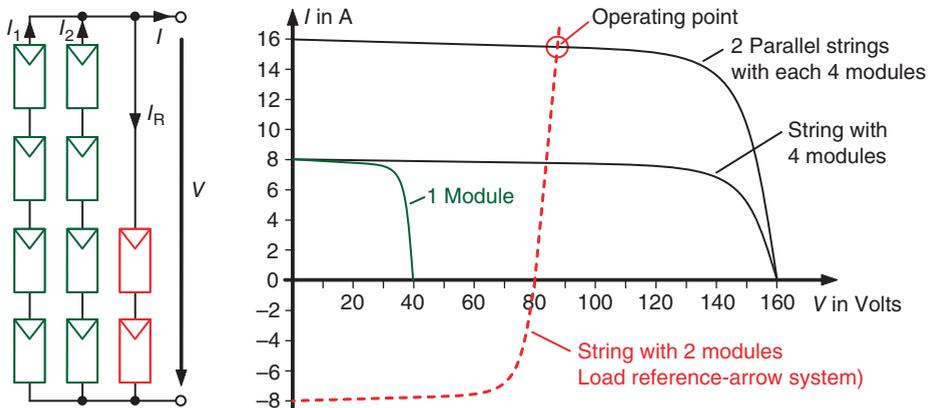
Figure 6.18 Structure of a solar generator with cabling error: The right-hand string has two modules too few so that a reverse current of almost double the module short circuit current is set
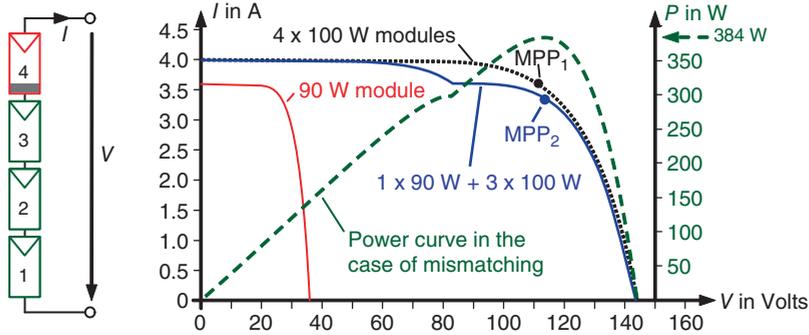
Figure 6.19 Effect of mismatching losses: The series connection of three good and one bad module leads to an overall power of only 384 W instead of the expected 390 W

6.2.3 Losses Due to Mismatching

If one purchases several modules of the same type, then they are not fully the same in their voltages and currents because of **manufacturing tolerances**. For this reason it can occur when connecting the solar modules to a generator that the overall power of the modules is not the same as the sum of the individual powers. The losses occurring in this way are called **mismatch losses**.

In order to explain this phenomenon we will assume a string of four 100 W modules (Figure 6.19). One of the modules will have a nominal power of only 90 W due to manufacturing tolerances. In principle, we can see this as though a normal 100 W module is only irradiated with 900 W/m^2. The *I/V* characteristic curve shows a new MPP$_2$ that lies at 384 W. This is about 6 W below the sum of the module power of 390 W.

The loss occurs because the three good modules can no longer contribute their full current to the MPP$_2$.

Thus, one can state for the installation of a photovoltaic plant:

> If the purchased **modules show** clear **manufacturing tolerances**, then they should be **sorted in such a way** that always **modules with the same short circuit current** are **combined** into a string.

6.2.4 Smart Installation in Case of Shading

In Section 6.1 we have discussed the shading losses in solar modules in detail. When connecting many solar modules, thought must also be given how the losses of shading can be kept as low as possible.

Let us assume that we wish to build up a solar generator of eight modules, each with 100 W. The first possibility is series connection of all modules into a single string (Figure 6.20). The unshaded modules will produce approximately 800 W in the MPP (MPP$_1$ in Figure 6.20). If module 8 is shaded by three quarters then the current also drops by three quarters. As the module is equipped with bypass diodes the remaining modules feed their power past module 8.
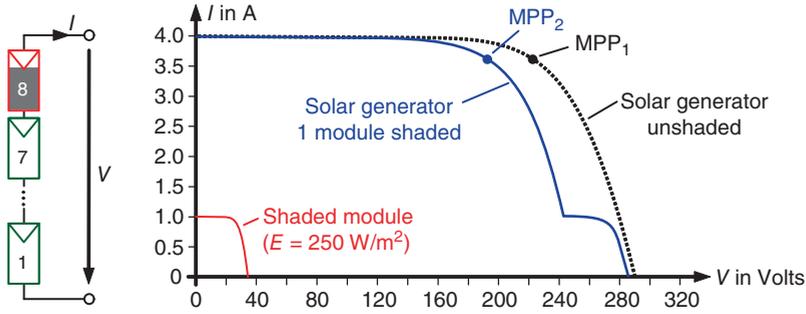
Figure 6.20   Series connection of all eight modules into a string: The shading of a module only has a small effect on the overall power

Thus the MPP moves by approximately one module voltage to the left so that the result is a new MPP power:

$$P_{MPP2} = 196\,\text{V} \cdot 3.57\,\text{A} = 700\,\text{W}$$

This means that the shaded module makes practically no contribution to the overall power.

What happens now if we build up the solar generator from two strings each with four modules (Figure 6.21)? In the unshaded condition the result is again the maximum power of 800 W. If module 8 is shaded again as before, then here too, the MPP will move by almost one module voltage to the left. The result is the new MPP_2 from Figure 6.21:

$$P_{MPP2} = 89\,\text{V} \cdot 7.1\,\text{A} = 632\,\text{W}$$

Compared to the first case we have lost almost 70 W.

> [?] Why do we have greater power losses now? As before, only one of eight modules is shaded!
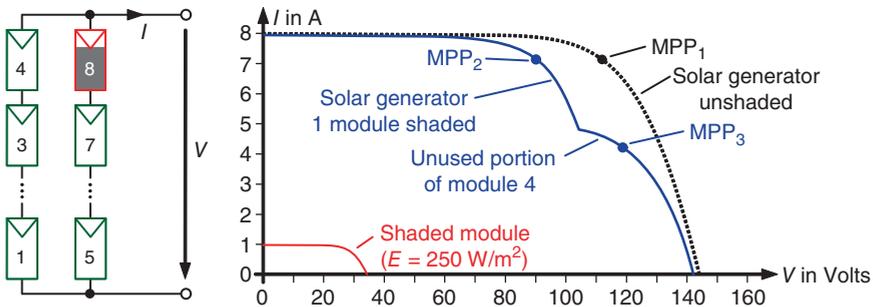
Figure 6.21   Connection of eight modules into two strings with each four modules: The losses for shading of a module doubles when compared to Figure 6.20

> [!] Due to the division of the solar generator into two strings, the shading of module 8 also affects the left string. Module 4 can make almost no contribution to MPP$_2$ power as a large part of its power is unused (see Figure 6.21). The shading of module 8 thus acts as if module 4 is shaded as well as module 8.

In general one can derive a rule-of-thumb from this:

> If there is a **danger of shading** in a solar plant then **all possible modules should be combined into a single string**. This string should possess its own MPP tracker (see Chapter 7).

6.3 Direct Current Components

6.3.1 Principle Plant Build-Up

The typical overall structure of a photovoltaic plant connected to an electric grid is shown in Figure 6.22. The current of the series-connected solar modules is fed via the **string line** to the **generator connection box (GCB)**. Besides the already discussed **string fuses**, this possibly contains a **DC disconnector** with which each individual string can be disconnected. The two **varistors** ensure protection against thunderstorm-caused voltage peaks.

From the generator connection box the main DC line leads to the inverter. The DIN VDE 0100-712, specially developed for photovoltaic plants, requires a main switch in order to safely disconnect the solar generator from the inverter. This main **switch must be specially designed for direct current** due to the fact that with **direct current** the resulting **electric arc** is not self-extinguishing when disconnected.
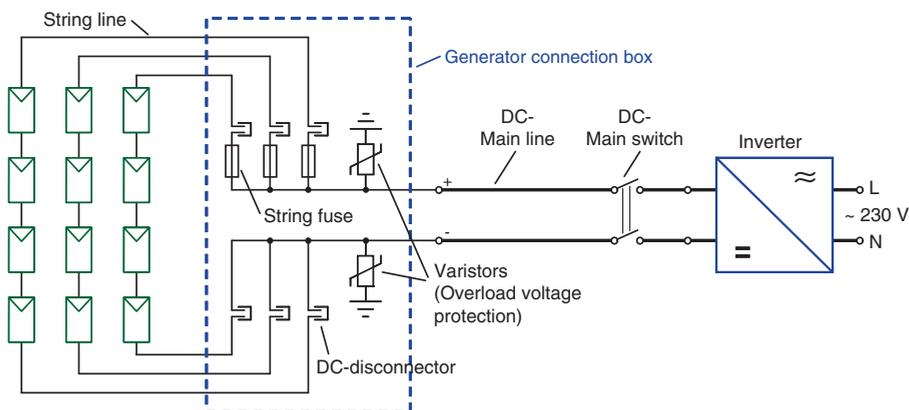
Figure 6.22 Structure of a typical photovoltaic plant connected to the electric grid: The individual strings are combined in the generator connection box and further connected via the main line to the inverter
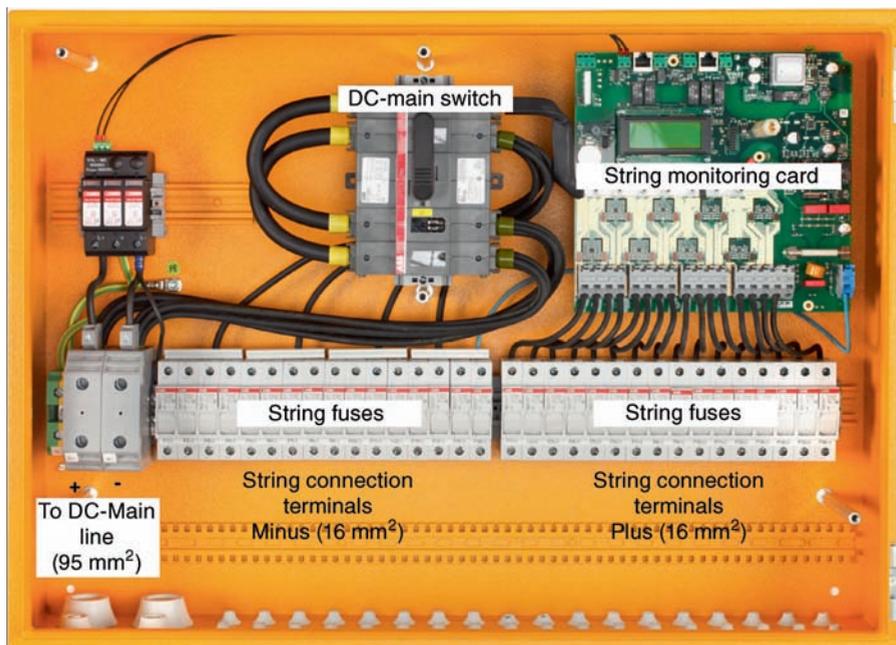
Figure 6.23   Interior of a modern generator connection box: Besides the typical components of DC main switch, string fuses and overload voltage protection, it also contains electronic instrumentation for remote monitoring of strings (photo: Sputnik Engineering AG)

Figure 6.23 shows the interior of a **generator connection box**. Besides string fuses and overload voltage protection, also the main DC switch was directly built-in here. In addition, the model contains the measurement instrumentation that monitors the string currents and string fuses and permits **remote control** by means of a network connection. For smaller plants, the components of the generator connection box are often included completely in the inverter.

If an individual string is to be disconnected, for instance, to carry out measurement on it, then the **DC disconnector terminals** must **not be pulled under any circumstances while under load**. The disconnection will immediately lead to an **electric arc**. Instead the plant must first be shut down by means of switching off the main DC switch.

6.3.2 Direct Current Cabling

There are also special requirements for **DC cables**. They should be **double-insulated** for protection against short circuits; mostly **positive and negative lines are carried in different cables**. As the string cables are subject to the weather, solar radiation and high temperatures, they must be **UV resistant, flame retardant** and designed for **high operating temperatures**. **Solar connectors** have been developed for connecting the modules and these provide simple and safe connections. They are designed such that no accidental touching of the contacts can occur. Figure 6.24 shows an example of the connectors from the Multicontact Company that have become a quasi-standard. The type MC-3 has meanwhile been mostly replaced by the newer type MC-4 as this possesses a lock against accidental disconnection.
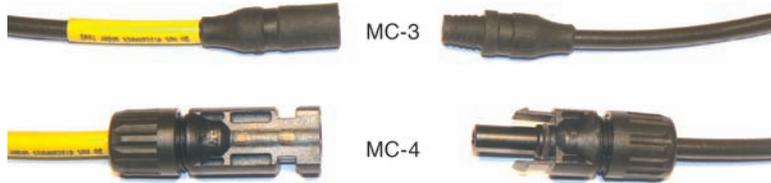
Figure 6.24 Solar plug assortment of the Multicontact Company: The MC-4 has a mechanical lock to prevent accidental disconnection

In order that the expensive electrical energy is not immediately turned into heat, care must be taken to ensure **sufficient cross-sectional area** of the cables. In order to determine the **losses**, resistance R of the cables is first calculated:

$$R = \frac{\rho \cdot l}{A} \tag{6.9}$$

with

l : length of cable
A : cross-sectional area of the cable
P : specific resistance of copper: $\rho_{Cu} = 0.0175\,\Omega\cdot\text{mm}^2/\text{m}$

The length l must be the overall length of positive and negative lines. The cable losses can then be determined with:

$$P_{\text{Loss}} = I^2 \cdot R \tag{6.10}$$

There is a simple dimensioning rule for the maximum cable losses:

The electrical **cable losses** on the direct current side should be **a maximum of 1%** of the **nominal power** of the **plant**.

Example 6.2   Cable losses on the DC side

A PV plant is made up of two strings with each 10 Bosch M-200 solar modules (see Table 6.1). Each string has a cable length of $2 \times 10\,\text{m}$, the length of the DC main line is 15 m. All the lines have a cross sectional area of $4\,\text{mm}^2$. Are the losses tolerable?
We first calculate the resistance of the lines:

$$R_{\text{String}} = \frac{0.0175\,\Omega \cdot \dfrac{\text{mm}^2}{\text{m}} \cdot 20\,\text{m}}{4\,\text{mm}^2} = 0.09\,\Omega$$

$$R_{\text{Main}} = \frac{0.0175\,\Omega \cdot \dfrac{\text{mm}^2}{\text{m}} \cdot 30\,\text{m}}{4\,\text{mm}^2} = 0.13\,\Omega$$

The losses are:

$$P_{\text{Loss}} = 2 \cdot I^2_{\text{String}} \cdot R_{\text{String}} + I^2_{\text{Main}} \cdot R_{\text{Main}} = 2 \cdot (8.1\,\text{A})^2 \cdot 0.09\,\Omega + (16.2\,\text{A})^2 \cdot 0.13\,\Omega$$

$$= 11.8\,\text{W} + 34.1\,\text{W} = 45.9\,\text{W}$$

Compared to the plant nominal power of 4 kWp the loss is 1.1% and is thus slightly too high. Here a DC main line with 6 mm^2 cross-sectional area would be advisable. ∎

The loss of 1.1% calculated in the example does not mean that the operator of the plant loses 1.1% of the generated power every year. Seen over the year, the plant mostly works in part-load operation. As the losses rise with the square of the current, then, for instance, with a half-power operation only a quarter of the calculated value of 1.1% is lost. In the consideration of the typical occurrence of the various power levels a **power loss coefficient k_{PL}** of approximately 0.5 [40] is defined. With the calculated power losses of 1.1% the energy loss would be approximately 1.1%·0.5 = 0.55%.

6.4 Types of Plants

Because of the modularity of the photovoltaic technology, solar power plants can be erected in fully different sizes and structural environments. We will look at the most important variants in the following.

6.4.1 Open Air Plants

Open air plants are mostly built as large plants such as **solar parks in the megawatt range**. As an example Figure 6.25 shows the citizen solar park Hofbieber-Traisbach in Bavaria, Germany that has a total power of 1.3 MW with 5586 polycrystalline modules. The second example is a 3.5 MW solar park near Mehring on the Moselle consisting of 45 560 CdTe modules installed by the First Solar Company.

The **types of construction** of open air plants range across a wide spectrum. The foundation of the overall structure is usually a **ram foundation** in which a long steel rod or profile is driven

Figure 6.25 View of two solar parks: *Left*: Citizen solar park Hofbieber-Traisbach with 1.3 MWp of polycrystalline modules (photo: IBC SOLAR AG). *Right*: 3.5 MWp solar park at Mehring on the Moselle with CdTe modules (photo: juwi Solar GmbH)

Figure 6.26 Typical construction of an open air plant: Galvanized steel posts are rammed into the ground and serve as the base for the module panel support. (photo: Schletter GmbH)

into the ground. The material for the **module support structure** is mostly aluminum or galvanized steel (Figure 6.26). The modules are fixed to these rails by means of module clamps.

A variant of the ram foundation is the **screw-in foundation** in which a spiral-shaped tube is screwed into the ground to ensure a secure support (Figure 6.27). If the ground is rocky or if construction must progress especially quickly, then use can be made of **concrete foundations**, which will support the overall construction with their own weight.

Some open air plants are also built with tracking systems. Here one differentiates between dual- and single-tracker plants. The **dual-axis plant** provides a much **greater yield** that is approximately 30% in Germany (see Chapter 2). However, the mechanically complex design means a substantial **price rise**. Besides this, the individual systems must be erected at relatively greater distances apart in order to prevent **mutual shading** with a low lying Sun. Most the plants make use of **astronomic trackers** in which the module always faces the Sun even when it is not visible. The **brightness tracker**, on the other hand, is based on a light sensor, in order to fix on a point in the sky on cloudy days that is brighter than in the direction

Figure 6.27 Alternative ground fixings: Screwed foundation as well as concrete heavy-load foundations (photos: Krinner Schraubfundamente GmbH, Schletter GmbH)

Figure 6.28 Tracked open air plants: Dual-axis Solon-Mover as well as single-axis system with horizontal axis (photos: Urnato © SOLON)

of the Sun. Which system is actually better suited will probably continue to be a matter of faith.

Figure 6.28 shows "Solon-Movers" on the left, each with 8 kWp power. The solar park Gut Erlasee in Germany was equipped with 1500 Solon-Movers from the Solon Company that follow the Sun in a dual-axis manner. However, the relatively **expensive dual-axis trackers** are hardly used today due to great price decreases for solar modules in the past few years.

Alternatives are the **single-axis tracker** plants. The right side of Figure 6.28 shows a system with a horizontal axis in which the south-facing modules always only follow the height of Sun (elevation). Here a hydraulically operated pusher rod moves up to 12 module rows simultaneously. These systems are relatively **cheap** to produce and hardly cause mutual **shading**. The **yield increase**, according to the information from the producer, is **between 12 and 18%** in Germany whereas in southern Europe, a yield increase between 21 and 27% is achieved.

6.4.2 Flat Roof Plants

In the case of flat roofs, **aluminum supports** originally dominated the market. Figure 6.29 shows an example of the photovoltaic teaching plant erected in 1994 on the roof of the Münster

Figure 6.29 Photovoltaic plant at the Münster University of Applied Sciences from 1994: The aluminum support structure is held down by means of flagstones (photo: W. Göbel)

Figure 6.30 Flat roof system on the roof of the Münster University of Applied Sciences of the year 2008: The modules are placed in plastic tubs that are again weighed down by paving stones

University of Applied Sciences in Steinfurt. A **heavy-load foundation** was achieved with the use of flagstones so that no roof penetrations were necessary.

Today more and more use is made of systems with plastic tubs. Figure 6.30 shows a 25 kWp photovoltaic plant from 2008 at the Münster University of Applied Sciences that was erected by the fair-Pla.net non-profit cooperative. The **polyethylene tubs** are weighed down with paving stones. Horizontal metal tubes serve to carry the string cables, which are thus protected from UV rays and movement.

In the case of roofs that can only carry **small area loads**, the classic heavy-load foundation is only recommended after investigation by a statics expert. As an alternative there are an increasing number of systems that manage to do with little weight. An example is shown in Figure 6.31 with the LORENZaero10 model: the **low, enclosed shape** provides the wind with hardly a surface of attack. Instead the elements are pressed down on the ground by the wind from the front (southerly wind). If, on the other hand, the wind blows from the back on to the system, then openings on the top side cause suction that keeps it on the ground. As all elements are interconnected, there is a high degree of stability for the overall system.

Figure 6.31 Solution for roofs with low bearing capacity: Because of the low closed form the system offers hardly any resistance to the wind; instead the elements are pressed down by the wind (source: LORENZ-Montagesysteme GmbH)

Figure 6.32 On-roof system on a private house: There should be at least a row of tiles spacing at the side in order to reduce attack possibilities for the wind

6.4.3 Pitched Roof Systems

Photovoltaic installations on pitched roofs are the most common form of PV systems and are found just as much in urban as in rural areas. They are relatively cheap to install as the **roof** is already available **as a base** and they fit harmoniously into the environment. An example of an **on-roof system** is shown in Figure 6.32: the modules are above and beside the dormer and there is enough spacing to minimize shading. **At the side** there is a **distance of** approximately **one row of tiles** to the edge of the roof in order to limit the wind attack possibilities as far as possible. The panel at the right bottom provides the power for a solar-driven watercourse pump.

The fixing of the module supports is carried out by means of **stainless steel roof hooks** that are screwed to the rafters of the roof (Figure 6.33). A sufficient distance of the hook from the
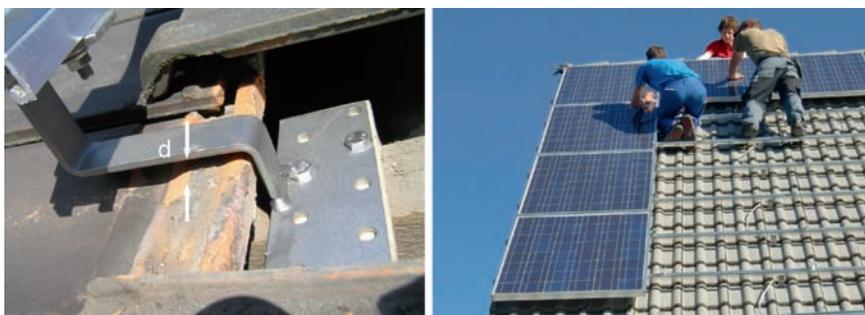
Figure 6.33 Fixing the on-roof system: the roof hooks are screwed to the rafters and thus form the base for holding the module supports. A sufficient distance between roof hooks and roof tiles is important in order to avoid damaging the tiles (photos: Ch. Niemann, A. Schroer)

InDax system (source: Schott solar AG)   In-roof system from Schüco (photo: Mertens)
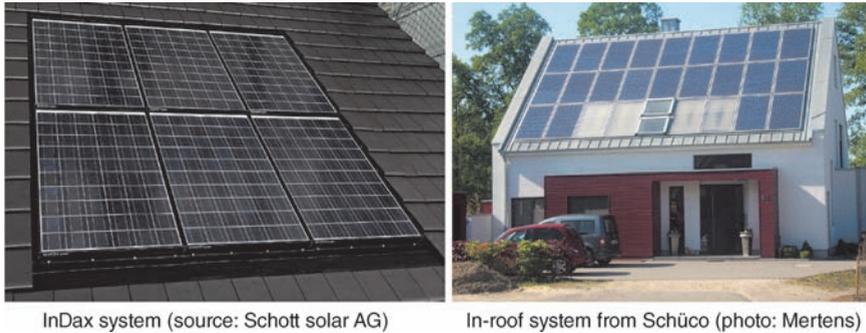
Figure 6.34 Examples on in-roof systems: The solar modules replace the actual roofing and are harmoniously integrated into the overall architecture

tiles is important, as the hook could bend with the weight of snow and damage the roof tiles below it. The horizontally arranged rails are made of special **aluminum profiles** that are usually also suitable for holding the module connection cables.

An alternative to erecting a photovoltaic system on the roof is to integrate it into the roof. Such an **in-roof system** (or **roof-integrated system**) consists of solar modules that form the actual roofing (Figure 6.34). With the InDax system by Schott Solar the individual solar modules are provided with special frames and then placed over each other like roof shingles. The model by Schüco, on the contrary, uses frame strips that are used for sealing between the individual modules.

A feature of this system is the combination with skylights and solar thermal collectors (to be seen at the left and right of the skylights). This provides a very harmonious overall view.

When using the in-roof system, special attention must be paid to **sufficient back ventilation** of the plant, **otherwise the module temperature rises** and the annual yield is less than a similarly arranged on-roof plant. A further problem is the **participation of various trades** during the installation of the plant. This requires the cooperation and clarification of whoever is responsible for the **warranty** in case of a leaking roof.

Figure 6.35 View of two façade installations: *Left*: a 50 kWp system of polycrystalline modules in Freiburg, Germany (source: Solarfabrik AG). *Right*: cold façade Prosol TF+ of a-Si modules (source: Schüco International KG)

6.4.4 Façade Systems

Façade systems are mostly installed on **industrial or office buildings**. Figure 6.35 shows on the left a solar façade erected in the year 2000 in the course of a renovation of a block of flats in Freiburg, Germany. With almost 200 multicrystalline modules, the system delivers 50 kWp of power and is designed as a back-ventilated hanging façade.

An alternative with thin film modules can be seen on the right in Figure 6.35: the cold façade ProSol TF+ by Schüco. It consists of large (approximately 6 m^2) thin film modules of amorphous silicon.

As can be seen from Table 2.4, the south oriented **façade provides only** about **70%** of an optimally arranged solar system. However, there are further limiting effects on the annual yield: shading due to trees, fire escapes, other buildings, and so on.

7

Photovoltaic System Technology

We are now well acquainted with the power generation chain of photovoltaics:

$$\text{Solar radiation} \rightarrow \text{cell} \rightarrow \text{module} \rightarrow \text{string} \rightarrow \text{PV generator}.$$

Now we will deal with how the electric power provided by the generator can best be utilized completely for feeding into the electric grid or other loads. For this purpose we will consider the possibilities of **adapting the PV generator to the** available electric **load**. An emphasis of this chapter is on **grid-connected systems** (also called on-grid systems) and the functional principles of the different types of inverters. Besides this we will look at **stand-alone systems** (also called off-grid systems) and examples of their dimensioning.

> Sometimes the expression **Balance of Systems (BoS)** is used to summarize all the components that are needed additionally to the solar modules to build up a complete PV system.

7.1 Solar Generator and Load

The power produced by the solar generator can be used by various consumers of electricity. Typical examples are for charging a battery, a solar driven water pump or a public supply grid. These different types of loads always have their own requirements of the provided voltages and currents. In most cases, therefore, a component must be interposed that makes the necessary adaptation possible.

7.1.1 Resistive Load

The load easiest to study is an **ohmic resistance**. In the *I/V* characteristic curve it is described as a linear equation:

$$I = \frac{1}{R} \cdot V \tag{7.1}$$
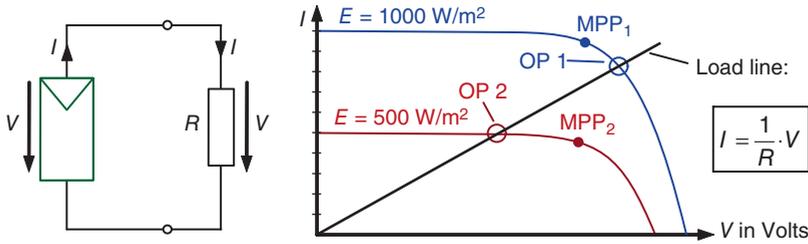
Figure 7.1 Operation of an ohmic load at a solar module: In the case of half the Sun's irradiance ($E = 500\,\text{W/m}^2$), the operating point (OP 2) is far away from MPP_2

Figure 7.1 shows the case of a direct connection of an ohmic load (e.g., a light bulb) to a solar module. If the solar generator is operated at $1000\,\text{W/m}^2$, then in this example, the operating point 1 is near the MPP_1 of the module. If the irradiance falls to half, then a new operating point 2 is adjusted that is, however, far away from the actual optimum MPP_2. In this case the solar module can **only** contribute **a portion** of the actually available **power** to the load. It is therefore desirable to **decouple** the voltage at the solar generator from the voltage at the load. For this purpose we use an electronic adaptation circuit, the **DC/DC converter**.

7.1.2 DC/DC Converter

7.1.2.1 Idea

A **DC/DC converter** (direct current converter) converts an input voltage V_1 into an output voltage V_2. The result of this is that the **voltage** at the solar module can be selected almost **independently** of the voltage at the load. Thus, for instance, in Figure 7.2 the voltage V_1 at the solar module can be kept constant. The self-adjusting operating point in both cases is very near to the respective MPP.
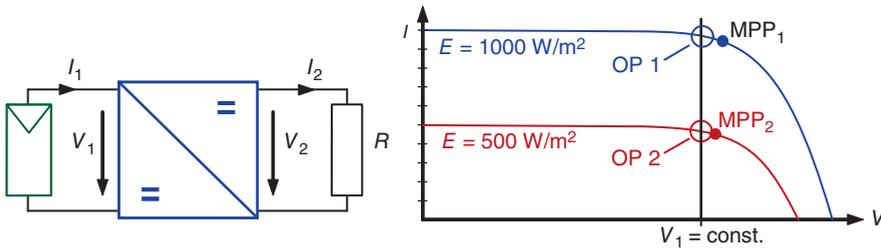
Figure 7.2 Application of a DC/DC converter: The voltage at the solar generator can be selected independently of that at the load; for example, it can be left constant

A direct current converter will never work without loss. However, good converters achieve **efficiencies of more than 95%**, the rest being converted into heat. In the case of an ideal converter with an efficiency of 100% the input and output power are the same:

$$P_1 = V_1 \cdot I_1 = V_2 \cdot I_2 = P_2 \tag{7.2}$$

If we choose V_1 differently to V_2 then the currents I_1 and I_2 must also be different. Thus the **voltage converter** works at the same time as an **impedance transformer**.

7.1.2.2 Buck Converter

Modules are often connected in series in order to obtain a high voltage. If this voltage is to be reduced then a **buck converter** (**step-down converter**) is used. The principle of the buck converter is to switch through the input voltage V_1 only for a certain time period T_{On} to the output voltage (so-called pulse width modulation – PWM, see Figure 7.3).

The result is a pulsed voltage $v_2(t)$ at the output that has a mean value of:

$$\bar{v}_2 = \frac{T_{On}}{T} \cdot a \cdot V_1 \tag{7.3}$$

with

T_{On} : On-time
$\;\;T$: time period

The quantity a is the **duty cycle** or **duty factor**:

$$a = \frac{T_{On}}{T} \tag{7.4}$$

In practical applications, a pulsed output component cannot be accepted. For this reason smoothing elements for current and voltage must be added. Figure 7.4 shows the complete circuitry.
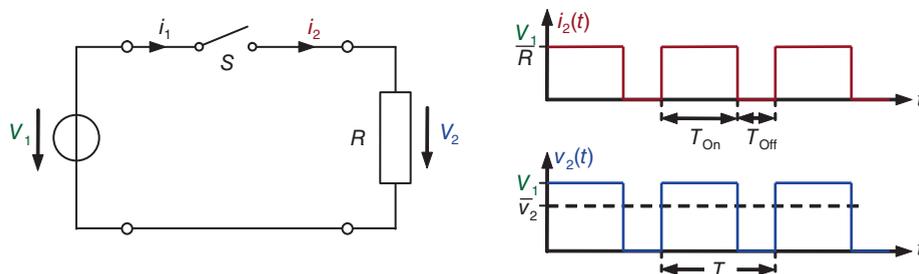
Figure 7.3 Simple model of a buck converter: At the output the result due to the pulse width modulation in the time average is a reduced voltage $\bar{v}_2$ compared to V_1
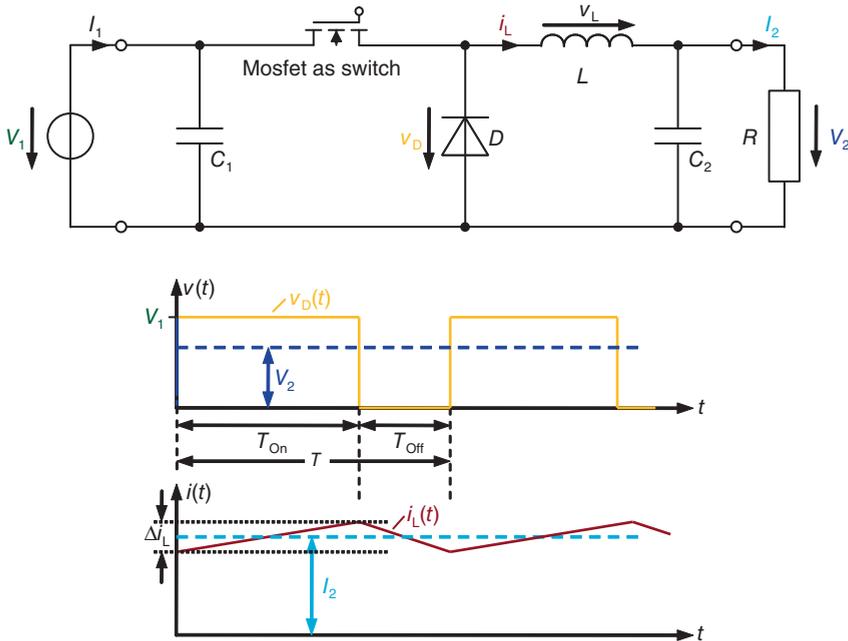
Figure 7.4   Circuit as well as current and voltage curves of the buck converter [91]

The **choke coil L** is used to ensure a continuous current i_L and the **capacitor C_2** is used for smoothing the output voltage. The capacity is to be large enough that we can assume a direct voltage V_2 at the output.

The function of the switch from Figure 7.3 is carried out in practice by a **semiconductor switch**, for example, a **power MOSFET** (Metal Oxide Semiconductor Field Effect Transistor). It can be switched like a normal switch via a positive potential at its gate terminal. The **capacitor C_1** serves to prevent that the source of the voltage is loaded at the input by pulsating currents.

In detail, how does this function? First we will look at the case of the MOSFET being switched on. For the voltage v_D at the diode there applies:

$$v_D = V_1 \tag{7.5}$$

The voltage at the choke coil there then follows

$$v_L = v_D - V_2 = V_1 - V_2 \tag{7.6}$$

Thus there is a constant voltage at the coil so that, according to the **induction law**:

$$v_L(t) = L \cdot \frac{d i_L}{dt} \tag{7.7}$$

We can say that for the time T_{On} the current will vary linearly with the time. The current rises with the **constant slew rate** (see Figure 7.4):

$$\frac{di_L}{dt} = \frac{v_L}{L} = \frac{V_1 - V_2}{L} \tag{7.8}$$

If the transistor is switched off at the time $t = T_{On}$, then the coil attempts to maintain the current i_L. It drives the current further via the **flyback diode D**. If we assume that this is an ideal diode ($v_D = 0$), then in an analogous manner to that previously mentioned, we can derive the slew rate of the current:

$$\frac{di_L}{dt} = \frac{v_L}{L} = -\frac{V_2}{L} \tag{7.9}$$

Thus, the current decays linearly with time. The value of the starting point is obtained from the thought that there can be no drop of direct voltage at an ideal coil. The constant voltage V_2 is derived from the mean average of the voltage v_D over time:

$$V_2 = a \cdot V_1 \tag{7.10}$$

with

a: duty factor

> Conclusion: By means of the variation of the duty factor, the **output voltage** of the **buck converter** can be set almost arbitrarily **between 0 and V_1**.

These results do not apply when the current i_L decays to zero during the time period T_{Off}. In this **discontinuous mode** the output voltage would no longer depend on the duty factor but also on the load current I_2. In order to prevent the undesired discontinuous mode one selects the switching frequency of the transistor to be as large as possible (e.g., 20 kHz). In this way a good quality of the output voltage can be achieved even for small values of L, C_1 und C_2. However, the cutoff frequency of the transistor presents an upper limit for the switching frequency. Besides, the switching losses increase with the rise of the switching frequency. Further details can be found, for instance, in [91].

7.1.2.3 Boost Converter

It is often necessary to convert a small solar generator voltage into a higher voltage, for example, in order to feed into the public grid. In this case use is made of a **boost converter** (**step-up converter**). The circuit is shown in Figure 7.5. First the transistor is switched on. With $v_S = 0$ follows $v_L = V_1$ so that the slew rate of the current can be immediately given as:

$$\frac{di_L}{dt} = \frac{v_L}{L} = \frac{V_1}{L} \tag{7.11}$$
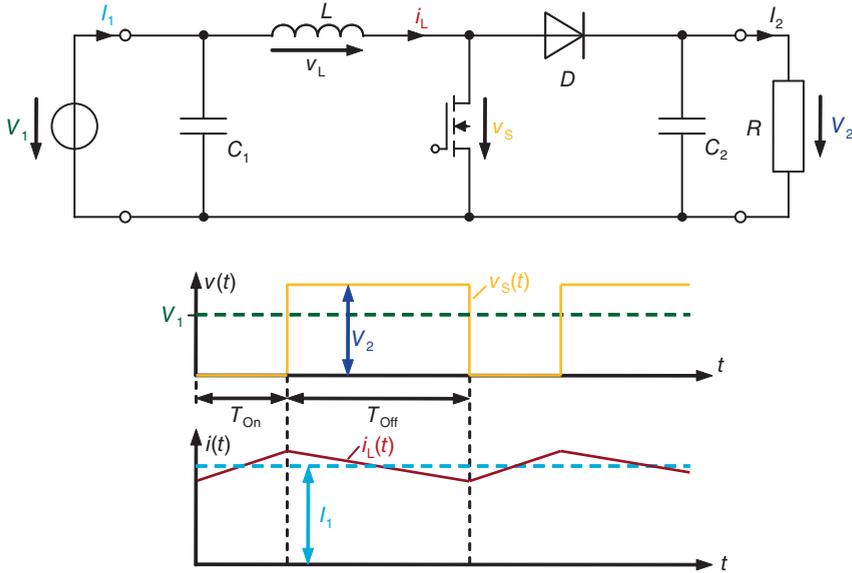
Figure 7.5 Connecting a boost converter with current and voltage progressions [91]

The transistor is switched off after the time period T_{On}. The choke attempts to maintain the current. We will assume that V_2 is greater than V_1. In this case the choke drives the current slowly down via the diode D at the output. The voltage at the choke is then:

$$v_{\text{L}} = V_1 - V_2 \tag{7.12}$$

and the current slew rate is:

$$\frac{\mathrm{d}i_{\text{L}}}{\mathrm{d}t} = \frac{v_{\text{L}}}{L} = \frac{V_1 - V_2}{L} \tag{7.13}$$

As i_{L} sinks the voltage v_{L} will be negative according to the Induction Law (7.7). If one solves (7.12) for V_2 then it will be clear that the **output voltage must be greater than the input voltage**, which will confirm our assumption:

$$V_2 = V_1 - v_{\text{L}} \tag{7.14}$$

Here, too, the following applies: the choke coil cannot accept direct current so that the temporal **mean value of $v_{\text{S}}(t)$ must be equal to V_1**. Therefore we obtain from the voltage progression in Figure 7.5:

$$V_2 \cdot T_{\text{Off}} = V_1 \cdot T \tag{7.15}$$

For the output voltage there is thus:

$$V_2 = \frac{T}{T_{\text{Off}}} \cdot V_1 = \frac{T}{T - T_{\text{On}}} \cdot V_1 = \frac{1}{1 - T_{\text{On}}/T} \cdot V_1 = \frac{1}{1 - a} \cdot V_1 \tag{7.16}$$

Example 7.1   Various duty cycles with the boost converter

Apply an input voltage of 10 V to a boost converter and adjust the duty cycles one after another to 0.1, 0.5, and 0.9. The output voltage results are 11.1 V, 20 V and 90 V.

∎

Conclusion: By varying the duty cycles one can set the **output voltage** of the **boost converter** by a **multiple of V_1**.

[?] Actually it is strange that with a longer switch-on phase of the transistor there is a greater output voltage of the boost converter. Should it not be the other way around?

[!] During the switch-on phase of the transistor the current at the choke coil rises. The longer the switch-on phase lasts the more power is stored in the choke, which it can then pass on in the switch-off phase to the output. To a certain extent the coil takes more impetus.

[?] What is the purpose of the diode D in Figure 7.5? In contrast to the buck converter we do not need a flyback diode here.

[!] Without the diode the output would be connected directly in parallel to the transistor. As soon as the transistor is switched on the capacitor would immediately be unloaded and the output voltage would be reduced to zero.

7.1.3 MPP-Tracker

After we have become acquainted with the DC/DC converter we can use it for MPP tracking (MPP control). Figure 7.6 shows the basic principle: At the output (or input) of the DC/DC converter the actual power is determined by means of measurement of current and voltage. The operating point can be varied by varying the duty factor a.

There are various methods of finding the MPP of which the ***Perturb and Observe method*** has become the most popular [92]. The flow diagram of the algorithm can be seen in Figure 7.7. Most of the MPP trackers start at the open circuit point of the *I/V* curve. First the actual power is determined and then the duty factor is increased. If the new power is greater than the old value, then the tracking was correct and the duty factor is raised further. If the MPP is exceeded then the measured power is decreased and the duty factor is reduced again. Thus the actual operating point varies slightly about the MPP.
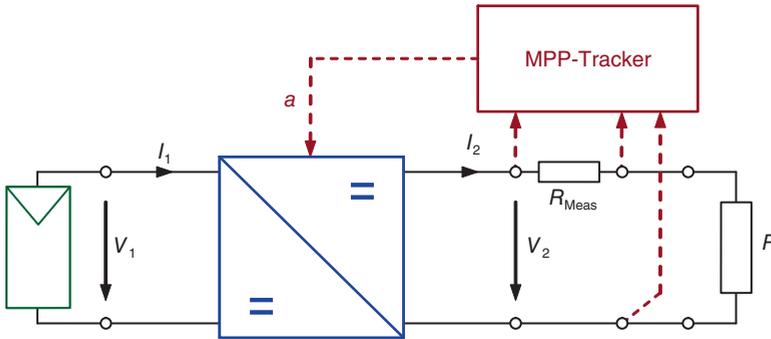
Figure 7.6 Principle of MPP tracking: The output power is maximized by measuring the current and voltage with the simultaneous variation of the duty factor
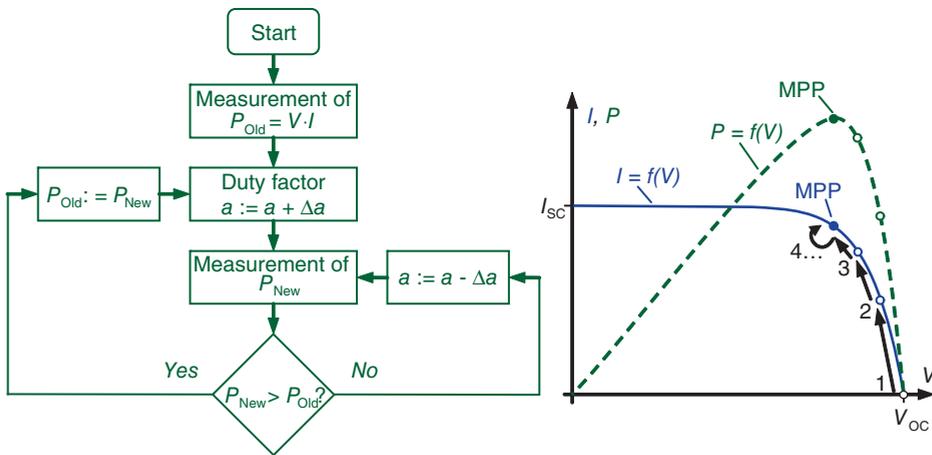
Figure 7.7 Algorithm of the *Perturb and Observe* method: Starting from the open circuit point the duty cycle is changed, the new power is determined and the duty cycle is further optimized depending on the result until finally the MPP is reached

7.2   Grid-Connected Systems

Although in the beginning, the main uses of photovoltaics were applications separated from the electric grid (see Chapter 1), today systems connected to the grid play a dominating role. In this, the electric power supply grid is used to a certain extent as storage that takes up the power that is fed to it.

The technical conditions of the worldwide energy supply grids differ from country to country. For example, the grid voltage of most countries in Europe is 230 V with a frequency of 50 Hz.

In contrast to this, the electric grids in the USA, Central America and a few other countries have a voltage of 110 V and a frequency of 60 Hz. This book deals with the European electric grid and the grid connection conditions refer to a large extent to Germany.
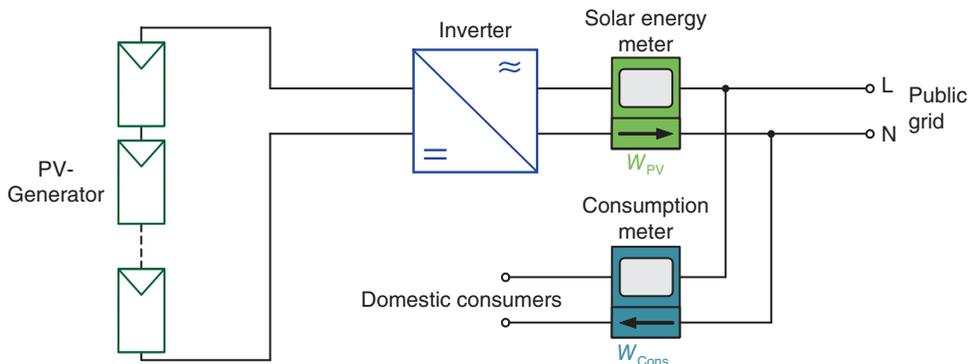
Figure 7.8 Classic connection of a photovoltaic installation to the public grid: The whole of the solar power is fed into the public grid via a feed-in meter whilst the domestic use is separately measured by means of a consumption meter

7.2.1 Feed-In Variations

The classic arrangement of a plant connected to the grid is shown in Figure 7.8. As most of the plants are refinanced by **feed-in tariffs**, the inverter feeds the generated power **completely** into the grid via a **feed-in meter**. Separated from this, the operator of the plant draws its normal **domestic energy requirements** via a **consumption meter**.

However, at present the feed-in tariffs in Germany are below the power consumption price for normal power tariff customers. For this reason it pays to use as much generated energy as possible for one's own use (the so-called **self-consumption**). Thus today a **bi-directional meter** is normally installed that measures both the fed-in and the energy taken from the grid separately (Figure 7.9).

If one still wished to know how much solar energy has been generated, then a **separate solar energy meter** is installed between the PV installation and the bidirectional meter as shown in Figure 7.9.

7.2.2 Installation Concepts

The various concepts for building up a solar power system suitable for connecting to the public grid are shown in Figure 7.10. The first type of installation with a **central inverter** is already
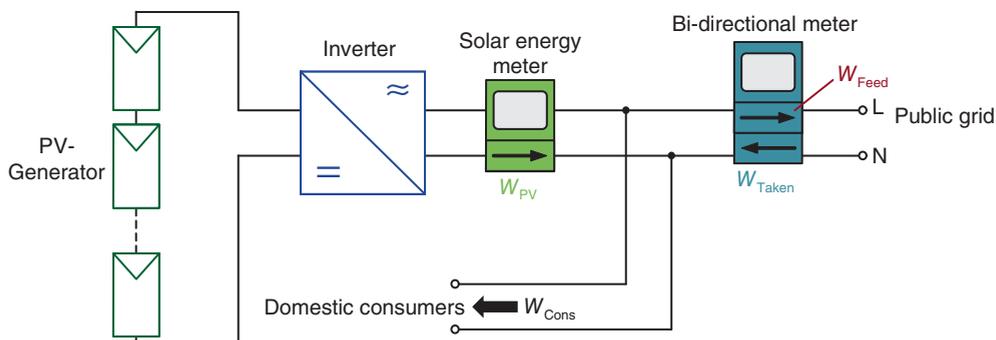
Figure 7.9 Use of bi-directional meter for separated acquisition of the fed-in and the energy taken from the grid. The solar energy meter is installed additionally if the overall generated solar energy also is to be measured
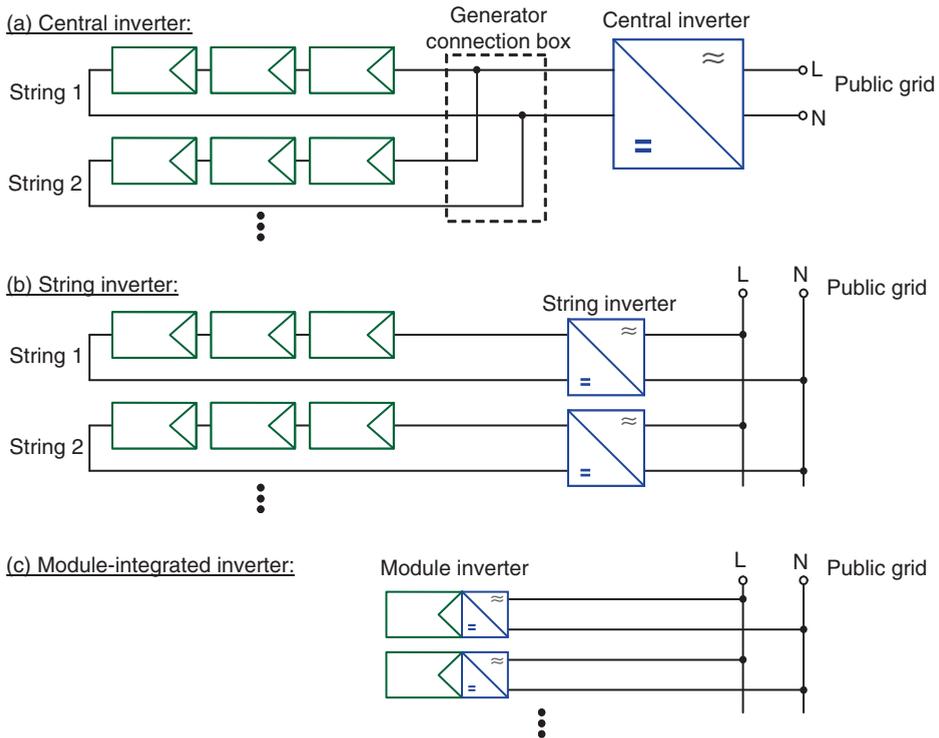
Figure 7.10 Variations of the arrangement of photovoltaic systems connected to the grid

familiar to us from Chapter 6. The individual strings are connected in parallel in the generator connection box and the generated power is fed into the grid via a central inverter.

The advantage of this concept is that only a single inverter is needed. However, we also know the disadvantages: If the individual strings are differently shaded then the parallel connection leads to mismatching losses. Added to this is the high effort (and possible losses) in the direct current cabling.

The second concept is much more elegant as it is based on **string-inverters** (Figure 7.10(b)). In the consistent application of this concept only one string is connected to each inverter.

A generator connection box is not necessary as each string is individually MPP-controlled and, in any case, is easy to monitor. Compared to the central inverter variant, the cabling effort on the direct current side is much simpler. In practice two parallel strings are often connected to one string inverter when it is certain that both strings have the same structure and will not be shaded.

One can dispense with direct current cabling altogether in the concept of the **module inverter** (Figure 7.10(c)). Here each module has its own inverter that is attached directly to the rear of the module. This means that each module is individually monitored and can be kept in the MPP. However, this concept also has clear disadvantages. An important problem is that the inverters are installed with the modules on the roof. Thus, they are subject to wind, weather and high temperature fluctuations, which do not really increase the life of the electronic

components. Added to this is that a failed inverter can only be replaced with much effort. These reasons have led to module inverters being almost only used in demo-projects.

7.2.3 Structure of Inverters

As already mentioned, besides the solar modules, the inverter is the heart of a photovoltaic system connected to the grid. For this reason we will look at it in greater detail in the following.

7.2.3.1 Tasks of the Inverter

We will now list the most important tasks of the inverter of a PV plant connected to the grid. The individual subjects will be dealt with in more detail next.

- Converting **direct current** into a possibly sinusoidal-form **alternating current**
- Achieving a **high degree of efficiency** (>95%) in partial as well as in peak loads
- **Feeding** the current **synchronously** with the grid frequency
- **MPP tracking**
- **Monitoring the grid** for voltage, frequency and grid impedance in order to prevent an inadvertent stand-alone operation
- Measures for **personnel protection**:
  – Inverter with transformer: insulation monitoring of the solar generator
  – Inverter without transformer: residual current monitoring of the solar generator
- Preparation of actual **condition data** of the plant (power, current, voltage, error codes) via an external data interface.

7.2.3.2 Line-Commutated and Self-Commutated Inverter

The **classic inverter** makes use of **thyristors** as switching elements. These have the disadvantage that they **cannot be turned off** by means of the control electrodes. In order to block them one must wait for the next zero pass of the mains voltage.

For this reason, this type of inverter is called a **line-commutated inverter**. The thyristors can only be switched on and off once per period, leading to a rectangular form of current flow. In order to fulfill the requirements of **electromagnetic compatibility** (EMC), the current must be smoothed by means of additional filters.

We obtain far fewer harmonics with **self-commutated inverters**. This switching principle is now standard for devices up to 100 kW as a series of suitable **components** that **can be switched off** are available: **GTOs** (Gate Turn Off thyristor), **IGBT**s (Insulated Gate Bipolar Transistor) and **power MOSFETs**. These permit quick on and off switching (e.g., 20 kHz) and thus a piece-by-piece copy of a sinusoidal current flow (see Figure 7.12). Therefore, we will consider only the self-commutated inverters.

7.2.3.3 Inverters without Transformers

We will use the example of an **inverter without transformer** to consider the complete arrangement of a modern string inverter. Figure 7.11 shows the principle circuit as used nowadays in many inverters. The **boost converter** raises the input voltage according to the requirement of the **MPP tracker** to a higher DC voltage level. This DC voltage is converted by
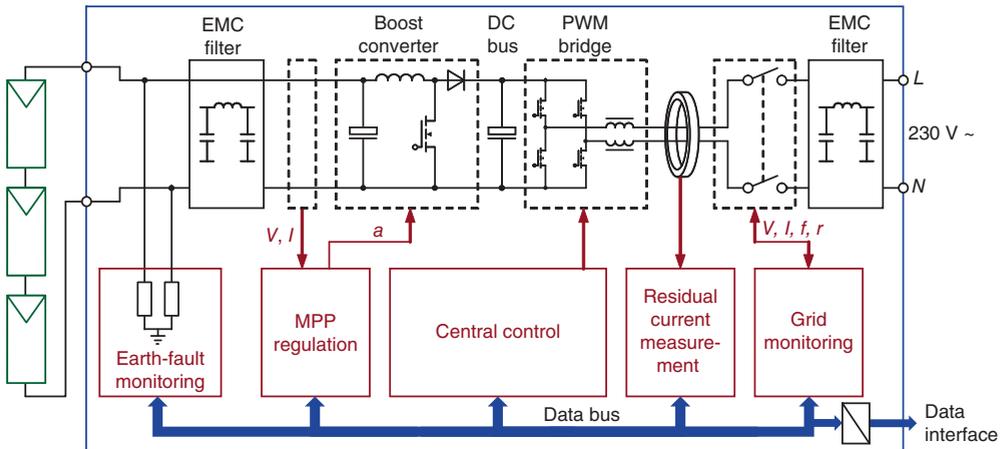
Figure 7.11 Overall arrangement of an inverter without transformer: Besides the actual grid feed-in it must fulfill a number of other functions such as MPP tracking, residual current measurement and grid monitoring

the **PWM bridge**, including the two **choke coils**, into a 50 Hz sinusoidal voltage and fed into the grid.

As there is **no galvanic separation** between the mains and the PV plant in the case of an inverter without transformer, an all-current sensitive (reacting to errors on the DC and AC side) **residual current protective device** (RCD) is prescribed for reasons of personnel safety. This must be specially designed so that it reacts to sudden current changes from 30 mA. A normal RCD is not enough as, in the case of larger PV generators in normal operation, high capacitive leakage currents against ground that can exceed 30 mA are possible.

Finally, the **grid monitoring** must ensure that voltage and frequency are within the permissible range so that feeding-in only takes place when a proper public grid is available (see Section 7.2.8.1)

The principle of pulse width modulation is explained in more detail in Figure 7.12. The direct voltage V_{DC} is chopped by the MOSFET bridge into pulses of various widths. In the **first half-period** of the grid AC voltage the **transistors ① and ④** are switched through and in the **second** half the **transistors ② and ③**. The downstream low pass filter ensures that only the moving average of this component arrives at the output; this is the desired 50 Hz signal. This has almost an ideal sinusoidal form, but because of the small impulses, high-frequency signal parts are generated that could disturb other devices connected to the grid (e.g., radios). For this reason an **EMC filter** is installed before the feed-in into the grid.

The transistors in Figure 7.12 all possess a so-called **body diode**. This makes certain that after switching off a transistor the current is not suddenly zero in the series-inductance (induced voltage peak!). Instead the diode of transistor ② takes over the current after switching off transistor ① and ensures a continuous flow of current.

The problem of **potential induced degradation of thin film modules** (PID) in connection with inverters without transformers has been known for some years. The background is the fact that the solar generator can have a high potential of approximately −500 V against earth due to
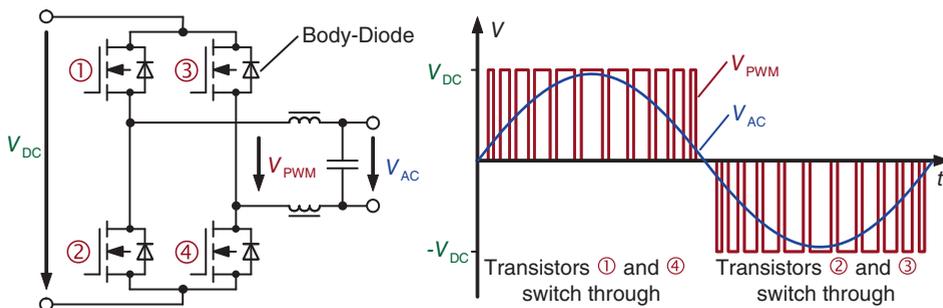
Figure 7.12 Principle of the self-commutated inverter: The direct current is chopped into pulses of varying widths and then filtered by means of a low pass filter so that a 50 Hz sinusoidal voltage is achieved

the lack of a galvanic isolation. With some thin film modules this leads to a diffusion of positively charged sodium ions from the cover glass to the TCO layer. When, at the same time, water vapor enters the cell, an electro-chemical reaction occurs causing the **TCO layer to corrode**. The result is **permanent damage** to the module with substantial power losses.

This problem only occurs with superstrate cells (e.g., CdTe and a-Si, see Chapter 5) in which the TCO layer is applied directly to the cover glass [93]. Meanwhile there are circuit concepts for inverters without transformers that permit a one-sided **earthing of the solar generator** [94]. In this case, the sodium ions are moved away from the cell so that electrical corrosion no longer occurs. In the case of thin film modules the planner should always first check the plant whether the selected **inverter** has been **released** by the producer for the respective type of module.

c-Si modules can also be affected by a degradation effect because of high existing voltages compared to the earth potential. Here, in a moist environment, there are possible leakage currents from the cell to the frame due to the high existing potential. The results are increased recombinations of the charge carriers generated by the light. The effect, also called **potential induced degradation (PID)** is not necessarily connected with damage to the module as is the case with thin film modules but in some types of modules it can lead to a **reduction in power** of **up to 20%**. Particularly affected up to now are the modules made by **Sunpower and Evergreen** [95].

In the following we will look more closely at the alternatives to inverters without transformers and discuss their advantages and disadvantages.

7.2.3.4 Inverters with Mains Transformer

Without exception, the first string inverters were equipped with **mains transformer**. The main reason for this was that solar generators were designed only for safety with **extra-low voltage** (<120 V) and low generator voltage was easily transformed to the desired level by means of a transformer. Besides this, the **galvanic isolation** between the solar generator and the mains was specifically desired for **personnel protection reasons**. Unfortunately, apart from these advantages, **50 Hz transformers** only **have disadvantages**: they are **large, heavy, expensive** and cause relatively **high electric losses**. For this reason one tries to do without them as much as possible. Nowadays practically all solar modules are built according to protection class II and are therefore checked for insulation voltages of 1000 V. Thus, string voltages of, for instance, 400 V are quite possible.
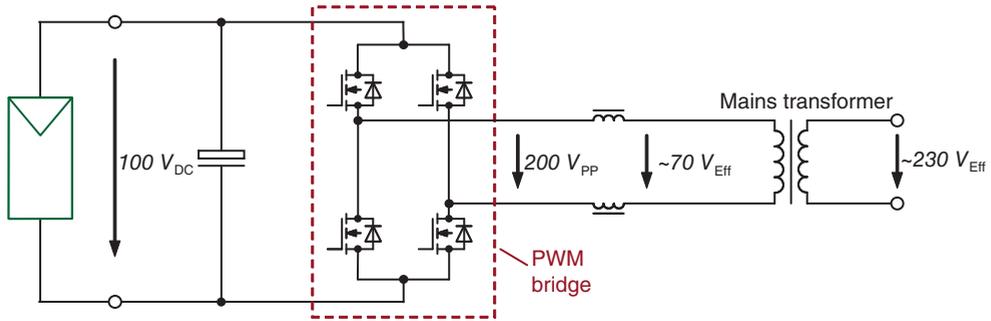
Figure 7.13 Principle of the inverter with mains transformer: The voltage signal received from the PWM bridge is converted to the desired mains voltage by the transformer

Transformer inverters are still required for **smaller plants** with voltages below 200 V. Besides this, the **galvanic isolation** ensures that the DC cabling presents no voltage fluctuations to earth. Thus, in principle, **no electro-magnetic radiation** can be caused as they may occur with inverters without transformers.

Figure 7.13 shows the basic structure of an inverter with mains transformer. In the example, a voltage of 100 V is delivered that is chopped in the PWM bridge into a peak-peak voltage of 200 V. The effective voltage of approximately 70 V caused by this is finally converted by the mains transformer into the desired 230 V.

7.2.3.5 Inverters with HF Transformer

There is a further type of inverter that permits a galvanic isolation of the DC and AC side and yet prevents the disadvantages of the mains transformer. This is the inverter with a **high-frequency transformer** (HF transformer). Figure 7.14 shows the arrangement with the occurring voltage progression: the direct voltage is converted by means of a fast PWM bridge into a high-frequency alternating voltage. At this high frequency the required **transformer inductance is smaller by some factors** than for the 50 Hz transformer. For this reason one can use a **small, light, low-loss and cheap high-frequency transformer** in order to achieve the galvanic isolation. The high-frequency alternating voltage is then rectified and filtered so that a pulsating half-wave voltage emerges. This must then be converted into the desired mains alternating voltage by means of a 50 Hz flip bridge (a bridge that changes the polarity every 10 ms).

Since the HF transformer inverters went into decline at the end of the 1990s we experienced a renaissance due to the potential problems with thin film modules described earlier.

Table 7.1 summarizes the advantages and disadvantage of the various types of inverters again.

7.2.3.6 Three-phase Feed-in

In past years the trend for on-roof installations has been for larger plants (e.g., for farms or industrial buildings). For this reason there are an increasing number of inverters with **powers above 5 kW** in the market that feed **three-phase power** into the grid.

Figure 7.15 shows the principle of one such inverter. A PWM bridge of **six semiconductor switches** is built up and generates three voltages V_1, V_2, V_3, each displaced about 120° between the lines.
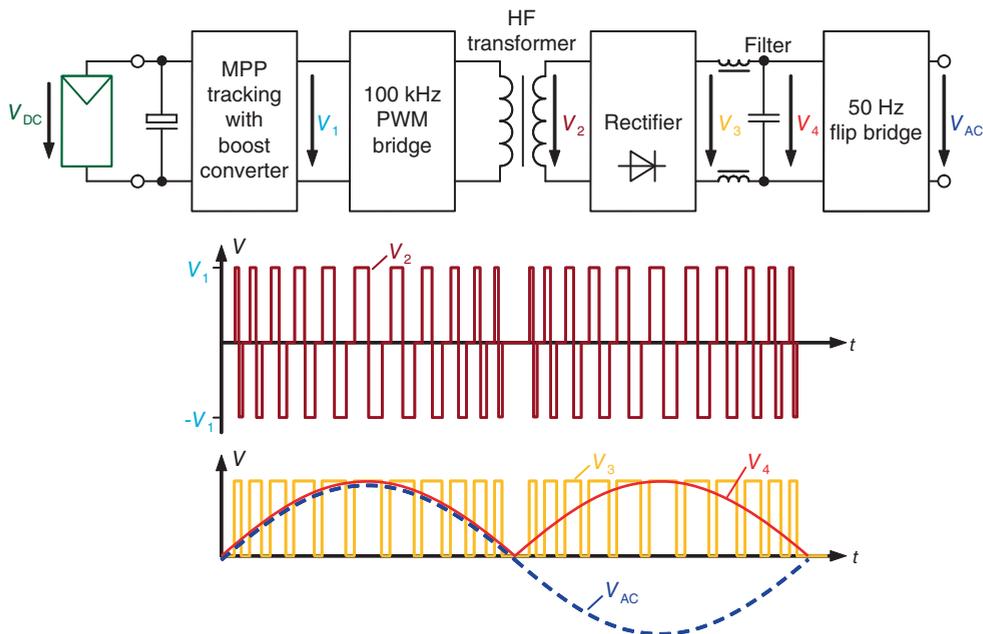
Figure 7.14 Principle of an inverter with high-frequency transformer: The DC voltage is chopped by means of a HF bridge and can thus be galvanically isolated by a low-loss transformer of low inductance. After rectifying and flip bridge the desired 50 Hz signal is finally available [40]

In order to generate a sufficient voltage for the 400 V three-phase grid, there must be at least a direct voltage of

$$V_{DC\_Min} = 400\ V \cdot \sqrt{2} = 567\ V \tag{7.17}$$

at the input of the inverter. Three-phase inverters without boost converters typically have an input voltage between 600 and 800 V. With this input voltage the **overall power** fed into the three-phase grid is **three times** that of a single phase feed-in. This is where one of the advantages

Table 7.1 Advantages and disadvantages of various types of inverters

Features	Inverter with grid transformer	Inverter with HF transformer	Inverter without transformer
Galvanic isolation	Yes	Yes	No
Residual current monitoring necessary	No	No	Yes
EMC radiation of the solar generator	Little	Little	Possibly high
Usage with $V_{DC} < 150\ V$	Quite possible	Possible	Hardly possible
Usage with thin film modules	Yes	Yes	Possibly
Size and weight	Large	Medium	Low
Efficiency	Poor	Medium	High
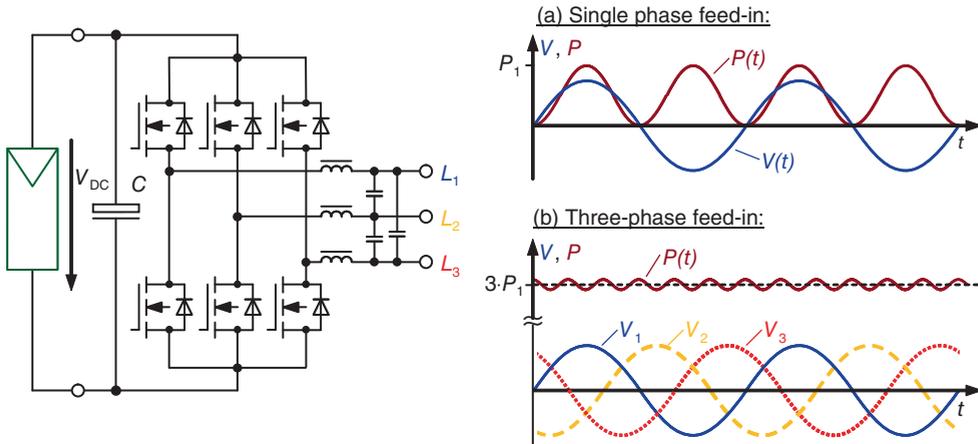
Figure 7.15 Principle of three-phase feed-in inverter: With six instead of four MOSFETS it is possible to feed-in the threefold power compared to the single phase case

of the three-phase inverter comes to the fore: With two additional power transistors (50% more in comparison with the original four transistors) it is possible to obtain **200% more power**. However, the transistors must be designed for the increased voltage region.

A further advantage of the three-phase inverter is that it feeds in equally on all three phases and therefore the **grid is symmetrically supplied**.

Added to this is the timely even feed-in: as the power progressions in Figure 7.15 show, the momentary value of the power fed into the grid in the case of the single phase feed-in pulses from zero to maximum. However, the solar generator continually supplies its direct current power to the inverter. For this reason the capacitor C must possess a very high capacity in order to provide intermediate storage of the energy of the solar generator. Relatively expensive and large electrolytic capacitors are necessary for this. In the case of **three-phase feed-in**, the momentary value of the fed-in power is nearly constant so that **only a small storage capacitor is required**.

7.2.3.7 Further Clever Concepts

In addition to the inverter concepts already discussed, there are now a multitude of mixed and special forms. A clever idea for reducing the mismatching losses is the **multistring inverter** (Figure 7.16). This contains two or three inputs each possessing a **separate MPP tracker**. The device is especially suited for plants with **partial shading** in which the string with shaded modules is to be individually MPP controlled (see Chapter 6). A further application case would be, for instance, plants with modules on a south as well as on a west-facing roof. Here, too, there is the possibility of controlling both solar generators separately in order to prevent **mismatching losses**. The alternative would be the application of two string inverters with two housings, double control electronics, and so on, which would result in high costs and low efficiencies. Table 7.2 lists, among others, the data of two multistring inverters.

A second idea for increasing the yield of photovoltaic plants is the **Master-Slave concept** (Figure 7.17). This is mainly used for large plants (>30 kW). In place of a central inverter use is made of several individual devices that are possibly positioned in a common housing. At times
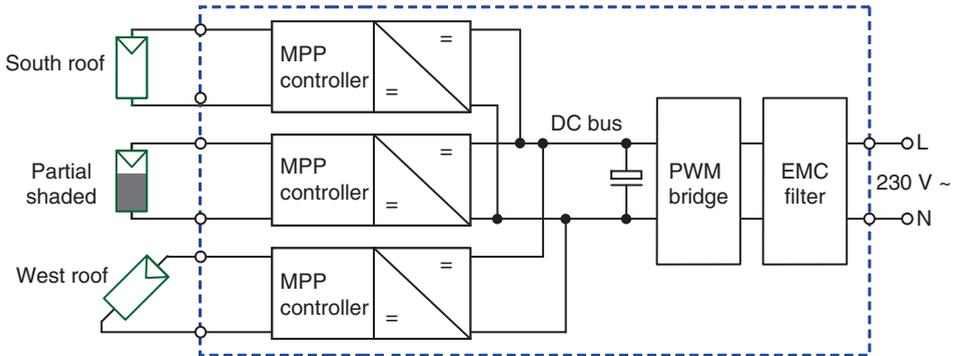
Figure 7.16 Arrangement of a multistring inverter for connecting different part-generators: The three inputs are separately MPP-controlled and then fed into a common direct voltage bus

of small radiation (e.g., mornings, evenings, or cloudy days) the whole of the PV power is switched to the Master inverter. This then achieves a **high loading** with a corresponding **good efficiency** (see Section 7.2.4). Slave 1 is only added when the Master no longer can take up the solar power by itself. With rising PV power the Slave 2 is then brought into the game. The control of the overall sequence is carried out by the Master.

It is particularly clever to allocate the role of the Master to a different inverter every day. In this case all inverters end up with the same mean operating hours. Master-Slave type concepts are also available for **plants to 30 kW** and these are marketed, for instance, under the names of **Team**- or **Mix-Concept**.

7.2.4 Efficiency of Inverters

Ideally, the complete power provided by the solar generator should be fed into the electric grid, which is not achievable in practice. Each inverter requires a central control with micro-controller that takes over the entire operation. More definite, however, are the **losses in the power part** of the device. Each real component possesses non-ideal properties. Thus, besides the **inductance**, the choke also has an **ohmic resistance** that leads to heat losses. Further, there are **switching losses in the semiconductor switches**, especially in the switch-off process.

7.2.4.1 Conversion Efficiency

In order to compare various inverters, the **conversion efficiency** η_{Con} is defined and shows what portion of the direct current power delivered by the solar generator is fed into the alternating current grid:

$$\eta_{\text{Con}} = \frac{P_{\text{AC}}}{P_{\text{DC}}} \tag{7.18}$$

with

P_{AC}: alternating current power at output of the inverter.
P_{DC}: direct current power at input of the inverter.

Table 7.2 Data for various types of inverters [www.photon.info]

Designation	Sunny Boy 1100	SMC 7000 HV	SMC 8000TL	SolarMax 6000S	IG Plus 100	Sunny Boy 5000TL	TLX 12.5k
Producer	SMA Solar Techn. AG	SMA Solar Techn. AG	SMA Solar Techn. AG	Sputnik Engin. AG	Fronius Int. GmbH	SMA Solar Techn. AG	Danfoss Drives AS
DC nom. power P_{DC_N} (kW)	1.1	7.35	8.25	5.3	8.42	4.83	12.9
AC nom. power P_{AC_N} (kW)	1	6.65	8	4.6	8	4.6	12.5
DC nom. voltage V_{DC_N} (V)	180	340	350	400	390	520	700
MPP region (V)	139–320	335–560	333–500	100–550	230–500	125–750	430–800
DC nom current I_{DC_N} (A)	6.1	21.5	25	12	21.05	9	12
Max. efficiency η_{Max} (%)	93	96.2	98	97	96	95.5	98
Europe efficiency η_{Eu} (%)	91.6	95.5	97.7	96.2	95.5	94.5	97.3
Number of inputs	2	4	4	3	6	3	3
Number of MPP-trackers	1	1	1	1	1	3	3
Feed-in	Single phase	Single phase	Single phase	Single phase	Single phase	Single phase	Three phase
Remarks	Mains transformer	Mains transformer	No transformer	No transformer	HF transformer	No transformer, Multistring	No transformer Multistring
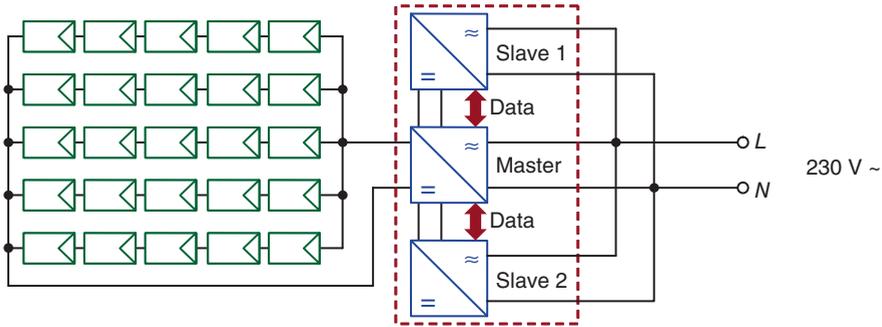
Figure 7.17 Master-Slave concept: With low radiation the whole PV power is switched to the Master that then works with a high part-load. If solar power rises then the Slaves successively take on a part of the work

Figure 7.18 shows the efficiency curves for various types of inverters. The x axis gives the actual input power P_{DC} with reference to the input nominal power P_{DC_N} of the inverter. For smaller powers the efficiency curve declines for all types as is to be expected, in medium and upper ranges it remains relatively stable. The lowest curve belongs to the **SMA Sunny Boy 1100** that came onto the market in 1999 and is thus a real **veteran**.

Because of its low power of 1.1 kW, its transformer and the old-fashioned design, it only achieves a maximum efficiency of 92.4%. A more up-to-date device with mains transformer is the **SMA SMC 7000HV** that achieves a maximum efficiency of 95.6%. A slightly better efficiency is reached by the **Fronius IG Plus 100** with 96.2%. It is equipped with a **high frequency transformer** for potential isolation. The somewhat irregular progression of the efficiency curve is due to a switching peculiarity: depending on the existing input voltage, there is a change-over between several primary windings of the transformer. The upper curve belongs to the **SMA SMC 8000TL,** an **inverter without transformer** that achieves a peak **efficiency** of 98%.

The curves shown in Figure 7.18 apply only for a particular existing DC voltage. The **efficiency** actually **varies** also for **different PV generator voltages**. Figure 7.19 shows as an
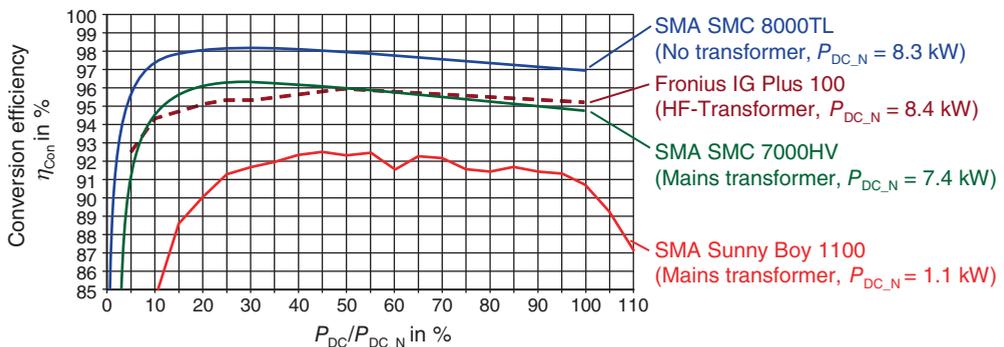
Figure 7.18 Conversion efficiency η_{Con} of different types of inverters: Clearly visible types with high frequency transformers and especially systems without transformers show the highest efficiencies [Data sheets, Photon inverter tests]
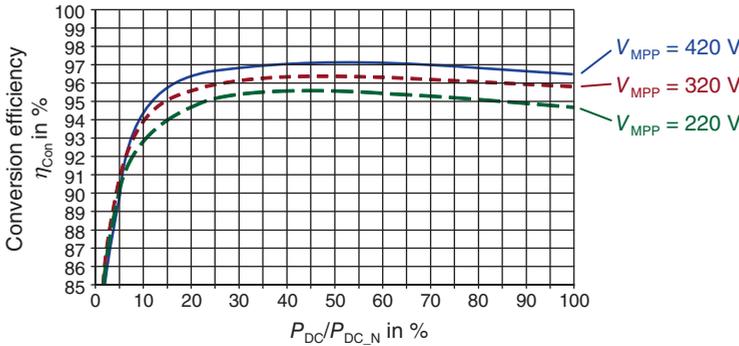
Figure 7.19 Conversion efficiency η_{Con} of the Sputnik Solarmax 6000S: The maximum efficiency depends greatly on the applied input voltage

example the efficiency curves of an inverter without transformer (Sputnik Solarmax 6000S). The inverter only reaches its maximum efficiency of 97% for an input MPP voltage of 420 V, at 220 V it is already 1.5% lower. This must be taken into account by the planner in the selection of the number of modules.

7.2.4.2   European Efficiency

Actually **the peak efficiency** of an inverter is **not that important** from the **point of view of the operator** of a photovoltaic plant. **Decisive** for the yield of the plant **is the mean efficiency over the whole year**. For the sake of clarity, Figure 7.20 shows an example from the year 2000 of the measured frequency with which various classes of radiation occurred at the site of Freiburg (Germany) (solid line). At the same time the vertical bars represent the energy portions that the respective radiation classes contribute to the overall solar annual energy. The first bar, for instance, shows that the irradiance between 0 and 50 W/m^2 contribute almost 1.5% to the annual energy. The irradiance up to 500 W/m^2 over the year amounts to approximately 30% of the overall energy.
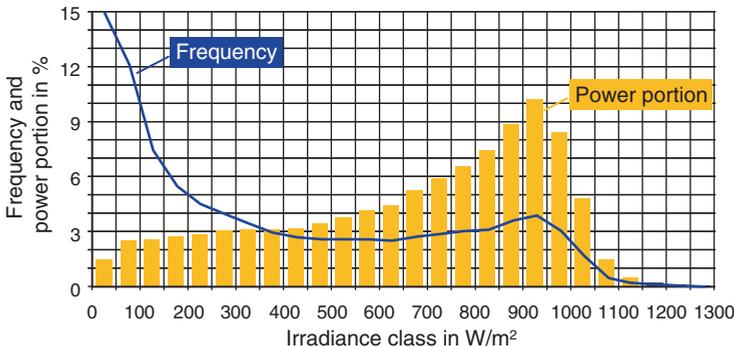
Figure 7.20 Relative frequencies of the radiation in the year 2000 as well as annual energy portions of the individual radiation classes in Freiburg: The low radiation classes seen over the year provide relatively high power portions [96]. The radiation measurements were taken at close intervals as "momentary values" (10 seconds averaged)

For the inverter this means that it is often working in the lower part-load region. For this reason the DIN EN 50524 standard specifies the **European Efficiency** η_{Eu} that weights the individual part load efficiencies according to how often they occur in Central Europe:

$$\eta_{\text{Eu}} = 0.03 \cdot \eta_{5\%} + 0.06 \cdot \eta_{10\%} + 0.13 \cdot \eta_{20\%} + 0,1 \cdot \eta_{30\%} + 0.48 \cdot \eta_{50\%} + 0.2 \cdot \eta_{100\%} \quad (7.19)$$

with

$\eta_{x\%}$: conversion efficiency at a respective part-load of x%

From the equation it can be seen that the inverter in this model is operated at 20% of its operating time with the nominal power ($P_{\text{DC}} = P_{\text{DC\_N}}$). The efficiency of the inverter at half of its nominal power ($\eta_{50\%}$) is weighted at 48%, and so on. If we apply this equation to the inverters in Figures 7.18 and 7.19 then the results are the values shown in Table 7.2 for the European Efficiency. The modern devices are all above 94% and almost 98% is achieved in part. Noticeable is the SMC 8000TL **device without transformer**: The efficiency η_{Eu} here is only 0.3% below η_{Max}, which shows **very good part-load behavior** of this inverter.

The efficiencies of photovoltaic inverters have improved continuously over recent years and further improvements can be expected. The availability of new **power components made with silicon-carbide** (SiC) shows especially that the losses can be further reduced.

This material has a very big bandgap of 3.2 eV that results in a small intrinsic carrier concentration even for high temperatures. Whereas silicon transistors can be used at approximately 150 °C, the critical temperature for SiC is about twice that. Thus much smaller heatsinks can be used. Further advantages of the material are high possible reverse voltages, low forward resistances and reduced switching losses. Further, SiC permits high switching frequencies, which allow smaller choke coils.

The use of flyback diodes of SiC is widespread today. There is a whole palette of SiC transistor types in the region of semiconductor switches. Although they are much more expensive than Si transistors, they can compete due to higher inverter efficiencies. Meanwhile the first prototypes with **peak efficiencies of 99%** are available [97,142].

7.2.4.3   Clever MPP Tracking

In the case of **shading** there is the possibility that **more than one power maximum** in the $P = f$ (V) curve of the solar generator exists. For this purpose we will look at the case presented in Figure 6.20 (1 module shaded). An inverter starting at the open circuit point would immediately seize up in the local MPP at 270 V and almost 1 A. The actual point of maximum power (MPP₂) would not even be found. Help is provided here by a better algorithm that every now and then **searches the whole** characteristic **curve** in order to find the global MPP and then tracks around it. Such a control for instance, is offered in the market under the name **OptiTrac Global Peak**.

7.2.5   Dimensioning of Inverters

A photovoltaic plant can only bring a maximum yield when PV generator and inverter are optimally adapted to each other. For this reason we will now consider the most important **dimensional requirements** for inverters.

7.2.5.1 Power Dimensioning

The inverters of the 1990s had relatively poor efficiencies in the lower part-load region. For this reason they were often **under-dimensioned** by 20%, meaning that for a PV plant with 2 kWp an inverter would be used whose maximum input power was 1.6 kW. This corresponds to a **solar generator over-dimensioning factor k_{Over}** of

$$k_{Over} = \frac{P_{STC}}{P_{DC\_N}} = \frac{2\,kWp}{1.6\,kW} = 1.25 \tag{7.20}$$

with

P_{STC}: nominal power of the PV generator (at STC)
P_{DC_N}: DC nominal power at the inverter input

Thus, these inverters achieved average part-load regions even for low radiation and thus higher efficiencies. The disadvantage, naturally, was that for nominal powers of the PV generator (e.g., on a sunny cold day in May) there was a limitation of the inverter and much energy was given away. Today's inverters have much better part-load behavior so that under-dimensioning of the inverter hardly makes sense any more.

Meanwhile increasing use is made of the so-called **design factor SR_{AC} (Sizing Ratio)**. This refers to the output power P_{AC_N} of the inverter

$$SR_{AC} = \frac{P_{STC}}{P_{AC\_N}} \tag{7.21}$$

The reason for this new reference value is that some inverter producers declare input powers that are too high so that the devices often work in overload operation.

What could possibly be the correct design factor? To find the answer, use is made of an investigation carried out by the Fraunhofer ISE Institute. There the radiation measurements of Figure 7.20 were used in order to determine a **realistic annual average efficiency** of an inverter without transformer. The result is shown in Figure 7.21: Taking into account the hourly mean values, one can afford to use a design factor of 1.1 without any energy losses. However, things are different when **using the momentary values** (10-second mean values). Here it is seen that SR_{AC} **should be a maximum of 1.0** in order not to reduce the yields.

[?] Why does the timely resolution of the weather data have an influence on the results of dimensioning the inverter?

[!] On sunny days with moving clouds there are repeated radiations of, for instance, 1000 W/m^2 that are reduced for short periods to for instance 500 W/m^2 by the clouds. If the data is averaged out over an hour then we could obtain a value of 800 W/m^2. From this we cannot see that the inverter was overloaded. This is the reason why momentary values are so important.
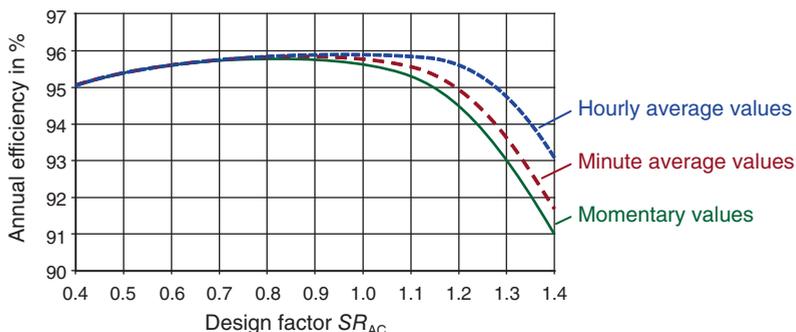
Figure 7.21 Annual efficiency of an inverter without transformer in dependence of the design factor: When viewing the radiation momentary values it is seen that the design factor should be less than 1.0 in order to reach the maximum yields [96]

7.2.5.2 Voltage Dimensioning

Besides the power also the voltage and the current of the solar generator must be adapted to the inverter. As a means of an overview of the relevant parameters, Figure 7.22 shows the **operating region** of the inverter with the example of the SMA SMC 8000TL.

First we will consider the **voltage dimensioning**: each inverter has a **maximum permissible voltage** V_{Inv_Max} that will cause it to shut down if it is exceeded. The most critical situation, for instance, would be a restart of the inverter on a cold sunny **winter's day** as the modules then possess their maximum open circuit voltage.

If one assumes the module temperature ϑ_M at $-10\,°C$, then the **maximum number of modules** η_{Max} per string is:

$$n_{Max} = \frac{V_{Inv\_Max}}{V_{OC\_M(-10°C)}} \tag{7.22}$$
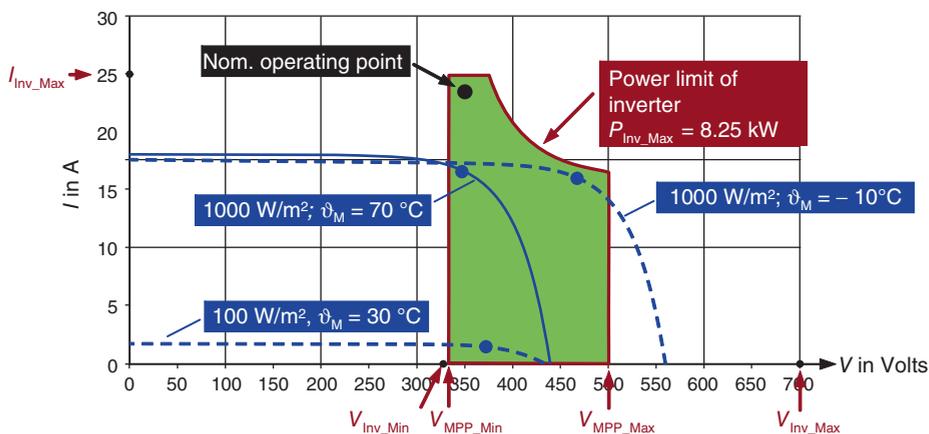
Figure 7.22 Possible operating region of an inverter using the example of the SMC 8000TL: It is limited to the left and right by the minimum and maximum MPP voltage, at the top by the maximum current and the maximum inverter input power [21]

The **minimum number of modules $\eta_{\textbf{Min}}$** is determined by the MPP working region of the inverter (Figure 7.22). We will therefore consider a **summer's day** at which the module temperature reaches 70 °C. In this case the string MPP voltage must not be less than $V_{\text{MPP\_Min}}$ of the inverter as otherwise it will not provide the maximum possible power or may even shut down. The equation is therefore:

$$n_{\text{Min}} = \frac{V_{\text{MPP\_Min}}}{V_{\text{MPP\_Module(70°C)}}}$$
(7.23)

7.2.5.3 Current Dimensioning

The **number of possible strings $n_{\textbf{String}}$** is prescribed by the **maximum current $I_{\textbf{Inv\_Max}}$** of the inverter and the **maximum string current $I_{\textbf{String\_Max}}$**:

$$n_{\text{String}} \leq \frac{I_{\text{Inv\_Max}}}{I_{\text{String\_Max}}}$$
(7.24)

As a precaution, because of occasionally assumed higher irradiances than 1000 W/m² one should assume for $I_{\text{String\_Max}}$ the **1.25 × MPP current**.

Today **simulation tools** are mostly used for dimensioning the inverter (see Chapter 9). Yet the rules and equations given here are helpful as they are immediately comprehensible and can at least be used for critically checking the simulation results.

7.2.6 Measures for Increasing Self-Consumption

Meanwhile the feed-in tariffs for solar power lie below the power consumption price for normal tariff customers (the so-called **Grid Parity**, see Section 10.3). Therefore it makes sense to improve the profit of a solar power plant in that as large a portion of the produced power as possible is consumed by oneself.

Let us consider the example of a four-person family with a typical power consumption of approximately 4500 kWh per year. Their 5 kW plant on the roof generates about the same quantity of solar energy so from a pure mathematical point of view the family can use the whole of solar energy by itself. But as the provision of solar power is distributed very unevenly over the year and over the day, one takes a **blanket** amount of only **30% self-consumption rate**. This portion, however, can be increased over the day by the deliberate switching-on of household devices (washing machine, dishwasher, etc.) during the day. Meanwhile there are various suppliers of **energy management systems** who optimize self-consumption by automatic switching on and off of household devices. Field tests and simulations show here that this permits self-consumption rates to be **increased to 45%** [99].

If the **self-consumption** is to be **increased further**, then batteries are required in order to provide intermediate storage for part of the generated solar energy. A possibility for this, for instance is the **Sunny Boy 5000 Smart Energy**. It is a 5 kW inverter with integrated lithium-ion **battery** that can provide intermediate storage for approximately 2 kWh. This effect can be

Typical household load profile with PV plant (5 kWp)

Load profile with Sunny Home Manager and Sunny Boy 5000 Smart Energy

- ■ Fed-in PV energy   ■ Directly used PV energy   ■ Stored PV energy
- ■ Energy drawn from the mains   ■ Energy drawn from the storage
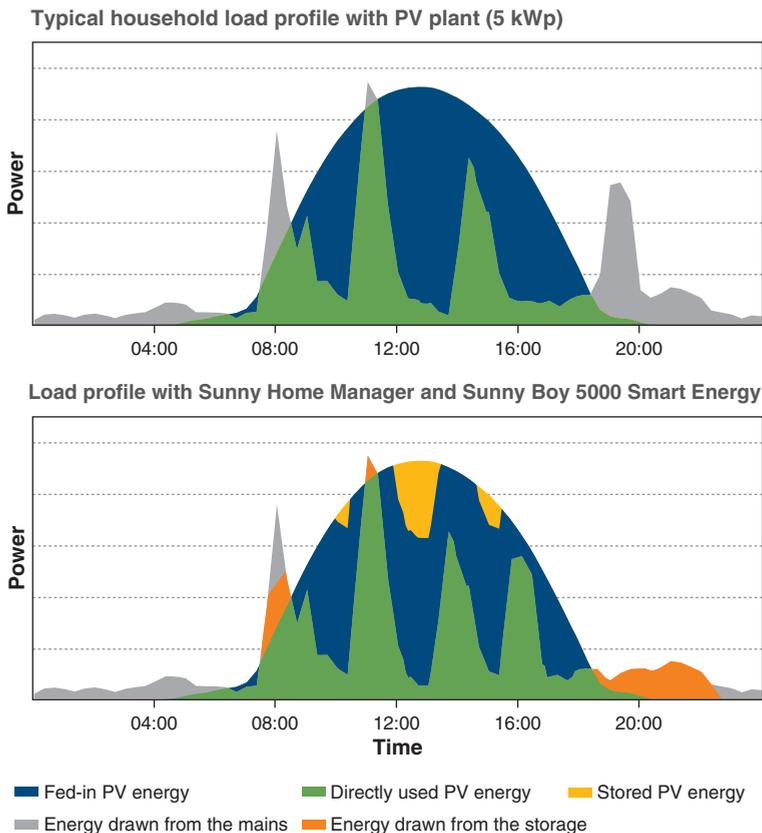
Figure 7.23 Increasing self-consumption rate with the help of an energy management system as well as an inverter with integrated battery: The lower figure clearly shows the reduced mains consumption (source: Solar Technology AG)

seen in Figure 7.23: The upper diagram shows the load profile on a sunny day without energy management system and intermediate storage resulting in a relatively low self-consumption rate. The lower picture shows the same load profile but with an energy management system of the domestic consumers ("Sunny Home Manager") and the use of the battery. The mains consumption can be substantially reduced. If one calculates these curves over the whole year, then according to the manufacturer, there is a **self-consumption rate** of approximately **60%**.

It can be assumed that increasingly refined systems for self-consumption will appear on the market in coming years. The **intermediate storage** of solar power can also **relieve the grid** as it permits a stabilization of the fed-in power (see also Section 10.4.3).

Furthermore the trend for higher self-consumption rates will also have **effects on heating technology**. Thus, for instance, the first suppliers to offer domestic hot water heat pumps, which – solar operated – will provide real competition for the present thermal solar collectors.

7.2.7 Requirements of Grid Operators

Inverters must fulfill certain **technical requirements** in order to be permitted to feed into the power supply grid. Beside the prescriptions of the **quality of** the fed-in **current** (low harmonic portion), these are primarily measures to exclude an **undesired stand-alone operation** of the inverter with associated danger to people. A feasible case, for instance, would be the uncoupling of a street of houses from the power supply grid, in order to carry out maintenance. If the inverters were to continue to feed-in, then the maintenance personnel would be in grave danger. For this reason the corresponding guideline [100] mandates that every PV plant must possess a **publicly available isolation unit** in order to separate it from the grid. However, plants below 30 kW power can dispense with this if they possess an automatic functioning **self-acting disconnection unit**.

7.2.7.1 Prevention of Stand-Alone Operation

In order that the inverter properly recognizes a stand-alone operation it must continuously **monitor all three phases** of the mains for adherence to **voltage and frequency tolerances**. The VDE V0126-1-1 standard has defined these as follows:

$$80\% < \frac{V}{V_N} < 115\% \tag{7.25}$$

with

V_N: nominal voltage of the power supply grid

$$47.5\,\text{Hz} < f < 50.2\,\text{Hz} \tag{7.26}$$

with

f: grid frequency

If one of these requirements is not fulfilled then the inverter must **switch itself off** from the grid **within 0.2 s**. However, the **50.2 Hz upper limit** has shown itself to be a problem. If this is exceeded then all the photovoltaic inverters suddenly shut themselves off from the grid, which could lead to **instability in the supply grid**. For this reason the **new low voltage guideline** VDE-AR-N 4105 mandates that the inverters must power down more and more between 50.2 and 51.5 Hz in order to prevent sudden power jumps. They are only fully switched off from 51.5 Hz.

Theoretically the case would be conceivable that the loads in a separated grid region use just as much power as the connected inverters generate. In this case the inverters would not recognize the undesired stand-alone operation and possibly feed-in for a longer period. However, this case is extremely improbable as the smallest deviation between supply and demand would generate an asymmetry in the three-phase grid that would immediately be recognized.

An **alternative** to recognizing the undesired stand-alone operation is the self-acting disconnection unit with **grid impedance measurement**. For this purpose the inverter increases the fed-in current for a short period by an amount ΔI and measures the **resulting voltage increase ΔV**. The quotient of both sizes is then the **grid impedance Z_{Grid}**:

$$Z_{Grid} = \frac{\Delta V}{\Delta I} \tag{7.27}$$
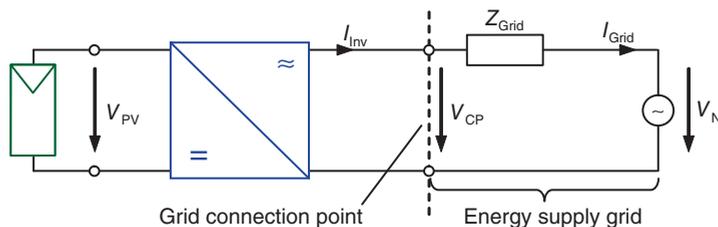
Figure 7.24 Simple equivalent circuit diagram of the energy supply grid built up of an ideal voltage source V_N and grid impedance Z_{Grid}: Depending on the size of the fed-in current, the voltage V_{CP} increases at the grid connection point compared to the nominal voltage V_N

If a value of $Z_{Grid} > 1\,\Omega$ is measured then the inverter must switch-off from the grid within 5 s. A great **advantage** of this method compared to the voltage/frequency measurement is that, according to the standard, **only the feeding-in phase need be checked**. For single-phase inverters no three-phase cable must therefore be laid up to the inverter.

> **[?]** Why do we recognize with grid impedance whether we are dealing with a stand-alone or regular grid?

> **[!]** An ideal grid should always operate at the same voltage of 230 V, independent of how much power is consumed or fed into it. This means that such a grid, when referred to the feed-in point, always has an internal resistance of $0\,\Omega$ (see Figure 7.24). Real grids lie typically at values below $0.5\,\Omega$ but in rural areas it could be above that (e.g., freestanding farmhouse).
>
> In an undesired stand-alone grid that is only formed of the consumers of a street, the voltage increases drastically when the inverter feeds in more current. Thus, it has a very high resistance.

7.2.7.2 Maximum Feed-in Power

In order to prevent an unbalanced load, the **feed-in power** from **the single phase** inverter is limited to **4.6 kVA**. If several single phase inverters are used then they must be distributed over individual phases so that there is no unbalanced load greater than 4.6 kVA [101]. However, it is more sensible to use three-phase inverters directly if possible.

Before connecting a PV plant to the grid we must check whether it can accept the planned power. The measuring limit here is that the **voltage** at the connection point must **not permanently rise by more than 3%over the nominal voltage** [101]. For plants below 30 kW the grid operator is required to extend the grid correspondingly if necessary. For **larger plants** the plant **owner must lay** a suitable **line** up to a suitable connection point (§ 5 and § 9 of the EEG 2009).

Since 2012, the German Renewable Energy Law requires a remote-controlled shut-down facility (so-called **feed-in management**, § 6 EEG 2012) for all photovoltaic plants. The background is the fact that the solar plants installed in Germany now produce so much power that on certain days there can be an excess supply of electrical power. The grid operators thus require the possibility to **shut**

down the power of **photovoltaic plants**. This consists, for instance, of special electronic ripple control receivers that sent shut-down commands to the inverters.

Owners of **smaller plants (<30 kW)** however have a (not really convincing) **alternative**. Instead of participating in the feed-in management, they can **under-dimension** their **inverters by 30%** from the start. In this way the typical midday peak on a sunny day is mitigated.

7.2.7.3 Reactive Power Provision

The voltage in the grid increases slightly as soon as a photovoltaic plant feeds into the power supply grid. With the increasing number of photovoltaic plants it often occurs that impermissible increases in voltage take place in the low and medium-voltage grids. An alternative to a grid expansion (larger cable cross sections, additional lines, etc.) is **reactive power provision**. In this case the inverters, in addition to effective power, also feed-in inductive or capacitive reactive power. This can partly moderate the generated voltage rise caused by effective power feeding (for instance see [40] for details). The low-voltage guideline VDE-AR-N 4105 mandates that the grid operator can prescribe a fixed **power factor** (cos φ). With larger inverters it is also possible to prescribe a power factor/effective power characteristic curve so that the cos φ can be **dynamically changed** in dependence of the presently fed-in power. Nowadays all newly installed inverters in Germany fulfill this requirement.

7.2.8 Safety Aspects

The most important aspects of safety of on-grid plants will be briefly discussed here.

7.2.8.1 Earthing of the Generator and Lightning Protection

For the **protection of persons, supports and module frames** must be **earthed** except when they are classed as protective class 2 or the open circuit voltage of the PV generator is less than 120 V. However, this earthing should also be carried out for inverters without transformers for modules of protective class 2. The reason is that there is a **high capacity** between the module frame and the cell strings and it is possible that **high voltages exist at the module frame** due to the changing generator potential [40].

The **earthing of the plant** also has advantages for **lightning protection** as lightning currents can be diverted to Earth. The earthing should be carried out with a massive copper line (at least 6 mm^2, better 16 mm^2) in the shortest path to the potential compensation rail. Basically it can be said that lightning protection is not a requirement for private residences. If, however, a lightning protection system exists then the PV plant must be connected to it [102]. A very comprehensive discussion on lightning protection of photovoltaic plants can be found, for instance in [40]. Contrary to constant rumors, it should be mentioned here that **a photovoltaic plant on the roof of a house does not increase the risk of a lightning strike** [102]!

7.2.8.2 Fire Protection

In past years there have been repeated reports of fire protection hazards in connection with photovoltaic plants. On the one hand a photovoltaic plant represents an extended electrical plant that, like other electric plants, can trigger a **fire in case of error**. There are known cases, for instance, of scorched junction boxes on modules of BP Solar caused by poor soldered

terminals [103]. However, these problems are special cases that can be prevented by means of better quality management on the part of the manufacturer.

Far more critical is the fact that a photovoltaic plant on a burning house can be a great **hazard for firemen**. This also exists with normal mains installations but that can be stopped relatively simply by switching the house off from the grid. Contrary to this, in the case of a solar power plant, even after switching off the inverter there is still **a voltage of several hundred volts** in the solar generator. Added to this is the fact that the possibly arising **electrical arcs** are not self-extinguishing. The first **proposals of a solution**, such as placing the string lines on the outer wall of the house or in metal tubes inside the house only lessen the danger slightly. There must be a permanent solution that will **safely short-circuit each module in case of fire** or that uncouples it from the string line. Conceivable would be a self-conducting semiconductor switch (e.g., MOSFET) in the module junction box that will cancel the short circuit only when it receives a signal from the inverter. If the inverter switches off in case of a fire, then this signal is missing and all modules are short-circuited. It is to be hoped that this type of solution becomes mandatory in the foreseeable future in order to spare the fire brigade unnecessary danger and the photovoltaic industry from damage to its image.

Section 9.4 contains concrete examples of photovoltaic plants. These will describe the build-up, the components used, the dimensioning of the inverters and the operating results.

7.3   Stand-Alone Systems

Photovoltaic stand-alone systems are typically used when there is no electric grid or the costs for connecting to a grid are too high. Examples of stand-alone applications were discussed in the historical overview in Chapter 1 with the discussion of power for satellites and telephone amplifiers.

Even today there are many application possibilities for photovoltaics in places that are remote from electric grids. As well as relatively limited use in mountain huts in the Alps or similar, the main use is in developing countries.

7.3.1   Principle of the Structure

Figure 7.25 shows the principle of the structure of a simple stand-alone system using photovoltaics. An important element is the **storage**, which in most cases is a **lead battery**.
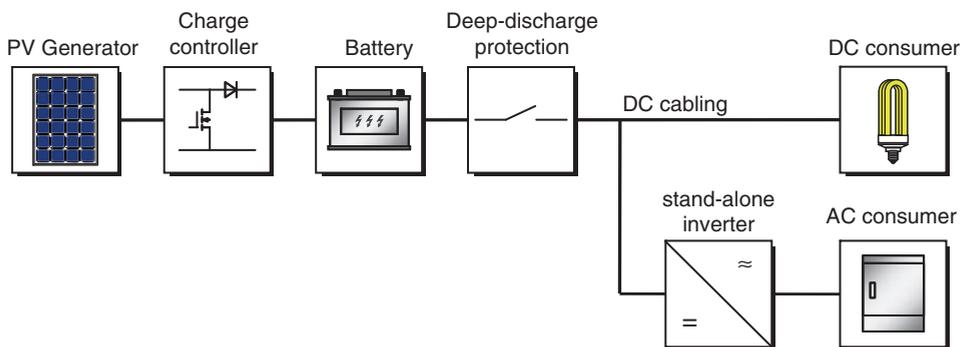
Figure 7.25   Principle of the arrangement of a photovoltaic stand-alone system: The battery fed by the module over a charge controller makes the power available for the DC consumer. An additional stand-alone inverter is provided in the case of AC consumers (e.g., refrigerator)

This is protected from overloading by a **charge controller**. Damage to the battery is prevented by means of a special **deep-discharge protection** in which the load is uncoupled in case the voltage falls below a critical level. **DC loads**, for instance, are energy saving **lamps, radios or also water pumps**. If, besides the direct current loads there are also alternating current loads then a **special** additional **stand-alone inverter** must be provided.
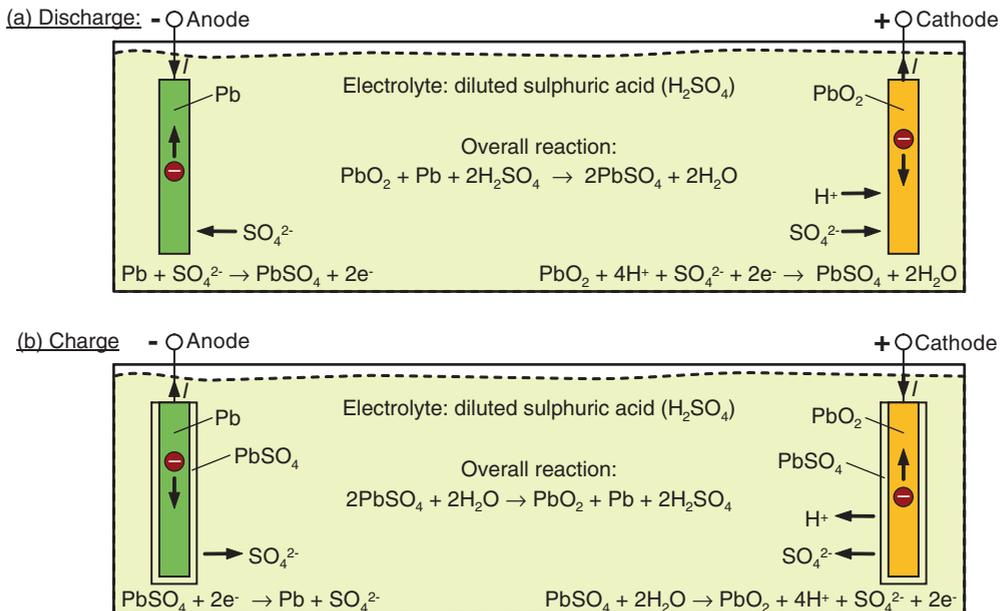
7.3.2 Batteries

Various types of batteries are can be used for storing electrical energy. Lead batteries, nickel metal hydrite batteries, lithium-ion batteries, lithium-polymer batteries, and so on. However, **lead batteries** are used almost exclusively in photovoltaic stand-alone systems although most other types of batteries have advantages such as high storage density or lower self-discharge. The decisive advantage of the lead battery is its **lower price**. This is especially important as the typical **life of a battery is less than 10 years** and this forms a high proportion of the **costs** of a stand-alone plant.

7.3.2.1 Principle of the Lead-Acid Battery

Figure 7.26 shows the principle of the **lead-acid battery** (or lead battery for short). It is filled with an **electrolyte** of diluted sulfuric acid (H_2SO_4). The negative electrode consists of lead whilst the positive electrode is of lead oxide (PbO_2).

Let us consider first the **discharging process**: The lead at the negative electrode reacts with the electrolyte under the loss of electrons to lead sulfate ($PbSO_4$). At the same time, the lead oxide of the positive electrode reacts with the sulphuric acid under the take-up of electrons to lead sulfate and water. This causes a layer of lead sulfate to grow on both electrodes.

(a) Discharge: − ○ Anode   + ○ Cathode

Electrolyte: diluted sulphuric acid (H_2SO_4)

Pb

PbO_2

Overall reaction:
$$PbO_2 + Pb + 2H_2SO_4 \rightarrow 2PbSO_4 + 2H_2O$$

SO_4^{2-} $H^+ \rightarrow$
$SO_4^{2-} \rightarrow$

$$Pb + SO_4^{2-} \rightarrow PbSO_4 + 2e^-$$ $$PbO_2 + 4H^+ + SO_4^{2-} + 2e^- \rightarrow PbSO_4 + 2H_2O$$

(b) Charge − ○ Anode   + ○ Cathode

Electrolyte: diluted sulphuric acid (H_2SO_4)

Pb
$PbSO_4$

PbO_2
$PbSO_4$

Overall reaction:
$$2PbSO_4 + 2H_2O \rightarrow PbO_2 + Pb + 2H_2SO_4$$

SO_4^{2-} $H^+ \leftarrow$
$SO_4^{2-} \leftarrow$

$$PbSO_4 + 2e^- \rightarrow Pb + SO_4^{2-}$$ $$PbSO_4 + 2H_2O \rightarrow PbO_2 + 4H^+ + SO_4^{2-} + 2e^-$$

Figure 7.26   Principle structure of a lead-acid battery: When discharging, a layer of lead sulfate ($PbSO_4$) forms at both electrodes, that is decomposed again during charging

In the **charging process** the reactions are exactly the reverse (Figure 7.26(b)): now the lead sulfate at the surfaces of the electrodes decomposes again and delivers sulfate ions to the electrolyte. The actual **storage of energy** thus takes place **in the electrolyte**. During charging its density increases so that the charge condition of the battery can be determined with a density measuring instrument (acid hydrometer).

If the battery is fully charged, then **gassing** occurs for **exceeding the end-of-charge voltage**: Oxygen forms at the positive electrode and hydrogen at the negative one, which together can form **explosive oxyhydrogen gas**. For this reason it must be ensured that the room has sufficient ventilation. Gassing also eventually leads to a loss of water that must be compensated by means of regular topping up with distilled water (once a year).

The **electrodes** mostly consist of a core of lead that is surrounded by the **active material** (lead or lead oxide). This has a porous structure in order to provide the largest possible surface for the electrochemical reaction. Unfortunately the lead sulfate does not decompose completely during the charging process; small quantities remain stuck to the electrodes. This **sulfation** has the effect that the active mass of the electrodes and thus the capacity of the battery decline with the continuous charge-discharge cycles. This decline in capacity becomes stronger the deeper the discharge of the battery. Frequent **deep discharges** thus result in an extreme **reduction in the length of life** of a lead battery. The lifespan is defined as the time at which the battery falls below 80% of its original nominal capacity [104].

> ? Why is that the end of its life? Surely the battery is still usable, or is this not the case?

> ‼ Actually the battery can still be used but only with reduced and further sinking capacity. At some time the lead sulfate deposits of the positive and negative electrodes touch each other and cause a short circuit. Figure 7.27 shows the linkage between depth of discharge and maximum achievable number of cycles for various types of batteries.
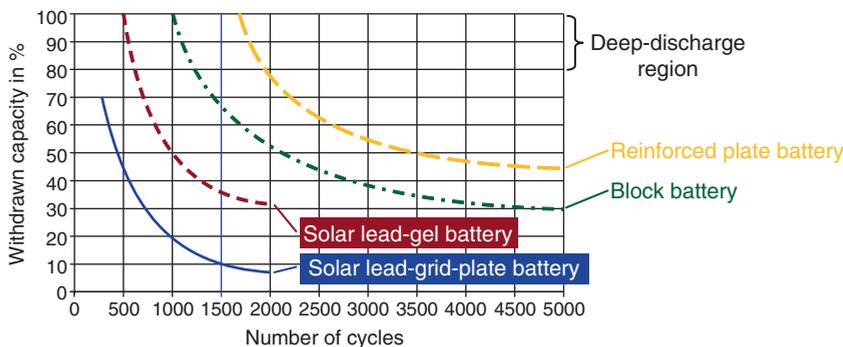
Figure 7.27 Lifespan of various types of batteries: The deeper the battery is discharged the fewer number of cycles it can carry out until it reaches the end of its life [21]

7.3.2.2 Types of Lead Batteries

Which types of batteries are to be used in a stand-alone system depends to a great extent on the particular requirements. First there is a difference between the method of operation of lead batteries in **buffer operation** and **cycle operation**. A normal **car battery** (starter battery), for instance, is operated in buffer mode. For most of the time it is fully charged but occasionally must **deliver short-term high currents** for starting the engine. Things are different with a forklift battery: It is fully loaded overnight and almost fully discharged on the next day and thus goes through **whole charge and discharge cycles**. This type of operation is called **cycle operation**, which tends also to be the case with solar stand-alone plants. The different requirements affect the method of construction of the different types of batteries.

A **starter battery** needs to provide high currents for short periods, which is why there are many electrodes close together in the form of plates that offer a large surface. With a stand-alone plant with typical cycle operation the starter battery would be **unusable in a few weeks** due to progressive sulfating and corrosion.

> A car battery is not suitable as storage in a stand-alone solar plant as it would become defective in a short period due to the cycle operation.

Solar lead grid-plate batteries are modified starter batteries in which thicker plates with larger spacings are used and the lead plates are hardened with an antimony additive (Figure 7.28). They only reach a lifespan of 300 cycles if they are discharged to a maximum to 30% of their capacity (depth of discharge 70%) (see Figure 7.27). They can reach 1000 cycles for a discharge of only 20%. Thus, they are only suitable for **sporadic use** such as in weekend cottages.

In **solar lead-gel batteries** the electrolyte is thickened to a gel by additives. Here the battery can be completely sealed and is thus leak-proof. In addition, no gas leaks so no distilled water needs to be topped up. A special charge controller that ensures adherence to the end-of-charge voltage is important as otherwise the battery will dry out due to gassing. In contrast to this, an occasional gassing is desirable for standard batteries in order to mix the electrolytes. Depending
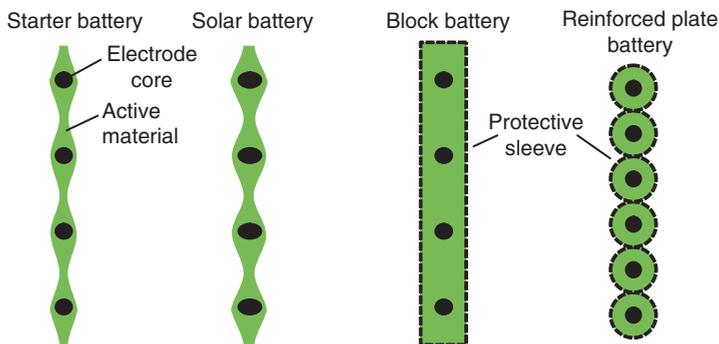
Figure 7.28 Principle arrangement of the electrodes of various types of batteries: Block and reinforced plate batteries keep the active material in place by means of an electrolyte-permeable protective sleeve

on the method of operation, the **length of life** of solar lead-gel batteries is almost **double that of the classic solar batteries** (see Figure 7.27).

If one wishes to achieve a continuous operation over 15–20 years then stationary **reinforced plate batteries** are the best choice. These are available in two variants: Stationary reinforced plate with special separation and fluid electrolyte batteries and sealed stationary reinforced plate batteries. They are normally used for battery-supported emergency power systems and cost 2–3 times more than simple solar batteries. The positive plate consists of lead rods that are individually surrounded by tubes. These keep the active material together and prevent premature loss of mass (Figure 7.28) [40].

A middle path finally is the **block battery** (also called the stationary grid plate block). Here several lead rods are surrounded by a common protective sleeve. They are therefore **cheaper** than reinforced plate batteries and yet achieve **relatively high life spans**.

7.3.2.3 Battery Capacity

The **capacity C** of a battery is not a fixed amount but **depends on** the **discharge current**. If the battery is discharged with a low current then the sulfate ions can penetrate deep into the active mass of the electrodes and convert into lead sulphates. With greater current draw-off the stored sulphur molecules at the start block the penetration of the following molecules so that the active mass cannot be fully utilized. For this reason the **nominal capacity** of a battery is **always mentioned in connection with a certain nominal charge current**. Mostly the nominal capacity is referenced to a **nominal charge current I_{10}**, a current that discharges the battery in 10 h.

This is shown for the sake of clarity in Figure 7.29 on the basis of a reinforced plate battery of the Hoppecke Company: if the battery is discharged within 5 h ($I_5 = 26.5$ A), then only a capacity of C_5 of 132 Ah is usable. The other extreme case would be a discharge over 100 h, which gives a capacity of C_{100} of 200 Ah at a current of $I_{100} = 2$ A. The type designation of the battery is called the *block solar power 200* but actually the nominal capacity C_{10} is only 150 Ah. This example emphasizes the **need to always check** on the datasheet as to **which discharge current** was used for the **nominal capacity**!

The **temperature** also has an effect on the usable capacity of a lead battery. Anyone who has not been able to start his car in winter knows that the **capacity is less at low temperatures**. It
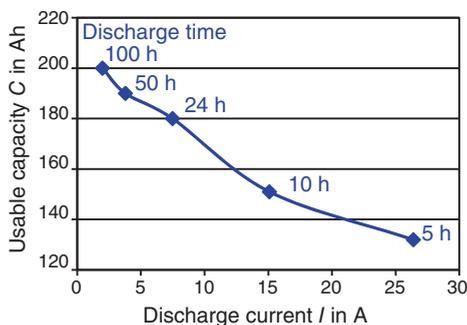
Figure 7.29 Dependency of the capacity of a reinforced plate battery (*block solar power 200*) on the amount of the discharge current
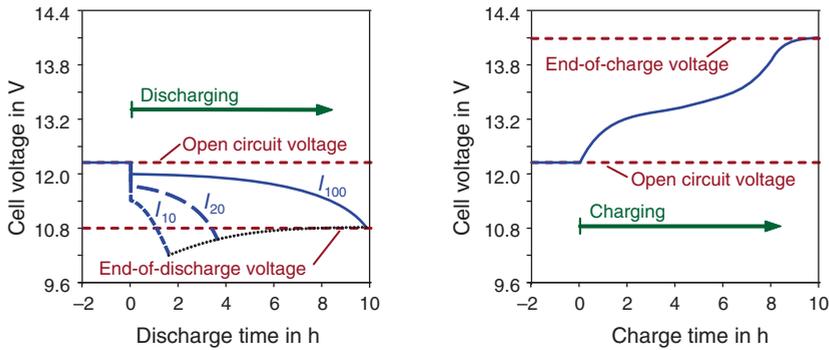
Figure 7.30 Progression of voltage of a 12 V battery when discharging and charging: The lower permissible limit is the end-of-discharge voltage whereas the upper permissible limit is the end-of-charge voltage [104]

lowers the capacity, for instance, at 0 °C to about 80% of the capacity at 20 °C. At much lower minus degrees the electrolyte freezes and limits the functionality of the battery completely.

#### 7.3.2.4 Voltage Progression

The nominal voltage of an individual battery cell is 2.0 V. Series connection of six individual cells is normal so that, depending on the charge condition, there is a **battery voltage of 12.0–12.7 V**. Figure 7.30 shows at the left the progression of the voltage in the **discharge** of the battery: Starting from the open circuit voltage, the voltage is reduced up to the **end-of-charge voltage of 10.8 V**. If current continues to be drawn off it will reach deep-discharge that can damage the battery.

The progression of the **charging** can be seen at the right in Figure 7.30. A voltage greater than the open circuit voltage must be applied to press the sulfate ions into the electrolyte again. Usually the so-called *I/V charging method* is used: First the battery is charged with a constant current. When the end-of-charge voltage has been reached then there is a change to constant charge voltage. The **charge voltage of 13.8–14.4 V** (depending on temperature) should not be exceeded in order not to overload the battery and to avoid gassing.

7.3.3 Charge Controllers

The previous section has shown that batteries require care in handling in order to enjoy their use for a long time. This depends on a series of tasks for the charge controller:

- Overload protection
- Deep-discharge protection
- Prevention of unwanted discharging
- State-of-charge monitoring
- Adjusting to battery technology (electrolyte/gel)
- Voltage conversion (possibly)
- MPP tracking (possibly)
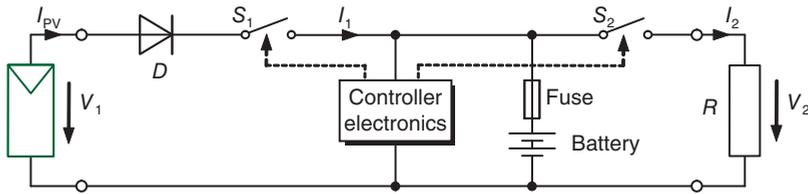
Figure 7.31 Principle of a series charge controller: Switch S_1 interrupts the charge current when reaching the end-of-charge voltage; switch S_2 serves for the deep-discharge protection of the battery

7.3.3.1 Series Controller

The arrangement of a classic series controller is shown in Figure 7.31. The control electronics constantly measure the battery voltage and when the end-of-charge voltage has been reached, turn the switch S_1 (mostly a MOSFET) off. **Switch S_2** separates the load from the battery in the case of falling below the end-of-discharge voltage and thus ensures **deep-discharge protection**. The **diode** at the input of the charge controller is meant to prevent the battery from being discharged at night by the inactive solar generator. A problem can arise when the battery is deep-discharged at night and there is insufficient power available to operate the control electronics. As switch S_1 is possibly opened, the battery cannot be reloaded again despite the Sun's radiation the next morning.
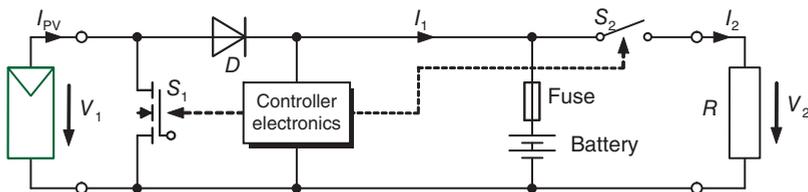
7.3.3.2 Shunt Controller

An alternative to the series controller is the **shunt controller (parallel controller)**. Here the transistor is connected in parallel to the solar module (Figure 7.32). As soon as the transistor conducts, it short-circuits the solar generator and interrupts the loading of the battery. An advantage of this concept compared to the series controller is the fact that the unavoidable (but relatively small) voltage drop at the switched-through MOSFET incurs no losses during charging.

The second advantage is that the MOSFET blocks without voltage signal at the gate and thus the battery can be charged in the morning after the deep discharge case described previously. These advantages result in the shunt controller being mostly used today.

7.3.3.3 MPP Controller

Naturally, MPP tracking makes sense also in stand-alone systems in order to obtain the **maximum energy** from the solar generator. Figure 7.33 shows a charge controller that realizes the MPP tracking similar to that described in Section 7.1.3 via a DC/DC converter. This is

Figure 7.32 Principle of the shunt controller: If the charge current is to be interrupted then the transistor S_1 short circuits the solar generator
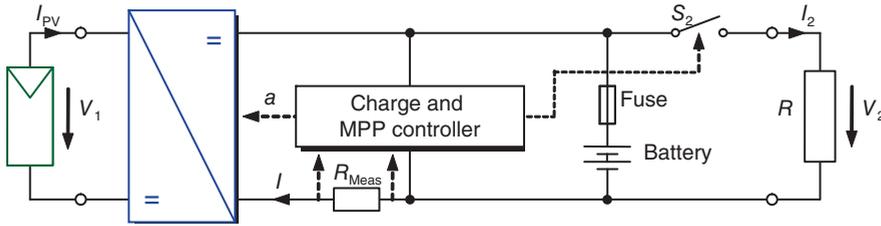
Figure 7.33 Principle of a charge controller with MPP controller: The voltage of the DC/DC converter is varied by varying the duty factor *a* and thus the MPP of the solar generator is reached

mostly a buck converter that, for instance, reduces the input voltage from up to 48 V to a system voltage of 12 or 24 V.

7.3.3.4 Examples of Products

Figure 7.34 shows two solar controllers of the Steca Elektronik Company: The technical data is listed in Table 7.3. The **PR 0505** is a **simple controller** for a module up to 78 Wp.

The maximum input voltage is 47 V and the maximum current is 5 A. The room temperature is determined by means of an internal sensor in order to determine the correct end-of-charge and end-of-discharge voltages. The controller is arranged as a **series controller** and controls the current in PWM operation with a switching frequency of 30 Hz.

The **PR 3030** is much **more powerful**, it is suitable for solar generators up to 900 Wp. It works as a **shunt controller** and offers various additional functions such as an external temperature sensor that is fixed directly to the battery. A further feature is the **intelligent charge condition determination** with which current, voltage and temperature are continuously monitored during charging and discharging. This makes possible a very exact representation of the actual battery charging state on the graphic display.

Both controllers make use of a variation of the already-mentioned *I/V charging process*: The current prescribed by the solar module is charged up to the end-of-charge voltage. Then the electronics control the MOSFET by means of a PWM signal such that the end-of-charge voltage is maintained.

Figure 7.34 Solar charge controller of the Steca Company: The PR 0505 shows the actual condition of the battery relatively coarsely via two LEDs, while the PR 3030 has a graphic display showing an intelligent charge monitoring

Table 7.3 Data for two different solar charge controllers [www.steca.de]

| Designation	Steca PR 0505	Steca PR 3030
System voltage	12 V	12 V (24 V)
Maximum charge current	5 A	30 A
Connectable PV power	78 Wp	900 Wp
Controller principle	Series controller, PWM-operation	Shunt controller, PWM-operation
Temperature compensation	Yes, with internal sensor	Yes, optional with external sensor
PWM control	Yes	Yes
Overload protection	Yes	Yes
Deep discharge protection	Yes	Yes
Polarity reversal protection	Yes	Yes
Charge condition determination	Via voltage and temperature	Via current, voltage and temperature
Charge condition display	2 LEDs	Graphic-LCD-Display
Features	–	Menu-controlled operation

7.3.4 Examples of Stand-Alone Systems

7.3.4.1 Solar Home Systems

There are **billions of people** in the world **without** access to an **electric supply grid**. Instead they often have to use inefficient kerosene lamps for lighting and this fuel must be transported over wide distances. Batteries are often the only source of energy for radios, and so on. Here **photovoltaics** are an **ideal alternative** for making a considerable contribution for improvement in quality of life and for environmental protection.

The expression **solar home systems (SHS)** denominates **mini solar systems** of one or two modules that provide the required electric energy for a house in the third world. Typical loads are DC-operated energy-saving lamps, radios and TV sets (Figure 7.35).

The main problems in the spread of solar home systems are the **high initial costs** of the plants. Here **micro-credit models**, for instance, are a help with which customers can make a down-payment and then monthly payments for their SHS. A pioneering role in this field is the *Grameen Shakti* (translation: "village energy") undertaking, a subsidiary of the Grameen Bank famous for its micro-credits. This undertaking is responsible for financing **more than 500 000**
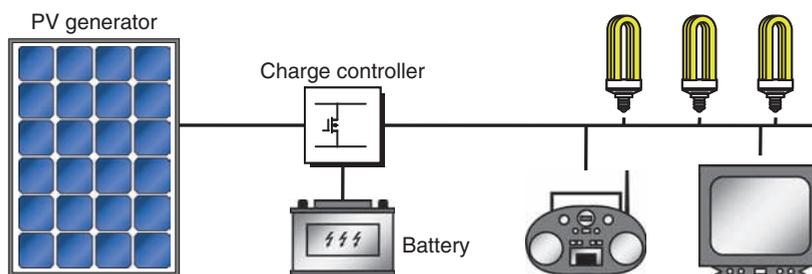
Figure 7.35 Typical arrangement of a solar home system: The loads are typically DC operated lamps, radio and television

Figure 7.36 Photos of solar home systems in Bangladesh: Arrival of the components by river and installation of the plant on a hut (photos: Grameen Shakti; Microenergy International)

solar home systems in Bangladesh (Figure 7.36). As the installations are erected by specially trained technicians and servicing of customers is organized through service offices, the result is high quality and a long life. If a system should fail then it is frequently due to the bridging of the charge controller by the owner of the installation [[105], www.gshakti.org].

The concept pioneered by Grameen Shakti now has many **imitators**. For instance there is a similar project in **Ecuador** that is sponsored by the government via a fund for rural electrification (FERUM – Rural and Marginal Urban Electrification Fund). The PV system consists of a **100 W module, charge controller** and a **105 Ah battery** with 3 DC **energy-saving lamps**. In addition systems with inverters and PV power of up to 800 Wp are also being installed [106].
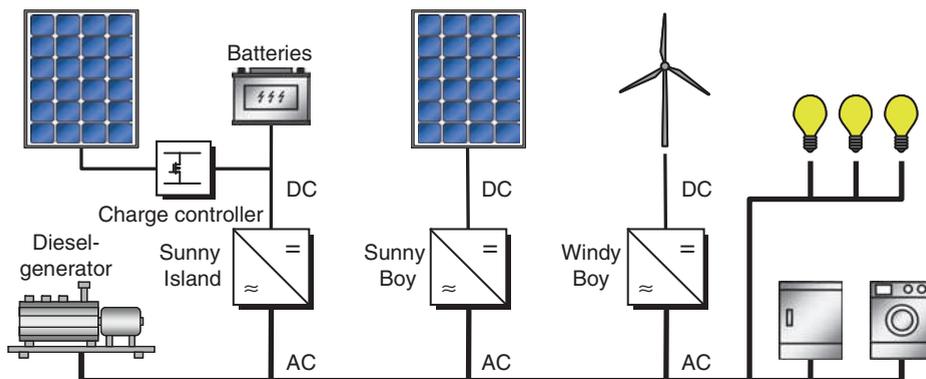
7.3.4.2 Hybrid Systems

If a whole year's continuous supply of electric energy is to be ensured then solar systems quickly reach their limits.

In order to equalize bad weather periods and even more seasonal fluctuations, high PV power and large storage capacities must be built up that lead to unreasonable costs. In this case the solution is **hybrid systems**, which are a **combination of various methods of generating electricity**. The combination with other renewable sources of energy such as water power, wind turbines and biomass is obvious. In addition the use of a diesel generator makes sense in order to bridge gaps in supply.

From an economic point of view hybrid systems with PV, diesel generator and large battery storage are **often cheaper** than plants in which only **diesel generators** are used. Reasons for this are the high servicing effort, short life span and very poor part-load efficiency of diesel generators [106].

Hybrid systems can be organized as pure DC systems, mixed DC/AC systems or also as pure AC systems. For larger plants, the trend is definitely to **pure AC systems** as they are **very flexible** and can be **easily extended**. Figure 7.37 shows an example of such a system that is equipped with inverters by SMA.

Figure 7.37 Arrangement of a hybrid system with pure AC coupling of generators and consumers: The Sunny Island generates a stable AC grid and can start the diesel generator or switch off loads in case of demand bottlenecks [107]

The heart is the **Sunny Island** battery inverter that generates a stable alternating current grid. The **batteries** serve as the **basis for** the **energy** and these again are charged by a PV generator. Other plants feed into the AC grid, for example, a further PV generator via a normal grid inverter **(Sunny Boy)** or a wind turbine via a special wind energy inverter **(Windy Boy)**.

If less power is used in the AC grid than is generated, then the Sunny Island feeds the excess energy into the batteries. If these are already full then other generators must be turned off. For this purpose SMA uses the **SelfSync**® process, which works in a similar manner to the power controls of large power stations in the energy supply grids. If the Sunny Island reduces the **frequency** of the AC grid then this is a command for the other inverters to reduce the fed-in **effective power**. At the same time the amount of **voltage** of the AC grid **determines** the quantity of the fed-in **reactive power**.

If, on the other hand, more power is consumed than can actually be generated then the Sunny Island accesses the batteries. If this is still insufficient then the device automatically starts the diesel generator or will switch off certain loads.

It is clear that this system is very **flexible** as further generators can simply be connected to the alternating current grid. Besides SMA, other producers also offer similar systems (e.g., Kaco).

If a whole village is connected to the hybrid system, this is also called a **Micro-Grid**. If, again several micro-grids are interconnected this is known as a **Mini-Grid**. Thus, it is clear that the technologies for developing countries offer a great opportunity to decentrally electrify rural areas in an **evolutionary manner** and then to interconnect to ever larger grid units.

7.3.5 Dimensioning Stand-Alone Plants

Dimensioning is relatively simple in the case of plants connected to the grid as one assumes that the public grid will be able to absorb the power generated at all times. This is much different for **stand-alone systems**: here the **consumption** must be **determined** as accurately as possible and then the PV generator and storage must be dimensioned in accordance with the radiation conditions at the plant location.

In the following we will become acquainted with a **simple scheme for planning a stand-alone system** that works with tables. The scheme was mostly taken over from the **guidelines**

for photovoltaic plants of the Deutsche Gesellschaft für Sonnenergie e.V. (German Association for Solar Energy) [21]. This method of calculation is naturally not nearly as accurate as an analysis with a stand-alone plant design program, but it can provide a **good first estimate**.

7.3.5.1 Acquiring the Energy Consumption

The best way of determining energy consumption is by means of a table in which the **nominal consumption of the individual consumers** and the **daily operating time** is listed. As an example we will assume a small holiday cottage near Munich that is to be used throughout the year (see Table 7.4). It is advisable to list the **summer season** (May–September) and the **winter season** (October–April) separately.

A special case is the refrigerator: In order to save energy especially in winter, it is assumed that the refrigerator is switched off in winter. Also one usually does not know the daily operating times of a refrigerator but the data sheet usually states the daily energy consumption (here 0.3 kWh).

After determining the energy consumption, we can turn our attention to the dimensioning of the PV generator.

7.3.5.2 Dimensioning the PV Generator

First we must find out what the yield of a solar module is in the respective months. Basic data is shown in Table 2.2 in Chapter 2, which gives the daily radiation H on a horizontal area for various places. Now we will look up in which month in the summer season the radiation is weakest. In the case of Munich this is September with an radiation of 3.53 kWh/(m^2·d).

Instead of the radiation we will simplify by considering **Sun full-load hours** (again - see Chapter 2). The Sun requires 3.53 full-load hours to generate the whole radiation on a September day. A 100 W module lying flat on the ground on this day will then generate energy of 3.53 h·100 W = 353 Wh. If we slant it then the yield is increased, which we can coarsely determine by means of a correction factor C_{Slant} according to Table 7.5. In the case of south alignment and a tilt angle of 30° we get a day's yield of 353 Wh · 1.25 = 441.3 Wh.

Finally we should take into account the **effects of temperature** on the module yield; this is done using a **correction factor C_{Temp}** that is listed in Table 7.6. As is to be expected, the warm climate of the south-oriented site makes a difference to the yield.

Table 7.4 Consumption balance of a small holiday cottage

Consumer	Nom. power P_{N} in W	Daily operating time t in h		Daily consumption W in Wh	
		Summer	Winter	Summer	Winter
3 lamps in living room	$3 \times 12 = 36$	1	3	36	108
2 reading lamps in bedroom	$2 \times 7 = 14$	1	2	14	28
1 outside lamp with motion detector	10	0,1	0,5	1	5
1 TV	50	2	3	100	150
1 refrigerator	50	Unknown	Switched off	200	Switched off
Total	160			351	291

Table 7.5 Correction factor C_{Slant} for deviations from the horizontal in Germany and other sites [21,40]

Site	Direction	Slant angle	Jan	Feb	Mar	Apr	May	Jun	Jul	Aug	Sep	Oct	Nov	Dec
Germany	South	30°	1.67	1.54	1.31	1.16	1.07	1.01	1.02	1.10	1.25	1.38	1.58	1.68
		45°	1.88	1.70	1.37	1.15	1.02	0.95	0.96	1.08	1.28	1.46	1.76	1.93
		60°	2.02	1.77	1.36	1.09	0.93	0.84	0.86	1.00	1.25	1.48	1.85	2.07
	Southwest	30°	1.55	1.36	1.21	1.08	1.02	0.97	0.96	1.05	1.16	1.29	1.42	1.48
		45°	1.73	1.46	1.24	1.06	0.98	0.91	0.90	1.02	1.17	1.35	1.54	1.61
		60°	1.83	1.49	1.22	0.99	0.89	0.82	0.81	0.94	1.13	1.34	1.56	1.68
	West	30°	1.10	0.98	0.98	0.93	0.92	0.90	0.88	0.93	0.96	1.02	1.01	0.95
		45°	1.12	0.97	0.95	0.87	0.86	0.83	0.81	0.87	0.92	1.00	0.99	0.93
		60°	1.10	0.93	0.90	0.80	0.78	0.76	0.74	0.79	0.86	0.95	0.96	0.91
	Southeast	30°	1.35	1.36	1.19	1.12	1.05	1.02	1.05	1.08	1.16	1.20	1.35	1.45
		45°	1.43	1.46	1.21	1.11	1.01	0.97	1.01	1.05	1.17	1.22	1.45	1.61
		60°	1.47	1.48	1.18	1.05	0.93	0.89	0.94	0.98	1.12	1.18	1.46	1.68
	East	30°	0.87	0.98	0.95	0.97	0.96	0.98	1.00	0.96	0.95	0.90	0.94	0.95
		45°	0.83	0.98	0.91	0.93	0.90	0.93	0.96	0.91	0.91	0.86	0.92	0.93
		60°	0.80	0.94	0.85	0.86	0.83	0.85	0.90	0.84	0.84	0.80	0.86	0.89
Marseille	South	60°	1.80	1.43	1.20	0.97	0.82	0.76	0.79	0.91	1.11	1.35	1.65	1.89
Cairo	South	60°	1.39	1.21	1.00	0.82	0.68	0.62	0.65	0.75	0.93	1.15	1.34	1.44

Table 7.6 Correction factor C_{Temp} for various sites in case of on-roof installations [40]

Site	Jan	Feb	Mar	Apr	May	Jun	Jul	Aug	Sep	Oct	Nov	Dec
Berlin	1.06	1.05	1.02	0.98	0.94	0.93	0.92	0.93	0.96	1.00	1.04	1.06
Marseille	0.98	0.98	0.95	0.93	0.91	0.89	0.87	0.88	0.91	0.93	0.97	0.98
Cairo	0.93	0.92	0.90	0.88	0.86	0.84	0.84	0.84	0.86	0.87	0.90	0.93

Added to the given correction factors there are also loss factors. First we will assume a fixed amount of up to 6% for the **electrical losses in the direct current lines**. These we will take into account with the line **loss factor $V_{\text{Line}} = 0.94$**.

In addition a battery can never completely output the full amount of energy that was put in during charging as the electro-chemical conversion processes incur losses. Experience values for temperate regions are 10% and in hot climates approximately double. For our cottage in Munich we will therefore calculate with a **conversion loss factor V_{Conv}** of 0.9.

Finally stand-alone plants to 500 Wp are usually produced without the MPP controller. This we will account for with the **adaptation loss factor V_{Adapt}** also of 0.9.

Now we can finally calculate the required module power with the following equation:

$$P_{\text{PV}} = \frac{W}{N_{\text{Sun}} \cdot C_{\text{Slant}} \cdot C_{\text{Temp}} \cdot V_{\text{Line}} \cdot V_{\text{Conv}} \cdot V_{\text{Adapt}}} \tag{7.28}$$

with

W: Energy consumed per day.
N_{Sun}: Sun full load hours.

For summer operation in the case of a south-oriented PV generator at a 30° inclination angle we get:

$$P_{\text{PV}} = \frac{351 \text{ Wh}}{3.53 \text{ h} \cdot 1.25 \cdot 0.96 \cdot 0.94 \cdot 0.9 \cdot 0.9} = 108.8 \text{ Wp} \tag{7.29}$$

A 110 W module would just about be good enough to cover the daily demand.

If we do the same calculation for the winter half year (with December as the critical month) then we get a required generator size of

$$P_{\text{PV}} = \frac{291 \text{ Wh}}{0.79 \text{ h} \cdot 1.68 \cdot 1.06 \cdot 0.94 \cdot 0.9 \cdot 0.9} = 271.7 \text{ Wp} \tag{7.30}$$

Winter thus clearly dominates the number of modules required.

> [?] December is the worst month as regards solar radiation. Could one not optimize the slant of the module for this month?

> ⚠️ This is really a good idea! According to Table 7.5 an inclination of 60° is the most advantageous for December. This results in a required PV performance of only 220.5 Wp. For instance, we could thus use two 120 W modules connected in parallel as a solar generator, which would then still be 10% over-dimensioned.

7.3.5.3 Selecting the Battery

Two aspects are especially important when selecting the battery:

1. The number of desired autonomy days.
2. The increase of the battery life for lesser discharge depth.

The term *autonomy days N_A* is understood to be the number of days on which the consumers can be further operated even in bad weather.

> A **rule-of-thumb value** for autonomy days in Germany is: **Summer: 3.5 days; winter: 5.5 days**

> In order to achieve a high **battery lifespan** we make the decision that batteries must **never** have a **state of charge of less than 30%**.

In the end, the user must decide what supply safety he wishes to achieve with the stand-alone system.

Accounting for these two conditions leads to the following equation:

$$C_N = \frac{W \cdot N_A}{0.7 \cdot V_N} \tag{7.31}$$

with

V_N: system voltage, here assumed to be $V_N = 12 \text{ V}$

In our case this results in summer:

$$C_N = \frac{351 \text{ Wh} \cdot 3.5}{0.7 \cdot 12 \text{ V}} = 146.3 \text{ Ah} \tag{7.32}$$

Naturally the requirements are higher in winter:

$$C_N = \frac{291 \text{ Wh} \cdot 5.5}{0.7 \cdot 12 \text{ V}} = 190.5 \text{ Ah} \tag{7.33}$$

Here, for instance a 12 V battery with 200 Ah capacity would be a good choice. As a result we will therefore select two solar modules each 120 W and a battery with a capacity of 200 Ah.
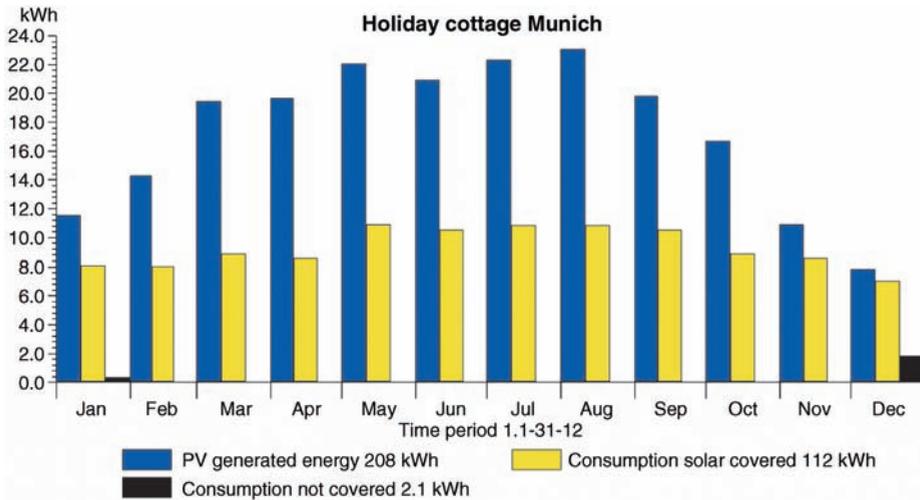
Figure 7.38 Simulation of the holiday cottage in Munich: With the design of the plant for the winter half of the year, only about half the generated electricity can be used (simulation with PV-Sol Expert)

On the home page *www.dgs-berlin.de* there is an Excel tool with which the calculation according to this scheme can be comfortably worked out for a series of other sites in the world. Further, the tool assists in the dimensioning of the DC line cross section. There are, of course, many other simulation programs with which stand-alone plants can be calculated (see also the overview in Chapter 9).

This example shows that in **summer** there will be a **large surplus of energy** that can normally not be used sensibly. Despite this, it is conceivable with the selected dimensioning that no full supply can be ensured in bad weather periods. If, for instance, one simulates this holiday cottage with the PV-Sol Expert simulation tool, then one actually obtains a solar coverage of 98% over the year (Figure 7.38). However, to cover the last 2 kWh with solar energy one would have to increase the battery capacity by 50%. This is in no relationship to the additional costs. Instead a small **emergency generator** would be recommended that in winter would occasionally recharge the battery. In this case one could even halve the battery capacity, for instance to 100 Ah, and still achieve a solar coverage of 93%.

8

Photovoltaic Metrology

Trust is good – control is better. This saying also applies to photovoltaics. That is why this chapter is devoted to presenting the most important principles for acquisition of solar radiation, and for performance and quality analysis of photovoltaic plants.

8.1 Measurement of Solar Radiation

It is necessary to use radiation sensors in order to determine the radiation behavior at various sites as accurately as possible. This measurement deals mostly with the determination of **global radiation** but sometimes also with the separate acquisition of **direct and diffused radiation** (see Chapter 2). For this purpose we will look at various types of sensors and discuss their special features.

8.1.1 Global Radiation Sensors

8.1.1.1 Pyranometer

The most accurate sensor for measuring global radiation is the **pyranometer**. The name is derived from the ancient Greek of *pyr*: "fire" and *ouranós*: "heaven"; to a certain extent the instrument measures the strength of the Sun's "fire" from the sky. The structure of a pyranometer is shown in Figure 8.1: The decisive element is the black absorber surface. The Sun's rays cause this to heat up compared to the environmental temperature so that the **temperature difference $\Delta\vartheta$** is a measure of the incident irradiance E:

$$\Delta\vartheta = \vartheta_1 - \vartheta_A = const \cdot E \qquad (8.1)$$

with

ϑ_1 : temperature of the absorber
ϑ_A: temperature of the ambience

The temperature difference is determined very accurately by means of a **thermopile**, which is understood to be a series connection of several thermal elements.
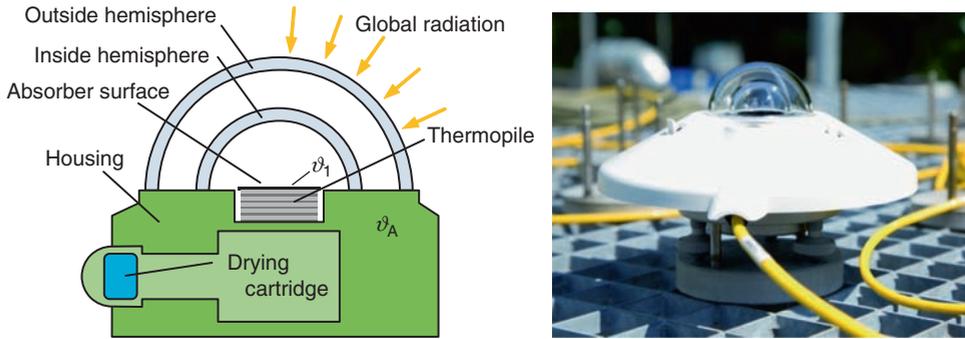
Figure 8.1 Structure and view of a pyranometer: The absorber surface is heated by the Sun's radiation so that via the temperature the irradiance can be acquired (photo: Kipp and Zonen)

The two **glass domes** have two tasks: First they ensure that the heated absorber surface re-radiates as little as possible of the heat taken up. Second, the hemispherical form secures that the sensitivity depends on the cosine of the incident angle (so-called **cosine response**). A vertical radiation thus has a maximum effect on the absorber surface whereas the horizontal one should have no effect at all.

In order to prevent the glass cover from misting, many pyranometers have a **drying cartridge** of silica gel that absorbs the moisture. The cartridge must be replaced after about 6 months.

The photo in Figure 8.1 shows the pyranometer with the normal white plastic cover; the **sunshade** is meant to prevent the pyranometer housing from heating up due to solar radiation. The black absorber surface detects practically the whole of the Sun's spectrum with a constant sensitivity. However, because of the glass dome, the measurable **spectrum** is limited to the range of **300–2800 nm**, but this is no problem as only a small portion of the solar radiation is not acquired (see Figure 8.2).

The voltage signal output by the thermopile is very small, typically around 10 mV with full Sun irradiance (1000 W/m^2). For this reason the signal is best increased by means of an external amplifier to manageable voltage values such as 0–10 V.
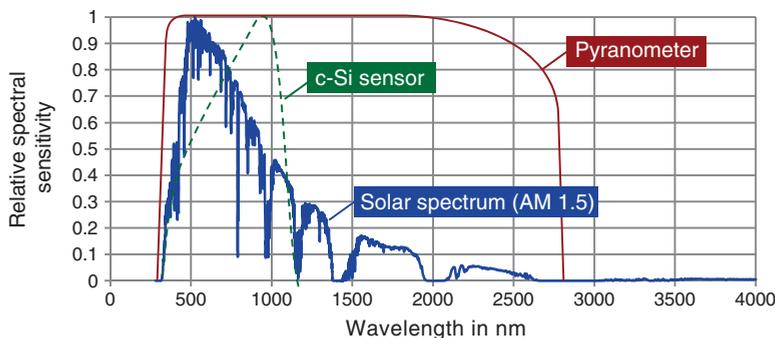
Figure 8.2 Spectral sensitivity of pyranometer and solar cell sensor: The pyranometer absorbs almost the whole of the solar spectrum whereas the solar cell only detects a limited portion

Table 8.1 Accuracy classes of pyranometers to ISO 9060

Property	Second class	First class	Secondary standard
Quality	Fair	Good	Excellent
Accuracy (daily sum) (%)	±10	±5	±2
Resolution (W/m²)	±10	±5	±1
Long-term stability (%)	±3	±1.5	±0.8
Response time (s)	< 60	< 30	< 15

Pyranometers are always used if as accurate as possible global radiation measurement data are required. For this purpose **various classes of accuracy** are defined in the **ISO Standard 9060** (see Table 8.1).

The table shows that there are great differences between the individual classes. Special note should be taken of the peculiar naming: **Best Class** is not the "First Class" but **"Secondary Standard"**!

8.1.1.2   Radiation Sensors from Solar Cells

A **pyranometer** costs **between 600 € and 2000 €**, depending on the class. For this reason radiation sensors from **solar cells** are an **economical alternative**. These are mostly small c-Si cells that have been specially encapsulated. In order to measure the irradiance, the solar cell is short-circuited with a low-ohmed shunt resistor and the voltage drop at the shunt is measured. As the short circuit current of a solar cell is proportional to the irradiance, a simple arrangement is possible. The temperature dependency of I_{SC} can be compensated for by building in a temperature sensor together with a downstream temperature-dependent voltage amplifier.

For a price range between 100 € and 500 € one obtains sensors with given accuracy of ±5 to ±10%. However, it must be noted that the c-Si solar cell always only measures a **small portion of the Sun's spectrum** (see Figure 8.2). If the sensor is calibrated to an AM 1.5 spectrum then it will show a deviation for a low-lying sun (e.g., AM 4). Added to this is that the **flat cover sheet** has a reflection that is dependent on the angle of incidence.

Therefore solar cell radiation sensors are mainly used for continuous **performance monitoring** of a PV plant. For this purpose they are **mounted at** the **module level** so that they receive the exact radiation available to the PV plant (Figure 8.3). This is why the radiation sensor should have the same technology (c-Si, a-Si, CdTe, etc.) as the modules in the plant.

In this case, the limited spectral sensitivity of the sensors is an advantage as they correspond exactly to that of the monitored modules. Table 8.2 summarizes the advantages and disadvantages of both types of sensors.

Nowadays there are also sensors on the market that are sold as **pyranometers with silicon photodiode**. These are actually c-Si sensors that possess a glass dome with a scatter pane in order to reduce the directional dependency of the sensor.

8.1.2   Measuring Direct and Diffuse Radiation

In Chapter 2 we saw that for the most accurate yield estimate, the separation of the global radiation into direct and diffuse radiation is necessary. There are special sensors for this. For

Table 8.2 Comparison of pyranometers and solar cell sensors

Pyranometer	Solar cell sensor
+ Very high accuracy	+ Economical
+ Sensitivity independent of λ	+ Behaves as a solar module
+ Hardly direction dependent	+ Small response time ($<1\,s$)
− Expensive	− Strong spectral dependency
− Sluggish	− Strong directional dependency
Use: measurement of global radiation for comparing various sites	Use: measurement of radiation in module level for plant monitoring

Figure 8.3 Various reference sensors of c-Si solar cells at the experimental rig of the Münster University of Applied Sciences: The modules are installed at module level in order to measure the incident radiation on the solar module

determining the **direct radiation** use is made of a *pyrheliometer* (*Helios*: a Greek Sun god). A typical model can be seen in Figure 8.4: The actual sensor is situated at the lower end of the tube. This only receives light when it comes exactly from in front through a pinhole at the start of the tube. For this reason, the pyrheliometer must continuously track the Sun.

In the case of **diffuse radiation** one uses a **normal pyranometer** in which the direct radiation is carried out by a **tracker shade ball** (Figure 8.5). The much **cheaper variant** is a **fixed shade ring** whose height however, must be adjusted every 10 days.

8.2 Measuring the Power of Solar Modules

When purchasing a fairly expensive solar plant, the customer expects the power of the module to correspond to what was agreed upon during the purchase. As we saw in Chapter 6 in the discussion about mismatching, it is not sufficient when the sum of all the power of the modules corresponds to the agreed-to nominal power; instead the powers of the individual **modules** should have the **smallest possible tolerance**. In order to ensure this, the modules must be measured very precisely by the producer. For this purpose almost exclusive use is made of **module flashers**.

Figure 8.4 Pyrheliometer for measuring direct radiation: The instrument must continuously track the Sun (photos: Kipp and Zonen)

8.2.1 Buildup of a Solar Module Power Test Rig

An important element of a module test rig is the **module flasher** (also called **solar simulator**). This designates a source or radiation that generates a flash of light corresponding to the spectrum of the sun. It consists mostly of a xenon flash lamp with a filter in front in order to approach as near as possible to **AM 1.5 spectrum**. During the **period of the flash** (e.g., **10 ms**) the *I/V* characteristic curve is electrically measured. For this one varies the resistance of the connected electronic load and at the same time measures, via computer control, the voltage and current of the module (Figure 8.6).

The reason for the use of a flash of light is the fact that the module scarcely heats up in the short time period. Thus one can assume a **constant temperature**. In order that the solar module is **homogenously illuminated**, the flash lamp should be placed at a great

Figure 8.5 Sensors for measuring diffuse radiation: Whereas the shade ball variant must continuously track the Sun, the shade ring is satisfied with an occasional adjustment of the tilt angle (photos: Kipp and Zonen)
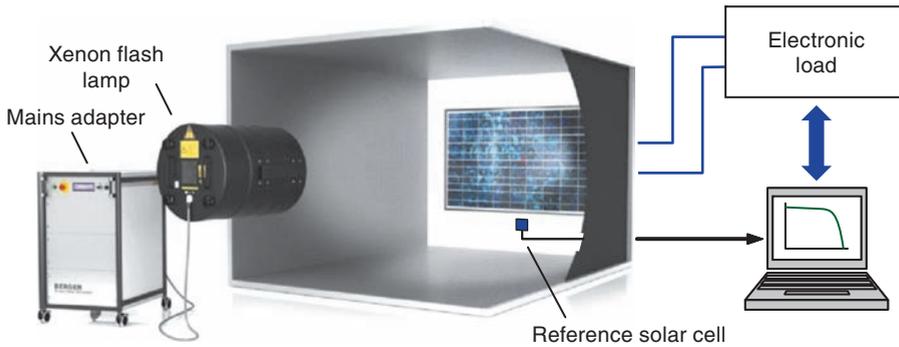
Figure 8.6 Principle arrangement of a solar module power test rig: The xenon lamp generates a flash of light with an AM 1.5 spectrum. During the flash the *I/V* characteristic curve of the solar module is measured with the help of an electronic load (source: Berger Lichttechnik)

distance (e.g., 5 m) from the module. A laser pointer acts as an aid to direction and must be aimed at the center of the module.

The **irradiance** during the measurement should be exactly **1000 W/m²**, which is why it is controlled by a **reference solar cell sensor**. The sensor must again be calibrated in order to achieve a high degree of accuracy during measurement. This calibration is carried out by means of a **reference module (the "golden module")**, which is understood to be a module that was measured by an accredited testing laboratory (e.g., TÜV Rheinland or Fraunhofer ISE) with an error of a maximum of ±2%. After the calibration of the reference sensor, the measurement of the golden module must have the same power as the value stated on the certificate of the test laboratory.

8.2.2 Quality Classification of Module Flashers

The EN 60904-9 standard specifies the requirements that a solar simulator must fulfill with regards to **spectrum** as well as **homogeneity** and **timely stability** of the irradiance [108]. For this purpose different classes are defined from which the quality of a flasher can be derived. Table 8.3 shows the conditions that lead to a division into the classes A, B or C.

In order to evaluate the **spectral adaptation**, an investigation is carried out in six defined spectral regions between 400 and 1100 nm on how well the flasher simulates the AM 1.5 spectrum. In order, for instance, to achieve Class A there must be no deviation of more than ±25% in any of the regions. Much more difficult to achieve is a **homogenous illumination** of the module area. The maximum deviation demanded of Class A of 2% between minimum

Table 8.3 Classification of solar simulators [108]

Classification	Spectral adaptation to AM 1.5 (%)	Inhomogeneity of irradiance (%)	Long-term instability of the irradiance (%)
A	± 25	2	2
B	± 40	5	5
C	± 60–100	10	10
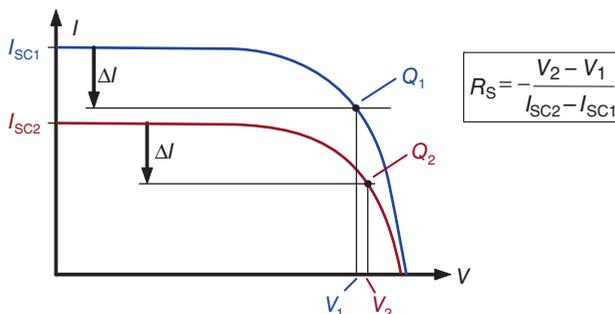
Figure 8.7 Determination of the series resistance R_S: After sketching the horizontal help lines the two operating points Q_1 and Q_2 that lead to the determination of R_S are found [109]

and maximum irradiance can be reached for large measurement areas of for example, 2 m × 2 m only with much effort. For this reason there are a number of ABA flashers on the market. However, from Chapter 6 we know that even a reduced radiation limited to a small area can have a large effect on the power of a solar module. For this reason one should **only accept measurements** that have been carried out with flashers of **Class AAA**. In this case the module performances should be determined with an **accuracy of ±3%**.

8.2.3 Determination of the Module Parameters

The most important parameters V_{OC}, I_{SC} and P_{MPP} can be directly derived from the received I/V curve of the module under standard conditions. In addition, one can determine the **shunt resistance R_{Sh}** and **series resistance R_S** of the module from the slope in the short circuit and open circuit point as described in Section 4.5.

However, a **more accurate determination** is possible with the flasher in the case of **series resistance**. For this, **two characteristic curves** must be taken **at different irradiances** (e.g., 1000 and 800 W/m^2) (see Figure 8.7). Now one determines an operating point Q_1 on the upper characteristic curve somewhat to the right of MPP and determines the **current difference ΔI** between I_{SC1} and the current in point Q_1. Then one determines the operating point Q_2 on the lower characteristic curve at which the current is $I_{SC2} - \Delta I$. R_S is calculated according to the following equation:

$$R_S = -\frac{V_2 - V_1}{I_{SC2} - I_{SC1}} \tag{8.2}$$

This method was specified in the DIN EN 60891 standard in 1994 and is now somewhat out-of-date [109]. A follow-up standard was issued in 2010 that specifies the taking of at least three characteristic curves at different irradiances. The series resistance is defined by means of a mathematical method, the details of which can be found in [110].

In order to estimate the quality of a solar module the **weak light behavior** should always be investigated. For this purpose the module is irradiated, for instance, in sequence with 100, 200, 400 and 700 W/m^2 and **the decay of the efficiency** compared to 1000 W/m^2 is determined (see

also Section 6.1.5). The different irradiances are obtained in that an optical weakener ("**fly screen**") is placed in front of the lamp.

> [?] Could we not just reduce the current of the lamp to get a lower irradiance?

> [!] Unfortunately, lowering the lamp current also lowers the lamp temperature and thus the lamp spectrum. The current should only be reduced to a maximum to $900 \, \text{W/m}^2$ where the change of the spectrum is still acceptable.

8.3 Peak Power Measurement at Site

When building up a photovoltaic plant one normally assumes that the power of the purchased modules corresponds to the data sheet values. A precautionary checking of all modules with the flasher would, in any case, be too expensive. A **cheaper alternative** to laboratory measurements is the **peak power measurement** of the whole plant at site.

8.3.1 Principle of Peak Power Measurement

In peak power measurement at site, a whole string or even the whole solar generator is measured at once. The source of light is the Sun; the actual irradiance is measured with a radiation sensor that points in the same direction as the solar modules. The module temperature is measured at the same time.

The actual measurement is carried out as follows: At time point $t = 0$ the solar generator is connected to a large capacitor (see Figure 8.8). The solar generator loads the capacitor, for instance, for one second. In this it **runs through the whole I/V curve** from the short circuit point (empty capacitor) to the open circuit point (charged capacitor). During the charging
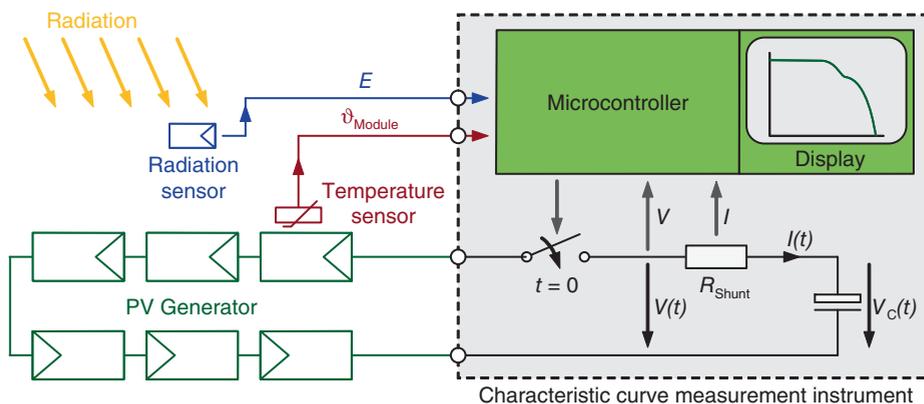
Figure 8.8 Arrangement of a characteristic curve measurement instrument: After the switch is closed, the solar generator charges the capacitor. In this it runs through the whole I/V characteristic curve from the short circuit to the open circuit point

process, the microcontroller continuously measures the voltage and current and can thus acquire the whole of the characteristic curve.

With simultaneously recorded radiation and module temperature, the determined **MPP power** can then be converted to the **value for STC conditions** (hence the designation **peak power measurement**).

> In the case of the module flasher, use was made of the changeable resistance in order to run through the characteristic curve. Why is a capacitor used here?

> When measuring a whole solar generator, high powers of, for instance, 10 kW are easily reached. The electrical load would therefore have to be very large and well cooled. With the capacitor, however, almost no power loss occurs so that the device can be relatively small.

8.3.2 Possibilities and Limits of the Measurement Principle

A large **disadvantage** of measurements at site is the **dependency on the weather**. Most of the producers of characteristic curve measurement instruments admit that exact measurements are only possible with irradiance over 500 W/m^2. A study carried out at the Münster University of Applied Sciences (Münster UAS), however, showed that even in this case the **peak power** was still strongly dependent on the **radiation** and **module temperature** [111]. The error tolerances of some producers of ±5% are certainly very optimistic because already the radiation sensors supplied have their own tolerances of ±5%.

Besides the peak power determinations also the reported **characteristic curve** is very informative. It can provide information on **cabling errors** or **defective modules**. Figure 8.9 shows two example characteristic curves.
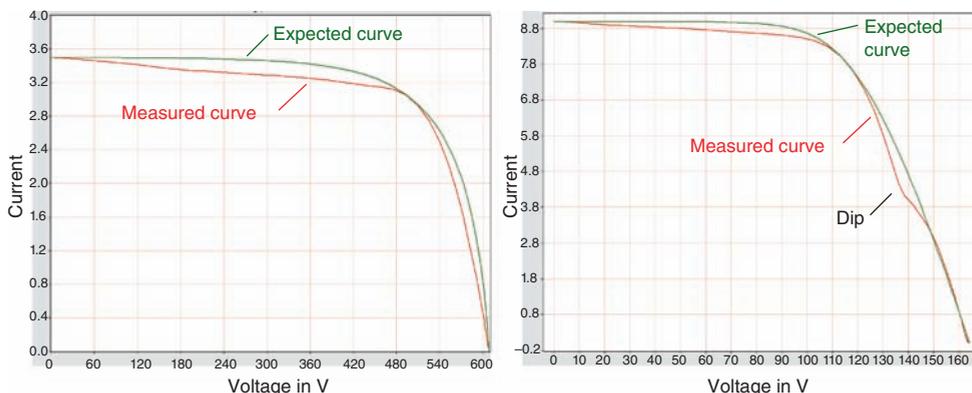
Figure 8.9 Recorded measurement curves: left; a string with modules of different quality, right; the effects of incorrect string cabling

The left picture shows an example of a curve of a string measurement, in which a slanted decay is noticeable in the upper region. This can be an indication of **partly shaded modules**. In this particular case, however, there was no shading; instead the **modules** were **of different qualities**. Because of this "proof curve" all the modules of the string were replaced by the producer. The picture on the right shows the effects of **errors in the string cabling**. Here a string of eight modules was connected in parallel with one string of seven modules shown by the dip in the right side of the characteristic curve.

The **series resistance** of the whole measured string can also be determined from this characteristic curve [11]. If this is much larger than the sum of the series resistances of the individual modules then it points to **high contact resistances** at the terminals of the string cabling.

To summarize, the characteristic curve measurement at site is a very **informative method** with information on quality of modules and cabling. Therefore is should be carried out as standard within the scope of plant acceptance for comprehensive quality control.

8.4 Thermographic Measuring Technology

Infrared thermography offers the possibility of carrying out a time-saving quality check of solar modules. We will first briefly deal with the principle of the function of thermography and then look at the two most important methods of bright and dark thermography.

8.4.1 Principle of Infrared Temperature Measurement

In Chapter 2 we learnt that the Sun is a **black body radiator**. An ideal black body radiator radiates a characteristic light spectrum depending on the surface temperature (**Planck's law of black body radiation**, see Figure 2.2). If this spectrum is integrated over the whole wavelength region, then the result is the ***Stefan–Boltzmann law***:

$$P_B = \sigma \cdot T^4 \tag{8.3}$$

with

P_B: optical power of the black body radiator
σ: Stefan–Boltzmann-constant: $\sigma = 5.67051 \cdot 10^{-8}\,\mathrm{W/(m^2 \cdot K^4)}$
T: surface temperature of the black body radiator

The **optical power** of the ideal black body radiator thus depends solely on a constant as well as the **surface temperature** of the radiator!

If the surface of the radiator is not ideally black then only a portion of the possible power is irradiated to the outside. This is accounted for in Equation 8.3 by the introduction of an **emission factor ε**:

$$P = \varepsilon \cdot \sigma \cdot T^4 \tag{8.4}$$

with

ε: emission factor

If the emission factor of a radiator is known then one can determine the surface temperature by means of a measurement of the radiation power. Table 8.4 lists the emission factors of some

Table 8.4 Emission factors of various materials [112]

Material	Emission factor	Material	Emission factor
Black body radiator	1	Aluminum, polished	0.18
Steel, black painted	0.96	Aluminum, oxidized	0.19
Steel, polished	0.07	Glass sheet	0.8–0.9

materials. From the example of steel it is clear that it is not the material in itself but the **surface properties** that are **decisive** in the **emission factor**. Basically one can say that the stronger the reflective effect of a surface the smaller the emission factor.

In simple IR thermometers, the radiation emitted by a surface is led by means of a lens to a sensor that detects the strength of the radiation. From this and the known emission factor, the surface temperature can be determined. Thermography cameras use the same principle but here a whole array of detectors is used so that a two-dimensional temperature picture can be generated.

8.4.2 Bright Thermography of Solar Modules

Bright thermography is understood to be the temperature analysis of solar modules in sunlight. In the simplest case one views the solar generator with a thermographic camera and searches for noticeable temperature peaks. Figure 8.10 shows an example in which an on-roof installation was investigated.

Two cells of the module at the bottom right whose temperatures are approximately 20 K above the other cells **are clearly noticeable**. Apparently they deliver too little current and thus heat up (load operation, see also Chapter 6). At the same time the region of the **module connection box** is clearly **heated up**, which indicates an active bypass diode. A characteristic curve measurement of the module confirmed that the module provided approximately 30% less power. On the basis of this malfunction picture the producer replaced all modules of the installation within the warranty period.
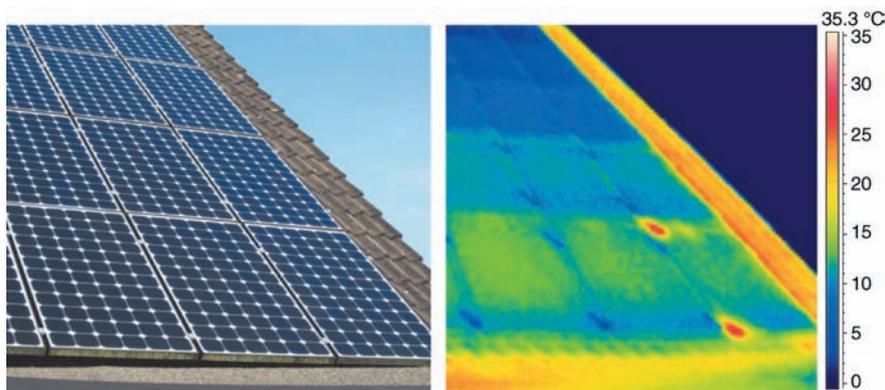
Figure 8.10 Example of thermographic measurement of an on-roof installation: Two cells of the module at the bottom right clearly show noticeable spots (photos: T. Stegemann, Münster UAS)
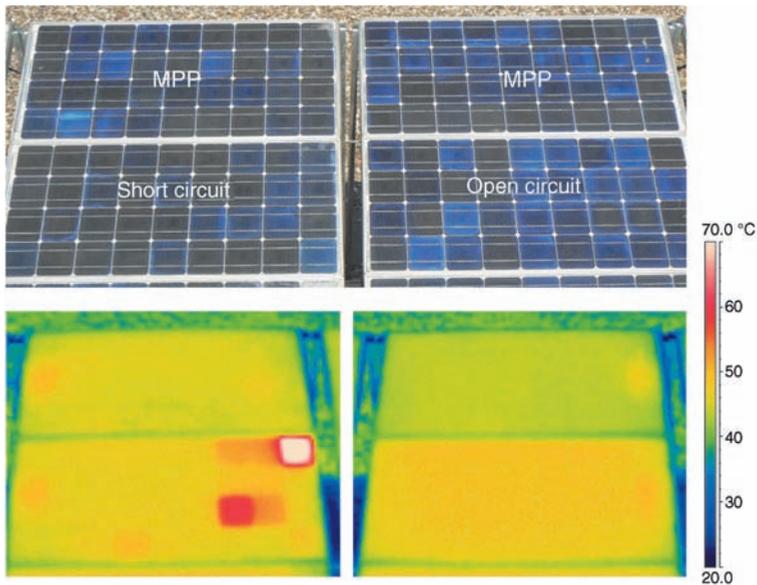
Figure 8.11   Thermography picture of modules in various operating conditions: The module in open circuit shows a homogenous heating, whereas the short circuit operation leads to different heating of the cells (photo: Münster UAS)

The thermography pictures in this chapter can be found in color on the Internet under *www.textbook-pv.org*.

The temperature picture of a solar module depends strongly on the actual operating condition. Figure 8.11 shows four modules of which one is in open circuit, one in short circuit and two are in MPP operation. The thermography picture of the module in **open circuit** is relatively homogenous, as here the light absorption has led to **even heating**. In the case of the **short circuited module**, there are **clear temperature differences** between the individual cells; here the load operation of the weaker cells can be seen. The cell at the top right has a temperature of 75 °C; it is approximately 30 K above the temperature of the other cells. In **MPP operation** the differences are **not** nearly **so distinct**.

After the short circuit operation, the bottom left module was changed to MPP operation and was measured by thermography again (not shown in Figure 8.11). In this case the weak cell only showed a temperature increase of 3 K compared to the other cells.

In the short circuit operation of a solar module the different cell qualities are much more in evidence in the thermography picture than in MPP operation.

> In Figure 8.11 the MPP modules seem to have the lowest temperatures while the open circuit and short circuit module are somewhat hotter. Is this a coincidence?

> It is really no coincidence! The MPP modules give up a part of their irradiated optical power as electrical power to the inverter. This part therefore does not lead to heating up the module. In the two other modules (open circuit and short circuit) no electrical power is output and therefore they heat up more strongly. In the particular case the difference is 2–4 K.

> A module in short circuit or open circuit operation heats up slightly more than one in MPP operation.

The knowledge of the characteristic thermo-pictures of the various operating conditions makes thermography a very effective means of quality control of photovoltaic plants. It is very easy to recognize incorrectly connected and defective modules.

> If a thermography camera is too expensive one can also do without it if need be. Figure 8.12 shows the module of Figure 8.10 taken on a cold November day with hoarfrost on the modules.

8.4.3 Dark Thermography

Besides thermography under illumination, measurements in the dark laboratory can also provide information on the module. In this the module is operated in **the IVth quadrant** (see Figure 6.1) with a high **reverse current** of, for instance, double the short circuit current.

Figure 8.12 "Thermography for the poor" on a cold November day: The two cells of the modules from Figure 8.10 can be clearly seen as free from hoarfrost (photo: T. Stegemann, Münster UAS)
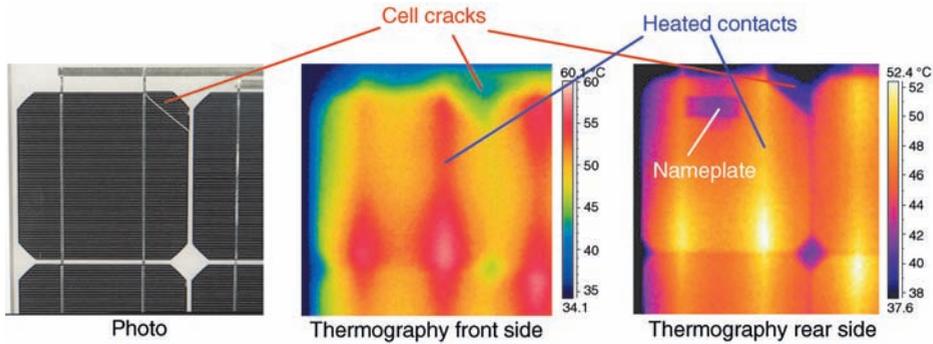
Figure 8.13   Dark thermography at the front and rear sides of a module: The inactive cell area top right can be much better recognized from the rear of the module (Photo: Münster UAS)

This current leads to heating of the finger contacts on the top side of the cell. Error positions with **high contact resistances** are clearly seen by means of temperature peaks (Figure 8.13). At the same time the reverse current ensures a relative even heating of the cells. Any **inactive cell region** can also be recognized. Measurement in the laboratory also has the advantage that the module can be viewed from the bottom. The thin rear side foil provides much better "picture resolution" than the thick front glass that strongly evens out the temperature picture.

8.5   Electroluminescence Measuring Technology

The last method of measuring we will look at is **electroluminescence measuring technology (EL measurement)**.

8.5.1   Principle of Measurement

The idea here is to **light up a solar module** as a large-surface LED. For this purpose the module is operated in the **diode pass region**, thus in the IVth quadrant (see Figure 6.1). A strong power supply is used to drive a reverse current to the level of the short circuit current through the module. With this the p-n junction is operated in the forward region and **light emission** is possible. However, we know from Section 3.6 that c-Si is an indirect semiconductor. As a phonon is required here for the interaction between photon and electron-hole pair, not only is the absorption of light relatively weak but, in the opposite case, the emission is too. Added to this is the fact that the bandgap of silicon leads to a **spectrum of about 1150 nm**. This wavelength can hardly be detected by a normal CCD camera.

Figure 8.14 shows the problem: the spectral sensitivity of the CCD sensor made of silicon decays strongly in the region of the bandgap of silicon. The already low light emission of the solar module can thus only be photographed at the noise limit. Nowadays special (and expensive) CCD cameras are available that can provide usable pictures.

A trick can be used in order to **improve** the **quality** of the photographed pictures: A **picture** of the current-less solar module is also taken, which is then "**subtracted**" from the electroluminescence picture. In this way the inherent noise of the camera and any foreign light can be well compensated.
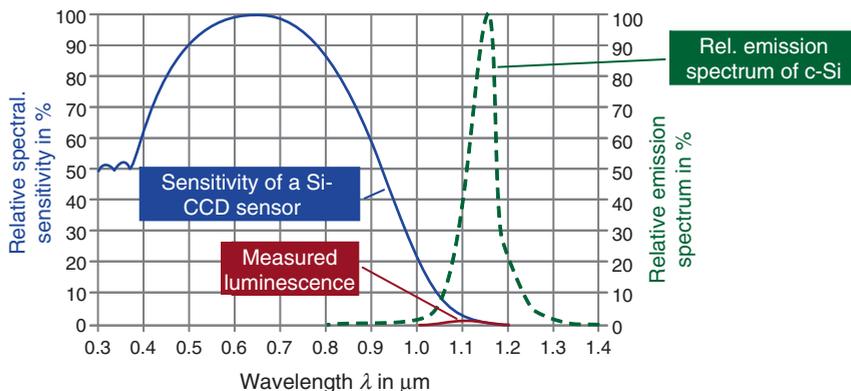
Figure 8.14   Problem with electroluminescence measurements: The emission spectrum of c-Si is at the sensitivity limit of CCD cameras and can therefore only be detected very weakly [113]

8.5.2   Examples of Photos

What do **typical electroluminescence pictures** look like? Figure 8.15 shows at the left a detailed photo of an individual cell taken with a special camera. **Spider web-type microcracks** can be clearly seen that have probably been caused by point mechanical loading.

Nevertheless the whole cell lights brightly as the current, as before, can be led through the two busbars and the contact fingers to all parts of the cell.

Things look different for cell 2: There is an inactive region that can be seen at the bottom right as the current cannot bridge the micro-crack. There is also a dark area at the top left indicating that the micro-crack runs parallel to the left busbar. The dark horizontal strip at the top right shows a **missing contact finger piece**, which could have been caused by a **blocked screen printing mask** (see also Section 5.1.3).
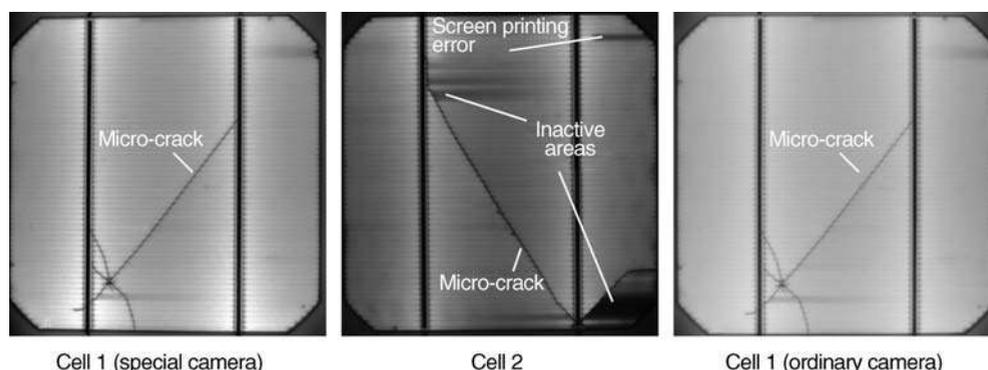
Figure 8.15   Photographed electroluminescence pictures of two solar cells: Both cells show a micro-crack that does not lead to a reduction of power at cell 1. In the case of cell 2, however, dark areas can be seen that can no longer contribute to the photocurrent. The right hand photo again shows cell 1 but here photographed with an altered cheap digital reflex camera (source: Münster UAS)
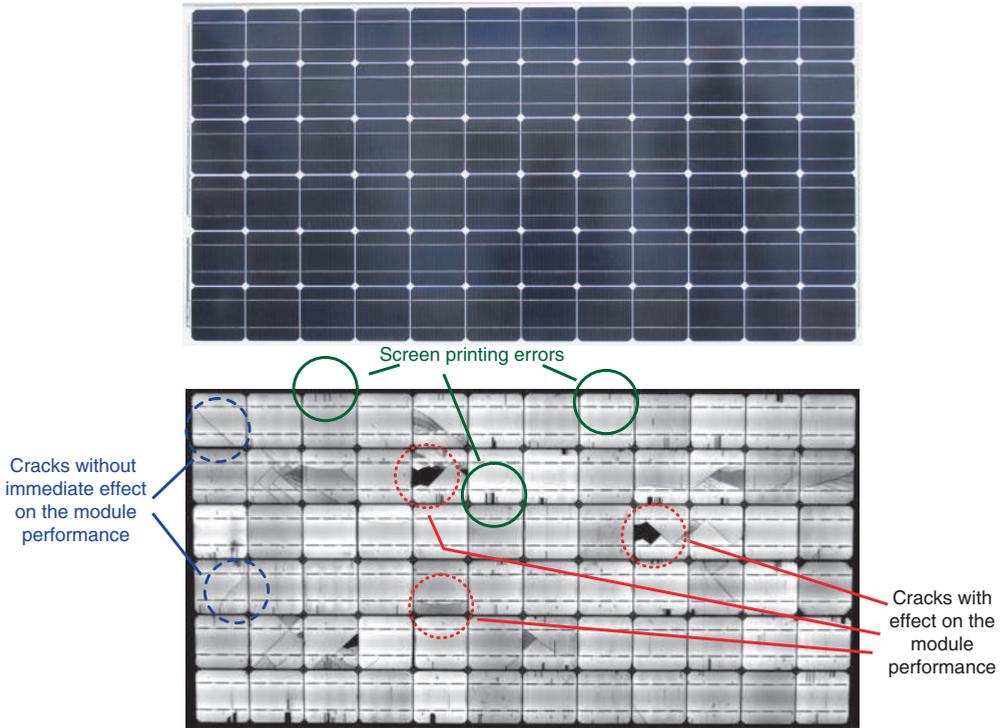
Figure 8.16   View and EL photo of a solar module that was improperly transported
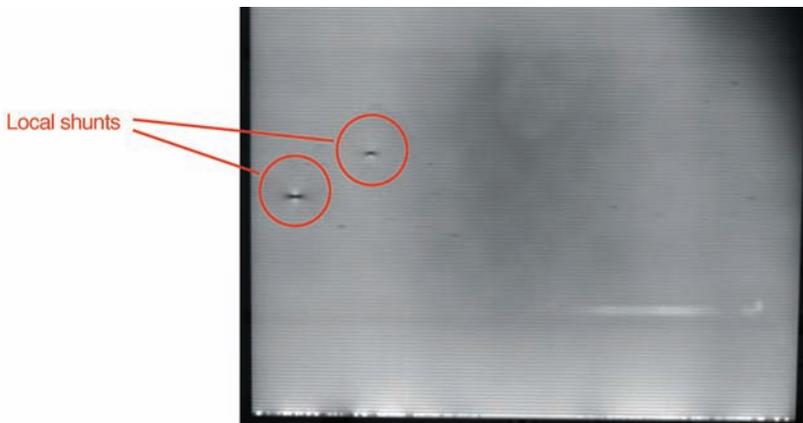
Figure 8.17   EL photo of a micromorphic thin film module: the two dark spots are caused by local shunts, which can already have been caused during module production

The **dark regions** are especially **critical** for cell performance. Although electron-hole pairs are also formed in normal operation of the solar cell, they cannot move to the bus bar and thus recombine without being used. This causes **sinking of** the **short circuit current** of the cell and also that of the cell string of the module.

An investigation at the Münster University of Applied Sciences showed that cheaper digital reflex single lens cameras (DSLR-camera) can also be used for electroluminescence photos after being altered [114,115]. This is shown in Figure 8.15 with the same cell as before, but now as a photo with a "**low-cost camera**". The picture is not quite as sharp and has less contrast, yet the relevant details can be well recognized.

Figure 8.16 shows a **module** that **seems completely undamaged** from the outside. The EL photo, however, shows many micro-cracks and electrically inactive regions. In this case the micro-cracks are due to **improper transport** of the module.

Naturally the dark regions in the **dotted circles** from the right are particularly unpleasant. In the case of the cells with the **dashed circles** from the left, the micro-cracks have no effect on the performance of the module. But if a micro-crack does exist, then it can grow in the course of time under the influence of wind, temperature changes and snow loads and also lead to **degradation of performance** [116]! Thus, by means of EL photos one can obtain **information on damage** to the module even before there are any electrical effects.

The top, **solid circles** in Figure 8.16 are **screen printing errors**. These are not necessarily dramatic for the purchaser of the solar module as they occur during production and do not propagate themselves. The problem is rather with the producer, who has to sell the module with a lesser power than is possible.

Thin film modules can also be investigated by means of the electroluminescence technology as is shown in Figure 8.17. This is a micromorphic module in which two dark points are noticeable. These are caused by local shunts (short circuits) that can occur during the module production in the integrated series connection (see also Section 5.2.7).

To summarize: Nowadays a row of mutually complementary measuring technologies are available that permit very accurate quality investigations of solar modules.

9

Design and Operation of Grid-Connected Plants

This chapter deals with the steps required for erecting a photovoltaic plant. The important aspects will be discussed starting with the choice of location and suitability of the roof, through yield estimates up to choice of components and plant installation. A further important subject is investment calculations for photovoltaic plants. Finally we will deal with methods of monitoring plants and operating results of actual plants.

9.1 Planning and Dimensioning

This subject will place the emphasis on the selection of the site as well as the effects of shading. In addition, software tools for plant dimensioning and yield estimates will be presented.

9.1.1 Selection of Site

Before an investment decision for a photovoltaic plant is made, there should be an exact investigation of the boundary conditions at the planned site. An important criterion for the economic viability of the plant is the **annual radiation at the site of the plant**. As was seen in Chapter 2, this varies in Germany between 900 and 1150 kWh/(m^2·a). A second important factor for roof installations is the **orientation of the roof and its pitch**. Here we determined that the optimum is a south-oriented roof with a pitch of approximately 35° (for Germany). Orientation of this roof to the southwest reduces the yield only by around 5% but in the case of a west-facing roof, the losses are already almost 20% (see Table 2.4). A check must also be carried out whether **shading** occurs and what effect this will have on the yield of the plant.

A further cause of loss is **module soiling**. This seldom occurs for a module inclination from 30 degrees as rainwater brings with it sufficient self-cleaning. Typical losses then are between 2 and 3%. For flatter inclination angles, losses due to bird droppings, dust, and so on can easily reach up to 10%. For agricultural operations the impairment from the dirt of stable ventilators can be even greater. In these cases regular cleaning is recommended.
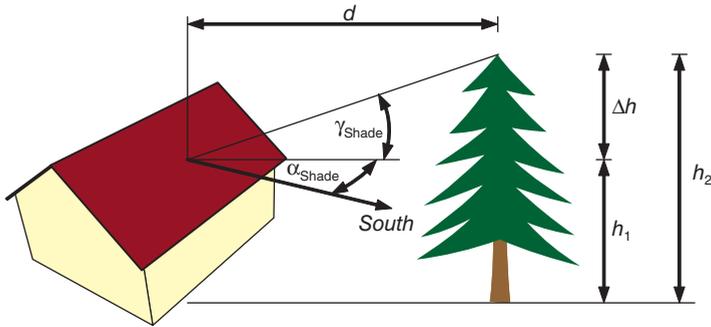
Figure 9.1   Determining the height angle of a shading object [21]

9.1.2 Shading

A shading analysis should be carried out in order to recognize possible shading and estimate its effects.

9.1.2.1 Shading Analysis

The **simplest shading analysis** is to stand at the installation site (on the roof) of the planned system and **look to the east, south and west** to see if there are any positions of possible shading. If there is only a single object (e.g., a high tree) then its sideways position can easily be determined by means of a compass. The **height angle γ_{Shade}** of the shade object is calculated from the distance d and the height difference Δh (see Figure 9.1):

$$\gamma_{\text{Shade}} = \arctan\left(\frac{h_2 - h_1}{d}\right) = \arctan\left(\frac{\Delta h}{d}\right) \tag{9.1}$$

This method is time consuming in the case of several shading objects. A **convenient aid** is the **Sun path indicator** with transparent film (Figure 9.2, left). This contains a compass with

Figure 9.2   Two variants of the shading analysis: The left picture shows the manually operated Sun path indicator and the right picture shows the SunEye device that permits automatic acquisition of the shading horizon
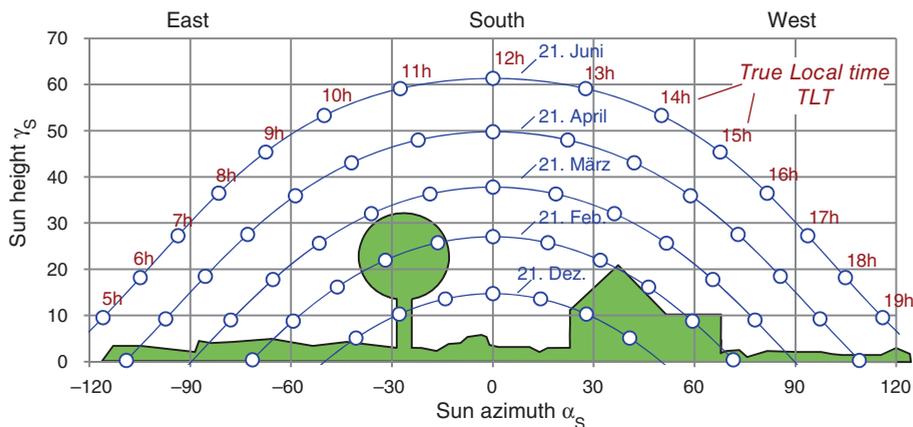
Figure 9.3 Example of a Sun path diagram with shading horizon: Whereas the house hardly has any effect, the tree provides daily morning shading from September to March

spirit level for aligning the device as well as a wide-angle lens through which the surroundings are viewed. A marker is then used to draw the silhouette of the surroundings on the film. As the film also shows the angle of the Sun during the course of the year, a rough estimate can be made of when the shading is likely to occur. These coordinates of the objects of shading can also be incorporated into a **simulation program** that carries out a relatively accurate determination of the effects on the energy yield (see Section 9.1.3.2).

More elegant than manually drawing-in the shading horizon is **automatic recording**. In the right-hand picture, Figure 9.2 shows the **SunEye device** that photographs the surroundings using a fish-eye lens. The shading horizon is then determined semi-automatically. At the same time with the use of a built-in GPS receiver, the device can determine the exact site and can thus carry out the site yield calculation directly.

Figure 9.3 shows the Sun path diagram known from Figure 2.12 with a shading horizon as an example.

Apparently the house on the right only has a slight influence as it causes shading only during the winter months from 14:00 h. However, the tree on the left provides morning shade for almost two hours from September to March.

9.1.2.2 Near Shading

The shading horizon is usually formed by far distant objects that often generate only a diffuse shade and do not lead to a full shading of the affected modules. **Nearby objects** such as roof dormers or chimneys are different as they form **deep shading**. A special case is caused by small objects such as aerial tubes, lightning protection rods or overhead lines. Whether these cause deep shading depends on the respective distances. Figure 9.4 explains the correlation on the basis of a sketch.

In the upper picture an **aerial tube** is positioned relatively near to the solar module. The result is broad deep shading that can lead to clear yield impairment. If the aerial tube is further away, then the width of the deep shading on the module is reduced. In the lower picture, the aerial tube is just far enough away that there is no more deep shading. This **minimal distance**
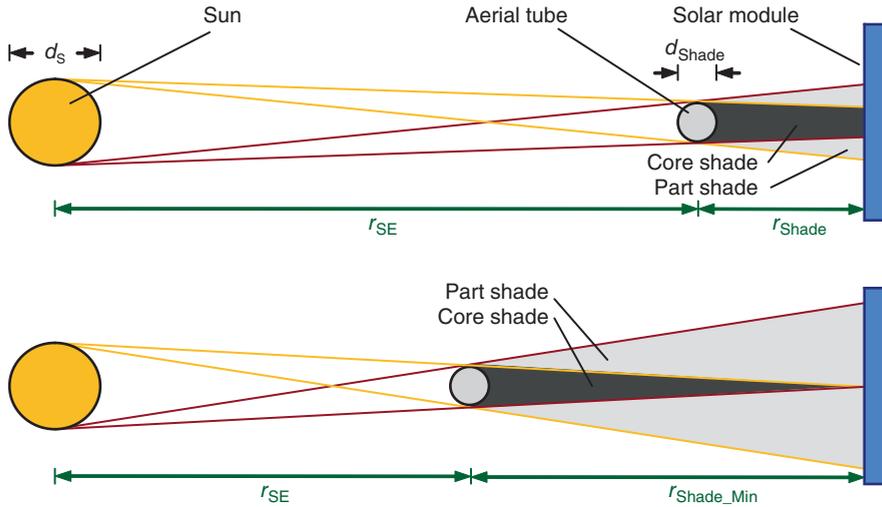
Figure 9.4   Problem of near shading: At short distances of the shading object there is a disadvantageous deep shade. The lower picture shows the minimum distance $r_{\text{Shade\_Min}}$, at which no deep shading will occur [21]

$r_{\text{Shade\_Min}}$ should be adhered to as far as possible. It can be simply calculated with the aid of the intercept theorem:

$$\frac{r_{\text{Shade\_Min}}}{d_{\text{Shade}}} = \frac{r_{\text{SE}} + r_{\text{Shade\_Min}}}{d_{\text{S}}} \approx \frac{r_{\text{SE}}}{d_{\text{S}}} \tag{9.2}$$

With the information for r_{SE} and d_{S} from Table 2.1 one can then derive an **approximation equation** for the minimum distance $r_{\text{Shade\_Min}}$ of the shading object of solar modules:

$$r_{\text{Shade\_Min}} = \frac{r_{\text{SE}}}{d_{\text{S}}} \cdot d_{\text{Shade}} = \frac{149.6 \, \text{M} \cdot \text{km}}{1.393 \, \text{M} \cdot \text{km}} \cdot d_{\text{Shade}} = 107 \cdot d_{\text{Shade}} \tag{9.3}$$

Example 9.1   Prevention of deep shading

Lightning protection rods of 1 cm are required in front of the installation. The minimum distance for preventing deep shading is:

$$r_{\text{Shade\_Min}} = 107 \cdot d_{\text{Shade}} = 107 \, \text{cm}$$

The distance of 1.07 m should not be undercut if possible.

∎

9.1.2.3   Self-Shading

In the case of flat-roof or free-standing plants, it is possible that the rows of modules **shade each other**. In order to prevent this certain **minimum spacings** must be adhered to.

A **rule of thumb** here is that at noon on December 21 (in the Northern Hemisphere) there must not be any shading. We can see from Figure 9.3 that this requires an angle of the Sun γ_S of 15°. The case is shown in Figure 9.5 in which the minimum spacing of the modules can be determined for a given angle of the Sun and defined module inclination angle.

The minimal module spacing d_{Min} in this case can be found by means of a similar calculation to that shown in Chapter 2 for Figure 2.14.

$$d_{Min} = b \cdot \frac{\sin(\gamma_S + \beta)}{\sin \gamma_S} \tag{9.4}$$

with

b: module width

Unfortunately, because of this condition only a part of the available area can be used. For this purpose we define the **area utilization ratio f_{Util}** that gives the relationship of module width b and module spacing d:

$$f_{Util} = \frac{b}{d} \tag{9.5}$$

In order to accommodate as much photovoltaic power on a flat roof surface as possible the optimum module inclination angle of 35° is often changed, for instance, to 20°.

Example 9.2   Area utilization ratios for various inclination angles

Two variations of flat-roof plants are planned: For a module width of 1 m in the first case the inclination angle is 35° and in the second case it is 20°. What is the area utilization ratio for an angle of the Sun of 15°?

In the first case, Equation 9.4 gives a minimum spacing of 2.96 m and in the second case $d_{Min} = 2.48$ m. The result of this is an **area utilization ratio of 34 and 45%** respectively. Therefore in the second case approximately 32% more photovoltaic power can be installed. The achievable energy yield per module area was only reduced by 2% (see Table 2.4). ∎
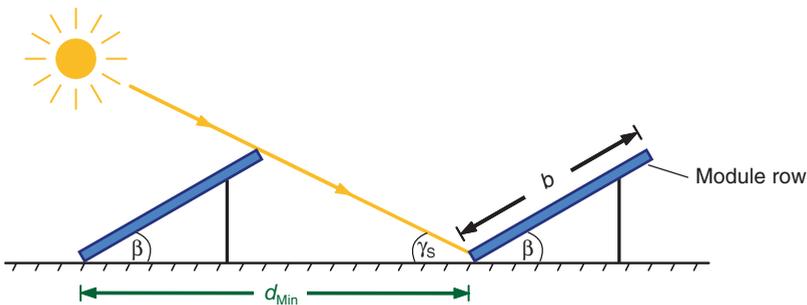
Figure 9.5 Prevention of self-shading: the spacing d_{Min} is the result of the requirement that there must be no shading even on the shortest day in the year (midday)
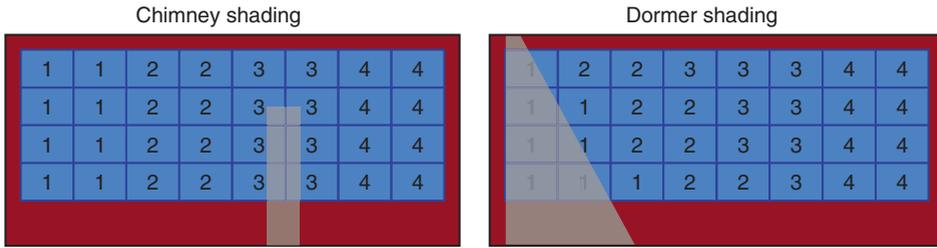
Figure 9.6   Optimized string connection for two cases of shading: Whereas the vertical chimney shading requires a vertical module connection, in the case of the slanted shading caused by the dormer this is better carried out diagonally [117]

9.1.2.4   Optimized String Connection

Section 6.2 showed that the effect of shading could be reduced by suitable string connections. We found there that simultaneously shaded modules should be connected into one string if possible. Figure 9.6 shows the application of this rule for two cases. The left picture shows a chimney, the shade of which wanders from left to right over the plant in the course of the day. Usually only one string is affected by the shading with vertical connections of the modules. In the picture on the right we see the slanted shading of a roof dormer that occurs in the late afternoon with the sun low in the horizon. Here the modules are best connected diagonally in order to limit the effects.

9.1.3   Plant Dimensioning and Simulation Programs

9.1.3.1   Inverter Design Tools

In Section 7.2 we dealt with the dimensioning of inverters and became acquainted with various rules for plant design. Nowadays practically all inverter manufacturers offer **design tools** for optimum combination of solar generators and inverters. Table 9.1 lists the tools of the five largest manufacturers.

Besides the actual **inverter dimensioning**, some of the programs also provide aids to **cable-loss calculations**. Further, some tools also comprise **simple yield estimates** but of different

Table 9.1   Summary of the dimensioning tools of various inverter manufacturers

Name	Sunny Design	Aurora Stringsizer	Kacocalc Pro	LynxPlanner	Solar Configurator
Manufacturer	SMA AG	Power One Inc.	Kaco New Energy GmbH	Danfoss GmbH	Fronius International GmbH
Inverter Dimensioning	Yes	Yes	Yes	Yes	Yes
Yield estimate	Yes	Only coarse	Yes	Yes	No
Cable loss calculation	Yes	No	Yes	No	Yes
Available as	Download	Online tool	Download	Download	Download
Web Address	www.sma.de	www.power-one.com/	www.kaco-newenergy.de/	www.danfoss.com	www.fronius.com
Remarks	–	Very little information	–	Large weather database	–

qualities. For exact yield prognosis it is better to turn to professional time-step programs as described in the following.

9.1.3.2 Simulation Programs for Photovoltaic Plants

An accurate **yield prognosis** for an actual plant at a particular site is best achieved with a **professional simulation program**. The program typically works in the time-step method in which the radiation (e.g., in the three-component model, see Chapter 2) is calculated for the whole year in minute or hour grids. At the same time the temperature coefficients and the weak light behavior of the solar modules are entered in the current and voltage calculation on the DC side. The efficiency curve of the inverters as well as cable losses are also taken into account in order to simulate the annual power fed into the public grid.

Table 9.2 shows the properties of a selection of the simulation programs available in the market. Besides two commercial programs it also contains free versions.

It is important for the accurate simulation results to have a **large number of weather data sets** in order to represent the situation at the planned site as accurately as possible. Besides the existing datasets, some programs provide the possibility of entering the data from additional sites.

There are many different ways of dealing with shading. Especially elegant is the **three-dimensional plant depiction** of the PV-Sol program with which the shading can be seen very clearly. Figure 9.7 shows, on the left the three-dimensional depiction of an on-roof installation, shaded by a chimney and a tree. The example shows the shading on the March 15 at 12:30 in Berlin: Because of the low position of the Sun in March, this causes heavy shading. The effect on the yield can be seen in the screenshot on the right hand picture: here the frequency of the shading is shown for every module over the year. The two modules above the chimney are the

Table 9.2 Collation of simulation programs for yield prognosis

Name	PV-Sol Expert	PV Scout	Greenius Free	RETScreen	PVGIS
No. of weather datasets	8000 worldwide	260	10	4700	From satellite pictures
No. of module datasets	6200	5700	1 (editable)	300	–
Time resolution of simulation	1 h	1 min	1 h	–	–
Shading simulation	Horizon and near objects, 3D visualization	Near objects (only visualization)	Horizon and near objects	No	Horizon
Suitable for island plants	Yes	No	No	Yes	No
Investment calculation	Yes	Yes	Yes	Yes	No
Price	1200 €	300 €	Free	Free	Free
Web address	www.valentin.de	www .solarschmiede .de	www.htw-berlin.de	www.retscreen.net	http://re.jrc.ec .europa.eu/pvgis
Remarks	Very comprehensive	Export of part lists and connection plans	Also for wind and solar thermal	Excel-based, also for wind, water, etc.	Online-Tool

3D-Overall view   Shading frequency
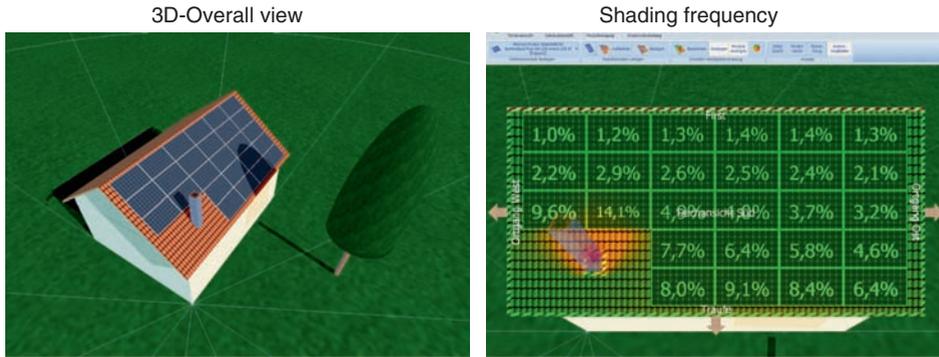
Figure 9.7   Shading simulation with PV-Sol: The three-dimensional depiction permits visualization of the shading for each time of the year. The picture on the right shows the frequency of shading of the individual modules

most affected with frequencies of 9.6 and 14.1%. This depiction can then be used in order to create a **shade-optimized string connection** and then to calculate the yield. For a simulation that is as near to reality as possible it is able to provide information on how many bypass diodes are contained in each module per type of module.

Besides the simulation programs, **photovoltaic online databases** are also available for forecasting the yield of a planned installation as accurately as possible. Thus, for instance, under *www.pv-ertraege.de* the yield data (in Germany) of approximately 16 000 photovoltaic plants are freely available. There it is possible to find **average yields of plants in one's own region**, which is a good estimation of the achievable yield. **Further online databases** are available in the **Appendix**. Besides this, there is a **checklist** that describes what is to be taken into account before and during the installation of a photovoltaic system.

9.2   Economics of Photovoltaic Plants

The economic operation of photovoltaic plants has only become possible in Germany with the **Renewable Energy Law (Erneuerbare-Energien-Gesetz: EEG)**. For this reason we will first look in more detail at the framework conditions of this law. Then we will look at a method for profit calculation with which the economics of the investment in a photovoltaic plant can be determined.

9.2.1   The Renewable Energy Law

The EEG was enacted by the German Bundestag in 2000. For the first time it provided a **country-wide regulation of cost-covering compensation of energy from photovoltaic plants**. The aim of the EEG is the provision of a continuous demand for photovoltaic plants in order to achieve **cost reductions** through **mass production**. The result was very impressive: within the first 10 years the prices for photovoltaic plants were reduced by approximately 70%.

The amount of the **compensation** depends on the year of erection of the plant and **remains constant for 20 years**. A plant that is built in the next year receives less compensation that

again remains constant for 20 years. The compensation regression of the EEG that was only 5% per year in its early years has been substantially increased as the prices of plants have been driven down over-proportionally.

9.2.2 Return Calculation

If one asks various providers of photovoltaic plants what the profit is, one receives greatly varying numbers as an answer. On the one hand, this is because different annual energy yields are assumed. On the other hand the cause is often in the **definition of "return"**. Thus, in some calculations, possible savings in tax are taken into account. Often it is assumed that the plant is in large part financed with a credit and only the **return on equity** is given in which the total return **only refers to the own capital** that was used. We want to make it simpler for ourselves but still achieve a high degree of transparency and traceability.

9.2.2.1 Input Parameters

The **input parameters** of any investment calculation are the **investment costs C_0** for the construction of the photovoltaic plant, the **annual operation costs C_{Oper}** and the expected **annual income C_{Inc}**. In the investment costs and all other amounts, use is made of the **net values** as the VAT is only a posting that is offset with the finance department in the following year.

The following applies for the annual operation costs C_{Oper}:

> The **annual operating costs C_{Oper}** (including service costs) are typically taken as **1.5% of the investment costs** of a photovoltaic plant.

The **operating costs** include expenditures for insurance, meter costs, electricity costs of a data logger, and so on. Besides this, in the lifetime of a plant one must take defects, especially of the inverter, into account. The calculated operating costs are also to be seen as reserve for repairs and should not be less than described above for the investment calculation.

The annual income depends on the amount of the **feed-in tariff c_{EEG}** and the achieved **annual energy yield W_{Year}**:

$$C_{Inc} = c_{EEG} \cdot W_{Year} \tag{9.6}$$

9.2.2.2 Amortization Time

The **simplest calculation model** is the view of the **amortization time**. This is understood to be the time it takes to recoup the capital expended. In the years after that one is in the profit zone. The amortization time T_{Amort} is obtained by the division of the **investment sum C_0** by the **annual surplus $C_{Surplus}$** that is further understood to be the difference between the annual income and operating costs:

$$T_{Amort} = \frac{C_0}{C_{Inc} - C_{Oper}} = \frac{C_0}{C_{Surplus}} \tag{9.7}$$

Example 9.3   Amortization time of a 5 kW plant

Susie Sunny purchases a 5 kW plant at a price of 9000 €. She calculates conservatively with a specific yield w_{Year} of 850 kWh/(kWp·a). She receives 18 cents/kWh as feed-in compensation.
    The annual income is:

$$C_{Inc} = W_{Year} \cdot P_{STC} \cdot c_{EEG} = \frac{850 \text{ kWh}}{\text{kWp} \cdot \text{a}} \cdot 5 \text{ kWp} \cdot 18 \text{ ct/kWh} = 765 \text{ €/a}$$

With the operating costs of 135 € this leads to an annual surplus of 630 €. Thus the amortization time is:

$$T_{Amort} = \frac{C_0}{C_{Surplus}} = \frac{9000 \text{ €}}{630 \text{ €/a}} = 14.3 \text{ a} \qquad \blacksquare$$

If one calculates this example with an annual specific yield of 900 kWh/kWp, then there is a better amortization time of 13.3 years. With an operating time of feed-in compensation of 20 years, Ms Sunny therefore has almost 7 years of making a profit.

9.2.2.3 Property Return

Although the amortization time is a very clear measurement, it does not take into account the **interest** of the capital used. For Ms Sunny the 765 € that she receives after the first year is to a certain extent more valuable than the amount of the second year as she can invest the money in the bank again and collect interest on it.
    For the sake of clarity we will present **two investors: Charles Cash** and **Susie Sunny**. Mr Cash has 9000 € available that he invests with his bank at **fixed interest p** for 20 years. At the end of each year he receives interest that is immediately invested again. With the **compound interest rate equation** one can now calculate how much money C_n he will have at the end of the n years:

$$C_n = C_0 \cdot (1+p)^n = C_0 \cdot q^n \qquad (9.8)$$

with

q: Interest factor: $q = 1 + p$

    Assume, for instance an interest rate of 3%, then after 20 years Mr Cash will have a sum of:

$$C_{20} = C_0 \cdot (1+p)^{20} = 9000 \text{ €} \cdot 1.0320 = 16.255 \text{ €} \qquad (9.9)$$

    Ms Sunny also has 9000 € available and invests the money in a photovoltaic plant. Every year she receives an income from the power feed-in and invests this money, less the deductions of the operating costs, also at an interest rate of p at the bank. Here, too, we can work out how much money she has saved after 20 years:

$$C_{20} = C_{Surplus} \cdot (q^{19} + q^{18} + q^{17} + \ldots + q^1 + q^0) \qquad (9.10)$$

    The sum in Equation 9.10 can be simplified with the help of the mathematically well-known **geometric series** so that we finally obtain the so-called **savings bank equation**:

$$C_{20} = C_{Surplus} \cdot \frac{q_{20} - 1}{q - 1} \qquad (9.11)$$

Assume that for Ms Sunny there is again an annual surplus of 630 € so that her income after 20 years is:

$$C_{20} = 630\,€ \cdot \frac{1.03^{20} - 1}{1.03 - 1} = 16928\,€ \tag{9.12}$$

In 20 years Ms Sunny has earned a bit more money than Mr Cash.

The **property return** is the interest that must be inserted in the Equations 9.8 and 9.11 so that in both cases the same money amount is calculated. In other words:

> We compare the investments in a photovoltaic plant with a money investment in a bank and define the appropriate rate of interest that applies to the same end amount as **property return of the photovoltaic plant**.

If we carry out this comparison for Ms Sunny's plant then we get a property return of 3.45%. In Figure 9.8 the capital development for this case of Charles Cash and Susie Sunny are compared. After 20 years both have about 17 700 €.

The return given in the example of 3.45% is quite low.

> In the **EEG** one normally orients oneself to the actual prices of photovoltaic plants and in the determination of the feed-in tariffs one assumes a **property return of 7.4%**.

> [?] A PV installer has told me that one can get a return on equity of more than 10% with a photovoltaic plant. What does he mean by this? Isn't this in contradiction with the previously mentioned returns?
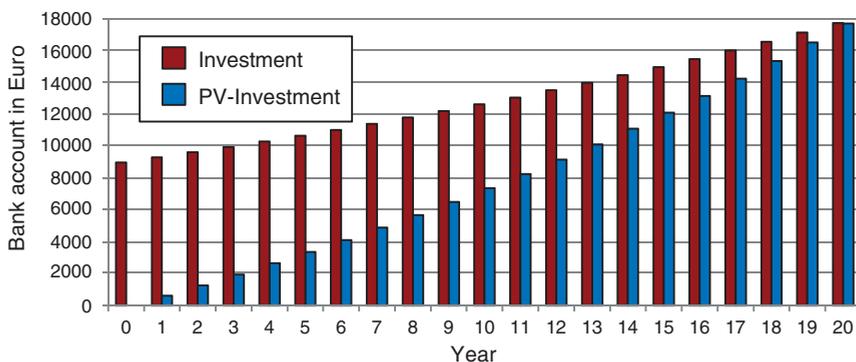
Figure 9.8 Explanation of property return: The investment in a photovoltaic plant is compared with an investment of money in which an amount is invested with compound interest for 20 years [118]

> ⚠️ The term "return on equity" refers to the return of a plant with the capital used. Assume that Ms Sunny buys her plant cheaply and thus achieves a property return of 7%. In order to finance this she takes out a credit at a bank of 8000 € with a rate of interest of 4%. The remaining 1000 € is her own resources. With the borrowed 8000 € she achieves a profit of around 3%. The return on equity refers to the return on the 1000 € of own capital and achieves, for instance, a value of 30%.

The result of this calculation depends greatly on the assumptions. If Ms Sunny were to take up the whole investment sum as credit then the **return on equity** is infinite. This shows that this return on equity **is no sensible measure** on which an investment decision can be based.

9.2.2.4 Profit Increase through Self-Consumption of Solar Power

As already described in Section 7.2.6, the profit of a photovoltaic plant can be increased in that the largest possible portion of the energy generated is used by oneself. If Susie Sunny and her family have the typical energy demand of 4500 kWh per year then she can assume a **self-consumption portion a_{Self} of approximately 30%** [99]. The price of the energy taken from the grid we will assume to be $c_{Taken} = 25$ ct/kWh. Thus the calculation of Example 9.3 can now be modified:

Example 9.4 **Amortization time of a 5 kW plant with 30% self-consumption**

We will first derive an "Average compensation" c_{Aver} from the two current parts:

$$c_{Aver} = a_{Self} \cdot c_{Taken} + (1 - a_{Self}) \cdot c_{EEG} = 0.3 \cdot 25 \text{ ct/kWh} + 0.7 \cdot 18 \text{ ct/kWh} = 20.1 \text{ ct/kWh}$$

If we calculate Example 9.3 with this feed-in tariff, then the amortization time with the self-consumption is reduced from 14.3 to 12.5 years. The return increases from 3.45% to almost 5%.

∎

With further **decreasing feed-in tariffs** and simultaneously **increasing power consumption costs**, solar power self-consumption will in future play an increasing role in the profitability of a photovoltaic plant.

9.2.2.5 Further Influences

The previous calculation can be further tweaked. Thus, for instance, one can integrate the general **price increase** on the assumption of an increase of almost 2% per annum.

Besides this there is the question whether the modules will perform at full power also after 20 years. The producers of the modules generally give a power guarantee of 90% within the first 10 years of operation and 80% on the nominal module power within 20 years. Thus one can factor in an assumption of a conservative **annual performance degradation** of 1% in the expected feed-in tariff. On the other hand, experience with c-Si standard modules **shows** that the degradation is more likely to be 0.5% per annum so that this value should be sufficient.

Finally, it should not be forgotten that a photovoltaic plant is **not valueless after 20 years**. The components can fulfill their tasks for many more years. If the plant continues to be connected to the grid it can reduce the own consumption costs. Further, it cannot be ignored that certain compensation will be paid also after 20 years as macroeconomic it will still be more advantageous than, for instance, building new coal-fired power stations. An Excel program is available under *www.textbook-pv.org* with which simple profit calculations can be carried out in a traceable manner.

9.3 Surveillance, Monitoring and Visualization

What do the three terms in this heading mean? **Plant surveillance** is an alarm system that gives early warning of failures or largely reduced yields. **Plant monitoring** goes beyond this aim: It is meant to compare the actual performance of a plant with other plants and in the best case give information on how the plant yield can be further increased. **Plant visualization**, on the other hand, is thought of as a descriptive information on the current status of the plant. In the following we will look at the respective aspects of the three measures.

9.3.1 Methods of Plant Surveillance

The simplest type of plant surveillance is to occasionally look at the **display of the inverter**. This should show that the inverter is feeding the grid and that the plant is running in MPP operation.

More accurate information is obtained when the generated energy is read off at the end of the month or the week and then compared with the **yields of other plants**. If the yield of the own plant is much lower then the cause must be searched for. Nowadays there are a series of **online databases** in which the yields of thousands of plants are available on a daily basis. Much more elegant than a manual comparison is the **use of a data logger** that compares the own daily yields with similarly oriented plants. If there is a large difference then, for instance, an SMS alarm message is output. The data logger's Internet connection has the additional advantage that the data is regularly saved on a central server and can even be called up years later. Examples of these types of databases are *home.solarlog-web.de* as well as *www.sunnyportal.com*.

An alternative for checking the plant on the basis of reference plants is the immediate comparison of the current plant performance with the present radiation. For this purpose a **solar cell radiation sensor** is mounted at generator level as described in Section 8.1. Besides this, the **measurement of the module temperature** is helpful in order in this way to obtain a preferably good estimate of the expected plant power. Various commercial data loggers offer this special function and can also trigger an alarm per e-mail, SMS or signal horn.

9.3.2 Monitoring PV Plants

9.3.2.1 Specific Yields

The yield of a photovoltaic plant depends primarily on the **radiation energy H_G** arriving at the generator. The **observation time** selected is usually a year but sometimes a month or even a day. The **reference yield Y_R** is defined as:

$$Y_R = \frac{H_G}{E_{STC}} \qquad (9.13)$$
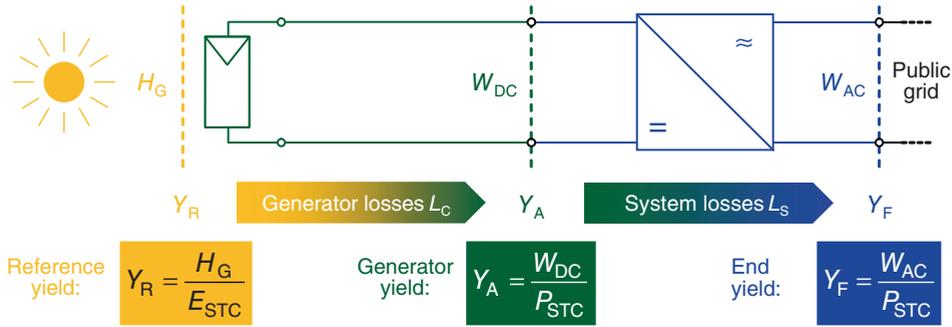
Figure 9.9 Specific yields of a photovoltaic plant: The generator yield Y_A is less than the generator loss and lower than the reference yield Y_R; the end yield Y_F again corresponds to the generator yield lessened by the system losses

With this, one references the radiation energy to the full irradiance of the Sun under STC conditions. The radiation energy H_G is given in kWh/m^2 and if this is divided by 1000 W/m^2 the result is the unit h (hours). The reference yield Y_R thus gives the number of hours during which the Sun would have to shine with full force on the solar generator in order to generate the energy H_G. Similar to that described in Chapter 2 we call this the **Sun full load hours**:

> The **reference yield Y_R** gives the **number of Sun full load** hours at the generator level per year.

Unfortunately, losses occur in a real photovoltaic plant so that the reference yield cannot be completely used for the production of electricity. This is shown clearly in Figure 9.9.

The result of the **generator losses L_C** (**capture losses**) means that only the **generator yield Y_A** (**array yield**) remains at the output of the solar generator.

$$Y_A = \frac{W_{DC}}{P_{STC}} \tag{9.14}$$

In the following inverter including cables there are also **system losses L_S** that finally lead to the **end yield Y_F** (**final yield**).

$$Y_F = \frac{W_{AC}}{P_{STC}} \tag{9.15}$$

Both the generator yield and the final yield are referenced to the STC power of the plant so that here, too, the result is the unit h.

> The **final yield Y_F** gives the **number of plant full load hours** per year.

Naturally, this quantity is the most important size for the owner of the photovoltaic plant as this is used to determine how much energy is fed into the public grid per year. Up to now we have also designated this as the specific annual yield w_{Year}.

9.3.2.2 Losses

How are these losses caused? There are many causes of **generator losses L_C**:

- The modules have less power than is stated in the data sheet
- The module temperature is higher than 25°C
- The modules are soiled or partly shaded
- There is a mismatch between modules of a string
- The modules are not being operated in MPP
- There are ohmic losses in the DC lines

The **system losses L_S** are primarily caused by the inverter:

- The efficiency of the inverter is less than 100%
- The inverter is under-dimensioned and limits the output power during high input power
- There are ohmic losses in the AC lines

9.3.2.3 Performance Ratio

If the desire is to determine the efficiency with which the photovoltaic plant handles the available radiation energy, then the **performance ratio PR** can be used as a measure. This compares the final yield with the reference yield:

$$PR = \frac{Y_F}{Y_R} \tag{9.16}$$

The **performance ratio** is typically **between 75 and 85%** and with very good plants it can even reach higher values.

Example 9.5   Yield and performance ratio of a 5 kWp plant

The annual radiation of a south-oriented roof with a pitch of 25° was 1100 kWh/m^2 in a year. The system installed there fed 4500 kW into the grid in the same year.

The reference yield is:

$$Y_R = \frac{H_G}{E_{\text{STC}}} = \frac{1100 \, \text{kWh}/(\text{m}^2 \cdot \text{a})}{1000 \, \text{W}/\text{m}^2} = 1100 \, \text{h}/\text{a}$$

The final yield is:

$$Y_F = \frac{W_{\text{AC}}}{P_{\text{STC}}} = \frac{4500 \, \text{kWh}/\text{a}}{5 \, \text{kWp}} = 900 \, \text{h}/\text{a}$$

The performance ratio is the quotient of the two results:

$$PR = \frac{Y_F}{Y_R} = \frac{900 \, \text{h}/\text{a}}{1100 \, \text{h}/\text{a}} = 81.8\% \approx 82\%$$
■

9.3.2.4 Concrete Measures for Monitoring

The minimum demands of power monitoring are the **acquisition of the radiation** and the **power fed into the grid**. Here Y_R and Y_F are known and the performance ratio as well as the total losses $L_{Tot} = L_C + L_S$ can be determined. However, proper information on improving the performance is obtained by means of a more accurate analysis. For this purpose, the data logger should **also log** the **energy W_{DC}** generated by the generator. The aim of this is to determine the generator and system losses and the logger can provide information on whether there is improvement potential on the DC or the generator side. In addition, in the case of a malfunction the error source can be quickly found. The **acquisition of the module temperature** also offers the possibility of dividing the generator losses into temperature-caused losses and other losses. In Section 9.4 we will look at simple monitoring results.

9.3.3 Visualization

A photovoltaic system installed on a roof is relatively unspectacular and can often not be seen, especially on office buildings. But some undertakings, especially public bodies, want to show off their dedication to photovoltaics. Here visualization the data can be used. The standard depiction is a **digital display** with kWh generated as well as the current plant power. More informative is the use of a **graphic display** that shows the daily or monthly yield as a bar diagram.

   In particular, **schools and kindergartens** like to show the power production in a way more appropriate for children. Unfortunately the normal displays of power and energy are **not very understandable** for children (and parents . . .). This has led the Münster UAS to develop the visualization unit VisiKid [119]. Figure 9.10 shows the inner structure of the prototype as well as a view of the licensed series device. The **power** of the photovoltaic plant is shown for children by the **number of** illuminated **bulbs**, which are in fact highly efficient LEDs. At the
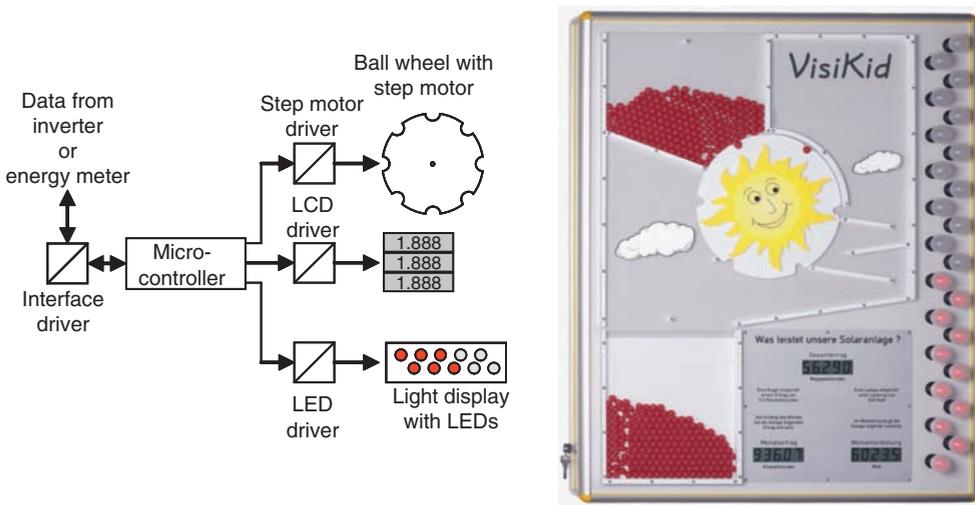
Figure 9.10 A child-centric visualization of a photovoltaic plant with Visikid: Left is the internal structure of the prototype developed by the Münster UAS; right is a view of the commercial series device (photo: IKS Photovoltaic GmbH)

same time the display of the **generated energy** is shown by means of **balls** that are moved by a ball wheel. Each ball deposited into the bottom container depicts a fed-in kWh. At the end of the calendar month the balls are poured back into the top container and the ball count starts at the beginning again. The number of devices sold so far shows that there is a considerable demand for this type of visualization.

9.4 Operating Results of Actual Installations

We will now look at the operating experiences of some photovoltaic plants.

9.4.1 Pitched Roof Installation from 1996

As a first example we will consider a 2 kW system that was installed in Aachen in 1996. Aachen was one of the first cities in Germany that paid cost-covering feed-in tariffs for photovoltaic plants. The tariff at that time was 2 DM (about 1 €) per kWh. Table 9.3 shows the most important data of the installation.

Figure 9.11 shows the final yield and the performance ratio of the installation in the course of the years. It is noticeable that in the first years there were relatively strong fluctuations in the yield. These were caused mainly by considerable **differences of the sun hours** of these years. A specialty was the year 2003 that in Aachen yielded an annual global radiation of 1200 kWh/(m^2·a). For the orientation of the modules this resulted in a reference yield Y_R of 1350 Sun full load hours. Also noticeable is the year 2001: In the summer of this year a **fuse** in the inverter line of an inverter **burned through**. The damage went unnoticed for two months and caused a **drastic reduction of the yield**.

Much more informative than the final yield is the course of the **performance ratio** that in most years was **between 70 and 75%**. Apparently we are dealing here with only a mediocre performing installation. The reasons here are two special aspects. On the one hand the type of inverter used, the Sunny Boy 700 is one that is superseded by today's standards. Its peak efficiency is only 93.4% and the European efficiency is a poor 92%. Moreover, the PV generator – as was normal at the time – was **clearly over-dimensioned**. Eighteen modules of 55 Wp were connected to an inverter with a maximum DC input power of 800 W. This corresponds to an over-dimensioning factor k_{Over} of 1.24 (see Section 7.2).

> In Figure 9.11 is seems as though the performance of the installation will continue to degrade. Is the reason for this a degradation of the modules?
> Degradation after so many years of operation cannot be excluded. However, module soiling can also be a reason as the installation was never cleaned.

Table 9.3 Data of the 2 kW plant in Aachen

Site, year of construction	Aachen, 1996	Power	1.98 kWp
Orientation	South	Solar modules	36 × Siemens SM 55
Module inclination	45 degrees	Inverters	2 × SMA Sunny Boy 700
Number of strings	4	Over-dimensioning factor k_{Over}	1.24
Length of string cable	12 m	Cross section of string cable	2.50 mm^2
Costs	15 000 DM/kWp	Feed-in tariff	2 DM/kWh

Figure 9.11 View and operating results of a 2 kW installation in Aachen: The poor yield in 2001 can be clearly seen and was caused by a burned-through fuse (photo: M. Pankert)

9.4.2 Pitched Roof Installation from 2002

As a comparison we will consider a 3.2 kWp installation that was installed in Steinfurt/ Münsterland in 2002 (Upper modules in Figure 6.32). Table 9.4 shows the data for this plant.

Table 9.4 Data of the 3.2 kW plant in Steinfurt

Site, year of construction	Steinfurt, 2002	Power	3.2 kWp
Orientation	South	Solar modules	$20 \times$ Isofoton I-159
Module inclination	48 degrees	Inverters	$1 \times$ SMA Sunny Boy 2500
Number of strings	1	Over-dimensioning factor k_{Over}	First 1.18, since 2007: 1.06
Length of string cable	14 m	Cross-section of string cable	6 mm^2
Costs	5200 €/kWp	Feed-in tariff	52.1 cents/kWh
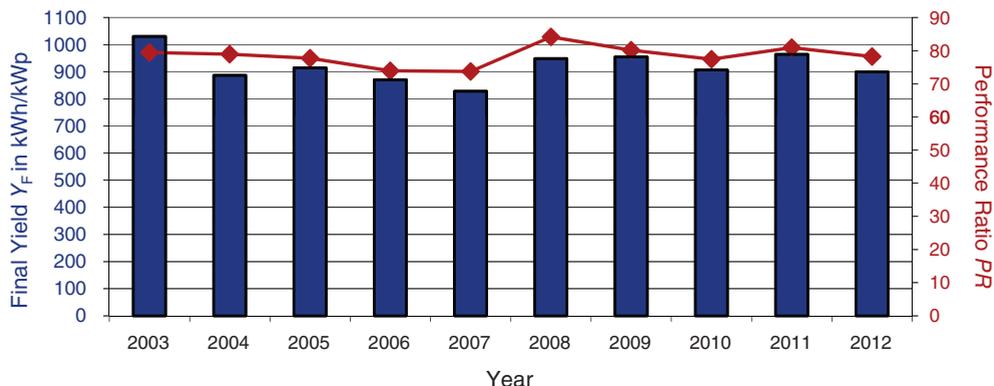
Figure 9.12 Operating results of the pitched roof plant in Steinfurt: In total the PR values were somewhat higher in comparison to Figure 9.11. The installation was optimized slightly in 2007 so that the performance improved further

Figure 9.12 shows the final yield and the performance ratio of the installation in the course of the years. In comparison with the installation in Aachen the **yield is somewhat better**. In the first years the performance ratio was an average of 4% above that of the other installation and in the last years this difference increased to about 8%. The reason was that in 2007 the installation was reduced by two modules and the over-dimensioning factor was reduced from 1.18 to 1.06.

9.4.3 Flat Roof from 2008

Finally we will consider a modern 25 kWp plant that was erected in 2008 on the flat roof of the Münster University of Applied Sciences (see Figure 6.30). Table 9.5 shows the data for this plant.

Figure 9.13 shows the results of this plant. It achieved on average a specific yield of a good 1000 kWh/kWp. The associated mean **performance ratio was 84%**. It shows that the use of a modern inverter without transformer and a lower over-dimensioning factor ($k_{Over} \approx 1$) can have clearly positive results!

Table 9.5 Data of the 25 kWp flat roof plant on the Münster UAS

Site, year of construction	Steinfurt, 2008	Power	24.84 kWp
Orientation	South	Solar modules	138 × Schüco S180-SP4
Module inclination	25 degrees	Inverters	2 × SMA Sunny Boy 9000 TL
			1 × SMA Sunny Boy 6000 TL
Number of strings	8	Over-dimensioning factor k_{Over}	0.99 and 1.05
Length of string cable	6 to 28 m	Cross section of string cable	6 mm^2
Costs	4496 €/kWp	Feed-in tariff	46.75 cents/kWh
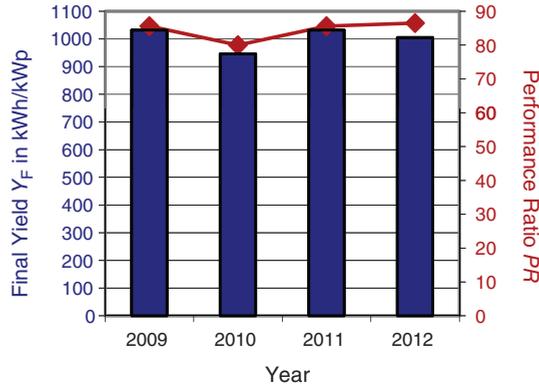
Figure 9.13 Results of a modern flat roof plant in Steinfurt: With the use of inverters without transformers and a low over-dimensioning factor there was a mean performance ratio of 84%

In all three installations it is noticeable that the performance ratio sinks from 2009 to 2010 and rises again in 2011. How can this be? In the calculation of the PR the influence of the annual radiation is calculated out.

In addition to the annual radiation there are also other influences to be taken into account. The temperature on the sunny days also plays a large role. Possibly this was higher in 2010 than in 2009. The year 2011, again, had a sunny but relatively cool spring.

10

Outlook

This chapter deals with the future of photovoltaics. First, we will look at the technical potentials of photovoltaics. How much of this can actually be put into practice depends on the scope of the finances. This leads to the question of what promotional instruments are best suited to achieving a further increase in market size and thus further lowering production costs. Finally, some thought should be given to how the future power supply will look with substantial participation of photovoltaics. For this purposes we will look at various scenarios.

10.1 Potential of Photovoltaics

In Chapter 2 we estimated the area necessary for covering the whole of **the primary energy needs of humanity** by means of photovoltaics. The result was the **Sahara miracle**: a **surface** area of only **800 km × 800 km** was required! As already mentioned, it makes no sense to concentrate the whole of the energy production at one site. Thus, we will limit the estimate of the potential to Germany.

10.1.1 Theoretical Potential

The theoretical potential is understood to be the whole of the radiation energy that reaches Germany in a year. In Chapter 2 we assumed an annual radiation of approximately $1000 \, kWh/m^2$. With a surface area of the Federal Republic of Germany of $357\,000 \, km^2$ we obtain a **theoretical potential** of $375{\cdot}10^{12} \, kWh$. This corresponds to about **100 times the overall primary energy requirement** of Germany!

10.1.2 Technically Useful Radiation Energy

Naturally, only a small part of this large amount is useful. On the one hand, the whole of Germany should not disappear under a sea of solar modules, and on the other hand, solar modules only convert a part of the irradiance into electrical power. Possible sites for solar systems are especially **roofs, façades and free areas** whose potential we will consider one after the other.

10.1.2.1 Roofs

According to [120], the **whole roof surface area** in Germany amounts to approximately **4345 M.m²** of which around 70% is pitched roofs and 30% is flat roofs. Of these, approximately 40% can be taken as being unsuitable for solar use [120] due to **building restrictions** (windows, chimneys and shading).

In the case of **pitched roofs** all those that have a maximum of 90° orientation turn to the south, meaning all roofs from east through south to west should be considered. Thus, only half the roof areas remain available. Also we want to reserve a third of the remaining surface area for **solar heat** so that there is an available **pitched roof surface area** A_{Pitch} for solar modules:

$$A_{\text{Pitch}} = 4345 \text{ M.m}^2 \cdot 0.7 \cdot 0.6 \cdot 0.5 \cdot 2/3 = 608 \text{ M.m}^2 \tag{10.1}$$

In the case of **flat roofs**, shading of the individual module rows must be prevented. We will therefore set the **area utilization factor** to 45% in accordance with Example 9.2. With the reduction for solar heat described above we will finally have available as usable **module area** A_{Flat} on flat roofs:

$$A_{\text{Flat}} = 4345 \text{ M.m}^2 \cdot 0.3 \cdot 0.6 \cdot 0.45 \cdot 2/3 = 235 \text{ M.m}^2 \tag{10.2}$$

In Chapter 2 we defined the annual radiation on a horizontal area in Germany has an average of 1000 kWh/(m²·a). In the case of optimum alignment (azimuth angle $\alpha = 0°$, inclination angle $\beta = 35°$) the global radiation is approx. 1200 kWh/(m²·a). The pitched roofs under consideration are angled from $\alpha = -90°$ to $+90°$ and we will assume a maximum inclination angle of $\beta = 60°$. According to Table 2.4, there are **inclination losses** of 0% to almost 30% so that we can set a mean of 15%. Finally, with Table 10.1 we obtain an overall **useable radiation energy** of **809 TWh/a**.

10.1.2.2 Façades

The **façade areas** of **6660 M.m²** available in Germany are much greater than the roof areas. However, relatively many areas fall away due to structural restrictions (extensions, doors, windows, shading, etc.). Further, we are only interested in façades with southeast to southwest orientations. If we reserve half the remaining area for solar heat usage then we are left with only approximately 200 M.m² (3% of all façade area) for photovoltaics. The vertical façades receive an average 850 kWh/(m²·a) of radiation energy so the total energy is **170 TWh/a**.

10.1.2.3 Traffic Routes

In Germany there are approximately **275 000 km** of regional **roads and rail routes**. For this reason it is also feasible to use them for photovoltaics. In [120] it is proposed to erect

Table 10.1 Usable radiation energy on suitable roof areas

Type of area	Useable area (M.m²)	Mean inclination losses (%)	Mean global radiation (reference yield) (kWh/(m²·a))	Overall useable radiation energy (TWh/a)
Pitched roof	608	15	1020	527
Flat roof	235	0	1200	282
Total	842	–	–	809

photovoltaic plants on both sides of almost 4% of these traffic routes. The idea is to use 2-m high **glass-glass modules** that permit radiation on both sides. Spread over all cardinal points, one can assume around 1250 kWh/(m² · a). With average losses (shading and soiling) of 15%, this provides a usable radiation energy of approximately **42 TWh/a**.

10.1.2.4 Free Areas

The largest potential is in the use of free areas. In [121], for instance, it is assumed that use is made of agricultural set-aside areas. However, since 2008 these have largely been used for planting biomass and are no longer available for photovoltaics. In 2010 in Germany approximately 18% of all arable areas were in use for renewable raw materials, which corresponds to an area of 21 500 M.m² [122]. We will assume that **1% of all arable areas** will be made available for photovoltaics. This would be an area of approximately 1200 M.m². With an area utilization ratio of 45% this gives a module area of 540 M.m² corresponding to a useable radiation energy of **648 TWh/a**.

10.1.3 Technical Electrical Energy Generation Potential

How much electrical energy can be obtained from the module areas in Section 10.1.2 depends to a great extent on the efficiency of the modules used. As we have seen from Chapter 5, standard solar modules are now available with an **efficiency** of almost **20%**. In the next 10 years this efficiency will continue to move upwards. Thus, we will easily achieve a **system efficiency** of **18%** (including the losses from inverter, cabling and deviations of module temperatures from STC conditions). The results are shown in Table 10.2.

We have an installable power of 325 GWp and 302 TWh/a of electrical energy from photovoltaics. This corresponds to **half** the current **German electrical energy consumption** of approximately 600 TWh/a! Even **without** taking the **free areas** into account we will still manage with a **portion of 31%**. Figure 10.1 shows the required module area as an amount of 0.3% of the total area of Germany. The areas taken into use are mainly on already available roofs and façades so that there is no competition for use.

Table 10.2 Photovoltaic energy generation potential in Germany with a module efficiency of 20% and a system efficiency of 18%

Type of area	Usable module area (M.m²)	Useable radiation energy (TWh/a)	Installed power ($\eta_{Mod} = 20\%$) (GWp)	Electrical energy ($\eta_{Sys} = 18\%$) (TWh/a)	Portion of energy requirement of 600 TWh/a (%)
Pitched roof	608	527	122	95	16
Flat roof	235	282	47	51	9
Façades	200	170	40	31	5
Traffic routes	38	42	8	8	1
Sub-total without free areas	1081	1021	217	183	31
Free areas	540	648	108	117	19
Total	1621	1669	325	302	50
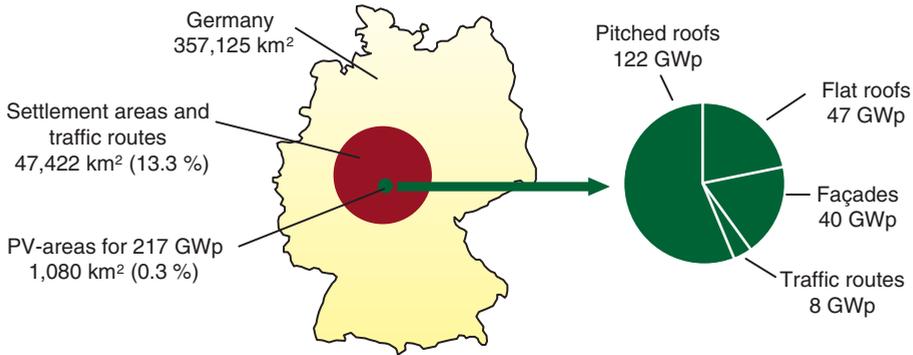
Figure 10.1 Surface area requirements for photovoltaics in Germany: A power of more than 200 GWp is available even without using free areas. The area required by this is not in competition with other types of utilization (e.g., biomass) [123]

10.1.4 Photovoltaics versus Biomass

If it is desired to generate much more electrical energy in the future (e.g., for electric cars or geothermal heat pumps for domestic heating), then free areas should also be used for photovoltaics. This represents an **area competition to biomass**. Therefore a comparison of the two technologies should be made:

A hectare of energy corn annually yields approximately 45 t of biomass (fresh mash), which again results in a biogas yield of 8000 m^3. With a methane portion of 52%, this corresponds to an energy of 41 600 kWh. If the biogas is used in a block power station ($\eta_{Elec} = 40\%$) then this provides electrical energy of almost **17 000 kWh/a** [124]. Per square meter of arable area we obtain an energy yield of $w_{Elec\_Bio} = 1.7\,\text{kWh/(m}^2 \cdot \text{a)}$. Compared with the solar radiation on a square meter of 1000 kWh/(m$^2 \cdot$ a) there is a **yield degree of efficiency** of only **0.17%**!

If we consider the photovoltaics, then in an open air plant ($\eta_{Mod} = 20\%$, area utilization factor $f_{Util} = 0.45$) we get an area-referenced annual yield of

$$w_{Elec\_PV} = f_{Util} \cdot \eta_{Mod} \cdot E_{STC} \cdot Y_F = 0.45 \cdot 0.2 \cdot \frac{1\,\text{kW}}{\text{m}^2} \cdot \frac{900\,\text{kWh}}{\text{kWp} \cdot \text{a}} = 81\,\frac{\text{kWh}}{\text{m}^2 \cdot \text{a}} \qquad (10.3)$$

The **yield efficiency of photovoltaics** is therefore **8.1%** and this gives a relationship to biomass use of 48:1. However, both heat and electricity are produced in a biomass block power station and that can also be used. On the other hand, the planting of corn requires energy for working the soil, transport, fertilizer, and so on that is not taken into account here.

> In comparison to photovoltaics, **biomass requires about 50 times the area** to generate the same electrical energy.

Up to now we have only considered the technical potential of photovoltaics. Whether this potential is actually realized in the erection of PV plants depends strongly on the legal and financial framework conditions. We will look at this more closely now.

10.2 Efficient Promotion Instruments

Germany already has a lot of experience with promotion programs for photovoltaics. At the start of the 1990s the **1000 Roofs Program** under the guidance of the Federal Ministry of Research commenced. This provided an investment subsidy for erection of on-grid plants amounting to 70% of the investment sum. The declared aim was the "Evaluation of the current state of the technology" and "Still needed development requirements" were to be determined [125]. Between 1991 and 1995 almost 2000 PV systems were erected within the framework of the program. Valuable operating experience was gathered with the use of a parallel measuring and evaluation program. The interaction of inverters with the power grid was investigated in particular, as there were originally great doubts from public utilities regarding safety. After the money pot was emptied the short-term market that had developed, collapsed.

The availability of the **high investment subsidy** of 70% led to a **flood of applications**. Apparently the prospect of **state money**, "cash on the barrelhead," is a high motivator. At the same time the plant operators hardly took notice of the high installation costs, the **plant prices** were mostly very near the prescribed upper limit of 28 000 DM/kWp. The evaluation of the program also showed that many plants became defective (especially the inverters) after one or two years. Often, however, they were not repaired as there was no financial support for repairs. In the following years some of the Federal States had further promotion programs based on investment subsidies. But no permanent market developed, as these were quickly over-subscribed, depending on the sums available.

Only after the development of cost-covering feed-in tariffs by various city departments (**Aachen Model**) and finally the start of the EEG in 2000 the situation did change. From the start, the EEG was conceived as a **market introduction program** and was meant to lead to a price reduction caused by mass production of PV plants.

What are the **important advantages** of this model in comparison to the promotion over investment subsidies?

1. As the money for feed-in compensation by the EEG levy is made by the electricity customers there are **no cyclically empty funding pots** as are typical with public investment programs. In this way the market is stabilized and **investment willingness** of the manufacturers is increased.
2. The **plant operator** only obtains a profit on his invested capital when he **works economically**. Thus he is obliged to purchase technically mature and also economic technology. Besides this he will repair the plant in his own interest and operate it as long as possible.
3. With the determination of a **reduction of the feed-in tariff** depending on the year of installation of the plant, the price and also the **market volume**, can be **controlled** to a certain extent.

The unplanned lowering of the tariff in Germany in recent years had the object of preventing the market from **overheating** and at the same time making further growth possible. Unfortunately, other countries such as Spain and Italy were not so consistent in this. In these countries too high feed-in tariffs were paid, which led to a cap of the promotable PV power and to a collapse of the respective markets. Yet, the aim of the reduction of costs due to mass production especially by the EEG (and the introduction of the concept in other countries) has been impressively reached as we will see in the next section.

10.3 Price Development

Figure 10.2 shows the **price development** for solar modules over the **past 30 years**. The prices have fallen drastically to approximately 70 cents; a **35th of the original value**. This corresponds to an average price fall of a good 10% per year! The curve shows some waves that were mainly caused by the temporary shortage of solar silicon.

A deeper understanding of the price development is given by the **learning curve theory**. It assumes that the production costs of a product (e.g., computers or solar modules) are continuously reduced with mass production. This is because the pressure of the competition causes production to become ever more efficient and that new technologies are introduced. The strength of the cost reduction is given by the **learning rate**:

> The **learning rate** is the percentage by which the costs of a product are reduced with a doubling of the quantity produced (accumulated).

A learning rate of 10%, for instance, means that the cost of the product is reduced by 10% with a doubling of the accumulated produced quantity. Figure 10.3 shows the price
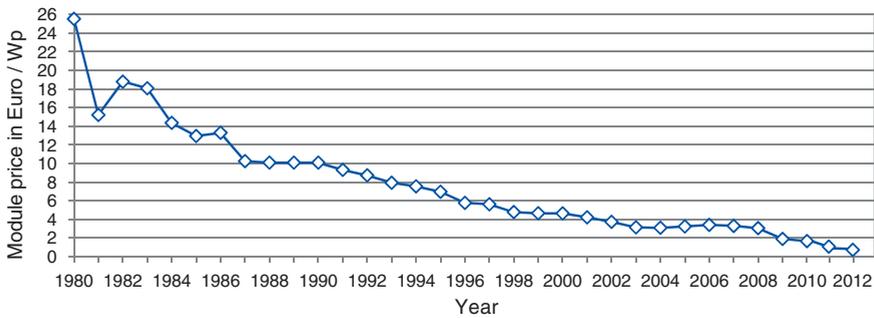
Figure 10.2 Price development of photovoltaic modules (inflation-weighted wholesale prices): Since 1980 the price has fallen to a 35th [126,127]
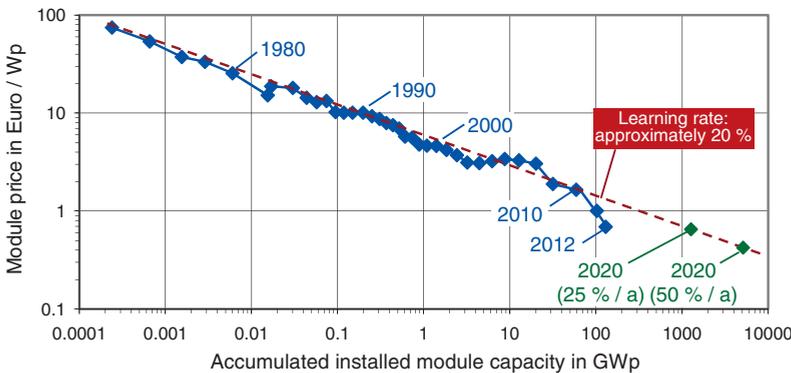
Figure 10.3 Module price development in doubled logarithmic depiction: For a doubling of the accumulated installed PV capacity there is a price reduction of approximately 20% [126,127]

development from Figure 10.2 in a doubled logarithmic form. The *x*-axis describes the accumulated installed solar module power and the *y* axis the price per Wp. Obviously one can average the price development in this form of depiction as a straight line. The slope of the straight line shows that the **learning rate of the solar modules is approximately 20%**.

What will the price look like **in the year 2020?** This depends on what the future growth will look like. From Figure 1.15 we can see that the PV world market has grown by more than 50% annually since 2000. If we extrapolate this growth to 2020 then we will have an installed PV capacity of about 4700 GWp. The price can then be expected to be approximately 42 cents. If the growth is only 25% then by 2020 we will land at a price of approximately 64 cents (Figure 10.3). It is important to note that the x-axis in Figure 10.3 is not a time axis. The learning curve will only continue when the market (e.g., due to suitable framework conditions) continues to grow.

Figure 10.3 shows a clear downwards dip of the price curve for the two years 2011 and 2012. This was triggered by the extreme price pressure by Asiatic producers. In the long run, though, it is to be expected that the price curve will again approximate the dashed straight line.

In this connection there is often talk of *grid parity*. This is the point in time at which the electric energy from a PV plant is cheaper than the normal price of electricity for the end user. Occasionally the opinion is expressed that no more feed-in compensation will be necessary from this point. This, however, does not take into account that the installation of a plant is only worthwhile for the customer when they can use the whole of the PV plant energy for themselves. But this is seldom the case (especially for larger plants). For this reason a certain form of **feed-in compensation will continue to be necessary**. Only in this way a stable market will be achieved that will lead to further cost reductions.

10.4   Thoughts on Future Energy Supply

What will the renewable energies in future contribute to energy supply and what will be the role of photovoltaics? This will be discussed in greater detail next. But first we will look at the present development.

10.4.1   Current Development in Renewable Energies

Figure 10.4 shows the **contribution of renewable energies** to the power supply in Germany over the past 20 years. In addition to the classical hydropower, wind power and biomass have also made great strides. In recent years photovoltaics with growth rates of more than 50% have also made much progress. In **2012** the renewable energies generated 135 TWh of electrical power, which corresponds to about **25% of German energy requirements**.

10.4.2   Consideration of Future Scenarios

How will this development continue? "Forecasts are difficult especially when they concern the future" – this fine sentence attributed to Mark Twain also applies to an accurate forecast of the energy mix of the future. There are many prognoses that concern the conversion of the current energy supply. Depending on the assumptions, the politically views and one's own economic relationship to the subject of the energy economy, one obtains very different results.

We will first look at the forecasts of the experts committee for environmental questions (SRU). The SRU is a committee of scientists that advises the German government.
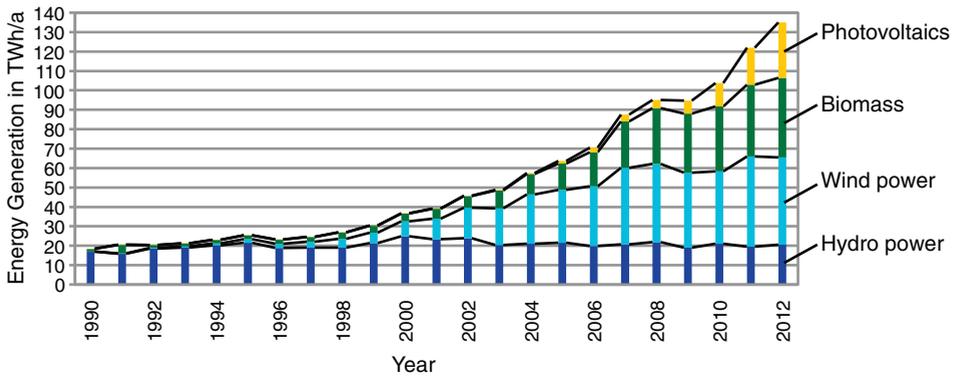
Figure 10.4 Development of renewable energies in Germany since 1990: In 2012 the contribution of energy generation was already more than 135 TWh/a, which corresponded to approximately 25% of the overall electricity demand [128]

A report presented at the start of 2011, discussed ways of achieving a 100% power supply with renewable energy.

In a **first scenario**, the scientists assumed that the German gross power consumption of 600 TWh/a today can be reduced to 450 TWh/a in 2050 by means of energy efficiency measures. At the same time it is assumed that by then **half of the road traffic** will be powered by means of **electricity** and therefore there will be an **overall energy consumption of approximately 500 TWh/a**. Figure 10.5 shows the assumed development up to the full supply with renewable energies in 2050. By far the largest portion will be borne by wind turbine plants; the contribution by off-shore wind generation alone is estimated to be 60%, whereas photovoltaics are only allocated 8%. This corresponds only to an installed capacity of approximately 40 GWp. In fact this value is thought to be reached by 2014.

A **further scenario** of the SRU assumes that all road traffic is converted to electric vehicles. In addition heat pumps are to be supplied from the electric grid in order to use geothermal energy for domestic heating. The result is an increased **power consumption of 700 TWh/a** in 2050. The energy mix is shown in Figure 10.6(b): here PV contributes 16%, for which approximately 110 GWp of installed capacity is necessary.
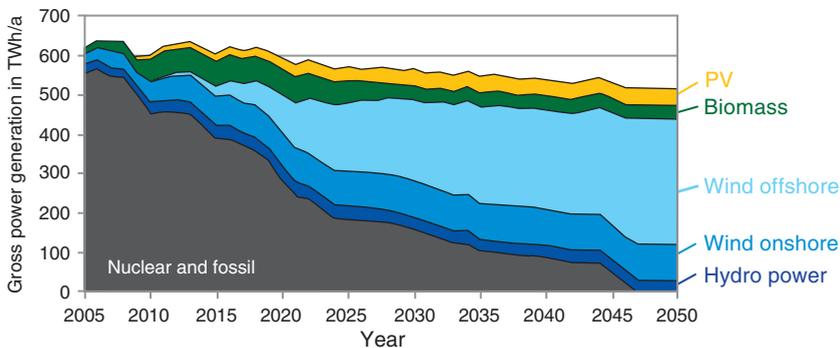
Figure 10.5 Conversion of the power supply to renewable energies up to 2050: In this scenario only a minimum part is covered by photovoltaics [129]
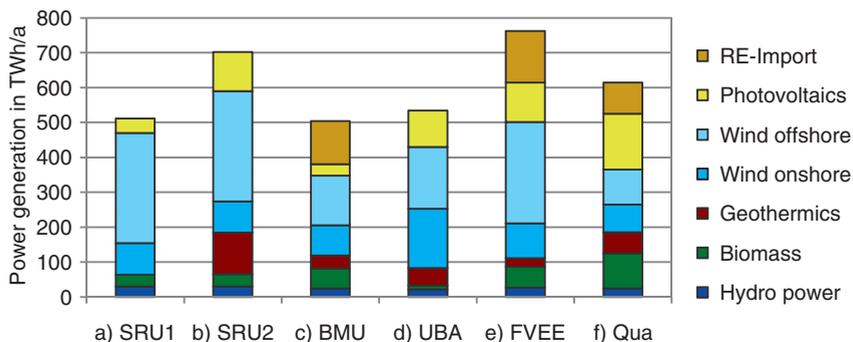
Figure 10.6 Results of various studies of the energy mix in 2050: The portion of photovoltaics is judged very differently [123,129–132]

Similar differences are shown in further studies; the scope ranges from 34 GWp in the somewhat earlier study of the Federal Ministry of Environment [130] up to 160 GWp for Quaschning [123]. The individual studies with authors and titles can be found in the References at the end of this book.

> Which of the studies would be most likely to foresee the future development correctly?

> Of course this cannot be generally answered. In fact all the studies of the past years have underestimated the actual development of photovoltaics. If photovoltaics continues to climb up the learning curve it could in the future take over 30% of energy generation.

The **import of renewable power** assumed in some studies is based on solar power stations (solar heat and photovoltaic) as well as wind turbines being erected in North Africa. The power generated is then transported by means of low-loss **HVDCT** (**High-voltage direct current transmission**) to Central Europe. This is basically a feasible option but up to now it is unclear whether it would be cheaper than generating on one's own soil. For reasons of **supply security**, this imported power should be limited to a **portion of 15%**.

10.4.3 Options for Storing Electrical Energy

As especially wind turbines and photovoltaics are very fluctuating power sources, it is necessary to develop possibilities of storing electrical energy. Various technologies can be used for this.

10.4.3.1 Pumped-storage Hydro Power Stations

Pumped-storage hydroelectric power stations use surplus energy to pump water into a high-lying dam. This can then be used to cover consumption peaks. The **storage efficiency** is relatively high at 80%. However, in Germany there are **hardly** any sites at which new

constructions would be possible. An **alternative** is to convert existing hydroelectric plants in the **Scandinavian** countries into pumped-storage hydroelectric dams [129].

10.4.3.2 Battery Storage

The storage of electrical power in batteries is feasible. Large technical batteries, for instance, **sodium-sulfur (NaS)** that are produced by the Japanese NGK Company are available and, according to the manufacturer's information, have an overall efficiency of 75%. In a pilot project, a 248 MWh storage of NaS batteries was installed in order to provide intermediate storage for a 51 MW wind park [133]. Also conceivable is **decentralized storage** of power **in households**; especially the combination described in Chapter 7 of **PV plant and battery storage**.

Besides increasing the own-use portion, these systems can also contribute to **grid relief**.

As an example, Figure 10.7 shows in the top diagram the real generating and consumption values of a four-person household with a 6.5 kW PV plant on a sunny day. The fluctuations of the grid exchange capacity in both directions are clearly seen. This is primarily due to switching on and off of heavy users (e.g., a stove) in the household.

The lower diagram shows the same load profile but with the use of an energy management system including storage (5.5 kWh capacity). In this case grid relief was expressly aimed at by means of **peak-shaving**. This means that occurring generating peaks are used for charging the storage and thus a defined feed-in power is not exceeded. In the reverse case the **"intelligent storage"** limits the power consumption from the grid in that it makes additional power available in times of consumption peaks.

Besides the stationary storage in buildings, **further battery storage** will become available through the future utilization of **electric vehicles**. If one integrates these into the intelligent energy management system, then the capacity and performance of the whole system can be much enhanced [134].

10.4.3.3 Compressed Air Storage

In **CAES plants** (**Compressed Air Energy Storage**), electrically driven pumps are used to pump air into underground caverns. This compressed air can then be used to drive gas turbines for generating electricity. Concretely, the air replaces the compression stage during which normally two-thirds of the losses of a gas turbine occur. However, there are substantial losses in the storage of air: when compressing in the underground cavern the air heats strongly and must be cooled. For this reason the **overall efficiency is a maximum of 55%**. At present new methods are being tested (**AA-CAES – Advanced Adiabatic Compressed Air Energy Storage**), in which the heat generated during compression is stored temporarily in a special heat storage. When discharging, this heats the air again so that an **overall efficiency of 70%** is possible [135].

10.4.3.4 Hydrogen as Storage

Hydrogen has long been mentioned as a possible storage carrier for renewable energies management. In fact it can easily be separated by means of electrolysis and then converted again by means of a fuel cell. The **overall efficiency is 44%** [129]. However, there is **no hydrogen infrastructure** (lines, storage, fuel cells, etc.) and these would have to be completely built up. For this reason one can assume that the methanizing of hydrogen will be used to begin with.
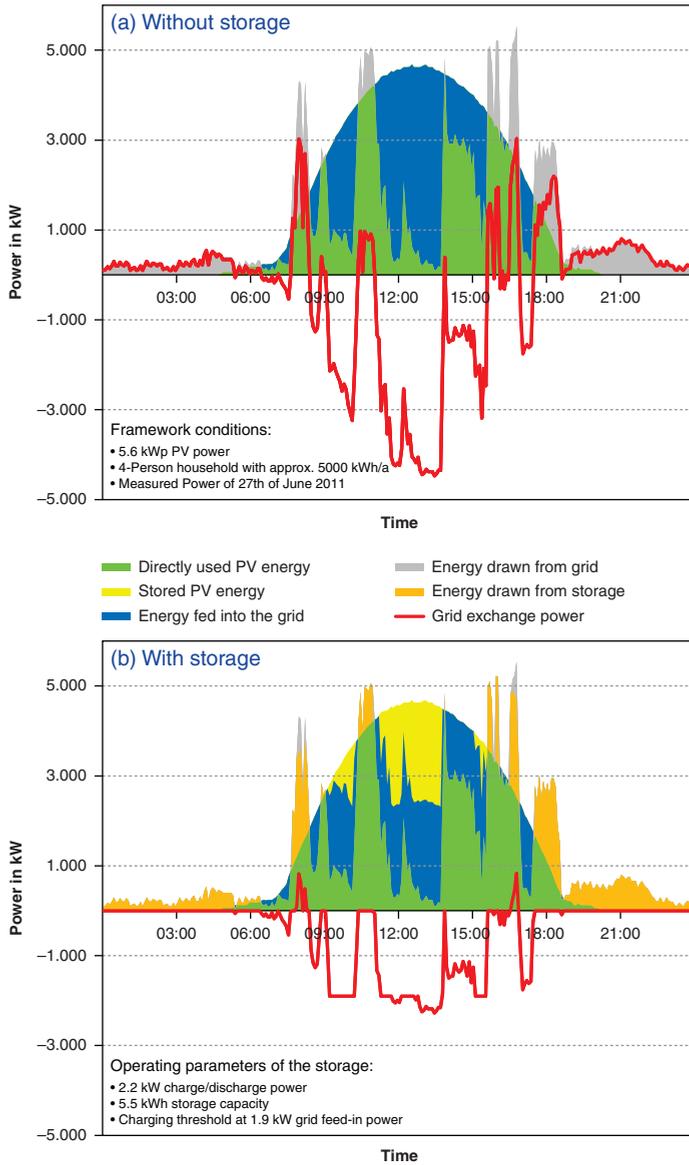
Figure 10.7 Peak-shaving using an intelligent storage: The high grid exchange power in the upper diagram is much reduced by the energy management system including battery as shown in the lower diagram (Source: Solar Technology AG)

10.4.3.5 Methanizing

A relatively new technology is the methanizing of electrical energy. For this purpose, use is made of **surplus wind** or **photovoltaic** power to **generate hydrogen** by means of electrolysis. This is converted to methane in a second step by the addition of carbon dioxide (see
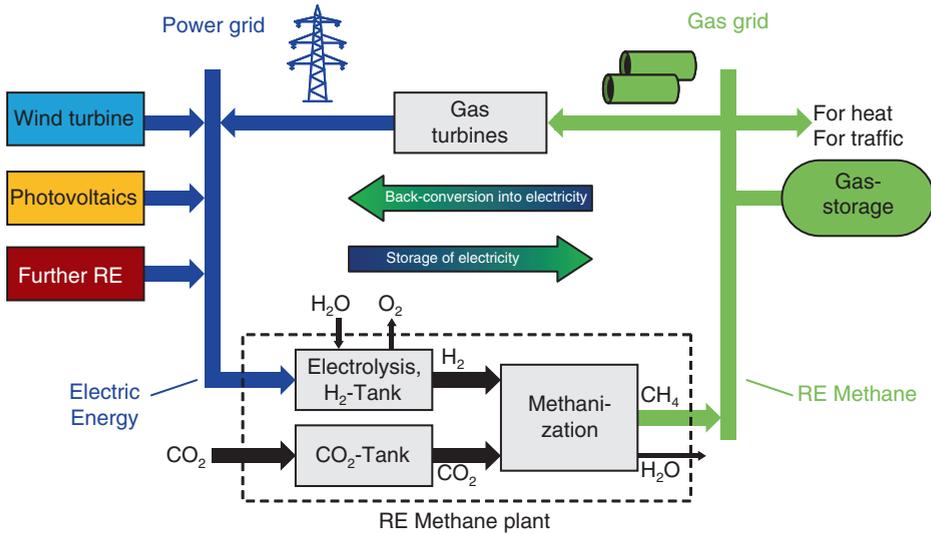
Figure 10.8 Power storage in RE methane: Surplus wind and PV power is methanized and fed into the gas grid. Then the RE methane can be re-electrified in gas turbines or used for heating and traffic purposes [136]

Figure 10.8). The generated **RE methane (Renewable Energy methane)** can then be used as normal natural gas. In order to re-convert the methane to electric power, it is fed into a gas turbine (block power station, gas power station or gas and steam power station). A decisive **advantage** is the **existing gas network** that can be seen as a **giant storage**. The storage capacity of the electrical energy is estimated to be approximately 120 TWh so that with the typical load of the German power grid of 70 GW even **seasonal storage** could be realized.

The **overall efficiency** starting from renewable electrical energy to the generated methane up to the re-electrification is **almost 40%**. This is somewhat lower than in the case of hydrogen generation as losses occur in the methanizing step. The largest realized system in Germany so far is a 6 MW plant. It was completed in 2013 and will produce about 1.4 M.m^3 renewable methane.

Besides the high storage capacity, the **Power-to-gas** systems have the advantage that use can be made of the existing infrastructure and the RE methane can also be used by other consumers (gas heating, gas-driven vehicles, etc.).

10.4.4 Requirements of the Grids

The requirements on the electric supply grid rise with the conversion of the energy system. Thus, for instance, **fast and controllable gas power stations** must be available in order to equalize the fluctuating supply of energy. At the same time a substantial **increase of the transport grids** is planned in order to distribute the large energy quantities of offshore wind turbines throughout Germany. Here, however, it should be weighed up as to whether the increased application of photovoltaics and the expansion of onshore wind turbines can be of greater assistance. In the first case the energy is generated near the consumer and need not be transported over great distances.

Besides the generator side there are also possibilities for optimization on the consumer side. The use of **smart grids** that influence the load curve is one of these. Thus, some consumers (e.g., air conditioning plants, heat pumps) can be uncoupled from the grid for a certain period without this leading to an impairment of the user. Other attempts would be the use of **different power tariffs** in order to run the washing machine for example, when there is a surplus of electricity.

In this way smart grids assist in adapting the load curve on the energy supply and in reducing the size of the necessary storages.

10.5   Conclusion

To conclude we can state that **photovoltaics** have **sufficient potential** in Germany for covering the overall electric energy requirements.

However, **Germany** is a relatively densely populated country with **limited free areas** and only a fair amount of solar offering. Thus, in most **other countries** there is even **greater potential** for solar power generation.

At the same time the mass production of photovoltaic components reduces costs further so that they approach those of other generating technologies. In this way photovoltaics can become an **important pillar** for the **future sustainable energy supply**. The building up of this new energy system is a **huge challenge** that we should meet with knowledge, imagination and perseverance. If this book makes a contribution to this it will have fulfilled its purpose.

11

Exercises

Exercises for Chapter 1

Exercise 1.1   Energy Content
You have a kilogram of coal available.

   a. How much energy content does it contain in J and kWh?
   b. How high could you theoretically lift 1 litre of water with this energy?
   c. To what speed (in km/h) could you theoretically accelerate a car (mass: 1 t) with this energy?

Exercise 1.2   Environmental Effects of the Present Energy Supply

   a. What are the main problems with the present energy supply?
   b. What is the mean temperature on Earth today and what could it be without the greenhouse effect?
   c. Explain the greenhouse effect in terms of key words and a sketch.

Exercise 1.3   Finiteness of Resources

   a. Assume every person has the present primary energy requirements of a person in Germany. For how many people would the present world primary energy consumption last?
   b. On the basis of Table 1.3, the scope of oil, natural gas and coal with varying annual growths p are to be estimated starting from 2008. Derive a general equation $scope = f$ *(annual extraction, reserves, p)*. Use the equation of the geometrical series (see Chapter 9, Equations 9.10 and 9.11.
   c. Calculate the scope of oil, natural gas and coal for an annual growth p of 2.2%.
   d. Calculate the scope of oil, natural gas and coal for an annual growth p of 4.4%.

Exercise 1.4   Properties of Renewable Energies

   a. What are the three primary sources of renewable energies?
   b. Name three advantages and three disadvantages of renewable energies.

Exercise 1.5 Yields of a Photovoltaic Plant

a. What is meant by STC and what boundary conditions are associated with it?
b. Family Meyer consumes 3500 kWh of electricity in a year. What should be the minimum power of a photovoltaic plant in order to generate this amount of energy?
c. What module area is required when the modules have an efficiency of 15%?

Exercises for Chapter 2

Exercise 2.1 Solar Constants

a. The Earth does not circle the Sun in an ideal circle but rather along an elliptical path $r_{SE\_Max} = 152$ M.km, $r_{SE\_Min} = 147$ M.km). Between what values does the solar constant fluctuate in the course of a year?
b. What solar constant do you expect from Mars that is approximately 58 M.km from Earth?

Exercise 2.2 Solar Spectrum

a. What does AM 0 stand for?
b. What does AM 1.5 mean and what solar elevation angle is associated with it?
c. Why is the sky blue?
d. What causes sunset glow?

Exercise 2.3 Global Radiation

a. What effects lead to the existence of diffuse radiation?
b. What approximately portion of the global radiation does the diffuse radiation in Germany have?
c. What is meant by "Sun full load hours" and what rule of thumb could one use for Germany?
d. How does the value of the previous sub-point change for a surface facing south and tilted at an angle of 35°?

Exercise 2.4 Radiation on Tilted Surfaces

On a cloudless summer's day, the measured global radiation is $E_{G\_Hor} = 850$ W/m². The Sun is at an angle of 50° to the horizon. Assume that there is no diffuse radiation.

a. What is the optimum inclination angle of the solar module and what is the irradiance E_{Gen} in this case?
b. What is the irradiance for a inclination angle of the solar module of 15° to the horizon?
Now take a winter's day: $E_{Direct\_H} = E_{Diffus\_H} = 300$ W/m². The sun is at an angle of 25° to the horizon.
c. What is the optimum inclination angle of the solar module and what is the irradiance in this case?
Determine the best angle by trial and error.

d. Solve the sub-point (c) not by trial and error but by means of an extreme value consideration of the equation $E_{\text{Gen}} = f(\beta)$. Make use of the following addition theorem:

$$\cos(x_1 + x_2) = \cos(x_1) \cdot \cos(x_2) - \sin(x_1) \cdot \sin(x_2)$$

Exercises for Chapter 3

Exercise 3.1   Charge Carriers in Semiconductors

a. Calculate the intrinsic carrier concentration of silicon at $100\,°C$.
b. Explain the difference between field current and diffusion current.

Exercise 3.2   p-n Junction

a. Describe the origin of the space charge region in the p-n junction.
b. Sketch the band diagram of a p-n junction in a qualitative manner.
c. Calculate the diffusion voltage of a pn junction of silicon at the following doping concentrations: $N_A = 5 \cdot 10^{16}/\text{cm}^3$, $N_D = 10^{18}/\text{cm}^3$.

Exercise 3.3   Light Absorption in Semiconductors

a. Verify the interconnection between the absorption coefficient and the penetration depth of light in a semiconductor (Equation 3.21). For this use suitable values in Equation 3.20.
b. What is the photon energy of light at the wavelength $\lambda = 560\,\text{nm}$?
c. What is the penetration depth of light at the wavelength $\lambda = 560\,\text{nm}$ in c-Si and a-Si?

Exercise 3.4   Anti-Reflection Films
Light with a wavelength of 600 nm and an irradiance of $E_0 = 500\,\text{W/m}^2$ impinges vertically on to a semiconductor of amorphous silicon. At this wavelength the material has a refractive index of 4.6.

a. What portion of the light is reflected at the semiconductor surface?
b. What thickness and what refractive index should an anti-reflective film possess in an ideal case?
c. In an actual case silicon nitride (Si_3N_4) is used as an anti-reflective film. What should the thickness of the film be in this case and how large is the remaining reflection factor?

Exercises for Chapter 4

Exercise 4.1   Recombination in the c-Si Solar Cell

a. What types of recombination do you know?
b. What is understood by the term "dead layer" in a cell?
c. A light photon is absorbed at a depth of $140\,\mu\text{m}$ and generates an electron-hole pair. The average carrier life span is $7\,\mu\text{s}$. Will the generated electron probably contribute to the photocurrent?

Exercise 4.2 Absorption Efficiency of a c-Si Cell

Given is a c-Si cell of thickness $d = 140\,\mu m$ that is illuminated by light with a strength of $E_0 = 1000\,W/m^2$, ($\alpha = 100/cm$; $n = 3.3$; $\lambda = 1000\,nm$).

a. How large is the penetration depth of the light?
b. How much light is reflected?
c. How much light is absorbed (assumption: rear side nonreflecting)?
d. How much light is absorbed when the rear side is mirrored and the front side is nonreflecting?
e. How big in the previous sub-point are absorption efficiency and the spectral sensitivity if one assumes that every electron-hole pair contributes to the photocurrent?

Exercise 4.3 Single Diode Equivalent Circuit Diagram

a. Sketch the single-diode equivalent circuit diagram and derive the characteristic curve equation.
b. What losses are incurred by the series resistance R_S and what by the parallel resistance R_{Sh}?
c. Sketch the characteristic curve of a solar cell for a rising series resistance R_S and explain the sequence for V_{OC} und I_{SC}.
d. Sketch the characteristic curve of a solar cell for a falling shunt resistance R_{Sh} and explain the sequence for V_{OC} and I_{SC}.

Exercise 4.4 Spectral and Theoretical Efficiency

a. What does the term "spectral efficiency" mean and what effects lead to the fact that it is not 100%?
b. What further losses does the "theoretical efficiency" take into account?
c. How large is the theoretic efficiency of c-Si cells and how near have we come to this optimum?

Exercise 4.5 Spectral Efficiency of Monochromatic Light

Assume we wish to convert monochromatic laser light into electrical energy as efficiently as possible. We select $\lambda = 1000\,nm$ as laser wavelength and the further data are: $E = 1000\,W/m^2$, $A_{Cell} = 10\,cm^2$, $m = 1$).

a. How large is the number N_{Ph} of photons per second that impinge on the cell and the maximum current density j_{Max}?
b. Determine the open circuit voltage of the cell.
c. Give the idealized fill factor of the cell.
d. How great is the theoretical efficiency of the cell?
e. Answer the previous question for a concentration factor of $X = 1000$.

Exercises for Chapter 5

Exercise 5.1   Production of c-Si Solar Cells

a. What do the following abbreviations mean: SG-Si, MG-Si, UMG-Si, CZ-Si, FZ-Si, EFG?
b. List the seven main steps for producing a c-Si standard cell starting from the p-doped wafer.

Exercise 5.2   a-Si Thin Film Cells

a. What is the basic difference between drift cells and diffusion cells?
b. Sketch the structure of an a-Si tandem cell with information on the materials and describe its function.
c. What is the Staebler–Wronski effect and how can it be moderated?

Exercise 5.3   CIS Cells

a. Sketch the structure of a CIS cell
b. What two functions does the CdS layer perform?
c. Explain the difference between superstrate configuration and substrate configuration in a thin film cell.

Exercise 5.4   Concentrator Systems

a. Sketch the two most important principles of concentrator systems.
b. Explain why an increased irradiance leads to an increase in the efficiency of a solar cell.
c. Describe a solar cell with the following data: $V_{OC} = 600\,mV; m = 1.5; \eta = 18\%$. What is the efficiency with the following concentration factors:
   i. $X_1 = 100$
   ii. $X_2 = 400$
d. Why does the efficiency not continue to increase with an increase of factor X?

Exercise 5.5   Ecology Questions

a. How do you judge the availability for cells of c-Si, CdTe and CIS?
b. An energy demand of 5500 kWh/kWp was required for the production of a complete PV plant. Calculate the energy amortization time T_A and the energy returned on the energy invested ERoEI:
   i. On a south facing roof (35° pitch) in Germany.
   ii. On a west facing roof (35° pitch) in Germany.

Exercises for Chapter 6

Exercise 6.1   Short Circuit Current and Open Circuit Voltage for a Variation of the Irradiance

A solar module with the data $V_{OC} = 43.2$ V, $I_{SC} = 10$ A is given. The installed cells have an ideality factor of $m = 1.5$.

  a. How many cells are probably built into the module?
  b. What short circuit current will adjust itself with an irradiance E' of $500 \, \text{W/m}^2$?
  c. What open circuit voltage will adjust itself with an irradiance E' of $500 \, \text{W/m}^2$?

Exercise 6.2   Series Connection of Modules

  a. Give two reasons for the use of bypass diodes.
  b. Now two modules of the type from Exercise 6.1 are connected in series. Module A is radiated with $1000 \, \text{W/m}^2$ and module B with $500 \, \text{W/m}^2$. Sketch the individual curves and the combined curve for the cases:
   i. The modules have no bypass diodes.
   ii. Both modules have at least one bypass diode.

Exercise 6.3   NOCT

  a. What is the meaning of NOCT and what boundary conditions are associated with it?
  b. What will be the temperature and module power of the FS-380 module from First Solar (see Table 6.1) at $900 \, \text{W/m}^2$ and an ambient temperature of $30 \, °\text{C}$?

Exercise 6.4   Mismatching

  a. What is understood by mismatching?
  b. On the basis of the generator I/V curves, explain: why, in the case of shading of a module it is particularly disadvantageous to connect the modules into two instead of one string?

Exercises for Chapter 7

Exercise 7.1   Buck Converter

  a. Sketch the circuit of a buck converter and explain the functions of the individual components.
  b. What are the advantages of a high switching frequency?
  c. What could be a disadvantage of a high switching frequency?

Exercise 7.2   Feed-in Variations

Sketch the two feed-in variations *full feed-in* and *feed-in with self-consumption* of a photovoltaic plant.

Exercise 7.3   Inverter Variations

    a. Give the advantages and disadvantages of the plant variations with central inverter, string inverter and module-integrated inverter.
    b. What is the advantage of a PWM bridge compared to a classic 50 Hz bridge?
    c. In what cases should inverters without transformers not be installed without investigation?
    d. Why inverters with high-frequency transformers are used?
    e. Give three advantages of the three-phase inverter.

Exercise 7.4   Inverter Dimensioning

Assume that you have an inverter SMC 8000 TL from SMA available and wish to drive as many modules of type c-Si M-200 from Bosch Solar with it.

    a. Determine the maximum possible number of modules per string.
    b. Determine the minimum possible number of modules per string.
    c. Determine the maximum possible number of strings.
    d. Determine the optimum plant configuration.

Exercise 7.5   Battery Systems

    a. Why does deep discharge reduce the life of lead batteries?
    b. Why is a car battery not suitable for an off-grid solar plant?
    c. In the data sheet of a battery the capacity of $C_{10} = 150$ Ah is given. What does this mean and how long do you estimate the battery can be discharged with a current of 20 A?
    d. What is understood by the I/V charging method?
    e. Give two advantages of the shunt charge controller compared to the series controller.

Exercise 7.6   Off-grid Systems

    a. What does a typical solar home system look like?
    b. What is understood by a hybrid system and what are the advantages compared to pure solar off-grid systems?

Exercises for Chapter 8

Exercise 8.1   Radiation Sensors

    a. What are the best class of pyranometers called and what is their accuracy?
    b. What two possibilities do you know in order to measure only diffuse radiation?
    c. Can a pyranometer be used as a reference sensor in a module flasher?

Exercise 8.2   Peak Power Measurement at Site

Sketch the structure of a characteristic curve measuring device for peak power determination with all relevant components.

Exercise 8.3 Thermographic Measuring Technology

a. In module checking what is the suitability of bright thermography and what of dark thermography?
b. In a temperature measurement of a solar module, the thermographic camera shows a value of 51 °C. However, in error you have set the emission factor of the camera at 0.9 instead of 0.8. What is the actual temperature of the module?

Exercise 8.4 Electroluminescence Measuring Technology

a. Why is a normal CCD camera unsuitable for EL measurements of c-Si modules?
b. What types of cell errors can hardly be recognized in the thermography measurement but readily in the EL measurement?

Exercises for Chapter 9

Exercise 9.1 Shading

An aerial tube of 5 cm in diameter is situated at a distance of 2 m from a photovoltaic plant.

a. Does the tube throw a deep shade on the plant?
b. How broad is the deep shade?
c. Assume the deep shading is unavoidable. Would you install the module rather vertically or horizontally?

Exercise 9.2 Yield Estimation

Farmer Jones would like to build a 30 kWp installation on a new barn in Attendorn, Sauerland, Germany. The roof has an orientation of 45° and a pitch of 12°. Determine the expected specific annual yield (final yield Y_F) in accordance with the following methods:

a. Use of the suitable fixed value for Germany of 900 kWh/(kWp · a) for optimum alignment and subsequent inclination loss reduction according to Table 2.4.
b. The fixed value in (a) is valid for a global radiation total H of 1000 kWh/(m² a). Take into account the approximate value for H' at Attendorn according to Figure 2.7 (about midway between Dortmund and Siegen).
c. Determine H'' at Attendorn using the PVGIS Internet database (see Table 9.2) and calculate analogously to the previous sub-point. Method: use the Internet address http://re.jrc.ec.europa.eu/pvgis/, *Interactive Maps*, *Europe*, enter the site, type in a location and press *Search*, Select menu *Monthly radiation*, Radiation database: *Climate-SAF PVGIS*, tick *Horizontal radiation*, press *Calculate*.
d. Determine Y_F''' at site Attendorn via the PVGIS Internet database in that you press Menu *PV estimation*, then *Climate-SAF PVGIS* Radiation database, enter slope and azimuth, leave all other values and then press *Calculate*.

Exercise 9.3   Return Calculation

Farmer Jones of Exercise 9.2 purchases his plant for 60 000 € net. The feed-in tariff is 28.7 cents. As an expected annual yield we use the results of Exercise 9.2d.

  a. Calculate the amortization time.
  b. Calculate the object return.

Exercise 9.4   Plant Monitoring

  a. What is the difference between reference yield and Sun full load hours?
  b. Does a southwestern aligned plant have a poorer performance ratio than a southern aligned one?
  c. What values for the performance ratio can one expect for actual plants?

Exercises for Chapter 10

Exercise 10.1   Potential Estimation for Pitched Roofs

The Saarland (small state in Germany) has an area of 2570 km^2.

  a. What theoretical potential does this area possess?
  b. Assuming approximately 0.3% of this area is available for the photovoltaics of suitable roof surfaces (east via south to west). What is the radiation energy on this surface?
  c. What PV power can be installed on this area ($\eta_{\text{Module}} = 20\%$) and what is the electrical energy generation potential ($\eta_{\text{System}} = 18\%$)?

Exercise 10.2   Potential Estimations for Free Areas

Assume you have a hectare of free surface available in the Saarland.

  a. What is the area utilization factor when there is to be no self-shading (degree of latitude $\varphi = 49°$, module inclination $\beta = 20°$)?
  b. What PV capacity can be erected on this surface and what is the electricity generation potential?
  c. What electrical energy could be generated on this hectare if energy corn is planted instead of using it for photovoltaics?

Appendix A: Checklist for Planning, Installing and Operating a Photovoltaic Plant

1. **Suitability of the roof**
   - Roof orientation: What yield can be expected?
     - Comparison with existing plants (e.g., with *www.sunnyportal.com*)
     - Yield prognosis as done in Exercise 9.2
   - Shading: Are there serious shading problems now or in the future?
   - Age of the roof: Will it need repairs in the next 20 years?
   - Roof statics: Can the roof bear the planned photovoltaic installation?

2. **Approvals**
   - Construction approval: Is this necessary (e.g., due to protection of historic buildings)?
   - In case of a rented roof: Close a roof utilization agreement with the owner.
   - Connection to the grid: Make an application to the public utility.

3. **Obtain and check quotes from solar installation companies**
   - Module manufacturer: Should be an established, known manufacturer.
   - Performance tolerance of the module: Acceptable is a maximum tolerance of ±3%.
   - Warranty conditions: Where is the place of jurisdiction?
   - Inverter:
     - Product guarantee should be more than 5 years.
     - European Efficiency should be more than 96% (see Section 7.2.4).
     - Design factor should be a maximum of 1 (see Section 7.2.5).
   - Cable dimensioning:
     - Line losses should be a maximum of 1% (see Section 6.3.2).

4. **Financing and insurance**
   - Investment appraisal:
     – Determine object return according to Section 9.2.2.
   - Close a credit agreement with bank.
   - Insurances:
     – Take out an operator liability insurance.
     – Take out an elementary damage or all-risks insurance.

5. **During installation**
   - Pre-sorting the modules (if desired, see Section 6.2.3).
   - Careful working of installers:
     – Is the rear side foil of the module damaged?
     – Is the module being stood upon (micro-cracks)?
     – Is the roof damaged?
     – Are the string cables clearly marked (numbering)?

6. **After installation**
   - Creating a startup protocol.
   - Acceptance of the system documents, including at least:
     – Roof sketch with modules drawn in and string arrangement plan.
     – Circuit diagram of the whole installation.
     – Datasheets of modules and inverter.
     – Information on the mounting system.
     – Information of length of warranty for modules and inverters.
   - Installation check (possibly):
     – Peak power measurement (see Section 8.3).
     – Bright thermography measurement (see Section 8.4).

7. **During Operation**
   - Function check (every 2 weeks):
     – Check whether inverter shows feed-in operation (status MPP).
   - Yield control (every 4–8 weeks):
     – Reading the meter.
     – Comparison with online databases.
   - Soiling check (annually):
     – Check whether solid dirt layers have formed on the module borders.
   - Mechanical check (annual or after a big storm):
     – Check whether the installation rattles with movement.

Appendix B: Physical Constants/ Material Parameters

Important Physical Constants

Boltzmann constant	$k = 1.3807 \cdot 10^{-23}\,\mathrm{J/K} = 8.6174 \cdot 10^{-5}\,\mathrm{eV/K}$
Elementary charge	$q = 1.6022 \cdot 10^{-19}\,\mathrm{As}$
Gravity	$g = 9.81\,\mathrm{m/s^2}$
Planck's constant	$h = 6.6261 \cdot 10^{-34}\,\mathrm{Ws^2}$
Solar constants	$E_\mathrm{S} = 1367\,\mathrm{W/m^2}$
Stefan–Boltzmann constant	$\sigma = 5.6705 \cdot 10^{-8}\,\mathrm{W/(m^2 \cdot K^4)}$
Speed of light in vacuum	$c_0 = 2.9979 \cdot 10^8\,\mathrm{m/s}$

Material Parameters of Silicon

Bandgap	$\Delta W_\mathrm{G} = 1.12\,\mathrm{eV}$
Mobility of electrons	$\mu_\mathrm{N} = 1400\,\mathrm{cm^2/Vs}$
Mobility of holes	$\mu_\mathrm{P} = 450\,\mathrm{cm^2/Vs}$
Refractive index at 600 nm	$n = 3.9$
Diffusion constant of electrons	$D_\mathrm{N} = 35\,\mathrm{cm^2/s}$
Diffusion constant of holes	$D_\mathrm{P} = 12\,\mathrm{cm^2/s}$
Effective density of state	$N_0 = 3 \cdot 10^{19}/\mathrm{cm^3}$
Melting point	$\vartheta_\mathrm{Melt} = 1414°\mathrm{C}$

References

1. International Energy Agency (2010) World Energy Outlook.
2. United Nations (2009) World Population Prospects – The 2008 Revision, New York.
3. International Energy Agency (December 19 2008) International Energy Annual 2006, www.eia.gov/iea/.
4. International Energy Agency (2010) Key World Energy Statistics.
5. Bundesministerium für Wirtschaft und Technologie (August 2010) Energie in Deutschland, aktualisierte Ausgabe.
6. Monnin, E., Steig, E.J., Siegenthaler, U. *et al.* (2004) EPICA dome C ice core high resolution holocene and transition CO2 Data, ftp.ncdc.noaa.gov/pub/data/paleo/icecore/antarctica/epica_domec/edc-co2.txt (accessed August 29, 2013).
7. Neftel, A., Friedli, H., Moor, E. *et al.* (1994) Historical carbon dioxide record from the Siple Station ice core Available at: http://cdiac.ornl.gov/trends/co2/siple.html (accessed September 1, 2013).
8. IPCC (2007) Climate Change 2007 – The physical science basis, contribution of working group Ito the fourth assessment report of the intergovernmental panel on climate change.
9. Lübbert, D. *et al.* (2006) Uran als Kernbrennstoff - Vorräte und Reichweite, Infobrief WF VIII G – 069/06, Wissenschaftlicher Dienst des Bundestages.
10. Becquerel, A.E. (1839) *Comptes Rendus de l'Academie des Sciences*, **9**, 561.
11. Wagner, A. (2010) *Photovoltaik Engineering – Handbuch, Entwicklung und Anwendung*, Springer.
12. Chapin, D., Fuller, C.S. and Pearson, G.L. (1954) A new silicon p-n junction photocell for converting solar radiation into electrical power. *Journal of Applied Physics*, **25** (5), 676–677.
13. Fatemi, N. (2005) Performance of high-efficiency advanced triple junction solar panels for the LILT mission DAWN. 31 Photovoltaic Specialists Conference and Exhibition, Lake Buena Vista, Florida, January 3–7.
14. Grochowski, J.. (1997) Minderertragsanalysen und Optimierungspotentiale an netzgekoppelten Photovoltaikanlagen des 1000-Dächer-Programms, Themen 96/97, Forschungsverbund Sonnenenergie, Köln.
15. International Energy Agency (2013) IEA Photovoltaic Power Systems Programme, www.iea-pvps.org.
16. Adams, W. and Day, R. (1877) *Proceedings of the Royal Society of London Series A*, **25**, 11.
17. Green, M. (2002) Photovoltaic principles. *Physica E*, **14**, 11–17.
18. NASA Langley Research Center (2013) Surface meteorology and solar energy, a renewable energy resource web site, release 6.0, http://eosweb.larc.nasa.gov/cgi-bin/sse/register.cgi.
19. Palz, W., Greif, J. and Scharmer, J. (eds) (1998) *European Solar Radiation Atlas*, Springer.
20. Deutscher Wetterdienst (2012) Strahlungskarten der Mittelwerte für Deutschland: Jahr – flächendeckende mittlere Jahressumme (1981–2010) www.dwd.de/Solarenergie 10.2.2012 (accessed September 1, 2013).
21. Deutsche Gesellschaft für Sonnenenergie (2010) *Planning and Installing Photovoltaic Systems*, 4th edn, DGS Berlin.
22. RWE (2010) *RWE Bau-Handbuch*, 14. edition, EW Medien und Kongresse GmbH, Frankfurt.
23. Goetzberger, A., Knobloch, J. and Vob, B. (1998) *Crystalline Silicon Solar Cells*, John Wiley & Sons, org.
24. Müller, R. (1995) *Grundlagen der Halbleiter-Elektronik*, Springer.
25. Kittel, Ch. (2006) Einführung in die Festkörperphysik, Oldenbourg.

---

26. McCandless, B. and Sites, J. (2003) Cadmium telluride solar cells, in: *Handbook of Photovoltaics Science and Engineering*, John Wiley & Sons, Ltd.

27. Lewerenz, H.-I. *et al.* (1995) *Photovoltaik – Grundlagen und Anwendungen*, Springer.

28. Roxlo, C. (1983) Comment on the optical absorption edge in a-Si:H. *Solid State Communications*, **47** (12), 985–987.

29. Hecht, E. (2003) *Optics*, Prentice Hall.

30. PVEducation (2013) website on the general properties of silicon http://pveducation.org/pvcdrom/materials/general-properties-of-silicon (accessed August 29, 2013).

31. v. Roos, O. (1978) A simple theory of back surface fields (BSF) solar cells. *Journal of Applied Physics*, **49** (6), 3503–3511.

32. Wagemann, H.-G. and Eschrich, H. (2007) *Photovoltaik – Solarstrahlung und Halbleitereigenschaften, Solarzellenkonzepte und Aufgaben*, Teubner.

33. Roth, T., Hohl-Ebinger, J., Warta, W. *et al.* (2008) Improving the accuracy of suns-V_{OC} measurements using spectral mismatch correction. 33. Photovoltaic Specialists Conference, San Diego, USA.

34. Schott Solar, DNR 500293-04 (2005) *Datenblatt multikristalline Solarzelle*, Schott Solar GmbH.

35. Green, M. (1995) *Silicon Solar Cells – Advanced Principles & Practice*, University of New South Wales, Sidney.

36. Green, M. (1982) *Silicon Solar Cells – Operating Principles, Technology and System Applications*, Prentice-Hall Inc.

37. Bosch Solar (2010) Data sheet of Bosch Solar Cell M-3BB, Position May.

38. Hovinen, A. (1994) Fitting of the solar cell I/V-curve to the two diode model. *Physica Scripta*, **T54**, 175–176.

39. Reference Solar Spectral Irradiance (n.d.) ASTM G-173, Online http://rredc.nrel.gov/solar/spectra/am1.5/ASTMG173/ASTMG173.html (accessed August 20, 2013).

40. Häberlin, H. (2012) *Photovoltaics System Design and Practice*, John Wiley & Sons, Ltd.

41. Swanson, R. (2005) Approaching the 29% limit efficiency of silicon solar cell, Photovoltaic Specialists Conference, Conference Record of the 31st IEEE, p. 889–894.

42. Ristow, A. (2001) Screen-printed back surface reflector for light trapping in crystalline silicon solar cells, Proceedings of the 17th European Photovoltaic Solar Energy Conference, p. 1335–1338, Munich.

43. Ransome, S. (2004) Quantifying PV losses from equivalent circuit models, cells, modules and arrays, Preprint of poster presented at 19th PVSEC, Paris.

44. Sinton, R., Kwark, Y., Swirhun, S. and Swanson, R.M. (1985) Silicon point contact concentrator solar cells. *IEEE Electron Device Letters*, **EDL-6** (8), 405–407.

45. Green, M. (2009) The path to 25% silicon solar cell efficiency: History of silicon cell evolution. *Progress in Photovoltaics – Research and Applications*, **17** (3), 183–189.

46. Suntech (2009) Mass production of the innovative plutoTM solar cell technology, White Paper, eu.suntech-power.com/de/technologie/pluto-zelle.html.

47. Sollmann, D. (2009) Was lange währt . . . , *Photon*, 7/2009, p. 76–78.

48. Alsema, E. de Wildy-Scholten, M.J. and Fthenakis, V.M. (4–8 September 2006) Environmental impacts of PV electricity generation – a critical comparison of energy supply options. 21st European Photovoltaic Solar Energy Conference and Exhibition, Dresden, Germany.

49. Sollmann, D. (2009) Sechs Neuner sind das Ziel, *Photon*, 4/2009, p. 42–45.

50. Basore, P. (1994) Defining terms for crystalline silicon solar cells. *Progress in Photovoltaics: Research and Applications*, **2** (2), 177–179.

51. Podewils, Ch. (2009) Diamantdraht zum Sägen, *Photon*, 4/2009, p. 77.

52. Chu, S.K. and Siemer, J. (2012) Zinn statt Silber für die Rückseite, *Photon*, 9/2012, p. 58.

53. Evergreen (2010) Evergreen Solar introduces new higher power string ribbon^TM Solar Panel at Solar Expo 2010 in Verona, Italy, press release, 05.05.2010.

54. Beneking, A. (2012) Neuer Kontakt, Photon, 2/2012, p. 58–61.

55. Rutschmann, I. (2008) Der Ruf nach Qualität, *Photon*, 03/2008, p. 52–56.

56. Glunz, S., Benick, J., Biro, D. *et al.* (June 20–25 2010) n-type silicon – enabling efficiencies > 20% in industrial production. 35th PVSC, Honolulu, Hawaii.

57. Repmann, T. (2003) *Stapelsolarzellen aus amorphem und mikrokristallinem Silizium, Dissertation*, Berichte des Forschungszentrums Jülich.

58. Gao, M. (2002) Optical band gap and electrical properties of a-Si:H, Workshop University of Lanzhou, China, 04.02.2002.

59. Zeman, M. (2006) Advanced amorphous silicon solar cell technologies, in *Thin Film Solar Cells – Fabrication, Characterization and Applications* (eds J. Poortmans, and V. Arkhipov), John Wiley & Sons, org.

60. Liang, I. *et al.* (2006) Hole-mobility limit of amorphous silicon solar cells. *Applied Physics Letters*, **88**, 063512.

61. Green, M. (2013) Solar cell efficiency tables (version 41). *Progress in Photovoltaics: Research and Applications*, **21**, 1–11.

62. Street, R. (2000) *Technology and Applications of Amorphous Silicon, Springer Series in Materials Science*, vol. **37**, Springer.

63. Staebler, D. and Wronski, C. (1977) Reversible conductivity changes in dischargeproduced amorphous Si. *Applied Physics Letters*, **31**, 292.

64. Carlson, D. and Rajan, K. (1998) Evidence for proton motion in the recovery of light-induced degradation in amorphous silicon solar cells. *Journal of Applied Physiology (Bethesda, Md: 1985)*, **83**, 1726–1729.

65. Yang, I., Banerjee, A. and Guha, S. (1997) Triple-junction amorphous silicon alloy solar cell with 14.6% initial and 13.0% stable conversion efficiencies. *Applied Physics Letters*, **70** (22), 2975–2977.

66. Hering, G. (2010) Das Kreuz mit der Dünnschicht, *Photon*, 9/2010, p. 64–72.

67. Burgelman, M. (2006) Cadmium telluride thin film solar cells – characterization, fabrication and modeling, in *Thin Film Solar Cells – Fabrication, Characterization and Applications* (eds J. Poortmans and V. Arkhipov), John Wiley & Sons, Ltd.

68. Gupta, A., Parikh, V. and Compaan, A.D. (2006) High efficiency ultra-thin sputtered CdTe solar cells. *Solar Energy Materials & Solar Cells*, **90**, 2263–2271.

69. Mitchell, K., Eberspacher, C., Ermer, J. and Pier, D. (1988) Single and tandem junction CuInSe$_2$ cell and module technology, 20th IEEE Photovoltaic Specialists Conference, Las Vegas, Conference Record, Vol. 2, p. 1384–1389.

70. Poortmans, J. and Arkhipov, V. (eds) (2006) *Thin Film Solar Cells - Fabrication, Characterization and Applications*, John Wiley & Sons, Ltd, p. 239, Fig. 6.2.

71. Nanosolar Inc. (2007) High performance thin-film photovoltaics using low-cost process technology, 17th Annual Photovoltaic Science and Engineering Conference (PVSEC) Fukuoka, Japan.

72. Rutschmann, I. (2009) Größter Coup oder größter Bluff, *Photon*, 10/2009, S. 34–37.

73. Green, M. (2001) Crystalline silicon solar cells, in *Clean Electricity from Photovoltaics* (eds M.D. Archer and R. Hill) Imperial College Press.

74. Mishima, T. *et al.* (2010) Development status of high-efficiency HIT solar cells. *Solar Energy Materials & Solar Cells*. doi: 10.1016/j.solmat.2010.04.030

75. Flamand, G. and Poortmans, J. (2006) Towards highly efficient 4-terminal mechanical photovoltaic stacks. *III–Vs Review*, **19** (7), 24–27.

76. Karam, N. *et al.* (2001) Recent developments in high-efficiency Ga$_{0.5}$In$_{0.5}$P/GaAs/Ge dual- and triple-junction solar cells – steps to next-generation PV cells. *Solar Energy Materials & Solar Cells*, **66**, 453–466.

77. Grätzel, M. (2006) Nanocrystalline injection solar cells, in *Thin Film Solar Cells – Fabrication, Characterization and Applications* (eds J. Poortmans and V. Arkhipov), John Wiley & Sons, Ltd.

78. Mozer, A. and Sariciftci, N.S. (2006) Charge transport and recombination in donor-acceptor bulk heterojunction solar cells, in *Thin Film Solar Cells Fabrication, Characterization and Applications* (eds J. Poortmans and V. Arkhipov), John Wiley & Sons, Ltd.

79. King, R. (2003) Lattice matched and metamorphic GaInP/GaInAs/Ge concentrator solar cells, 3rd World Conference on Photovoltaic Energy Conversion, Osaka.

80. Concentrix Solar, FAQ zur Technologie, www.soitec.com/en/technologies/concentrix/components/ (accessed September 1, 2013).

81. Fthenakis, V. and Zweibel, K. (2003) CdTe PV: Real and Perceived EHS Risks, NCPV Meeting, March 24–26.

82. Umweltbundesamt (2010) Nationale Trendtabellen für die deutsche Berichterstattung atmosphärischer Emissionen (Schwermetalle) 1990–2008, Stand: 15.02.2010, Dessau.

83. Schwarzburger, H. (2010) Kein Persilschein für Silizium, photovoltaic, 02/2010, p. 58–64.

84. Kreutzmann, A. Vorteil Wacker, *Photon*, 5/2008, p. 30–35.

85. Müller, A. (2009) Das zweite Leben, Sonne Wind und Wärme, 08/2009, p. 182–187.

86. BINE Informationsservice, Recycling von Photovoltaikmodulen, Projektinfo 02/2010, www.bine.info.

87. Gellings, R. (2006) Vom Regen in die Traufe, *Photon*, 6/2006, p. 52–62.

88. Iken, J. (2010) Abhängigkeiten und Alternativen, Sonne Wind & Wärme, 2/2010, p. 42–49.

89. Bunk, O. (issue 03/ 2002) Positive Umweltbilanz – Anlagen amortisieren sich nach wenigen Monaten, Windblatt – Das Enercon Magazin, p. 12–13.

90. Hering, G. (2012) Das Jahr des Drachens, *Photon*, 4/2012, p. 42–72.
91. Hagmann, G. (2009) *Leistungselektronik*, 4. issue, AULA-Verlag.
92. Femia, N. (2005) Optimization of perturb and observe maximum power point tracking method. *IEEE Transactions on Power Electronics*, **20** (4), 963–973.
93. Laschinski, I. (2008) Systemspannung, TCO-Korrosion und Generatorerdung bei Dünnschichtmodulen. *IHKS Fach Journal*, 129–131.
94. Sahan, B. (2010) *Wechselrichtersysteme mit Stromzwischenkreis zur Netzanbindung von Photovoltaikgeneratoren*, Kassel University Press GmbH.
95. Siemer, J. *et al.*, Hohes Schadenspotential, *Photon*, 12/2010, p. 58–66.
96. Burger, B. (2005) Auslegung und Dimensionierung von Wechselrichtern für netzgekoppelte PV-Anlagen, 20. Symposium Photovoltaische Solarenergie, Staffelstein.
97. Burger, B. and Kranzer, D. (2009) Extreme high efficiency PV-power converters, 13th European Conference on Power Electronics and Applications, Barcelona.
98. Wraneschitz, H. (2009) Das Henne-Ei-Problem, photovoltaik, 03/2009, p. 62–65.
99. Rothert, M. (2012) Ein Jahr Felderfahrung: PV-Anlagen mit Speicherlösung zur Eigenverbrauchserhöhung. 27. Symposium Photovoltaische Solarenergie, Staffelstein.
100. Richtlinie für Anschluss und Parallelbetrieb von Eigenerzeugungsanlagen am Niederspannungsnetz, 4. issue 2001 mit VDN-Ergänzungen, position September (2005).
101. Erzeugungsanlagen am Niederspannungsnetz (2010) Technische Mindestanforderungen für Anschluss und Parallelbetrieb von Erzeugungsanlagen am Niederspannungsnetz, Draft, July 2010.
102. Blitzschutz – Teil 3 (2009) Schutz von baulichen Anlagen und Personen – Sheet 5: Blitz- und Überspannungsschutz für PV-Stromversorgungssysteme, VDE 0185305-3 Sheet 5, October 2009.
103. Schlumberger, A. (2006) Der Tanker bewegt sich – ein Stück, *Photon*, 10/2006, p. 106–109.
104. Ladener, H. (1999) *Solare Stromversorgung*, 3. edition, Ökobuch Verlag.
105. Wiese, R. (2010) Empowering a rural revolution, *Renewable Energy World Magazine*, 15 April.
106. Strauß, P. *et al.* (2009) Netzferne Stromversorgung und weltweite Elektrifizierung, Themen 2009, Forschungs-Verbund Erneuerbare Energien, p. 94–101.
107. SMA AG (2010) *Produktkatalog Sunny Family 2010/2011 – the future of solar technology*, SMA AG, Kassel.
108. Photovoltaische Einrichtungen – Part 9 (2007) Leistungsanforderungen an Sonnensimulatoren, German edition of the IEC 60904-9:2007, VDE 0126-4-9.
109. Verfahren zur Umrechnung von gemessenen Strom-Spannungs-Kennlinien von photovoltaischen Bauelementen aus kristallinem Silizium auf andere Temperaturen und Einstrahlungen, German edition of the EN 60891 (1994).
110. Photovoltaische Einrichtungen (2010): Verfahren zur Umrechnung von gemessenen Strom-Spannungs-Kennlinien auf andere Temperaturen und Bestrahlungsstärken, Deutsche Fassung der EN 60891:2010, VDE 0126-6.
111. Mertens, K. (2008) Feldstudie zur tatsächlichen Leistung von Photovoltaikanlagen mittels Peakleistungsmessgerät. 23. Symposium Photovoltaische Solarenergie, Staffelstein.
112. Omega Newport Electronics GmbH (2011) Emissionsfaktoren – Technische Hintergrund informationen, www.omega.de (accessed August 29, 2013).
113. Köntges, M. *et al.* (2008) Elektrolumineszenzmessung an PV-Modulen, ep Photovoltaik aktuell, 7–8/2008, p. 36–40.
114. Mertens, K., Stegemann, Th., and Stöppel, T. (2012) LowCost EL: Erstellung von Elektrolumineszenzbildern mit einer modifizierten Standard-Spiegelreflexkamera. 23. Symposium Photovoltaische Solarenergie, Staffelstein.
115. Mertens, K., Stegemann, Th., and Stöppel, T. (2012) LowCost-EL – Preisgünstige Erstellung von Elektrolumineszenzbildern mit einer Spiegelreflexkamera, Der Bausachverständige, annual 8, 4 (August), p. 38–39.
116. Köntges, M. *et al.* (6–10 September 2010) Quantifying the risk of power loss in PV modules due to micro cracks. 25th European Photovoltaic Solar Energy Conference, Valencia, Spain, p. 3745–3752.
117. Antony, E.A. (2009) *Photovoltaik für Profis*, Solarpraxis AG.
118. Kreutzmann, A. Dünnschicht als Preisbrecher, *Photon*, 12/2006, p. 100–108.
119. Mertens, K. (2005) Kindgerechte Visualisierung von Photovoltaikerträgen. 20. Symposium Photovoltaische Solarenergie, Staffelstein.
120. Quaschning, V. (2000) Systemtechnik einer klimaverträglichen Elektrizitätsversorgung in Deutschland für das 21., Jahrhundert, Fortschritt-Berichte, VDI Series 6, No. 437, VDI Verlag.
121. Kaltschmitt, M. *et al.* (2007) *Renewable Energy: Technology, Economics and Environment*, Springer.

122. Top Agrar (2010) Biogas – Nawaro-Anbau legt kräftig zu, Pressemitteilung vom 10.09.2010, www.topagrar.com/news.

123. Quaschning, V. (2011) Bewertung von Methoden zur Bestimmung des PV-Anteils sowie von Ausbauszenarien und Einflüssen auf die Elektrizitätswirtschaft. 26. Symposium Photovoltaische Solarenergie, Staffelstein.

124. Fachagentur nachwachsende Rohstoffe e.V. (June 2010) Biogas – Basisdaten Deutschland, Info-flyer.

125. Hoffmann, V. (2008) Damals war's – Ein Rückblick auf die Entwicklung der Photovoltaik in Deutschland, Sonnenenergie, Nov.–Dec. 2008, p. 38–39.

126. PVXCHANGE (2012) Preisindex PV-Module, http://www.pvxchange.com/priceindex/priceindex.aspx?lang Tag=en-GB (accessed August 29, 2013).

127. Weber, E. (2009) Entwicklung des PV-Marktes aus Sicht der Forschung. 24. Symposium Photovoltaische Solarenergie, Staffelstein.

128. Quaschning, V (2012) website in German www.volker-quaschning.de/datserv (accessed August 29, 2013).

129. Sachverständigenrat für Umweltfragen (2011) *Wege zur 100% erneuerbaren Stromver-sorgung*, Sondergutachten.

130. Bundesministerium für Umwelt (August 2009) Leitszenarien 2009 – Langfristszenarien und Strategien für den Ausbau erneuerbarer Energien in Deutschland.

131. FVEE – Forschungsverbund Erneuerbare Energien (2010) Energiekonzept 2050, Köln, www.fvee.de/publika-tionen (accessed August 30, 2013).

132. Umweltbundesamt (2010) Energieziel 2050 – 100% Strom aus erneuerbaren Quellen.

133. Kawakami, N. *et al.* (2010) Development and field experiences of stabilization system using 34 MW NAS batteries for a 51 MW wind farm. IEEE International Symposium on Industrial Electronics, p. 2371–2376.

134. Sauer, D. (2008) Stromspeicher in Netzen mit hohem Anteil erneuerbarer Energien. 23. Symposium Photo-voltaische Solarenergie, Staffelstein.

135. Neupert, U., Euting, T., Kretschmer, T. *et al.* (2009) *Energiespeicher – Technische Grundlagen und ener-giewirtschaftliches Potenzial*, Fraunhofer IRB Verlag.

136. Sterner, M., Gerhardt, N., Saint-Drenan, Y.-M., *et al.*, (2010) Erneuerbares Methan – Ein innovatives Konzept zur Speicherung und Integration Erneuerbarer Energien sowie zur regenerativen Vollversorgung, LIFIS Online, ISSN 1864-6972, 09.07.2010.

137. NOAA Earth System Research Laboratory (2012) Trends in atmospheric carbon dioxide, www.esrl.noaa.gov.

138. Quaschning, V. (2005) *Understanding Renewable Energy Systems*, 1st edn, Earthscan London.

139. First Solar (2010) Corporate Datasheet, Available at: www.firstsolar.com/About-First-Solar/~/media/Files/Corporate/First%20Solar%20Corporate%20Datasheet.ashx (accessed August 29, 2013).

Further Information on Photovoltaics

Information on the Internet

home.solarlog-web.de	Yield database for data loggers of the Solare Datensysteme Company
re.jrc.ec.europa.eu/pvgis	Interactive solar radiation cards with yield estimates
www.dgs.de	Site of the Deutsche Gesellschaft für Solarenergie e.V.
www.photon.info	Module and inverter database (reached via *Publishing/Databases*)
www.photovoltaikforum.com	Forum on photovoltaic with module, inverter and company database
www.pveducation.org/pvcdrom	Interesting and instructive information and applets on photovoltaics
www.pv-ertraege.de	Yield database of the Solarenergie-Fördervereins Deutschland e.V. (SFV)
www.satel-light.com	Individual creation of an radiation map of the whole of Europe
www.sfv.de	Information of the Solarenergie-Fördervereins Deutschland e.V. (SFV)
www.solarserver.de	Comprehensive information on the subject of solar energy
www.sonnenertrag.eu	Yield database, company-independent
www.sunnyportal.de	Yield database for inverters of the SMA AG Company
www.volker-quaschning.de	Comprehensive information on the subject of renewable energies
www.textbook-pv.org/links	Additional interesting links can be found on this site

Journals

Global Solar Technology	www.globalsolartechnology.com
Photon	www.photon.de
Photon International	www.photon-international.com
Photovoltaics International	www.solarmediastore.com/journals.html
Photovoltaic Production	www.photovoltaic-production.com
Photovoltaik	www.photovoltaik.eu
pv magazine	www.pv-magazine.com
Solar Australia	www.solarmagazine.com.au
Solar Energy	www.journals.elsevier.com/solar-energy
Solar Industry	www.solarindustrymag.com
Solar Pro	www.solarprofessional.com
Solar Today	www.ases.org/solar-today-magazine
Solarthemen	www.solarthemen.de
Sonnenenergie	www.sonnenenergie.de
Sun & Wind Energy	www.sunwindenergy.com

Recommended Books

Quaschning, V. (2007) *Understanding Renewable Energy Systems*, Earthscan, London.
Good and comprehensive introduction to the subject of renewable energies.

Häberlin, H. (2012) *Photovoltaics: System Design and Practice*, John Wiley & Sons, Ltd.
Detailed description of the system technology of photovoltaic plants (inverters, lightning protection, etc.).

Haselhuhn, R. and Hartmann, U. (2013) *Planning and Installing Photovoltaic Systems*, DGS Deutsche Gesellschaft für Sonnenenergie.
Comprehensive work for the practical person with descriptive illustrations.

Index